

Joana  
Quaresma

Homemade Explosives based in Ammonium and Urea Nitrates

September  
2013



• U

Joana Filipa Pires d'Oliveira Quaresma

# Homemade Explosives based in Ammonium and Urea Nitrates

Forensic Chemistry Master Degree

Chemistry Department

FCTUC

September, 2013



UNIVERSIDADE DE COIMBRA

*(primeira folha no interior da tese, em branco nas costas)*

Joana Filipa Pires d'Oliveira Quaresma

# **HOMEMADE EXPLOSIVES BASED IN AMMONIUM AND UREA NITRATES**

**Dissertação apresentada para provas de Mestrado em Química, Área de especialização em  
Química Forense**

Professor Doutor José Leandro Simões de Andrade Campos

Professora Doutora Marta Piñeiro Gomez

**Setembro de 2013**

**Universidade de Coimbra**

*Quando se luta nem sempre se ganha. Quando não se luta perde-se sempre.*

Álvaro Cunhal



## ACKNOWLEDGMENTS

Este projecto científico é o culminar da grande Luta Académica que foi para mim a passagem pela Universidade de Coimbra. Apesar de todos os contratemplos, não lutar nunca foi uma hipótese. Por isso, nunca perdi.

Muitas vezes me faltaram as forças, sobretudo no Departamento de Física - o terreno das mais duras batalhas e de onde saí victoriosamente licenciada. Algo que sempre me ensinaram (e que bem aprendi) é que só podemos lutar se tivermos objectivos e, sem luta, a vida perde o seu encanto.

Esta Luta Académica não é só a mim que se deve. Muitos intervenientes tiveram um papel fundamental para que nunca me esquecesse dos objectivos que moviam a minha Luta Académica. A todos estou eternamente grata.

Aos meus pais agradeço por cedo me terem ensinado o significado da palavra “luta”, por nunca terem desistido de mim, por sempre terem acreditado nos meus potenciais. À minha mãe, por sempre ter sido e ainda ser um modelo a seguir e que muito admiro. Ao meu pai, por todo o esforço económico e apoio ao longo destes anos, que muito reconheço e agradeço.

Ao meu irmão João, que sempre me apoiou e que teve um papel fundamental no meu crescimento. À Teresa, que é como uma mãe para mim e a primordial incentivadora do meu percurso escolar. Talvez também graças à tabuada feita por ela (à mão) ter nascido o meu gosto pelas ciências.

Aos meus orientadores, um muito obrigada por toda a atenção prestada e conhecimento partilhado. À Professora Doutora Marta Piñeiro, por ter sido a primeira Professora a acreditar em mim e nas minhas capacidades, por toda a boa disposição e empenho ao longo dos últimos três anos. Ao Professor Doutor José Campos por, além de acreditar e confiar nas minhas capacidades, as testar todos os dias e investir nelas, por toda a sabedoria partilhada, dedicação empenhada e por todos os dias me fazer ver o mundo um pouco mais além. Sem dúvida que são pessoas que deixarão para sempre a sua marca na minha vida, mesmo que ausentes um dia.

## ACKNOWLEDGMENTS

Aos meus colegas de laboratório, Jaqueline e João, agradeço sobretudo o companheirismo. À Jaqueline agradeço pelo empenho, compreensão e pelas boleias que tanto me facilitaram a vida durante esta luta final. Ao João, um muito obrigada pelo bom humor constante, positivismo, acessibilidade e amizade que se gerou num tão curto espaço de tempo.

Aos meus amigos, Carolina e Leandro, estou agradecida pelo apoio dado em casa, sobretudo nas horas de maior agonia por que passei, que se traduziram num mau feito insuportável que eles estoicamente suportaram.

A todos os meus amigos, com especial relevo para o Paulo, a Inês, a Mariana e a Sara, um muito obrigada por fazerem parte da minha vida e por sempre me terem apoiado ao longo dela, mesmo quando as escolhas não eram as melhores.

Ao Laboratório de Energética e Detónica, ao Departamento de Engenharia Mecânica e ao Departamento de Química, obrigada pelo fornecimento de infraestruturas e material, essenciais em toda esta Luta.

## RESUMO

Nitrato de Amónio ( $\text{NH}_4\text{NO}_3$ ) é a componente base de uma conhecida família de misturas geradoras de gases e compósitos pirotécnicos. Nitrato de Ureia ( $(\text{NH}_2)_2\text{COHNO}_3$ ) é um nitrato recentemente utilizado em estudos de deflagração e detonação. Ambos os nitratos foram utilizados em grandes atentados terroristas e são frequentemente utilizados em explosivos ocasionais.

Foram testadas misturas de nitrato de amónio (AN) e de nitrato de ureia (UN). Foram utilizados poliuretano como ligante e, como aditivos, pó de Al e uma mistura de Magnésio com Teflon (MT). A decomposição dos reagentes foi prevista em função da temperatura através do código THOR. As temperaturas de combustão também foram teoricamente previstas, de modo a otimizar composições e a avaliar as performances esperadas. Os termogramas dos reagentes, adquiridos por DSC/TGA, ajudaram a definir as composições testadas, pois demonstram os seus níveis de decomposição. Os termogramas adquiridos do AN e do UN mostram algumas diferenças significativas entre eles. O UN apresenta um pico exotérmico a baixas temperaturas. Os testes experimentais recorreram a duas configurações: amostras cilíndricas, cuja ignição era feita no topo, e contentores em forma de disco, compostos por uma base cilíndrica de PVC e uma tampa de PMMA. As amostras cilíndricas foram testadas antes dos discos para verificar propriedades de combustão. O sistema de termopares permitiu a medição de temperaturas de combustão. Filmagens, acima de 1000 fps, permitiram a visualização directa da propagação da chama. Assim, as velocidades fundamentais de chama puderam ser medidas.

A combustão com aditivos, Al e MT, demonstram aumentos de temperatura de chama na ordem dos  $1300^\circ\text{C}$  e apresentam, sempre para a pressão atmosférica, velocidades de propagação de chama de mm/s e velocidades fundamentais de chama superiores a cm/s. A mistura de MT, como aditivo, parece aumentar a expansão dos produtos de combustão, mais do que o Al. O UN tem um comportamento semelhante ao do AN neste tipo de composições energéticas. Foi observada a auto-ignição de uma mistura de UN/PU com MT durante o tempo de cura. Este facto parece ser devido a complexos fenómenos (reações entre os reagentes), onde foi observada a produção de gás proveniente do UN. Estudos suplementares são necessários antes de realizar novas experiências.

## RESUMO

A espectroscopia de infra-vermelho (IV) foi utilizada para caracterizar os reagentes utilizados nas misturas, bem como a sua presença nas respectivas misturas, e para avaliar a formação de novas ligações, devido a reacções entre os reagentes. Os espectros de IV confirmam as capacidades de detecção para este tipo de misturas e provam a existência dos reagentes “frescos” nos resíduos de combustão.

Palavras-chave: Nitrato de Amónio, Nitrato de Ureia, ligante Poliuretano, explosivos ocasionais, aditivo alumínio, aditivo Magnésio/Teflon, código THOR, termogramas DSC/TGA, testes de combustão de amostras, velocidades fundamental de propagação de chama, espectroscopia de infra-vermelho.

## ABSTRACT

Ammonium Nitrate ( $\text{NH}_4\text{NO}_3$ ) is the base component of a known family of gas generators and pyrotechnic composite mixtures. Urea Nitrate ( $(\text{NH}_2)_2\text{COHNO}_3$ ) is a recent used nitrate in deflagration and detonation studies. Both of these nitrates were used in huge terrorist attacks and are frequently used on Homemade Explosives (HME). Mixtures of Ammonium Nitrate (AN) and Urea Nitrate (UN) with polyurethane solution, as binder, were tested, having Al and a mixture of Magnesium/Teflon as additives. Decomposition of reactants, as a function of temperature, was predicted using THOR code. Combustion temperatures were also theoretically predicted in order to optimize compositions and evaluate expected performances. DSC/TGA thermograms of reactants help to define tested compositions, showing their decomposition levels. AN and UN thermograms show some significant differences between them. UN presents an exothermic peak at quite low temperature. Experimental tests use two configurations: cylindrical samples, ignited at the top, and a cylindrical disk box, formed by a PVC cylindrical cup covered by a PMMA lid. Cylindrical samples were tested before cylindrical disk boxes, verifying burning properties. A thermocouples system allowed to measure burning temperatures. Video records, up to 1000 fps, allowed the direct visualization of the flame propagation. Fundamental flame velocities can then be measured.

Combustion with additives, Al and MT, show an increasing flame temperature on the levels of 1300 °C and present, always for atmospheric pressure, flame propagation velocities of mm/s and fundamental flame velocities higher than cm/s. MT additive seems to present an increased contribution, to the expansion of combustion products, more than Al. UN has a quite similar behaviour of AN in this kind of energetic compositions. It was observed the self-ignition of one of UN/PU compositions with MT, during curing time. It seems to be due to complex phenomena (reactions between reactants) where the production of gas, from UN, was observed. Supplementary studies are required before new experiences.

Infra-Red (IR) spectroscopy was used to characterize the reactants used on the mixtures and their presence on respective mixtures, to evaluate the formation of new bounds due to the reactions between reactants. IR spectra confirm detection capabilities for these kind of mixtures and prove the existing unburnt reactants at found residues.

## ABSTRACT

**Keywords:** Ammonium Nitrate, Urea Nitrate, Polyurethane binder, homemade explosives, Aluminum additive, Magnesium/Teflon additive, THOR code, DSC/TGA thermograms, burning test samples, propagation and fundamental flame velocities, IR spectroscopy.

## TABLE OF CONTENTS

|   |        |
|---|--------|
| Acknowledgments .....   | iii    |
| Resumo .....  | v      |
| Abstract.....   | vii    |
| Table of Contents .....   | ix     |
| List of figures .....   | xv     |
| List of tables .....  | xxxi   |
| Abbreviations .....   | xxxvii |
| Chapter 1 – Introduction.....                                       | 1      |
| 1.1. Forensic Sciences Framework.....                               | 1      |
| 1.1.1. Terrorism definitions – HME and IED.....                     | 1      |
| 1.1.2. IED – worldwide panorama.....                                | 2      |
| 1.1.3. Terrorist incidents in Portugal .....                        | 6      |
| 1.1.4. HME and supply chain security improvements.....              | 9      |
| 1.2. HME’s reactants – open market possibilities .....              | 15     |
| 1.2.1. HME’s reactants - market products selection.....             | 18     |
| 1.3. AN and UN reactants.....                                       | 20     |
| 1.3.1. Historical terrorist attacks using AN and UN.....            | 21     |
| 1.3.2. Selected oxidants, binder and additives.....                 | 22     |
| 1.3.2.1. Ammonium Nitrate .....                                     | 22     |
| 1.3.2.2. Urea Nitrate .....   | 23     |
| 1.3.2.3. Polyurethane .....   | 24     |
| 1.3.2.4. Additives.....   | 24     |
| 1.4. Thesis description .....                                       | 25     |
| Chapter 2 – Ammonium and Urea Nitrates Thermal Decompositions ..... | 27     |
| 2.1. Literature Review .....  | 27     |
| 2.1.1. Thermal Decomposition Mechanisms .....                       | 27     |
| 2.1.1.1. Ammonium Nitrate.....                                      | 27     |

## TABLE OF CONTENTS

|   |    |
|---|----|
| 2.1.1.2. Urea Nitrate .....   | 30 |
| 2.1.2. THOR - thermochemical evaluation code .....  | 33 |
| 2.1.2.1. Introduction .....   | 33 |
| 2.1.2.2. General equations .....  | 34 |
| 2.1.2.3. Results and discussion from literature.....  | 40 |
| 2.1.3. Thermal Analysis.....  | 43 |
| 2.1.3.1. Fundamentals of Differential Thermal Analysis (DTA), Differential Scanning Calorimetry (DSC) and Thermogravimetric Analysis (TGA)..... | 43 |
| 2.1.3.2. The Arrhenius approach to thermal decomposition .....  | 44 |
| 2.1.3.3. Results and discussion from literature.....  | 48 |
| 2.1.3.3.1. Ammonium Nitrate (AN) .....  | 48 |
| 2.1.3.3.2. Urea Nitrate .....   | 54 |
| 2.1.4. Infra-Red Spectroscopy .....   | 56 |
| 2.1.4.1. Introduction fundamentals.....   | 56 |
| 2.1.4.2. Results and discussion from literature.....  | 59 |
| 2.1.4.2.1. Ammonium Nitrate.....  | 59 |
| 2.1.4.2.2. Urea Nitrate .....   | 60 |
| 2.2. Predicting calculations.....   | 63 |
| 2.2.1. Ammonium nitrate thermal decomposition prediction.....   | 63 |
| 2.2.1.1. Methodology and results .....  | 63 |
| 2.2.1.2. Comparison between experimental results and literature.....  | 65 |
| 2.2.2. Urea nitrate thermal decomposition prediction .....  | 66 |
| 2.2.2.1. Methodology and results .....  | 66 |
| 2.2.2.2. Comparison between prediction results and literature .....   | 67 |
| 2.2.3. DSC/TGA .....  | 69 |
| 2.2.3.1. Ammonium Nitrate.....  | 69 |
| 2.2.3.2. Urea Nitrate .....   | 75 |

|  |     |
|--|-----|
| Chapter 3 – Experimental testing of selected compositions.....                               | 83  |
| 3.1. Mixtures compositions - Thermodynamic Properties .....                                  | 83  |
| 3.2. Thermochemical properties predictions for studied mixtures .....                        | 86  |
| 3.2.1. Mixtures based on Ammonium Nitrate .....  | 86  |
| 3.2.1.1. Free Gibbs enthalpy and temperatures of combustion predictions.....                 | 86  |
| 3.2.2.2. Prediction of temperature combustion as a function of additives concentration ..... | 86  |
| 3.2.2. Mixtures based on Urea Nitrate.....   | 88  |
| 3.2.2.1. Free Gibbs enthalpy and predictions of combustion temperatures.....                 | 88  |
| 3.2.2.2. Combustion temperature prediction as a function of additives concentration .....    | 88  |
| 3.3. Combustion experimental study .....   | 90  |
| 3.3.1. Introduction .....  | 90  |
| 3.3.2. Simplified combustion model – cigar burning approach.....                             | 91  |
| 3.3.3. Experimental testing.....   | 94  |
| 3.3.3.1. Reactants.....  | 94  |
| 3.3.3.2. Mixing Procedure .....  | 96  |
| 3.3.3.3. Preparation of the samples.....   | 96  |
| 3.3.3.4. Experimental set-ups .....  | 98  |
| 3.3.3.5. Thermocouples and time delay calibrations .....                                     | 100 |
| 3.3.3.6. Typical testing procedure .....   | 102 |
| 3.3.4. Experimental results .....  | 105 |
| 3.3.4.1. Mixture nº 1.2 - heterogeneous mixture based on AN, PU and Al .....                 | 105 |
| 3.3.4.2. Mixture nº 1.4 - heterogeneous mixture based on AN, PU and MT ...                   | 107 |
| 3.3.4.3. Mixture nº 1.5 - heterogeneous mixture based on AN, PU and MT ...                   | 109 |
| 3.3.4.4. Mixture nº 1.8 - heterogeneous mixture based on AN, PU and Al .....                 | 115 |
| 3.3.4.5. Mixture nº 2.6 - heterogeneous mixture based on UN, PU and Al .....                 | 121 |
| 3.3.4.6. Mixture nº 2.7 - heterogeneous mixture based on UN, PU and MT ...                   | 125 |

## TABLE OF CONTENTS

|  |     |
|--|-----|
| 3.3.4.7. Mixture nº 3.1 - heterogeneous mixture based on AN, PU and MT ...   | 126 |
| 3.3.4.8. Mixture nº 3.2 - heterogeneous mixture based on AN, PU and Al ..... | 131 |
| 3.3.4.9. Mixture nº 3.3 - heterogeneous mixture based on AN, PU and MT ...   | 137 |
| 3.3.4.10. Mixture nº 3.4 - heterogeneous mixture based on AN, PU and Al ...  | 143 |
| 3.3.4.11. Mixture nº 4.1 - heterogeneous mixture based on UN, PU and MT .    | 149 |
| 3.3.4.12. Mixture nº 4.2 - heterogeneous mixture based on UN, PU and Al ...  | 154 |
| 3.4. Infra-Red Spectroscopy .....  | 159 |
| 3.4.1. Reactants.....  | 159 |
| 3.4.1.1. Ammonium Nitrate.....   | 159 |
| 3.4.1.2. Urea Nitrate .....  | 161 |
| 3.4.1.3. PolyUrethane .....  | 162 |
| 3.4.1.4. Aluminium.....  | 164 |
| 3.4.1.5. Magnesium and Teflon mixture .....                                  | 164 |
| 3.4.2. Studied Mixtures .....  | 165 |
| 3.4.2.1. Mixture nº 3.1 - heterogeneous mixture based on AN, PU and MT ...   | 165 |
| Fresh mixture characterization .....   | 165 |
| Burnt mixture characterization .....   | 167 |
| 3.4.2.2. Mixture nº 3.2 - heterogeneous mixture based on AN, PU and Al ..... | 172 |
| Fresh mixture characterization .....   | 172 |
| Burnt mixture characterization .....   | 173 |
| 3.4.2.3. Mixture nº 4.1 - heterogeneous mixture based on UN, PU and MT ...   | 175 |
| Fresh mixture characterization .....   | 175 |
| Burnt mixture characterization .....   | 177 |
| 3.4.2.4. Mixture nº 4.2 - heterogeneous mixture based on UN, PU and Al ..... | 179 |
| Fresh mixture characterization .....   | 179 |
| Burnt mixture characterization .....   | 180 |
| Chapter 4 - Results Discussion.....  | 185 |

|   |     |
|---|-----|
| 4.1. Ammonium and Urea Nitrates Thermal Decompositions .....  | 185 |
| 4.1.1. THOR prediction .....  | 185 |
| 4.1.2. DSC/TGA .....  | 186 |
| 4.1.2.1. Ammonium Nitrate .....   | 186 |
| 4.1.2.2. Urea Nitrate .....   | 187 |
| 4.2. Development and detection of studied mixtures .....  | 188 |
| 4.2.1. THOR predictions of combustion products properties.....  | 188 |
| 4.2.1.1. Free Gibbs enthalpy and temperatures of combustion, for oxidants (AN and UN) and binder (PU) mixtures.....   | 188 |
| 4.2.1.2. Predicted temperature of combustion as function of additives for previous mixtures (AN and UN with PU) ..... | 188 |
| 4.2.2. Combustion experiments .....   | 189 |
| 4.2.2.1. Densities of the fresh mixtures .....  | 189 |
| 4.2.2.2. Temperature profiles of mixtures in cigar burning tests.....   | 191 |
| 4.2.2.3. Velocity of propagation of PMMA .....  | 193 |
| 4.2.2.4. Flame velocity propagation jumps on explosions .....   | 195 |
| 4.2.2.5. Velocity of the flame propagation on the studied mixtures.....   | 196 |
| 4.2.2.6. Fundamental flame velocities .....   | 197 |
| 4.2.2.7. Local explosions areas and time delay in disk combustion samples...  | 198 |
| 4.2.3. Infra-Red Spectroscopy .....   | 200 |
| 4.2.3.1. Reactants IR characterization .....  | 200 |
| 4.2.3.2. IR characterization of fresh mixtures .....  | 201 |
| 4.2.3.3. IR characterization of burned mixtures .....   | 203 |
| Chapter 5 – Synthesis and Conclusions.....  | 207 |
| Bibliographic References .....  | I   |



## LIST OF FIGURES

|   |   |
|---|---|
| Figure 1: Threat continuum. (Joint Improvised Explosive Device Defeat Organization, 2012-1026) .....  | 2 |
| Figure 2: Domestic Terrorist IED attack cycle. (Science & Technology to Counter Improvised Explosive Devices, 2010).....  | 3 |
| Figure 3: Terrorist incidents occurred in from the beginning of 2010 to the end of 2011 using bombing and explosion (dynamite is included as weapon). (START, 2012).....  | 3 |
| Figure 4: Target types of terrorist incidents during 2010 and 2011 which used explosive and incendiary devices. (START, 2012) .....   | 4 |
| Figure 5: Statistic of the use of explosives, bombs dynamite and incendiary devices as weapon on the 4930 terrorist incidents which used that kind of weapon (at left), and common weapons used on 9889 reported terrorist incidents during the years 2010 and 2011. (START, 2012)..... | 4 |
| Figure 6: Casualties –fatalities on the left and injuries on the right - resultant of 4930 terrorist incidents, occurred worldwide between 2010 and 2011. (START, 2012).....  | 5 |
| Figure 7: Regions affected by terrorist attacks with resource to explosives and bombs. (START, 2012).....   | 5 |
| Figure 8: Representation of monthly global terrorist events that employed IED's, excluding Iraq and Afghanistan cases, for 2010. (Caldwell, 2011) .....   | 6 |
| Figure 9: Terrorist incidents that occurred in Portugal since 1970 to 2011 (START, 2012).....   | 7 |
| Figure 10: Attacks types used on terrorist incidents (left) and number of occurrences of the top three along the years (right) registered in Portugal since 1970 to 2011. (START, 2012).....  | 7 |

## LIST OF FIGURES

|  |    |
|--|----|
| Figure 11: Most common target types (left) and number of occurrences of each top three target (right) of the terrorist attacks performed in Portugal from 1970 to 2011. (START, 2012)..... | 8  |
| Figure 12: Attack (left) and weapon (right) types used by FP25 between 1980 and 1987. (START, 2012).....   | 9  |
| Figure 13: Components of Supply Chain Security (Oosterhout, et al., 2007).....   | 10 |
| Figure 14: Supply Chain Processes and security risks. (Oosterhout, et al., 2007) .....   | 11 |
| Figure 15: Supply chain security sense and respond model. (Oosterhout, et al., 2007)   | 13 |
| Figure 16: Information blocks and coverage (in width) in Port of Rotterdam IT systems. (Oosterhout, et al., 2007) .....  | 14 |
| Figure 17: Thermal decomposition mechanism of UN at low temperatures (Désilets, et al., 2011).....   | 31 |
| Figure 18: Some of the condensed phase species formed during UN thermal decomposition (Désilets, et al., 2011) .....   | 33 |
| Figure 19: Data access and results output of THOR Code. (Durães, 1999).....  | 39 |
| Figure 20: Evolution of Gibbs free energy and combustion temperature as a function of absorbed enthalpy, $\Delta H$ , for AN decomposition (Durães, et al., 1996(2)) .....                 | 41 |
| Figure 21: The influence of products selection, as a function of obtained combustion temperature and Gibbs free energy value, for AN (Durães, et al., 1996(2)) .....                       | 41 |
| Figure 22: Gas products composition, as a function of calculated decomposition temperature, for AN (Durães, et al., 1996(2)) .....   | 41 |
| Figure 23: theoretical prediction of (a) temperature and (b) products composition of the thermal decomposition of AN (Morgado, et al., 2002) (Morgado, et al., 2003) .....                 | 42 |
| Figure 24: Phase modifications and respectively temperature transitions for ammonium nitrate (Oommen, et al., 1999).....   | 48 |

|  |    |
|--|----|
| Figure 25: DSC trace of AN on thermal cycling (Oommen, et al., 1999).....  | 50 |
| Figure 26: DSC thermogram of pure AN, acquired with a heating rate of 50°C/min (Davis, et al., 1996) .....   | 51 |
| Figure 27: DSC traces of AN and PSAN samples (Oommen, et al., 1999(2)).....  | 51 |
| Figure 28: PSAN thermogram acquired by DSC/TGA at an heating rate of 10°C/min (Portugal, et al., 2000) .....   | 53 |
| Figure 29: Typical DSC/TGA thermograms for PSAN (Simões, et al., 1998) .....   | 53 |
| Figure 30: DSC thermograms at 20°C/min (Oxley, et al., 2009) and 10°C/min (Oxley, et al., 2013), respectively.....   | 55 |
| Figure 31: UN thermograms, with a heating rate of 5°C/min. (Désilets, et al., 2011(2))   | 56 |
| Figure 32: IR spectra of the decomposition products of AN in the gas phase after 10 s at (a) 15 psi, (b) 280 psi of argon. The thermal decomposition was made by DSC/TGA coupled with rapid-scan FT-IR, at a heating rate of 80°C/min..... | 60 |
| Figure 33: IR spectrum of urea nitrate residue obtained from the UN thermal decomposition at low temperatures (Désilets, et al., 2011).....  | 61 |
| Figure 34: FTIR spectra acquired during the thermal decomposition, made by TGA, of UN at: (A) 143°C, (B) 150°C and (C) 190°C (Désilets, et al., 2011(2)).....  | 62 |
| Figure 35: FTIR spectras of (A) time dependence of the IR spectra of decomposition products of UN in Ar, and (B) decomposition products of UN and urea in Ar , both for 8 atm and 400°C (Hiyoshi, et al., 2002) .....                      | 63 |
| Figure 36 Products decomposition of AN as a function of temperature .....  | 65 |
| Figure 37: Products decomposition of UN as a function of temperature .....   | 67 |
| Figure 38: DSC/TGA thermograms for AN (blue and red, respectively) heated at 5°C/min, contained on an open alumina cup (M <sub>1</sub> = 34.40 mg) .....   | 69 |

## LIST OF FIGURES

|  |    |
|--|----|
| Figure 39: DSC/TGA thermograms for AN (green and orange, respectively) heated at 5°C/min, contained on an open alumina cup ( $M_2 = 13.30$ mg) .....   | 70 |
| Figure 40: DSC/TGA results for AN (blue and red, respectively) heated at 10°C/min, contained on an open alumina cup ( $M_3 = 35.40$ mg).....   | 70 |
| Figure 41: DSC/TGA results for ammonium nitrate (green and orange, respectively) heated at 10°C/min, contained on an open alumina cup ( $M_4 = 20.80$ mg).....   | 71 |
| Figure 42: DSC/TGA results for urea nitrate (blue and red, respectively) heated at 5°C/min, contained on an open alumina cup ( $M_1 = 41.0$ mg).....   | 76 |
| Figure 43: DSC/TGA results for urea nitrate (green and orange, respectively) heated at 5°C/min, contained on an open alumina cup ( $M_2 = 9.28$ mg).....   | 76 |
| Figure 44: DSC/TGA results for urea nitrate (blue and red, respectively) heated at 10°C/min, contained on an open alumina cup ( $M_3 = 34.50$ mg).....   | 77 |
| Figure 45: DSC/TGA results for urea nitrate (green and orange, respectively) heated at 10°C/min, contained on an open alumina cup ( $M_4 = 7.69$ mg).....  | 77 |
| Figure 46: Evolution of predicted Gibbs Free Enthalpy (left) and combustion temperature $T_b$ (right) of isobar adiabatic reaction of Ammonium Nitrate – PolyUrethane, as a function of equivalence ratio $r$ (adimensional) (Quaresma, et al., 2013)..... | 86 |
| Figure 47: Influence of mass percentage of MT (left) and Al (right) at temperature of combustion in a mixture composed by AN and PU (for % (m/m) additives = 0: 76% AN + 24%PU).....   | 87 |
| Figure 48: Comparison between the influences of mass percentages of additives in mixtures composed by AN and PU (for % (m/m) additives = 0: 76% AN + 24%PU)..  | 87 |
| Figure 49: Evolution of predicted Gibbs Free Enthalpy (left) and combustion temperature $T_b$ (right) of isobar adiabatic reaction of Urea Nitrate – PolyUrethane, as a function of equivalence ratio $r$ (adimensional) (Quaresma, et al., 2013).....     | 88 |

Figure 50: Influence of mass percentage of MT (left) and Al (right) at temperature of combustion in a mixture composed by UN and PU (for % (m/m) additives = 0: 86% UN + 14%PU) ..... 89

Figure 51: Comparison between the influences of mass percentages of additives in mixtures composed by UN and PU (for % (m/m) additives = 0): 86% UN + 14%PU). 89

Figure 52: Scheme of the simplified combustion phenomena for cigar burning test. Zone I is the condensed-phase zone, zone II the condensed-phase reaction zone and zone III is the gas phase reaction zone. .... 92

Figure 53. Aluminum (Al black 000 India - Carob) particle size distributions obtained by Laser Diffraction Spectrometry (left figure) and Simultaneous thermal analysis (DSC/TG) of Al black 000 India (Carob), in Ar/H<sub>2</sub>(48%) atmosphere and heating rate of 40°C/min (right figure). .... 95

Figure 54: Cigar burning test samples ..... 97

Figure 55: Disk test samples (all dimensions in millimeters). Adapted from Durães, et al., 2006. .... 97

Figure 56: disk samples ..... 98

Figure 57: Experimental set-up for cigar burning tests ..... 99

Figure 58: Recording equipment ..... 99

Figure 59: horizontal experimental set-up for disk burning test ..... 100

Figure 60: vertical experiment set-up for disk burning test ..... 100

Figure 61: Thermocouples assembly for calibration of temperature equipment..... 101

Figure 62: Temperature records showing thermocouples delay allowing flame velocity measurement (2 V/div↔ 200 °C/div.) as a function of time (500 ms/div.) ..... 101

Figure 63: Temperature record in function of time of 5 s of lighter flame in each thermocouple. Between the heating of two thermocouples, 15 s elapsed. .... 101

## LIST OF FIGURES

|   |     |
|---|-----|
| Figure 64. Example of experimental temperature record of AN/PU mixture with MT (5 V/div $\Leftrightarrow$ 500 °C/div.) as a function of time (5 s/div.).....  | 102 |
| Figure 65: Visualization of the combustion of a cigar with the help of a magnifying glass .....   | 103 |
| Figure 66: Disk of mixture n°. 1.2. Image on the right shows the fresh mixture on the disk. Image on the left shows the disk after the partial combustion of the mixture. ....  | 106 |
| Figure 67: Combustion of the disk with mixture n°. 1.2. ....  | 107 |
| Figure 68: Disk of mixture n°. 1.4 before its combustion .....  | 107 |
| Figure 69: Frames which shows the moment before explosion one (at left) and the first appearance of explosion one (at right). The measurement of the area was made at right image. ....   | 109 |
| Figure 70: Frames which shows the moment before explosion two (at left) and the first appearance of explosion two (at right). The measurement of the area was made at right image. ....   | 109 |
| Figure 71: Mixture n°. 1.5 prepared for a cigar burning test (left) and its residues after combustion (right) .....   | 110 |
| Figure 72: Flame of combustion of mixture n°.1.5 on a cigar burning test.....   | 111 |
| Figure 73: Frames used to study the velocity of flame propagation of PMMA. The initial position is image on the left, final position the image on the right. ....   | 112 |
| Figure 74: Frames used to study the velocity of propagation of explosion in mixture n°. 1.5. The frame of the left shows the bigger burning area of this explosion and the frame of the right shows the end of the explosion (when no more incandescence on the mixture was seen). .... | 112 |
| Figure 75: Frames used to study the velocity of propagation of the mixture n°. 1.5. The frame at the left is correspondent to the initial position, and the frame at right, the final position. ....  | 113 |

Figure 76: Disk of mixture nº. 1.5 before its combustion ..... 113

Figure 77: Flames generates by explosion. Frame of the left shows the maximum intensity of light during explosions. Frame of the right shows the flame on the end of the explosion..... 114

Figure 78: Combustion flames generated by the burning of mixture nº.1.5..... 114

Figure 79: Frames which shows the moment before explosion one (at left) and the first appearance of explosion one (at right). The measurement of the area was made at right image. .... 115

Figure 80: Frames which shows the moment before explosion two (at left) and the first appearance of explosion two (at right). The measurement of the area was made at frame of the right. .... 115

Figure 81: cigar of the fresh mixture nº.1.8 (left) and its residues of combustion (right) ..... 116

Figure 82: Flame of combustion of mixture nº. 1.8 on a cigar burning test..... 117

Figure 83: Frames used to study the velocity of the propagation of the flame on PMMA. The initial position is image on the left, final position the image on the right..... 118

Figure 84: Frames used to study the velocity of propagation of explosion in mixture nº. 1.8. .... 118

Figure 85: Frames used to study the velocity of propagation of the mixture nº. 1.8. The frame at the left is correspondent to the initial position, and the frame at right, the final position. .... 119

Figure 86: Disk of mixture nº. 1.8 before its combustion ..... 119

Figure 87: Flames of combustion of mixture nº.1.8 when it had mass consumption (at left) and when there was no mass consumption (at right). .... 120

## LIST OF FIGURES

|  |     |
|--|-----|
| Figure 88: Frames which shows the moment before explosion one (at left) and the first appearance of explosion one (at right). The measurement of the area was made at right image. ....                    | 121 |
| Figure 89: Frames which shows the moment before explosion two (at left) and the first appearance of explosion two (at right). The measurement of the area was made at frame of the right. ....             | 121 |
| Figure 90: Mixture n°. 2.6 prepared for a cigar burning test (left) and its residues after combustion (right) .....  | 122 |
| Figure 91: Flame of combustion of mixture n°. 2.6 on a cigar burning test.....   | 123 |
| Figure 92: Frames used to study the velocity of the propagation of the flame on PMMA. The initial position is image on the left, final position the image on the right.....                                | 124 |
| Figure 93: Frames used to study the velocity of propagation of explosion in mixture n°. 2.6. ....  | 124 |
| Figure 94: Frames used to study the velocity of propagation of the mixture n°. 2.6. The frame at the left is correspondent to the initial position, and the frame at right, the final position. ....       | 125 |
| Figure 95: Mixture n°. 3.1 prepared for a cigar burning test (left) and its residues after combustion (right). ....  | 126 |
| Figure 96: Flame of combustion of mixture n°. 3.1 on a cigar burning test.....   | 127 |
| Figure 97: Frames used to study the velocity of the propagation of the flame on PMMA. The initial position is image on the left, final position the image on the right.....                                | 128 |
| Figure 98: Frames used to study the velocity of propagation of explosion in mixture n°. 3.1. ....  | 128 |
| Figure 99: Frames used to study the velocity of flame propagation in the mixture n°. 3.1. The frame at the left is correspondent to the initial position, and the frame at right, the final position. .... | 129 |

Figure 100: Disk of mixture nº. 3.1. Image on the left shows the fresh mixture on the disk. Image on the right shows the disk after the combustion..... 129

Figure 101: Frames which shows the moment before explosion one (at left) and the first appearance of explosion one (at right). The measurement of the area was made at right image, on area surrounded by blue. .... 131

Figure 102: Frames which shows the moment before explosion two (at left) and the first appearance of explosion one (at right). The measurement of the area was made at right image. .... 131

Figure 103: Mixture nº. 3.2 prepared for a cigar burning test (left) and its residues in the end of the combustion (right). .... 132

Figure 104: Flame of combustion of mixture nº.3.2 on a cigar burning test. .... 133

Figure 105: Frames used to study the velocity of the propagation of the flame on PMMA. The initial position is image on the left, final position the image on the right. .... 134

Figure 106: Frames used to study the velocity of propagation of explosion in mixture nº. 3.2. .... 134

Figure 107: Frames used to study the velocity of flame propagation in the mixture nº. 3.2. The frame at the left is correspondent to the initial position, and the frame at right, the final position. .... 135

Figure 108: Disk of mixture nº. 3.1. Image on the right shows the fresh mixture on the disk. Image on the centre shows the disk after combustion. Image on the left shows the mixture after the combustion (disk without the PMMA lid). .... 135

Figure 109: Frames which shows the moment before explosion one (at left) and the first appearance of explosion one (at right). The measurement of the area was made at right image, on area surrounded by blue. .... 137

## LIST OF FIGURES

|  |     |
|--|-----|
| Figure 110: Frames which shows the moment before explosion two (at left) and the first appearance of explosion one (at right). The measurement of the area was made at right image surrounded by a blue circle. .... | 137 |
| Figure 111: Mixture n°. 3.2 prepared for a cigar burning test (left) and its residues in the end of the combustion (right). ....   | 138 |
| Figure 112: Flame of combustion of mixture n°. 3.3 on a cigar burning test.....  | 139 |
| Figure 113: Frames used to study the velocity of the propagation of the flame on PMMA. The initial position is image on the left, final position the image on the right. ....  | 140 |
| Figure 114: Frames used to study the velocity of propagation of explosion in mixture n°. 3.3. ....   | 140 |
| Figure 115: Frames used to study the velocity of flame propagation in the mixture n°. 3.3. The frame at the left is correspondent to the initial position, and the frame at right, the final position. ....          | 140 |
| Figure 116: Disk of mixture n°. 3.3. Images on the top shows the fresh mixture on the disk. Images on the bottom shows the disk after combustion. ....   | 141 |
| Figure 117: Frames which shows the moment before explosion one (at left) and the first appearance of explosion one (at right). ....  | 143 |
| Figure 118: Frames which shows the moment before explosion two (at left) and the first appearance of explosion two (at right). ....  | 143 |
| Figure 119: Mixture n°. 3.4 prepared for a cigar burning test (left) and its residues of combustion (right). ....  | 144 |
| Figure 120: Aspect of the flame during the combustion of the mixture n°. 3.4 on a cigar burning test .....   | 145 |

Figure 121: Frames used to study the velocity of the propagation of the flame on PMMA. The initial position is image on the left, final position the image on the right. .... 146

Figure 122: Frames used to study the velocity of propagation of explosion in mixture n°. 3.4. .... 146

Figure 123: Frames used to study the velocity of flame propagation in the mixture n°. 3.4. The frame at the left is correspondent to the initial position, and the frame at right, the final position. .... 146

Figure 124: Flame of combustion of mixture n°. 3.4 used for measurements of fundamental flame velocity. .... 147

Figure 125: Disk of mixture n°. 3.4. Image on the left shows the fresh mixture on the disk. Image on the right shows the disk after the combustion..... 147

Figure 126: Frames which shows the moment before appearance of  $A_1$  (at left) and the first appearance of  $A_1$ . .... 148

Figure 127: Frames which shows the moment before  $A_2$  (at left) and the first appearance of  $A_2$  (at right). .... 149

Figure 128: Mixture n°. 4.1 prepared for a cigar burning test (left) and its residues after combustion (right). .... 149

Figure 129: Aspect of the mixture n°. 4.1 during its combustion on a cigar burning test ..... 151

Figure 130: Frames used to study the velocity of the propagation of the flame on PMMA. The initial position is image on the left, final position the image on the right. .... 152

Figure 131: Frames used to study the velocity of flame propagation in the mixture n°. 4.1. The frame at the left is correspondent to the initial position, and the frame at right, the final position. .... 152

## LIST OF FIGURES

|   |     |
|---|-----|
| Figure 132: Flame of combustion of mixture nº. 4.1 on a cigar burning test.....   | 153 |
| Figure 133: Disk of mixture nº. 4.1. Image on the left shows the fresh mixture on the disk. Image on the right shows the disk after the combustion.....   | 153 |
| Figure 134: Mixture nº. 3.2 prepared for a cigar burning test (left) and its residues of combustion (right). .....  | 154 |
| Figure 135: Aspect of the mixture nº. 4.2 and its flames during its combustion on a cigar burning test .....  | 155 |
| Figure 136: Frames used to study the velocity of the propagation of the flame on PMMA. The initial position is image on the left, final position the image on the right. ....                               | 156 |
| Figure 137: Frames used to study the velocity of flame propagation in the mixture nº. 4.2. The frame at the left is correspondent to the initial position, and the frame at right, the final position. .... | 157 |
| Figure 138: Flame of combustion of mixture nº. 4.2 on a cigar burning test.....   | 157 |
| Figure 139: Disk of mixture nº. 4.2. Image on the left shows the fresh mixture on the disk. Image on the right shows the disk after the combustion.....   | 158 |
| Figure 140: Combustion of disk with mixture nº. 4.2 where it is possible to see the PMMA's flame and hotspots of the mixture. ....  | 158 |
| Figure 141: IR spectrum of pure Ammonium Nitrate .....  | 160 |
| Figure 142: Overlap of AN (red) and AN with DMF (blue) spectra.....   | 161 |
| Figure 143: IR spectrum of pure Urea Nitrate.....   | 162 |
| Figure 144: IR spectrum of commercial PolyUrethane.....   | 163 |
| Figure 145: IR spectrum of aluminium lined with a greasy coat .....   | 164 |
| Figure 146: IR spectrum of Magnesium and Teflon (MT) mixture .....  | 165 |

Figure 147: (a) Overlap of IR spectra of AN with DMF (red) and PU (blue) and (b) the acquired IR spectrum for AN with PU mixture..... 166

Figure 148: (a) overlap of IR spectra of AN / PU (orange) mixture and MT mixture (blue); (b) IR spectrum for mixture 3.1 (84%AN/ 7%PU/ 9%MT) ..... 166

Figure 149: IR spectra of: (a) burnt mixture n°3.1 in experimental isobaric conditions; (b) overlap of spectra of burnt material (orange) and fresh mixture n°3.1 (blue). The transmittance of burnt mixture, in (b) was increased 5 times, in order to be possible the visualization of its characteristic bands. .... 168

Figure 150: IR spectra of: (a) burnt mixture n°3.1 in experimental adiabatic conditions; (b) overlap of spectra of burnt (orange) and fresh (blue) materials of mixture n°3.1... 170

Figure 151: (a) IR spectra of fresh mixture 3.2 (b) Overlap of IR spectrum of: fresh mixture 3.2 (same as (a) – blue) and of mixture AN/PU (same as figure 44 (b) – dashed orange)..... 173

Figure 152: (a) IR spectrum of combustion products of mixture 3.2., burnt at isobaric conditions; (b) overlap of IR spectra of fresh (blue) and burnt material (red) from mixture 3.2..... 173

Figure 153: (a) IR spectrum of the collected residues after “disk” test had been employed to mixture 3.2; (b) IR spectrum of fresh mixture 3.2 (also shown in Figure 151 (a)) ..... 175

Figure 154: (a) Overlap of IR spectra of pure UN (blue) and PU (orange) and (b) the acquired IR spectrum for pure UN with PU mixture..... 176

Figure 155: (a) overlap of IR spectra of UN / PU mixture (blue) and MT mixture (orange); (b) IR spectrum for mixture 4.1 (84%UN/ 7%PU/ 9%MT) ..... 177

Figure 156: IR spectra of: (a) burnt mixture n°4.1 in experimental isobaric conditions; (b) overlap of spectra of burnt (red) and fresh material (blue) from mixture n°4.1 (the last one is also present at Figure 155 (b))..... 178

## LIST OF FIGURES

|  |     |
|--|-----|
| Figure 157: (a) IR spectrum of combustion products of mixture 4.1, burnt at adiabatic conditions; (b) overlap of IR spectra of fresh (blue) and burnt material (red) from mixture 4.1.....   | 179 |
| Figure 158: (a) IR spectra of fresh mixture 4.2; (b) Overlap of IR spectrum of: fresh mixture 4.2 (same as (a) – blue) and of mixture UN/PU (same as Figure 154 (b) – dashed orange).....  | 180 |
| Figure 159: IR spectra of: (a) burnt mixture n°4.2 in experimental isobaric conditions; (b) overlap of spectra of burnt (dashed orange) and fresh material (blue) from mixture n°4.2 (same as presented at Figure 154 (b)) .....   | 181 |
| Figure 160: (a) IR spectrum of combustion products of mixture 4.2, burnt at adiabatic conditions; (b) overlap of IR spectra of fresh (blue) and burnt material (orange) from mixture 4.2.....  | 182 |
| Figure 161: Overlap of IR spectra of burnt material, from mixture 4.2. The blue spectrum shows IR spectrum of burnt mixture on the “cigar” burning test (Figure 159 (a)), and the orange one shows the burnt material IR spectrum of “disk” burning test (Figure 160 (a))..... | 183 |
| Figure 162: Thor predicted decomposition species of AN in function of temperature.   | 185 |
| Figure 163: Thor predicted decomposition species of UN in function of temperature.   | 186 |
| Figure 164: Densities of all studied mixtures, for each test. ....   | 190 |
| Figure 165: densities of the mixtures separated by tests. At left are presented the densities of the mixtures on cigars. At right, the densities of the same mixtures, but in disks. Mixtures 1.2 and 1.4 just were performed in disks burning tests.....                      | 190 |
| Figure 166: Temperature profiles of the studied mixtures. Left image is correspondent to samples which has MT mixture as additive. Right image corresponds to mixtures with Al as additive. ....   | 192 |
| Figure 167: Velocities of the flame propagation on PMMA for each studied sample, on cigar burning tests.....   | 194 |

Figure 168: Velocities of the flame propagation on explosions ( $D_{\text{explosion}}$ ) in cigar burning tests. Mixtures 4.1 and 4.2 are not present because they not presented this kind of combustion. .... 195

Figure 169: velocities of the flame propagation on the studied mixtures ( $D_{\text{mixture}}$ ) in cigar burning tests..... 196

Figure 170: fundamental flame velocities ( $V_{\text{Flame}}$ ) for studied mixtures, in cigar burning tests..... 197

Figure 171: Time needed by each mixture to reach explosion by deflagration. On the legend, the number after the underscore means the number of the studied explosion. 199

Figure 172: Areas (A) of explosion by deflagration of each mixture in logarithmic scale. On the legend, the number after the underscore means the number of the studied explosion..... 199

## LIST OF FIGURES

## LIST OF TABLES

|  |    |
|--|----|
| Table 1: Examples of security measures. (Oosterhout, et al., 2007) .....   | 12 |
| Table 2: Chosen reagents selected from the market with commercial name, type and motive of selection. ✓ for “selected” and ✗ for “not selected” (Quaresma, et al., 2013(2)) .....  | 19 |
| Table 3: Synthesis of five most known terrorist attacks using AN as oxidizer. Attacks described by their known name (outrage), date and place of occurrence, quantities of used explosives, type of used bombs, circumstance and damage from the occurrence. | 21 |
| Table 4: Enthalpy of reaction of AN thermal decomposition as function of selected products (Durães, et al., 1997) (Durães, et al., 2000) (Campos, et al., 2006) .....  | 42 |
| Table 5: Internal energy of reaction of AN thermal decomposition as function of selected products (Durães, et al., 1997) (Durães, et al., 2000) (Campos, et al., 2006) ..  | 43 |
| Table 6: Crystallographic data and stability ranges of the AN phases (Oommen, et al., 1999).....   | 49 |
| Table 7: Heat of phase transitions of AN from Figure 25. (Oommen, et al., 1999).....   | 50 |
| Table 8: Endothermic peak temperatures (K) for each phase transition and decomposition of PSAN, where $\beta$ is the used heating rate.....  | 53 |
| Table 9: Experimental values for activation energy and pre-exponential factor for thermal decomposition kinetics of AN and PSAN.....   | 54 |
| Table 10 Arrhenius activation energy ( $E_a$ ) and Z (pre-exponential factor) calculated for Figure 30 and Figure 31, respectively .....   | 56 |
| Table 11: IR characteristic bands of explosives and some correlations (Yinon, et al., 1981).....   | 57 |

## LIST OF TABLES

|  |     |
|--|-----|
| Table 12: Mode assignment and respective wavenumber range, with examples of known explosive types or energetic materials (EM), for spectral features commonly observed in the IR spectra of explosives (McNesby, et al., 2002).....  | 58  |
| Table 13: DSC Peak temperatures and kinetic parameters obtained from figures 23 to 26. The kinetic parameters were calculated by Borchardt & Daniels method .....  | 71  |
| Table 14: DSC Peak temperatures and kinetic parameters obtained from Figures 42 to 45. ....  | 78  |
| Table 15: First serie of mixtures – composition in mass percentage.....  | 83  |
| Table 16: Second serie of mixtures – composition in mass percentage .....  | 84  |
| Table 17: Thermodynamic properties of Ammonium Nitrate (ICT, 2005) (Jolkkonen, 2012).....  | 84  |
| Table 18: Thermodynamic properties of Urea Nitrate (ICT, 2005) (Oxley, et al., 2013) .....   | 84  |
| Table 19: Thermodynamic properties of PolyUrethane (ICT, 2005) .....   | 84  |
| Table 20: Thermodynamic properties of Aluminium (ICT, 2005) (Jolkkonen, 2012)...   | 85  |
| Table 21: Thermodynamic properties of Magnesium (ICT, 2005) .....  | 85  |
| Table 22: Thermodynamic properties of Teflon (ICT, 2005) .....   | 85  |
| Table 23. Aluminium physical properties (experimentally measured) .....  | 95  |
| Table 24: Results obtained from the combustion of mixture n°. 1.4. ....  | 108 |
| Table 25: Results obtained from the combustion of mixture n°. 1.5 on cigar burning test. There was studied: density of the fresh mixture ( $\rho$ ), maximum temperatures acquired by thermocouples ( $Th_1$ is the upper one and $Th_2$ is the downer), velocities of flame propagation of PMMA, explosion, mixture and fundamental flame velocity..... | 111 |
| Table 26 Results obtained from the disk burning test of mixture n°. 1.5. ....  | 114 |

Table 27: Results obtained from the combustion of mixture n°. 1.8 on cigar burning test. There was studied: density of the fresh mixture ( $\rho$ ), maximum temperatures acquired by thermocouples ( $Th_1$  is the upper one and  $Th_2$  is the downer), velocities of flame propagation of PMMA, explosion, mixture and fundamental flame velocity..... 117

Table 28 Results obtained from the disk burning test of mixture n°. 1.8. .... 120

Table 29: Results obtained from the combustion of mixture n°. 2.6 on cigar burning test. There was studied: density of the fresh mixture ( $\rho$ ), maximum temperatures acquired by thermocouples ( $Th_1$  is the upper one and  $Th_2$  is the downer), velocities of flame propagation of PMMA, explosion, mixture and fundamental flame velocity..... 123

Table 30: Results obtained from the combustion of mixture n°. 3.1 on cigar burning test. There was studied: density of the fresh mixture ( $\rho$ ), maximum temperatures acquired by thermocouples ( $Th_1$  is the upper one and  $Th_2$  is the downer), velocities of flame propagation of PMMA, explosion, mixture and fundamental flame velocity..... 127

Table 31 Results obtained from the disk burning test of mixture n°. 3.1. .... 130

Table 32: Results obtained from the combustion of mixture n°. 3.2 on cigar burning test. There was studied: density of the fresh mixture ( $\rho$ ), maximum temperatures acquired by thermocouples ( $Th_1$  is the upper one and  $Th_2$  is the downer), velocities of flame propagation of PMMA, explosion, mixture and fundamental flame velocity..... 133

Table 33 Results obtained from the disk burning test of mixture n°. 3.2. .... 136

Table 34: Results obtained from the combustion of mixture n°. 3.3 on cigar burning test. There was studied: density of the fresh mixture ( $\rho$ ), maximum and average temperatures acquired by thermocouple, velocities of flame propagation of PMMA, explosion, mixture and fundamental flame velocity. .... 139

Table 35 Results obtained from the disk burning test of mixture n°. 3.3. .... 142

Table 36: Results obtained from the combustion of mixture n°. 3.4 on cigar burning test. There was studied: density of the fresh mixture ( $\rho$ ), maximum and average temperatures acquired by thermocouple, velocities of flame propagation of PMMA, explosion, mixture and fundamental flame velocity. .... 145

## LIST OF TABLES

|   |     |
|---|-----|
| Table 37 Results obtained from the disk burning test of mixture n°. 3.4. ....   | 148 |
| Table 38: Results obtained from the combustion of mixture n°. 4.1 on cigar burning test. There was studied: density of the fresh mixture ( $\rho$ ), maximum and minimum temperatures acquired by thermocouple, velocities of flame propagation of PMMA, explosion, mixture and fundamental flame velocity. ....  | 151 |
| Table 39: Results obtained from the combustion of mixture n°. 4.2 on cigar burning test. There was studied: density of the fresh mixture ( $\rho$ ), maximum temperature acquired by thermocouple, velocities of flame propagation of PMMA, explosion, mixture and fundamental flame velocity. ....               | 156 |
| Table 40: IV spectra band types, wavenumber ranges of appearance and characteristic vibrational modes for pure ammonium nitrate. The assignment of vibrational modes to the spectrum bands were made comparing with early reports. (Théorêt, et al., 1964) (Silverstein, et al., 1998) (Chattopadhyay, 1996)..... | 160 |
| Table 41: Most relevant band types, wavenumber ranges of appearance and characteristic vibrational modes of pure urea nitrate. The assignment of vibrational modes to the spectrum bands were made comparing with early reports. (Oxley, et al., 2013) (Désilets, et al., 2011).....                              | 162 |
| Table 42: Most relevant band types, wavenumber ranges of appearance and characteristic vibrational modes of the used commercial PU. The assignment of vibrational modes to the spectrum bands were made comparing with early reports. (Silverstein, et al., 1998) (Neves, 2010).....                              | 163 |
| Table 43: Most relevant band types, wave number ranges of appearance and characteristic vibrational modes of Teflon. The assignment of vibrational modes to the spectrum bands were made comparing with early reports. (Silverstein, et al., 1998) (Hopp, et al., 2007).....                                      | 165 |
| Table 44: Analysis of the presence of reactants in fresh mixture 3.1 by compound, typical peak band wavenumber from Tables 40, 42 and 43, new wavenumber of the typical peak in Figure 148 (b) and respective presence.....   | 167 |

Table 45: Analysis of the presence of reactants in burnt mixture 3.1 (cigar test burning) by compound, typical peak band wavenumber from Tables 40, 42 and 43, new wavenumber of the typical peak at Figure 149 (a). ..... 168

Table 46 Analysis of the presence of reactants in burnt mixture 3.1 (disk test burning) by compound, typical peak band wavenumber from Tables 40, 42 and 43, new wavenumber of the typical peak in Figure 150 (a). ..... 170

Table 47: Analysis of the presence of reactants in burnt mixture 3.2 (cigar test burning) by compound, typical peak band wavenumber from Tables 40 and 42, new wavenumber of the typical peak in Figure 152 (a). ..... 174

Table 48: Analysis of the presence of reactants in fresh mixture 4.1 by compound, typical peak band wavenumber from Tables 41 to 43 and Figure 154 (b), new wavenumber of the typical peak in Figure 155 (b) and respective presence. .... 177

Table 49: Analysis of the presence of reactants in burnt mixture 4.2 (cigar burning test) by compound, typical peak band wavenumber from Table 41 to Table 43, new wavenumber of the typical peak in Figure 159 (a). ..... 181

Table 50: Analysis of the presence of reactants in burnt mixture 4.2 (disk burning test) by compound, typical peak band wavenumber from Tables 41 to 43, new wavenumber of the typical peak at Figure 160 (a). ..... 182

Table 51: Analysis of the presence of reactants and common combustion products in burnt mixture 4.2 in experimental isobaric (cigar) and adiabatic (disk) conditions by compounds, typical peak band wave number from tables 42 to 44, new wave number of the typical peak in Figure 159 (a) and Figure 160 (a). ..... 183

Table 52: Chosen bands and respective bands intensities, ranges and peaks wavenumbers for characterization of the reactants in the mixtures, before and after their combustion. .... 201

Table 53: Analysis of the presence of reactants in fresh mixtures 3.1 and 3.2 (AN as oxidant) by compound and typical peak band wavenumbers (see tables above). ✓ used to “yes”, ✗ used to “no”. ..... 202

## LIST OF TABLES

|  |     |
|--|-----|
| Table 54: Analysis of the presence of reactants in fresh mixtures 4.1 and 4.2(UN as oxidant) by compound and typical peak band wavenumbers (see tables above). ✓ used to “yes”, ✗ used to “no”. .....                            | 202 |
| Table 55: Chosen bands and respective peaks wavenumbers for characterization of the mixtures after combustion. ....  | 203 |
| Table 56: Analysis of the presence of reactants and combustion products in burned mixtures 3.1 and 3.2 (AN as oxidant) by compound and typical peak band wave numbers (see tables above). ✓ used to “yes”, ✗ used to “no”. ..... | 203 |
| Table 57: Analysis of the presence of reactants and combustion products in burned mixtures 4.1 and 4.2 (UN as oxidant) by compound and typical peak band wavenumbers (see tables above). ✓ used to “yes”, ✗ used to “no”. .....  | 204 |

## ABBREVIATIONS

$A$  - Arrhenius equation pre-exponential factor resultant of the combination of reaction parameters or area

$A_F$  - Flame area

Al - aluminium

AN – Ammonium Nitrate

ANFO – Ammonium Nitrate / Fuel Oil

AP – Ammonium Perchlorate

$a_0$  - sound velocity

$B_i$  - covolume of component  $i$

[ $b$ ] - concentration of burned species

C4 – Plastic Bound Explosive based in Hexogene and plastic binder

$C_p$  – specific heat capacity at constant pressure

$C_v$  – specific heat capacity at constant volume

$D$  - Detonation velocity

$D$  - Propagation velocity

DSC - Differential Scanning Calorimetry

DSC/TGA - Differential Scanning Calorimetry coupled with ThermoGravimetric Analysis

DTA - Differential Thermal Analysis

$E$  - internal energy or absorbed energy

$E_a$  - Activation energy

$e_i$  - internal energy of  $i$  component

fps – frames per second

FP25 - (Forças Populares do 25 de Abril) Popular Forces of April 25

FUP – (Força de Unidade Popular) Popular Unity Force

FTIR – Fourier Transform Infra-Red

$G$  - Gibbs free energy

$G_{0i}$  - minimum value of global Gibbs free energy for  $i$  component

GTD – Global Terrorism Database

$h$  - Planck's constant

$H$  – enthalpy

## ABBREVIATIONS

HME – Home Made Explosive

IED - Improvised Explosive Device

IR – Infra-Red

IT – Information Technology

JIEDDO - Joint Improvised Explosive Devices - Defeat Organization

$k$  - Boltzmann constant

$K_p$  - Equilibrium constant

$\dot{m}$  - Mass burning rate

$m_b$  - Burned species mass

$m_f$  - fresh species mass

$M$  – Molar mass

$M_j$  -Arbitrary property common to all species involved in the chemical reaction

MT – Magnesium/Teflon

MTV - Magnesium/Teflon/Viton

$M_0$  - Total mass present in reaction

$n$  – Mole number or the reaction order.

$n'_j, n''_j$  - Reactants and products stoichiometric coefficients of the reaction, respectively

$N_{AV}$  - Avogadro number

$P$  – Pressure

PMMA - PolyMethylMethAcrylate

PVC - PolyVinylChloride

PU – Polyurethane

$Q$  – Heat

$R$  – Perfect gases constant

$R$  – Richness

$S$  – Entropy

$t$  – Time

$T$  – Temperature

TATP - TriAcetone TriPeroxide

TGA - ThermoGravimetric Analysis

Th – thermocouple

THOR – Thermochemical Code (from initials of “Thermodynamics of Heuze Olivier Reformulated”)

UN – Urea Nitrate

$\dot{V}$  - Fresh gases formation rate

$\mathbb{W}$  - Fundamental flame velocity

Z - Arrhenius equation pre-exponential factor for thermal decomposition

u - Velocity of mass consumption

$u_p$  - particular velocity

V – Volume

$v_F$  - Flame fundamental velocity

$x_i$  – molar fraction of i component

$X_i$  - mole number of i compound

$\alpha$  - exponent part of the intermolecular potential or percent conversion (reaction progress or mass loss rate)

$\gamma = C_p/C_v$

$\lambda$  - Mass loss in the reaction or reaction advancement degree

$\mu_i$  - Gibbs free energy of i component

$$\Gamma = \left. \frac{\partial H}{\partial S} \right|_s$$

$\nu$  -Total number of involved species or molecule vibrational frequency

$\omega$  – Potential parameter for component i

$\Omega$  – Potential parameter

$\rho$  - Density

$\rho_f$  -Fresh species density

$\sigma$  - Fifth order polynomial obtained from virial expansion

$\theta$  - Adimensional temperature







## CHAPTER 1 – INTRODUCTION

### 1.1. Forensic Sciences Framework

#### 1.1.1. Terrorism definitions – HME and IED

United Nations defined terrorism (vd. United Nations, 1994) as: “all criminal and unjustifiable methods and practices which can jeopardize friendly relations among States, territorial and human integrity and the security of the States, wherever and whoever committed; all acts, methods and practices which can put in risk international peace and security, the good relationships between countries, which can encumber international cooperation, and which as the aim of the destruction of human rights, fundamental freedoms and the democratic base of society; all criminal acts intended or calculated to incite a state of terror in the general public, organized or individual persons for political purposes are always unjustifiable and acts justifiable by political, philosophical, ideological, racial, ethnic, religious or any nature beliefs”. (Quaresma, et al., 2013(2)).

A quite different definition is given by American law, on Title 18 USC Section 2331, (5), specifying domestic terrorism as: “activities that involve acts dangerous to human life that are a violation of the criminal laws of the United States or of any State; appear to be intended to intimidate or coerce a civilian population; to influence the policy of a government by intimidation or coercion; or to affect the conduct of a government by mass destruction, assassination, or kidnapping; and occur primarily within the territorial jurisdiction of the United States”. (US Code, 1992)

The Science and Technology (S&T) Directorate of the U.S. Department of Homeland Security (Doherty, 2009) determined that “the term HME (Home Made Explosive) has been used to cover a wide range of materials from pure explosive compounds, such as triacetone triperoxide (TATP), that can be synthesized from readily available articles of commerce to home-made variants of explosives, such as ammonium nitrate (ANFO), that are used in very large commercial blasting operations. The former is a very sensitive material and so ordinarily is not made in large quantities. The latter is relatively insensitive and can be made in very large quantities.”

According to the Army United States Marine Corps, 2005, an Improvised Explosive Device (IED) “is a device placed or fabricated in an improvised manner incorporating

destructive, lethal, noxious, pyrotechnic, or incendiary chemicals and designed to destroy, incapacitate, harass, or distract. It may incorporate military stores, but is normally devised from non-military components”.

IED can vary widely in shape and form – ranging from small pipe bombs to multiple artillery shells linked together to create a device with greater explosive weight. They can be used in various forms: planted alongside a road, magnetically attached to a target, placed in a vehicle, or be loaded in a car or truck and driven into markets or buildings. Generically, IED’s can be divided by method of detonation or by method of delivery. The first one is divided into three basic methods to initiate detonation, they are by command, time and victim. The method of delivery can be divided into vehicle-borne IED and suicide bombers. (Caldwell, 2011)

### 1.1.2. IED – worldwide panorama

The IED is the weapon of choice for adversaries operating along the threat continuum, represented on Figure 1.



Figure 1: Threat continuum. (Joint Improvised Explosive Device Defeat Organization, 2012-1026)

Bombs threats, as international domestic explosive events, occurred on 82000 terrorist incidents between 1970 and 2007 (START, 2009). The top three terrorist targets are private citizen’s property (20%), government (17%), and business (16%). Bombing was 51% of the employed terrorists’ tactic. Between Augusts of 2008 and 2009 occurred an average of 600 IED attacks per month worldwide (excluding Iraq and Afghanistan). (Science & Technology to Counter Improvised Explosive Devices, 2010)

When a domestic terrorist IED attack occurs, it normally follows a cycle (Figure 2).

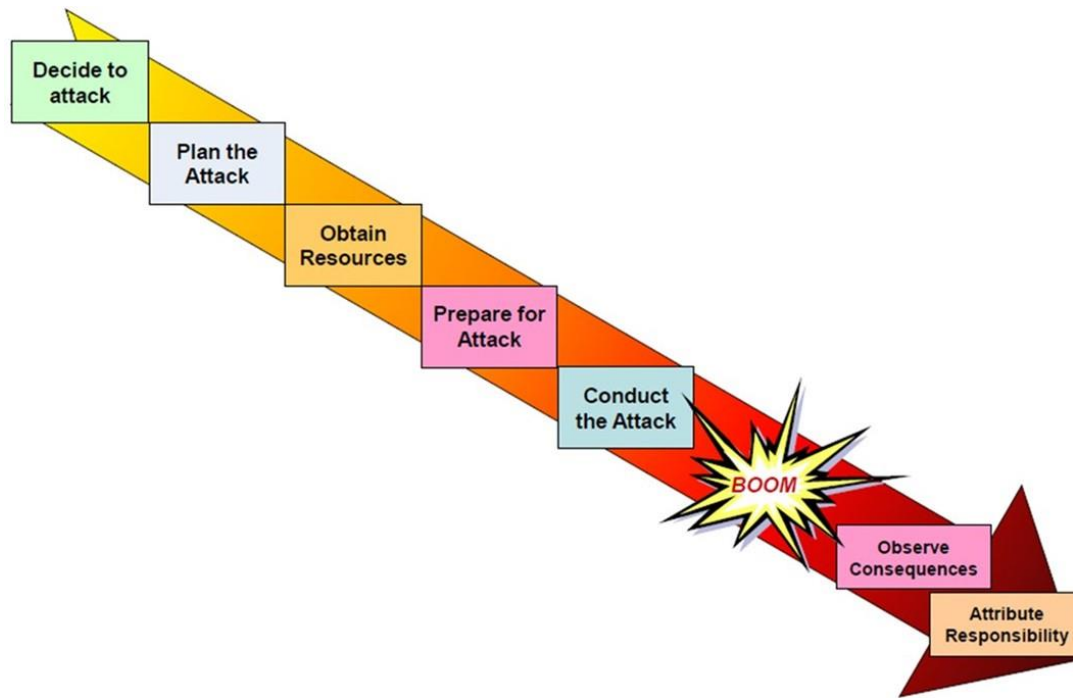


Figure 2: Domestic Terrorist IED attack cycle. (Science & Technology to Counter Improvised Explosive Devices, 2010)

To have a good overview about worldwide terrorism, a search on Global Terrorism Database (GTD) was made. (START, 2012)

An example is presented in Figure 3 related to 4930 incidents from January of 2010 to December of 2011. The incidents varied between 150 and 250 per month, being the worst months September and November.

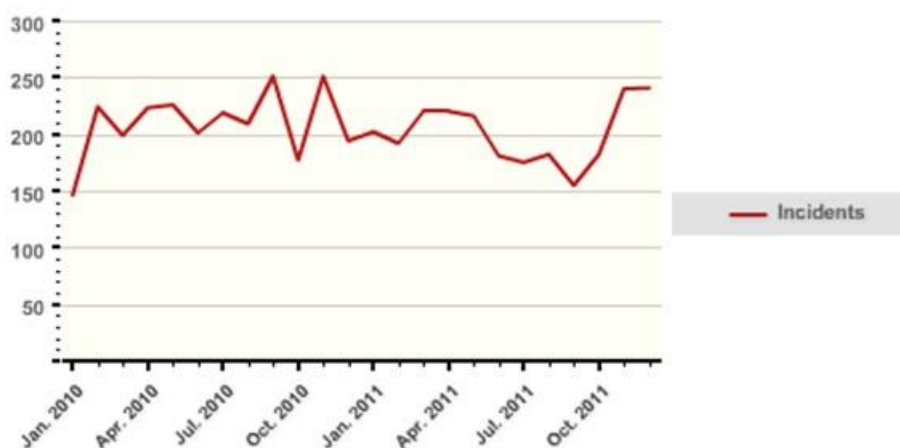


Figure 3: Terrorist incidents occurred in from the beginning of 2010 to the end of 2011 using bombing and explosion (dynamite is included as weapon). (START, 2012)

During the referred years the top three target not varied so much, just the third position changed from business to police (Figure 4).

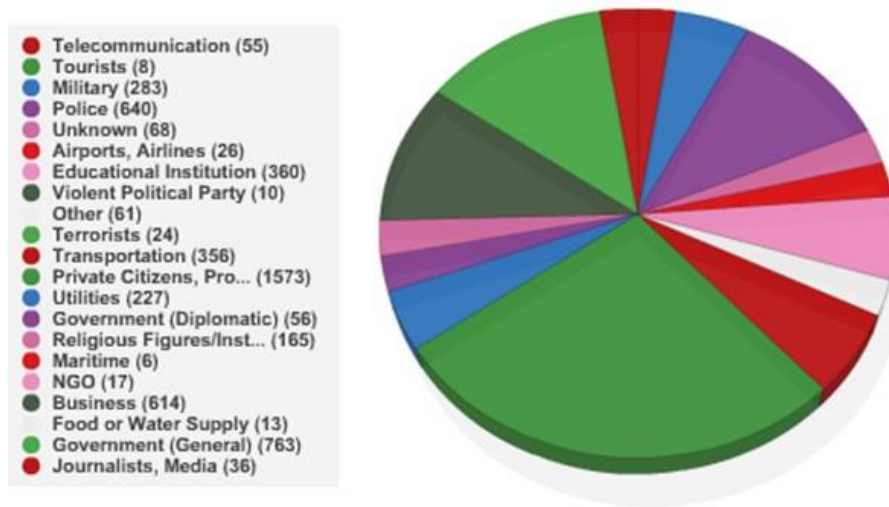


Figure 4: Target types of terrorist incidents during 2010 and 2011 which used explosive and incendiary devices. (START, 2012)

Explosives, bombs and dynamite were used two hundred times more than incendiary devices, during worldwide terrorist incidents on years of 2010 and 2011 (Figure 5 at left). On the 9889 incidents (considering all possible weapon types by GTD), explosives, bombs and dynamite were the most used weapon on terrorist incidents and incendiary devices occupied the third position of the known used weapons (Figure 5 at right).



Figure 5: Statistic of the use of explosives, bombs dynamite and incendiary devices as weapon on the 4930 terrorist incidents which used that kind of weapon (at left), and common weapons used on 9889 reported terrorist incidents during the years 2010 and 2011. (START, 2012)

## HOMEMADE EXPLOSIVES BASED ON AMMONIUM AND UREA NITRATES

On 4930 terrorist incidents, more than a half not had fatalities or injuries as casualties. Occurred more injuries than fatalities, but still this, the values are large. Figure 6 illustrate the statistic of the casualties occurred on terrorist incidents.

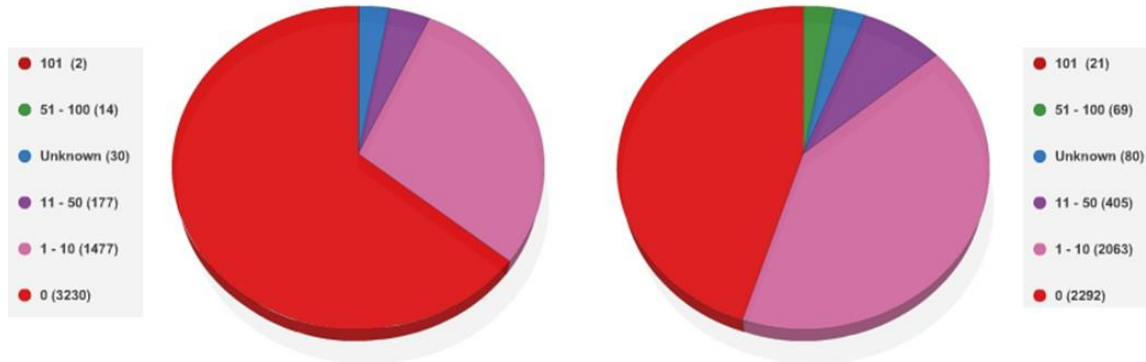


Figure 6: Casualties –fatalities on the left and injuries on the right - resultant of 4930 terrorist incidents, occurred worldwide between 2010 and 2011. (START, 2012)

Terrorism is a worldwide problem. The zones which suffer more with terrorist attacks using explosives, bombs, dynamite and incendiary devices, including recourse to suicide, are Middle East, North Africa and South Asia. East Asia is the most pacific zone (Figure 7).

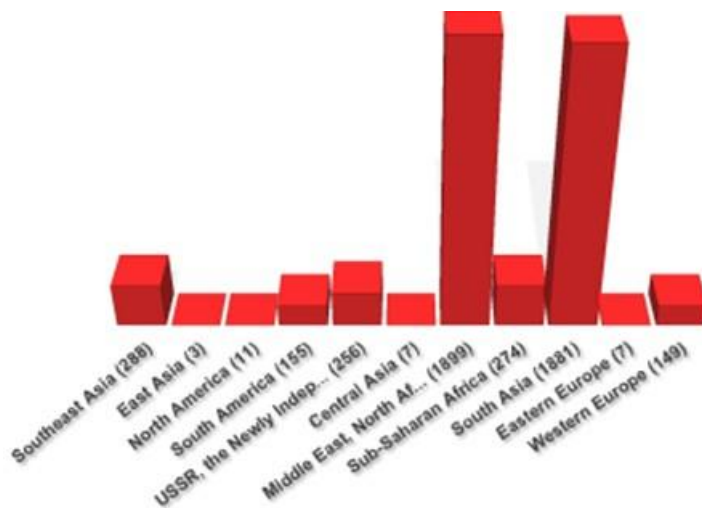


Figure 7: Regions affected by terrorist attacks with resource to explosives and bombs. (START, 2012)

The Joint IED-Defeat Organization (JIEDDO), a US military command, detailed from their 2010 annual report, that IEDs still are the weapon of choice for global insurgents, with approximately 260 IED incidents per month, excluding Afghanistan and Iraq. (Caldwell, 2011) (vd. Figure 8)

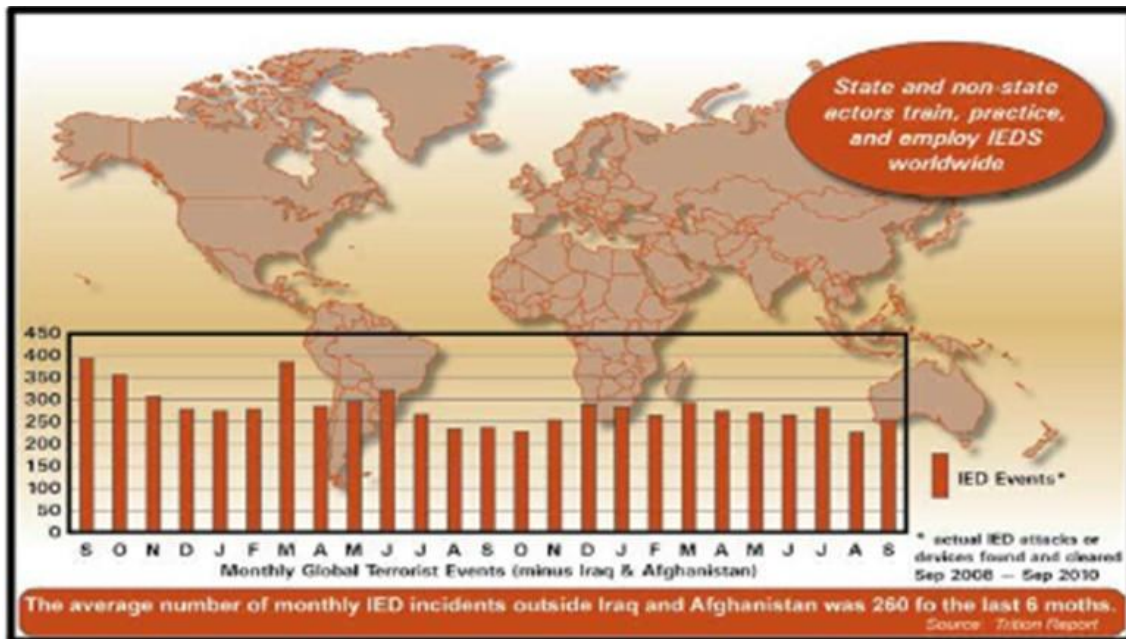


Figure 8: Representation of monthly global terrorist events that employed IED's, excluding Iraq and Afghanistan cases, for 2010. (Caldwell, 2011)

More recently, from January to November 2011, JIEDDO reported (outside of Iraq and Afghanistan) 6832 IED events averaging 621 per month, 12286 casualties at 111 countries conducted by individuals, supported by 40 regional and transnational threat networks. Many of these acts, methods and practices are always worldwide employed, concerning Israel/Palestine, Egypt, Syria, Libya, Russia /Chechnya conflicts, Iraq and Afghanistan, between many others. (Deen, 2005)

### 1.1.3. Terrorist incidents in Portugal

Portugal is a quiet country on west coast of Europe, but it already suffered with terrorism. According to GTD (START, 2012), since 1973 until 2011 happened 139 terrorist incidents in Portugal. As it is possible to see on Figure 9, the worst years were from 1976 to 1985.

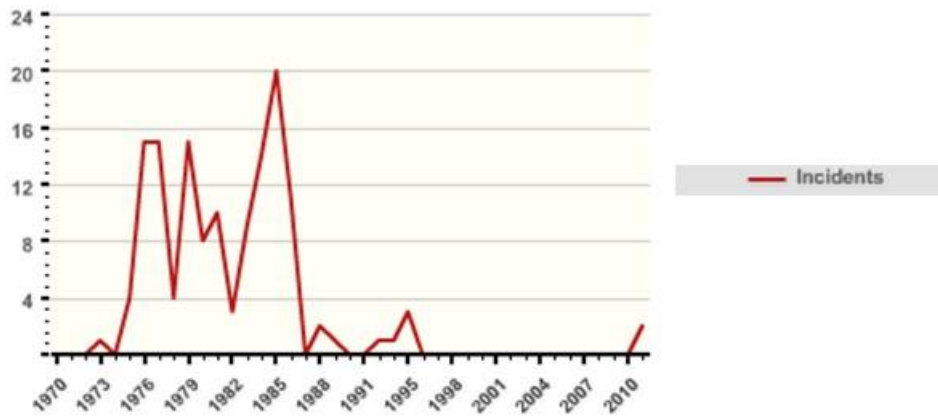


Figure 9: Terrorist incidents that occurred in Portugal since 1970 to 2011 (START, 2012)

The top three attack type of the reported attacks were armed assault, assassination and bombing/explosion (Figure 10, left), being the last one the most used along the years (Figure 10, right).

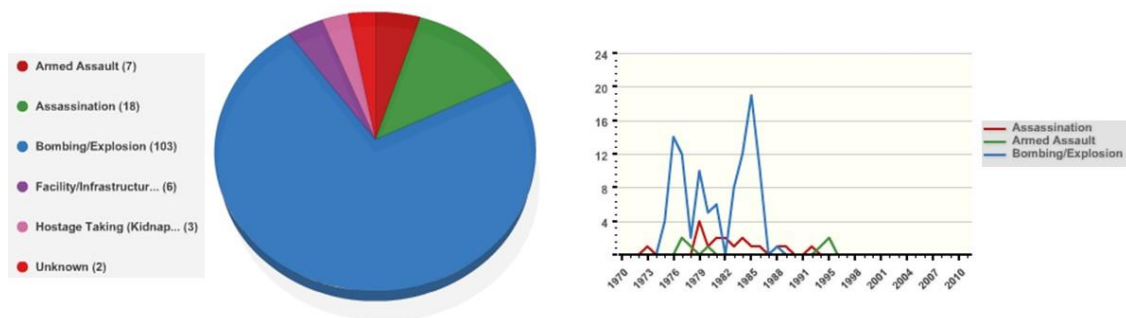


Figure 10: Attacks types used on terrorist incidents (left) and number of occurrences of the top three along the years (right) registered in Portugal since 1970 to 2011. (START, 2012)

The preferred targets on terrorist attacks were business, government (general and diplomatic) and private citizens and property (Figure 11, left). As referred above, the worst decades of terrorism in Portugal were 70's and 80's, due to the April 25<sup>th</sup> Revolution, 1974, when Portugal suffered the transition from a dictatorial regime to a democratic one. This fact is observable in statistics, because government (general plus diplomatic) was the most affected target (Figure 11, right).

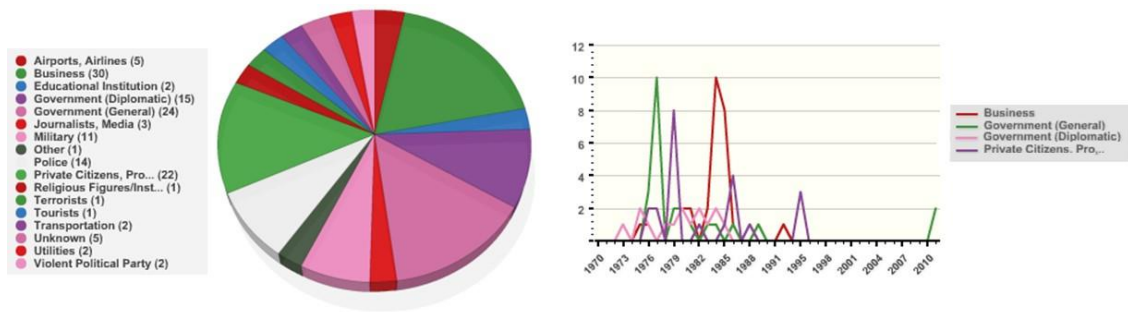


Figure 11: Most common target types (left) and number of occurrences of each top three target (right) of the terrorist attacks performed in Portugal from 1970 to 2011. (START, 2012)

The most known terrorist group in Portugal whose was responsible for 47 terrorist incidents, was Popular Forces of April 25 (START, 2012), known in Portugal by FP25 (acronym for Forças Populares). This was the armed organization that supported FUP (Força de Unidade Popular – Popular Unity Force), an extreme left political organization which was unhappy with the ideological and practical measures taken after the Revolution. (Infopédia, 2003 - 2013).

According to Govern Lopes (FP-25/30 anos, 2010), one of the founders of this extreme left armed organization, the objective of FP25 was the military formation of the Portuguese workers, on a defensive perspective, never with the objective of reaching the armed fight. In 1980, the FP25 appears on the restructuration process of the revolutionary left wing, which started in 1976 by extreme left political organizations (Brigadas Revolucionárias – Revolutionary Brigades - and Partido Revolucionário do Proletariado - Revolutionary Party of the Proletariat). FP25 felt there were an offensive against a set of achievements that workers had succeeded after the Revolution like the end of worker’s control, the companies’ self-management and the end of the agrarian reform. 1987 was the last year of terrorist attacks performed by this armed organization. (FP-25/30 anos, 2010).

As it is possible to observe in Figure 12, the most used tool and form to attack were explosives and bombing, respectively. (START, 2012) FP25 was responsible for 17 murders, 66 bombing outrages and 99 bank robberies. (FP-25/30 anos, 2010)

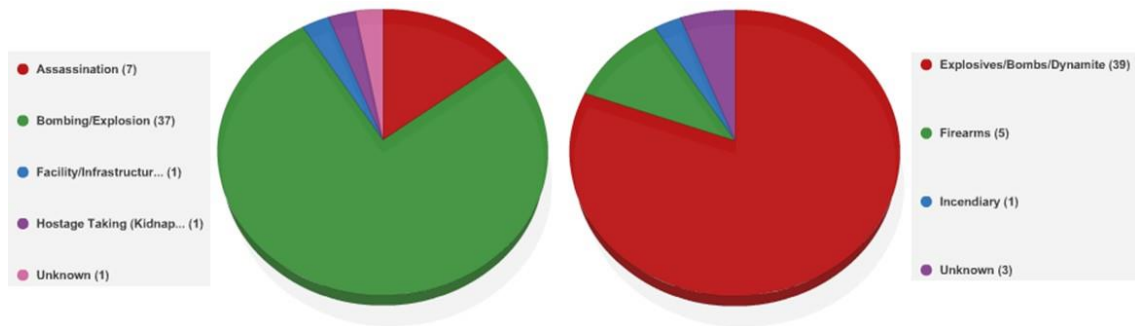


Figure 12: Attack (left) and weapon (right) types used by FP25 between 1980 and 1987. (START, 2012)

Nowadays, terrorism in Portugal is not usual, but still exists individual cases, as occurred in 2011 where groups of anarchist threw cocktails Molotov to State buildings. These kind of occurrences has tendency to grow, due to financial and economic recession that has been feeling in Europe since 2008. Good examples of this are the conflicts that have been occurring in Greece and Spain.

#### 1.1.4. HME and supply chain security improvements

In our occidental quotidian life products, energy, medicine and food are provided by a complex global supply chain. These global systems depend on an interconnected web of transportation infrastructure and pathways, information technology, cyber and energy networks. (The White House, 2012) All these dependencies can be profitable for economic activities, but with the development, the world-wide supply chains had become more and more complex. Due to that complexity, the supply chains become more vulnerable to terrorist or criminal attacks. Consequently, companies started to implement regulations and measures in order to improve their supply chain security. (Quaresma, et al., 2013(2))

A secure supply chain is a supply chain where various measures have been taken to guarantee a certain level of security. Security measures can be taken with regards to (a combination of) physical flows, information flows and/or money flows. (Oosterhout, et al., 2007) In order to achieve secure supply chains, technology, clear procedures and rules and cooperation between government and companies have to be combined effectively. The human factor has always to be considered, because it determines the ultimate success or failure of each system. (Quaresma, et al., 2013(2))

Supply chain security is a wide concept (vd. Figure 13) (Quaresma, et al., 2013(2)), composed by physical and non-physical security and by a preventive versus more corrective measures (examples in the figure). The supply chain security has to be organized in a way that if a security emergency occurs, the supply chain will quickly recover into a normal state of operations.

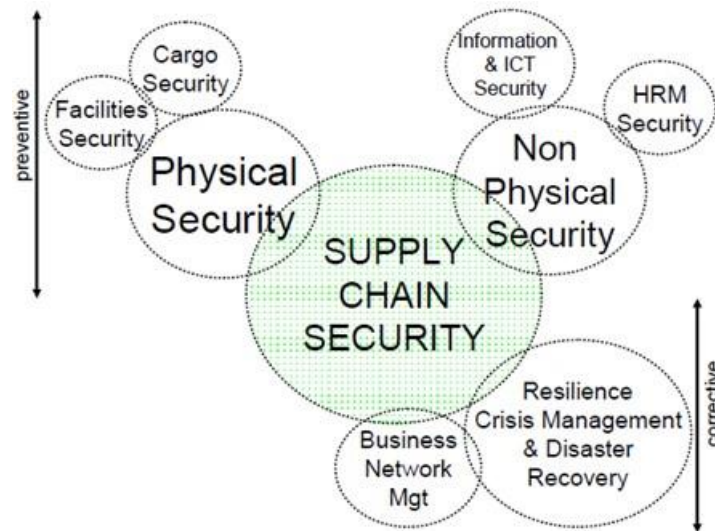


Figure 13: Components of Supply Chain Security (Oosterhout, et al., 2007)

Three different layers are used (Oosterhout, et al., 2007) to analyze supply chains:

- physical activities, such as transport and transshipment, are the first layer;
- the second layer is in respect to contracting or transaction activities that cover all commercial relationships between parties in the chain;
- the third layer is the governance layer, where are included all governing bodies with their inspection and verification activities. (Quaresma, et al., 2013(2)).

An overview of a typical port supply chain with an export flow, ocean transport and an import flow, as well as some possible areas of security risks is shown in Figure 14. (Oosterhout, et al., 2007)

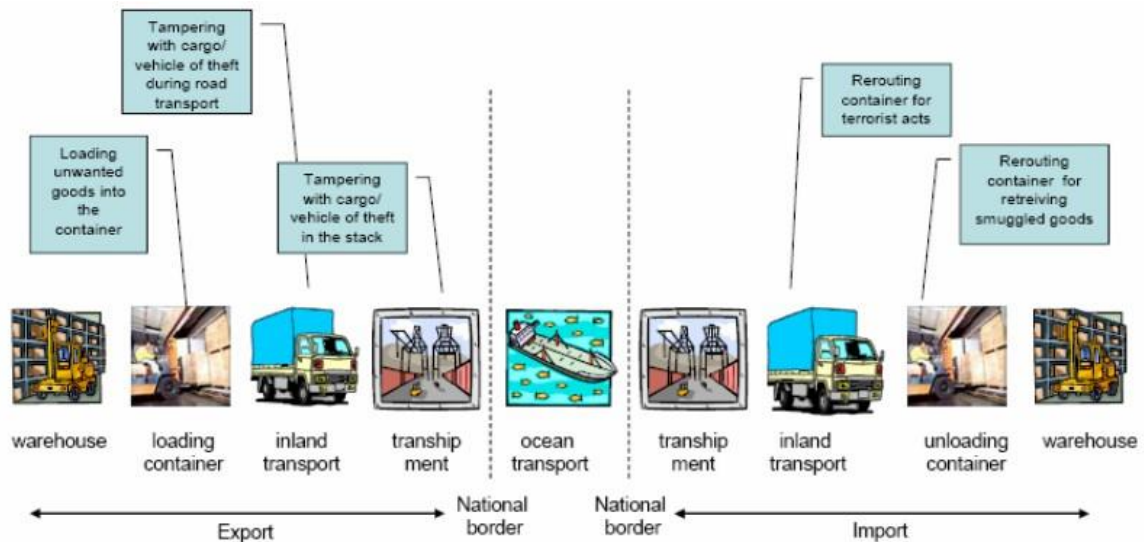


Figure 14: Supply Chain Processes and security risks. (Oosterhout, et al., 2007)

**Security risks in the physical layer.** The transport supply chain can be seen as a terrorist target. (Quaresma, et al., 2013(2)) In the physical layer, risk points are the points of stuffing and stripping of a container, plus stop points (used for workers rest, in case of truck motorists, for example) where the cargo is not touched. At these points, the load can more easily be altered/ stolen by terrorists or criminals. A cargo is safer in movement than in rest. Empty containers are easy targets, because they have little attention than the loaded ones. (Oosterhout, et al., 2007)

**Security risks in the transaction and governance layer.** The security risks in the transactional and governance layers are related (more or less) to the security of the information accompanying the logistical process, like criteria confidentiality, integrity, availability and non-repudiation. (Quaresma, et al., 2013(2))

These criteria were defined as confidentiality of data that ensures information only accessible to authorized people. (Oosterhout, et al., 2007) Once again, the information transparency has advantages and disadvantages. The biggest advantage is the safety on planning routes, where preventive measures can be taken in case of disturbs. The major disadvantage of information transparency is the detailing which a terrorist has access, in case of an attack or theft. (Oosterhout, et al., 2007)

**Security measures and requirements.** Security measures can be categorized by two ways: layers (examples in Table 1) and timing.

Table 1: Examples of security measures. (Oosterhout, et al., 2007)

| Layer       | Type of Measure         | Examples   |
|-------------|-------------------------|--|
| Governance  | Legal/policy measures   | Laws, Incentives                                       |
| Transaction | Organizational measures | Protocols & procedures, structuring, HRM-policy        |
|             | IT measures             | authentication, VPN, encryption, chip card, biometrics |
| Physical    | Physical measures       | physical gates, camera's, smart cards                  |

Oosterhout et al., 2007, distinguished between three types of possible measures: preventive measures, such as surveillance cameras, high fences and gates around the place where load and/ or load transport are stored; detective measures, like scanning containers or trucks where the cargo will be transported; and corrective measures, which are the security measures taken when an incident results in damage, to correct it and recover from it.

To create a secure freight system, Lee and Wolf describe three generic requirements or measures from a security perspective (Oosterhout, et al., 2007):

1. *Assuring integrity of conveyance loading, documentation and sealing*
2. *Reduce risk of tampering in transit (with comprehensive monitoring of tampering and intrusion)*
3. *Provide accurate, complete and protected information about shipments to those who need it in a timely manner*

By the same authors, four critical requirements from security processes are applied to supply chain managers (Oosterhout, et al., 2007):

- i. *Commit to processing and inspecting qualifying shipments in ways that permit highly reliable and predictable processing times*
- ii. *Protect all commercial information given to authorities*
- iii. *Harmonize and standardize security processes internationally*
- iv. *Security and anti-tampering practices should be by-products of excellent supply chain management practices.*

A supply chain security sense and respond model (Figure 15) was developed by Dove (2001) and by Christopher and Lee (2004). This model is divided in two phases, sense and respond. The sensing phase has preventive and detective measures, while

responding phase has detective and corrective measures. A learning phase should be added to make security measures effective in the long term. (vd. Quaresma et al., 2013(2))

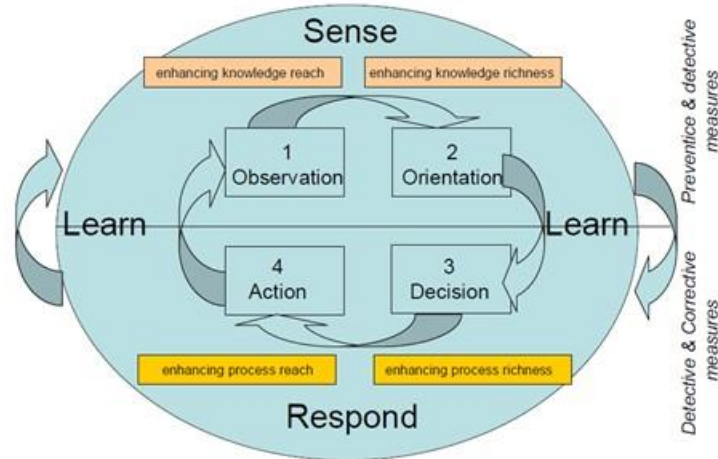


Figure 15: Supply chain security sense and respond model. (Oosterhout, et al., 2007)

**Implementing security measures: information needs.** Nine information blocks were created to improve the supply chain security. Beside these, specific data can be required for preventive, detective or corrective measures. The nine information blocks are (Quaresma, et al., 2013(2)):

1. Booking information
2. Cargo information
3. Nuclear detection
4. X-ray scan
5. Status (of container, for example)
6. Operator and location information
7. Seal
8. Certificate information
9. Personnel
- 10.

The diagram in Figure 16 shows the interconnection between information blocks in Rotterdam Port. The rectangles are the information blocks, the diamond shapes are the relationships between them. (Oosterhout, et al., 2007)

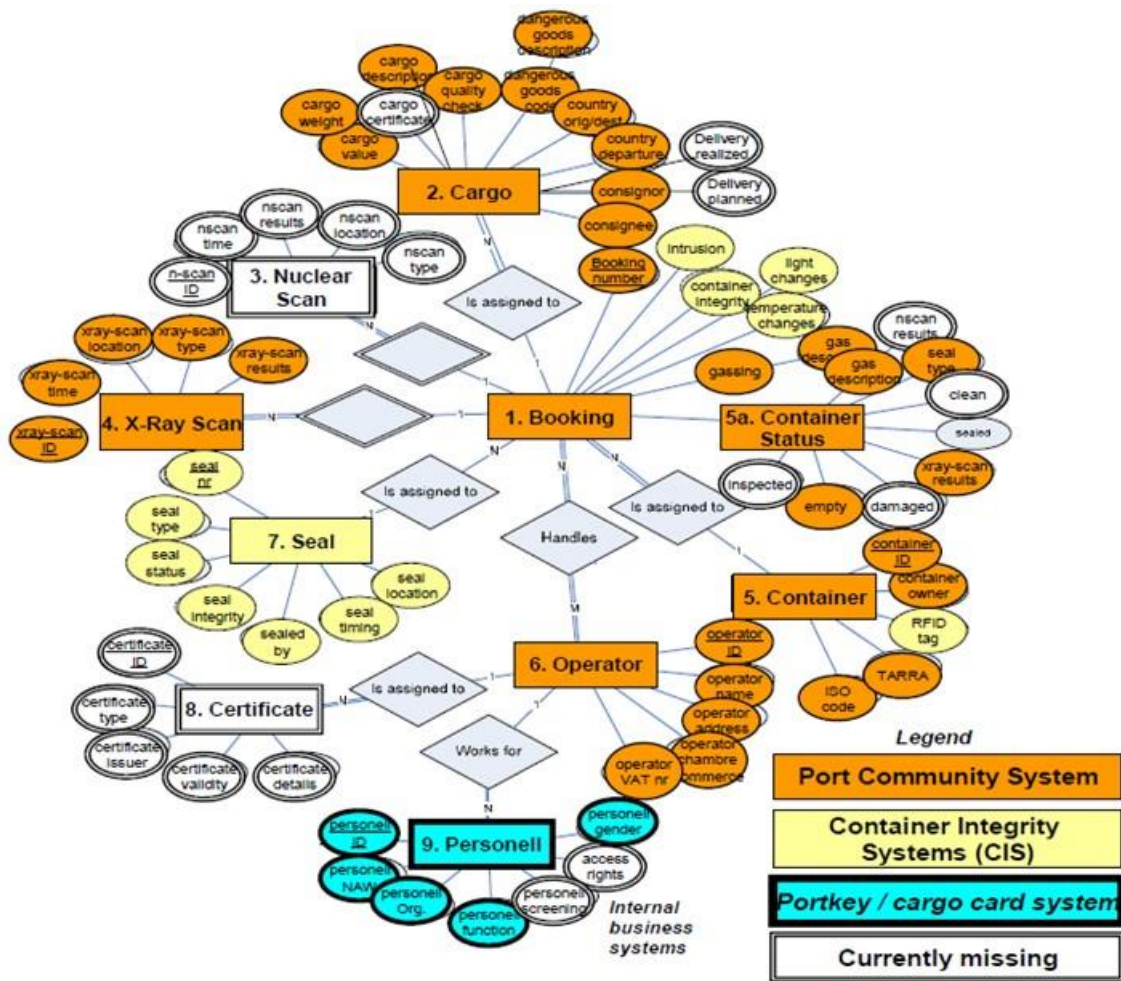


Figure 16: Information blocks and coverage (in width) in Port of Rotterdam IT systems. (Oosterhout, et al., 2007)

**Gap analysis.** Gap analysis, or largest security risks analysis, is defined as the “information need versus information availability”. The gaps are found where vulnerability for disruption is relatively high and security controls (or measures in place) are relatively low. (Oosterhout, et al., 2007)

Analyzing Figure 16 is understandable that a lot of security relevant information is accessible in electronic format and at supply chain workers. The most favorable situation, from a supply chain security perspective, is the most difficult challenge: the coverage of security relevant data elements by combining data from different IT (interconnection) systems of 100%. This situation is extremely hard to achieve, given the number of the parties involved, the limited readiness to share data and the complexity of a typical supply chain, as the port cases. A way to achieve this situation is making a selection of the most relevant data elements, combining all different IT

systems into a broader visibility platform. This visibility platform will cover the most relevant chain security data elements. (Oosterhout, et al., 2007)

### **1.2. HME's reactants – open market possibilities**

A search on an online open market was made to prove how easy is selecting and acquiring products to produce HME's. (Quaresma, et al., 2013(2))

In a similar way, information about the possible products, many documents were founded on internet, for terrorist proposes. Between them, it must be cited "The Terrorist's Handbook (Akira, 1998)) and "Indicators and Warnings for Homemade Explosives" (Bureau of Alcohol Tobacco Firearms and Explosives; Federal Bureau of Investigation, 2007).

"The Terrorist's Handbook" (Akira, 1998) shows clearly:

- The ways of acquiring explosives and propellants, both in common market or as illegal acquisitions, for illegal acquisition it also teaches picking locks techniques.
- A list of useful household chemicals and their availability.
- The preparation of some chemicals (ammonium nitrate is one of them).
- Some notions about explosions theory;
- Explosives recipes, which are divided into impact, low order (as Fuel + Oxidizer mixtures and perchlorates), high order (ammonium nitrate, ANFOs) and other explosives (like the much known Molotov Cocktails).
- Advices about using explosives as: safety, ignition devices and its construction, impact ignition, electrical and electro-mechanical ignitions, delays of fuse, timers and chemicals;
- Types of explosive containers: paper, metal, glass and plastic.
- Advanced uses for explosives where are presented techniques which just can be used by a person who had some degree of knowledge on the use of explosives, as shaped charges, tube explosives, atomized particles explosions, lightbulb bombs, book bombs and phone bombs.
- Special ammunition for primitive weapons like: bow and crossbow ammunition, blowguns, wrist rockets and slingshots.

- Special ammunition for firearms: handguns, shotguns, compressed air/gas weapons, B.B. guns, .22 calibre pellet guns.
- Rockets and cannons.
- Pyrotechnic as perpetrator of violence: smoke bombs, coloured flames, tear gas, fireworks, firecrackers, skyrockets, roman candles.
- A list of suppliers and more information.
- A checklist for raids on labs.
- Useful pyrochemistry, where it is possible to find reactions with the reagents in study on this thesis.

Consequently, between free open market materials:

- **Aluminium powder** can be found in explosives recipes as fuel in fuel-oxidizer mixtures. It can be explosive when added to: potassium chlorate, potassium permanganate, ammonium perchlorate and a small amount of iron oxide, potassium perchlorate, potassium perchlorate and sulphur or barium nitrate, barium peroxide and magnesium powder, potassium permanganate and icing sugar. The mixture of aluminium and iron oxide powders generates enormous quantities of heat and is known as Thermit. (Akira, 1998) (Quaresma, et al., 2013(2))
- In fuel-oxidizer mixtures is possible to find **icing sugar** as fuel in some mixtures with: potassium chlorate and charcoal, potassium permanganate, potassium permanganate and aluminium or magnesium powder. The “Chemical Fire Bottle” is composed by sugar, potassium chlorate, concentrated sulphuric acid and gasoline. (Akira, 1998) (Quaresma, et al., 2013(2))
- **Fuel oil** can be found as kerosene at kerosene stoves and can be bought at surplus or camping stores. (Akira, 1998) (Quaresma, et al., 2013(2))
- **Ammonium nitrate**, besides of being the main ingredient in fertilizers, can be bought at drug or medical supply stores in products as “Cold-Packs” or as “Instant Cold”, where it can be found in the second plastic bag, which is surrounding the bag of water. This handbook also explains how to synthesize ammonium nitrate from nitric acid (which synthesis is also referred) and ammonia household products, and how to detonate it with a conventional fire train. (Akira, 1998) (Quaresma, et al., 2013(2))

- **Potassium perchlorate** appears as oxidizer in fuel-oxidizers mixtures with: aluminium or magnesium powder and sulphur (optional), barium nitrate and aluminium powder. Potassium perchlorate is easily synthesized with perchloric acid and potassium hydroxide. (Akira, 1998) (Quaresma, et al., 2013(2))

The second cited document “Indicators and Warnings for Homemade Explosives” (Bureau of Alcohol Tobacco Firearms and Explosives; Federal Bureau of Investigation, 2007) focus on the problematic of homemade explosives. (Quaresma, et al., 2013(2)) In this manual it is possible to find the following information:

- Small introduction about characteristics of homemade explosive which are important to users (anti-terrorist forces) know them.
- List of examples of oxidizers, fuels, precursors and binders.
- Generalities about determining whether or not anti-terrorist forces are in a homemade explosives laboratory:
  - Most common homemade explosives: ammonium nitrate, chlorate/ perchlorate mixtures, urea nitrate, etc.
  - Chemical components: aluminium powder, ammonium nitrate, urea, etc.
  - Manufacturing equipment.

According to “Indicators and Warnings for Homemade Explosives” (Bureau of Alcohol Tobacco Firearms and Explosives; Federal Bureau of Investigation, 2007), **aluminium powder** can also be identified as having colours like silver, grey or black or may look whitish and it is odourless. Aluminium powders are extremely flammable; they should not be near oxygen rich chemicals, acids, moistures or water, because when in contact with water, they release flammable gases and their vapours can be explosive and spread in the adjacent areas of their location. They have commercial use in paints, pyrotechnics and in manufacture of engines, cars, structural members, etc. They can be found at plastic and steel containers, at supply stores of hardware, paint, chemicals and pyrotechnics. (Quaresma, et al., 2013(2))

The referred document gives also information about **ammonium nitrate mixtures**. Ammonium nitrate and fuel oil (ANFO) is the most common mixture, it appears in form of off-white to pinkish granules or spherical pellets and has the smell of

the fuel oil. These mixtures are sensitive to impact, friction, static spark and heat. They are commercially used as exploding targets (Tannerite), as blasting agent (ANFO), in dynamites, emulsions, water gels and in other packaged high explosives. Ammonium nitrate can be found at fertilizers, fuel oil at gas stations or in additives for motors and the icing sugar can be found at any market. (Quaresma, et al., 2013(2))

**Urea nitrate** is in form of colourless to off-white crystals which tends to create a deposit in the bottom of the recipients where it is contained, however, some additives can alter its physical appearance and it is odourless. These crystals are very sensitive to impact, friction, static spark and heat. It has not known commercial uses, but it can be easily synthesized with nitric acid, which is an industrial chemical, and urea, which is present in fertilizers. (Quaresma, et al., 2013(2))

Lastly, **urea** is a white crystalline, granular or powder and it has ammonia-like odour. It is used in fertilizers, road de-icers, food supplement and in manufacture of plastics and it is accessible in agricultural and hardware supply stores. (Quaresma, et al., 2013(2))

This document just gives general information about chlorates and perchlorates mixtures. All these mixtures are odourless and the most common are: flash powders, which appear in form of silver or gray powders/granules and used in fireworks; Poor Man's C4, a white putty-like, solid or clumps; Armstrong's Mix, a red powder present in toy gun caps. They are extremely sensitive to impact, friction, static spark, and heat. **Potassium perchlorates** are normally used on airbag initiator formulas and pyrotechnics. (Quaresma, et al., 2013(2))

### **1.2.1. HME's reactants - market products selection**

The preliminary search of HME's reactants was performed using online information of a public Portuguese supermarket (Continente Online). Selection criteria was based in oxidant properties and explosive previous reported characteristics. 19 products were selected as potential oxidants or fuels to construct homemade explosives. (Quaresma, et al., 2013(2)) (vd. Table 2).

## HOMEMADE EXPLOSIVES BASED ON AMMONIUM AND UREA NITRATES

Table 2: Chosen reagents selected from the market with commercial name, type and motive of selection.

✓ for “selected” and ✗ for “not selected” (Quaresma, et al., 2013(2))

| No. | Commercial name                                  | Selection | Motive of selection  |
|-----|--|-----------|--|
| 1   | Acetone  | ✗         | Highly volatile solvent  |
| 2   | Citric acid ACS reagent                          | ✗         | Very rich ( $r=2.29$ ) for our purposes, limited atomic composition (only has atoms of carbon, oxygen and hydrogen). |
| 3   | Icing Sugar “Sidul”                              | ✓         | Fuel easily obtained from common markets, with a satisfactory richness ( $r=1.12$ )                                  |
| 4   | Aluminium cellulose Paint                        | ✗         | Very complex composition   |
| 5   | Aluminium powder                                 | ✓         | Oxidant which improve the power of explosions  |
| 6   | UHU The all Purpose Adhesive                     | ✗         | Complex solvent and not has melamine   |
| 7   | Cellulose thinner                                | ✗         | Although complex, it has a favorable composition to produce explosives, because it has a lot of fuels in it.         |
| 8   | DMFA   | ✗         | Dangerous oxidant, can easily explode by a static discharge  |
| 9   | Flour “Branca de Neve Flor”                      | ✗         | Fuel with few disponible information and unknown composition   |
| 10  | Fuel oil   | ✓         | Very efficient fuel ( $r=3.35$ ) and easily obtained from common markets.  |
| 11  | Glycine ReagentPlus                              | ✗         | Oxidant easily inflammable in the presence of heat. Not stable enough for the main objectives                        |
| 12  | Harpic toilet bowl cleaner 2 in 1                | ✗         | Oxidant which products in its composition have unknown thermodynamic properties.                                     |
| 13  | Melamine   | ✗         | Dangerous fuel, can easily explode by a static discharge   |
| 14  | Ammonium nitrate ACS reagent                     | ✓         | Oxidant very used in terrorist attacks   |
| 15  | Potassium nitrate ReagentPlus                    | ✗         | Oxidant which can easily explode by a static discharge. To unstable for the purposes                                 |
| 16  | Urea nitrate                                     | ✓         | Very effective oxidant   |
| 17  | potassium perchlorate                            | ✓         | Oxidant very used in terrorist attacks   |
| 18  | CTX-300/GR TRICLORO GRANULADO (grainy trichloro) | ✗         | Oxidant with unknown thermodynamic composition   |
| 19  | Urea powder, BioReagent                          | ✓         | Innovative oxidant. Few studied in explosive reactions   |

An academic example exercise (Quaresma, et al., 2013(2)) was made in order to build a reactivity matrix of combined fuels and oxidants.

|                       | Aluminium Powder | Icing Sugar | Fuel Oil | Ammonium Nitrate | Urea Nitrate | Potassium perchlorate | Urea |
|-----------------------|------------------|-------------|----------|------------------|--------------|-----------------------|------|
| Aluminium Powder      | ■                | ✗           | ✗        | ✓                | ✓            | ✓                     | ✓    |
| Icing Sugar           |                  | ■           | ✗        | ✓                | ✓            | ✓                     | ✓    |
| Fuel Oil              |                  |             | ■        | ✓                | ✓            | ✓                     | ✓    |
| Ammonium Nitrate      |                  |             |          | ■                | ✗            | ✗                     | ✗    |
| Urea Nitrate          |                  |             |          |                  | ■            | ✗                     | ✗    |
| Potassium perchlorate |                  |             |          |                  |              | ■                     | ✗    |
| Urea                  |                  |             |          |                  |              |                       | ■    |

Legend:

Orange materials – fuels

Blue materials – oxidizers

■ Indifferent

✓ Selected

✗ Excluded

This exercise proves the complexity of selection, but also shows the effective possibility of producing a HME from free market products.

### 1.3. AN and UN reactants

Previous reactant matrix shows clearly the use of AN and UN due to the easy availability of large quantities in the open market.

### 1.3.1. Historical terrorist attacks using AN and UN

Several terrorist attacks were performed using ANFO (Ammonium Nitrate/Fuel Oil)

The explosive hazards of AN were early founded and many catastrophes occurred since the beginning of the XX century (Oxley, et al., 2002). Table 3 has a list with the story of AN accidents.

Table 3: Synthesis of five most known terrorist attacks using AN as oxidizer. Attacks described by their known name (outrage), date and place of occurrence, quantities of used explosives, type of used bombs, circumstance and damage from the occurrence.

| Outrage                              | Where  | When                          | Amount of explosive                 | Type of bomb   | Circumstance / Damage   |
|--------------------------------------|--|-------------------------------|-------------------------------------|--|---|
| Sterling Hall Bombing (Lee, 2012)    | University of Wisconsin campus, Madison, USA                         | August 24th, 1970             | ≈ 900 Kg                            | ANFO – vehicle born IED  | Students in protests anti-war of Vietnam; 1 dead, 4 injured         |
| Bishopsgate bombing (BBC, 1993)      | London, UK   | April 24 <sup>th</sup> , 1993 | 1000 Kg                             | Ammonium Nitrate and NitroMetane (ANNM) vehicle born (truck) IED | IRA (Irish Republican Army); 1 dead, 44 injured                     |
| Oklahoma City Bombing (Silva, 2013)  | Bureau of Alcohol, Tobacco, and Firearm (AFT) offices, Oklahoma, USA | April 19 <sup>th</sup> , 1995 | ≈ 2300 Kg                           | ANFO (fertilizer bomb) vehicle born (van) IED                    | McVeigh, protests against FBI measures; 168 dead, 680 injured       |
| Shijiazhuang bombings (Tang, 2001)   | Shijiazhuang, China  | March 16 <sup>th</sup> , 2001 | ≈ 600 Kg                            | ANFO (fertilizer bomb) - plastic bags                            | Jin Ruchao, Familiar and emotional problems; 108 dead, 38 injured   |
| Oslo bombing (Stigset, et al., 2011) | Oslo, Norway   | July 22 <sup>nd</sup> , 2011  | 950 Kg (150 kg of aluminium powder) | aluminium-powder enriched (ANNM) explosive                       | Anders Breivik, political and religious issues; 8 dead, 209 injured |

The use of UN on terrorist attacks is not as popular as the use of AN, but for over a decade; urea nitrate has been used by terrorists to make improvised explosives.

In 1992, use of urea nitrate became so common on terrorist incidents made by the Shining Path (a South American terror cell), that sales of urea were outlawed in Peru. (Oxley, et al., 2009). It was used in many car bombings in Palestine, in improvised mines, which destroyed three Israeli Merkava tanks, in suicide bomber belts, which caused the loss of well over 100 lives in Israel during the years 2001–2004, in mortar shell and in rockets on Gaza Strip. These kind of terrorist attacks has been the motivation for several forensic studies. (Oxley, et al., 2009) (Tamiri, et al., 2009) (Almog, et al., 2007) (Tamiri, 2005)

The most famous terrorist attack using UN was in the bombing of the World Trade Center, which occurred on February of 1993, in New York City. According to journalist references, Islamic radicals drove a truck loaded with about 680 kg of UN and hydrogen-gas cylinders into a garage underneath the World Trade Center. It leaved a crater 18 meters wide and caused the collapse of several steel-reinforced concrete floors in the surrounding area of the blast. Although the terrorist bomb failed to critically damage the main structure of the high-rise building, six people were killed and more than 1,000 were injured. The World Trade Center itself suffered more than \$500 million in damage. After the attack, authorities evacuated 50,000 people from the buildings, hundreds of whom were suffering from smoke inhalation. Investigators determined that the cell built the bomb in New Jersey by consulting manuals brought from Pakistan. (Whitlock, 2007) (History.com, 1996-2013)

### **1.3.2. Selected oxidants, binder and additives**

#### **1.3.2.1. *Ammonium Nitrate***

In some kind of applications, ammonium nitrate (AN) is the base component of a recent family of gas generators and pyrotechnic composite mixtures, as a candidate to substitute ammonium perchlorate (AP), due to its chlorine free characteristics. (Quaresma, et al., 2013) (FPNEM, 2013)

Other factor that contributed for the selection of AN were experimental results from its decomposition processes, which show significant influence (Kolaczkowski, 1980) of endothermic dissociation and exothermic elimination of some products components, in a good agreement with theoretical predictions (Durães, et al., 1996(2)). (Quaresma, et al., 2013) (FPNEM, 2013)

Previous work, related to the model of combustion of ammonium nitrate based propellants (Carvalho, et al., 1995), proves the influence of pressure and phase transition on the stability of flame regression, which are important characteristics to know when we want to study the deflagration of mixtures based on AN. (Quaresma, et al., 2013) (FPNEM, 2013) This lack of information conciliated with this work shows the hazards of using additives on explosive mixtures and the importance of the study of the combustion phenomena using these starting materials, for forensic and academic proposes.

### *1.3.2.2. Urea Nitrate*

Urea Nitrate ( $(\text{NH}_2)_2\text{COHNO}_3$ ) is a recent used nitrate in deflagration and detonation studies motivated, most of them, by forensic research works concerning HMEs and IEDs used in terrorist attacks. Urea Nitrate (UN) has a quite similar behaviour of AN in this kind of energetic compositions. (Quaresma, et al., 2013)

UN become an oxidant candidate because it allows the existence of a carbon atom inside its original molecule, which changes the contribution of this nitrate in flame propagation of UN/Polyurethane compositions. (Quaresma, et al., 2013) (FPNEM, 2013)

The main reasons for the use of UN as energetic raw material comes from the easy availability of the precursor chemicals, ease preparation in large quantities (Oxley, et al., 2009), relatively low cost, low sensitivity (considerably stable) and high-performance energetic material (releases a large amount of energy upon explosion) (Kohno, et al., 2003) (Tokmakov, et al., 2006). The detonation velocity of UN reached 5300m/s, which is comparable to that of emulsion explosives, and depended on the bulk density (Oxley, et al., 2009). This new candidate is also enclosed in commercial two-component polyurethane binder solution. (FPNEM, 2013)

According to Kohno et al., 2003, the decomposition of UN occurs via internal hydrogen transfer from one of the amino groups to the others, producing  $\text{NH}_3$  from the  $\text{NH}_2$ . It is formed HNCO (isocyanic acid) with  $\text{NH}_3$  (ammonium) and  $\text{HNO}_3$  (nitric acid), or with  $\text{NH}_4\text{NO}_3$  (ammonium nitrate). The urea nitrate starts to decompose when the hydrogen bonds between oxygen's in urea and in nitrate are broken, suggesting that these bonds may play an important role in "stabilizing" energetic materials. (FPNEM, 2013)

Another theoretical study (Hiyoshi, et al., 2002) states that the UN molecule in the gas-phase has the structure of an acid-base complex stabilized primarily by the hydrogen bonding interactions due to partial donation of the acidic proton from nitric acid (HNO<sub>3</sub>) to urea. In urea the electronegative O- and N-atoms can serve as the proton acceptor sites. It also predicted the enthalpy of formation of gaseous urea nitrate ( $\Delta_f H_{298}^\circ = -102.3$  kcal/mol). (FPNEM, 2013).

### ***1.3.2.3. Polyurethane***

This component was used as a binder, so it is the responsible for the mechanical properties of the mixture. The polyurethanes are a synthetic polymeric materials family, resulting from the reaction between a prepolymer (molecular weight from 1 000 to 2 000) with molecules hydroxyl terminated (both sides of the molecule) and a diisocyanate. For tests it will be used a commercial polyurethane foam obtained from two liquid solutions, A and B, mixed in the ratio 50% of A to 100% of B. (FPNEM, 2013)

As it was already said, the AN propellant mixtures generally use the same binder type (a PolyUrethane solution system - PU) of the Hydroxyl Terminated PolyButadiene of the classic AP based composite propellants, very well justified in previous works. The required concentration, near 20 %, is due to the rheological properties. (Carvalho, et al., 1995). However it is possible to reduce this concentration if, during mixing process, it is used a high pressure twin screw extruder or other equivalent mixing system that pressurize propellant mixture. (Quaresma, et al., 2013)

### ***1.3.2.4. Additives***

Self-propagating high temperature reaction, between oxidizer filler and combustible binder, assumes combustion characteristics based in flame propagation due to heat transfer, from existing flame to fresh material. Consequently, the fresh material presents an increasing temperature that originates the transition of phase of materials, diffusion and reaction between decomposed reactants. Combustion products expand and local pressure is increased. The expansion of products changes heat transfer complex phenomena and it is possible to react, in post combustion, other reactants with previous reaction products. This is the contribution of aluminium (Al) powders as additive of basic propellants. (Quaresma, et al., 2013)

Our suggestion is to use, alternatively to Al, a condensed mixture based in Teflon and Magnesium. The prediction of reaction path, partial and final compositions of the combustion products of Magnesium/Teflon, as the main components of Magnesium/Teflon/Viton (MTV) mixtures (Campos, et al., 2007(2)), show the strong influence of decomposition of Teflon and easier ignition of Magnesium (Mg), comparatively to Aluminium. (Quaresma, et al., 2013)

The increased temperature of the products of reaction, demonstrated and well explained by (Koch, 2002), allows an increasing gas formation and pressure. (Quaresma, et al., 2013)

Aluminium powder, as referred on 1.2., can be found at plastic and steel containers, at supply stores of hardware, paint, chemicals and pyrotechnics. Magnesium is acquirable on sports stores and Teflon on industries of pans.

### **1.4. Thesis description**

On the following thesis, the *Chapter 2* is dedicated to ammonium and urea nitrate thermal decompositions. In this chapter it will be presented a detailed literature review (2.1) about the thermal decomposition mechanisms of these nitrates; the history and fundamentals of THOR, the computational code used along this work for thermochemical calculations; the experimental techniques employed during this work to characterize AN and UN and their thermal decomposition mechanisms (infrared spectroscopy and thermal analysis, respectively)

Chapter 3 is dedicated to the development and detection of studied mixtures. Initially, in 3.1, it will be presented details about the thermodynamic properties of the reactants used and about the mixtures' composition. After the thermochemical predictions about the mixtures based on AN and UN using THOR Code (3.2), the combustion process occurred on selected mixtures was studied. This point, 3.3, approach the fundamentals about the combustion phenomena, the laboratorial work developed to study that phenomena and exposes the acquired results. Infra-red spectroscopy (3.4) was performed to characterize the reactants and the mixtures (before and after combustion) in the IR spectrum of light.

This characterization was made in order to enable the detection, in future, of these mixtures by this analytical and inexpensive technique, if used for terrorist or malicious purposes or even in case of accidents with the chosen reactants.

The discussion about the exposed results on *Chapters 2 and 3* is presented on *Chapter 4*. This chapter is only dedicated to the relevant results acquired and presented along this work.

Lastly, the *Chapter 5* is dedicated to the conclusions about the presented work and further developments.

## CHAPTER 2 – AMMONIUM AND UREA NITRATES THERMAL DECOMPOSITIONS

### 2.1. Literature Review

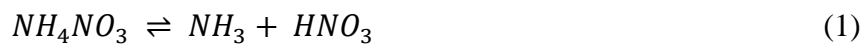
#### 2.1.1. Thermal Decomposition Mechanisms

##### 2.1.1.1. Ammonium Nitrate

Thermal decomposition is assumed as the reaction processes which reactant materials become reaction products, under increased temperature ranges and heating modes (slowly or quickly).

The thermal decomposition of ammonium nitrate (AN –  $\text{NH}_4\text{NO}_3$ ) has been extensively studied. (Patil, et al., 1992) (Durães, et al., 1996(2)) (Durães, et al., 1997) (Oommen, et al., 1999) (Portugal, et al., 2000) (Oxley, et al., 2009)

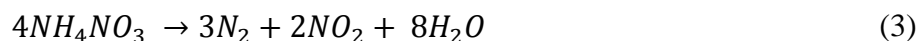
The global reaction mechanism starts, above  $169^\circ\text{C}$ , when occurs the endothermic dissociation in ammonia ( $\text{NH}_3$ ) and nitric acid ( $\text{HNO}_3$ ) (reaction (1)):



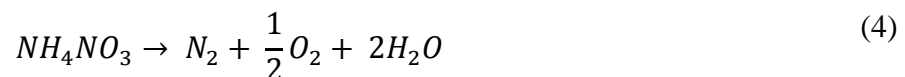
When solid AN is carefully heated at  $200^\circ\text{C}$ , heat is released by the exothermic elimination of nitrous oxide ( $\text{N}_2\text{O}$ ) (reaction (2)).



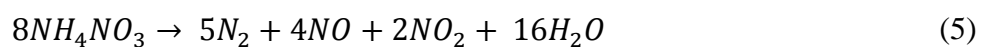
Reaction (3) corresponds to exothermic elimination of nitrogen gas ( $\text{N}_2$ ) and nitrogen dioxide ( $\text{NO}_2$ ) which occurs for temperatures above  $230^\circ\text{C}$ .



Detonation can arise, in a short time delay, AN is decomposed in nitrogen gas ( $\text{N}_2$ ), oxygen ( $\text{O}_2$ ) and water ( $\text{H}_2\text{O}$ ), being the elimination of  $\text{N}_2$  and  $\text{O}_2$  exothermic (reaction (4))



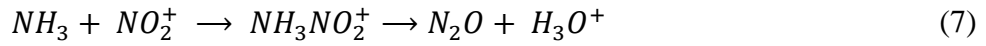
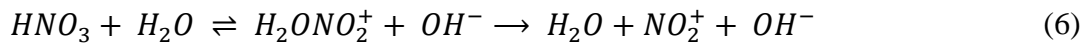
Reaction (5) occurs when ammonium nitrate goes under inducted explosion:



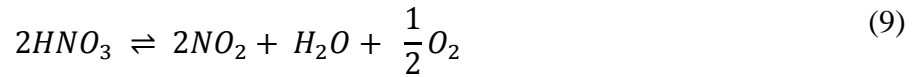
Basically, two main mechanisms have been proposed for thermal decomposition of AN, where the prevalence of one over the other is dependent of the temperature levels. (Patil,

et al., 1992) (Oommen, et al., 1999) So, it is possible separate the thermal decomposition mechanisms of AN when it occurs for low and high temperatures. For both mechanisms, the initial step is the AN dissociation (reaction (1)).

For **low temperatures**, which is considered to be under 270°C (Patil, et al., 1992) (Oommen, et al., 1999), the nitric acid (HNO<sub>3</sub>) from the AN dissociation (reaction (1)), produces nitronium ions (NO<sub>2</sub><sup>+</sup>). These ions will react with ammonia (NH<sub>3</sub>) to form nitrous oxide (N<sub>2</sub>O) and water (H<sub>2</sub>O). This mechanism is represented by reactions (6), (7) and (8). The global reaction is reaction (2).



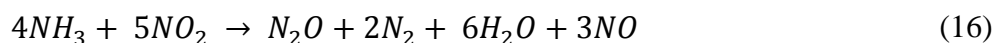
At **high temperatures** (Patil, et al., 1992) (Oommen, et al., 1999) (Oxley, et al., 2002) , the nitric acid is no more an intermediary specimen, but a formed decomposition product. This formed nitric acid (HNO<sub>3</sub>) goes under dissociation too (reaction (9)), due to high temperatures. Its dissociation products are nitrogen dioxide (NO<sub>2</sub>), water (H<sub>2</sub>O) and oxygen (O<sub>2</sub>).



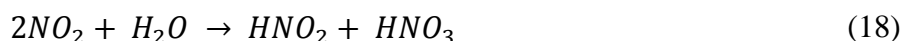
On a temperature range of 342 to 387°C, the formed nitrogen dioxide (NO<sub>2</sub>) oxidizes the ammonia (NH<sub>3</sub>). This oxidation is shown on reactions (10) to (15).



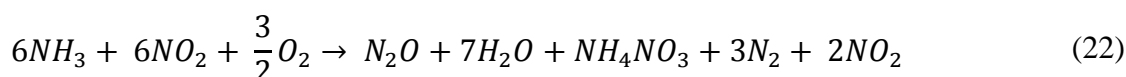
These reactions can be reduced to the global stoichiometry (reaction (16)), where the oxidation of ammonia (NH<sub>3</sub>) by nitrogen dioxide (NO<sub>2</sub>) forms nitrous oxide (N<sub>2</sub>O), nitrogen gas (N<sub>2</sub>), water (H<sub>2</sub>O) and nitric oxide (NO)



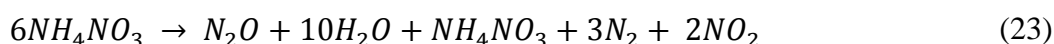
The oxygen, formed by nitric acid dissociation, slowly reacts with ammonia but has high reactivity on presence of nitric oxide. As a result, the oxygen (O<sub>2</sub>) is limited to oxidize nitric oxide (NO) (from reaction (16)). The subsequent reactions of this oxidation are reactions from (17) to (21).



These equations can be reduced to their global stoichiometry (reaction (22)).



Reaction (22) is typical of AN aerosol decomposition under a high heating rate (80°C/s). The resulting products are nitrous oxide (N<sub>2</sub>O), water (H<sub>2</sub>O), ammonium nitrate (NH<sub>4</sub>NO<sub>3</sub>), nitrogen gas (N<sub>2</sub>) and nitrogen dioxide (NO<sub>2</sub>) - this AN decomposition can be represented by reaction (23):



Other proposal for AN thermal decomposition at high temperatures is explained by the formation of a nitramide intermediary (NH<sub>2</sub>NO<sub>2</sub>) which produces nitrous oxide (N<sub>2</sub>O) and water (H<sub>2</sub>O) (reactions (24) and (25)):



Systematizing, The thermal decomposition of AN is highly dependent of heating rates. Low heating rates result on a bulk decomposition, which is exothermic and produces the gaseous species nitrous oxide (N<sub>2</sub>O) and water (H<sub>2</sub>O). High heating rates, AN goes under an endothermic surface decomposition and produces nitric acid (HNO<sub>3</sub>) and ammonia (NH<sub>3</sub>).

### 2.1.1.2. Urea Nitrate

The thermal decomposition mechanisms of urea nitrate (UN) (Hiyoshi, et al., 2002) (Kohno, et al., 2003) (Tokmakov, et al., 2006), (Oxley, et al., 2009) (Désilets, et al., 2011) (Désilets, et al., 2011(2)) (Oxley, et al., 2013) are dependent of pressure and temperature rates and levels. In similar way of AN, the thermal decomposition mechanisms of UN will be explained for low and high temperatures.

At **low temperatures**, for thermal decomposition mechanism (Désilets, et al., 2011) (Oxley, et al., 2009), UN decomposes at 100°C, which is a temperature below of its melting point (157-159°C). Its decompositions products are:

- the condensed-phase ammonium nitrate ( $\text{NH}_4\text{NO}_3$ ), urea ( $(\text{NH}_2)_2\text{CO}$ ) and biuret ( $\text{NH}_2\text{C}(\text{O})\text{NHC}(\text{O})\text{NH}_2$ );
- the gaseous products are ammonia ( $\text{NH}_3$ ), isocyanic acid ( $\text{HNCO}$ ) and nitric acid ( $\text{HNO}_3$ ).

This mechanism can be represented by reactions (26) to (29), shown on Figure 17.

At an early stage of this thermal decomposition, some UN dissociates into nitric acid ( $\text{HNO}_3$ ) and urea ( $(\text{NH}_2)_2\text{CO}$ ) (vd. reaction (26)). Reaction (27) shows the urea's thermolysis under 100°C, which products are ammonia ( $\text{NH}_3$ ) and isocyanic acid ( $\text{HNCO}$ ). Dependent on the temperature applied to urea, its thermolysis can generate more products besides these ones.

The formed urea reacts with the isocyanic acid ( $\text{HNCO}$ ), which is highly reactive, to produce biuret ( $\text{C}_2\text{H}_5\text{N}_3\text{O}_2$ ) (vd. reaction (28)).

Ammonium nitrate ( $\text{NH}_4\text{NO}_3$ ) is a product formed through the reaction of ammonia coming from urea's thermolysis (reaction (27)), with nitric acid formed due to urea nitrate dissociation (reaction (26)). This reaction is represented by equation (29).

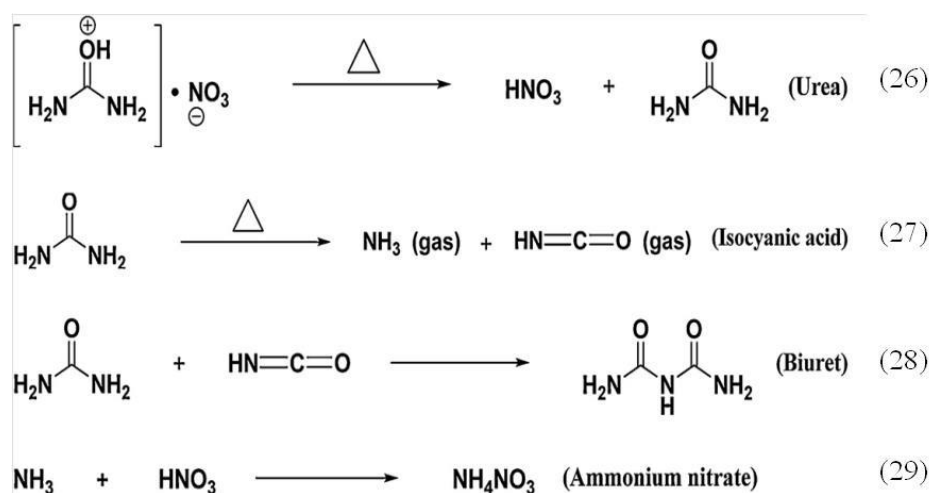


Figure 17: Thermal decomposition mechanism of UN at low temperatures (Désilets, et al., 2011)

At **high temperatures**, the thermal decomposition mechanism of UN (Oxley, et al., 2013) (Désilets, et al., 2011(2)) (Oxley, et al., 2009) (Hiyoshi, et al., 2002) is much more complex

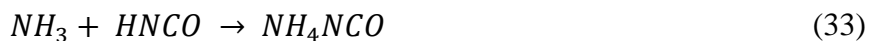
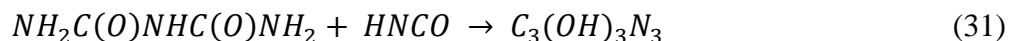
The initial phase of this mechanism is identical to the thermal decomposition mechanism at low temperatures (Désilets, et al., 2011(2)), which consists on UN's dissociation into nitric acid and urea (Figure 17, reaction (26)), followed by urea's decomposition into ammonia and isocyanic acid (Figure 17, reaction (27)); biuret is formed due to the reaction between urea (which not suffered decomposition) with isocyanic acid (Figure 17, reaction (28)); the reaction between ammonia and nitric acid yields ammonium nitrate (Figure 17, reaction (29)).

From ambient temperature until 190°C the urea ((NH<sub>2</sub>)<sub>2</sub>CO), suffers thermolysis or reacts to form biuret (NH<sub>2</sub>C(O)NHC(O)NH<sub>2</sub>), which reaches its maximum of formation at 190°C (reactions of formation (28), (30)). Condensed phase species formation, as cyanuric acid and ammelide structures (shown on Figure 18), starts at this temperature.



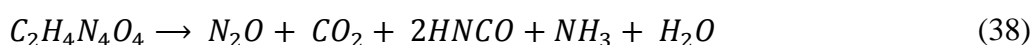
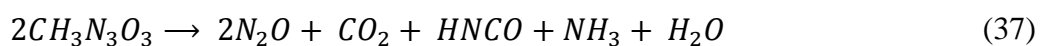
From 190°C to 250°C, urea's degradation is still occurring and starts biuret's decomposition. Reactions (31) and (32) shows the interactions between biuret and isocyanic acid, and from isocyanic acid (from urea) rearrangement to form cyanuric acid (C<sub>3</sub>(OH)<sub>3</sub>N<sub>3</sub> ↔ O<sub>3</sub>C<sub>3</sub>(NH)<sub>3</sub>; molecular structure on Figure 18). The productions of cyanuric acid and ammelide (C<sub>3</sub>H<sub>4</sub>N<sub>4</sub>O<sub>2</sub>, molecular structure on Figure 18) are accelerated and new compounds, as ammonium isocyanate (NH<sub>4</sub>NCO - reaction (33)), ammeline (C<sub>3</sub>H<sub>5</sub>N<sub>5</sub>O, molecular structure on Figure 18) and melamine (C<sub>3</sub>H<sub>6</sub>N<sub>6</sub>)

(reactions (34), (35) and (36), molecular structure on Figure 18), start appearing in small quantities. At 250°C all urea and biuret are totally decomposed.



From 250°C to 360°C, all material starts to decomposed by the reverse reactions, forming ammonia and isocyanic acid as gaseous products. The AN formed during the initial phase of UN's thermal decomposition, as referred before (vd. 2.1.1.1), suffers thermal decomposition at high temperatures. It is generally accepted that AN's thermolysis follows two distinct reactions which occur simultaneously. The first one is a proton-transfer reaction (reaction (1), vd. 2.1.1.1.), the second is the irreversible reaction (reaction (2), vd. 2.1.1.1.). All thermal decomposition mechanism at low temperatures is dependent on individual reaction rates, products stability and interactivity, as well as gaseous species evaporation. Ammonia, nitric acid and nitrous oxide and water are products from these two reactions.

At this temperature range, urea and biuret decompositions generate nitrate compounds as nitrourea ( $CH_3N_3O_3$ , molecular structure at Figure 18) and nitrobiuret ( $C_2H_4N_4O_4$ , molecular structure at Figure 18), which also thermally decomposes into carbon dioxide ( $CO_2$ ), nitrous oxide ( $N_2O$ ), isocyanic acid ( $HNCO$ ), ammonia ( $NH_3$ ) and water (reactions (37) and (38), respectively). The nitration of amine compounds can occur at high temperatures due to the presence of  $NO_2^+$  derived from AN decomposition (remember reactions (6) and (7) at 2.1.1.1.), or due to the nitric acid formed at high temperatures. These instable compounds just decompose in gaseous species.



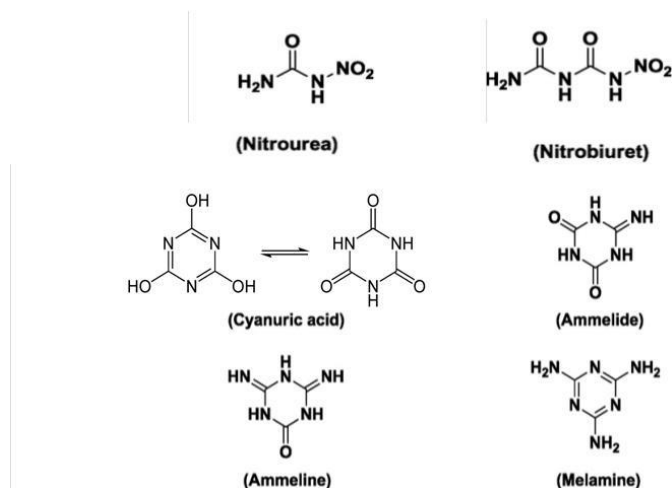
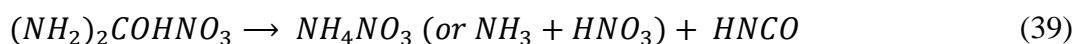


Figure 18: Some of the condensed phase species formed during UN thermal decomposition (Désilets, et al., 2011)

Other study that made the thermolysis of UN in ever harsher conditions (Hiyoshi, et al., 2002), from 400 to 500°C through the reaction monitoring with T-jump/FT-IR, concluded that in that temperature range UN decomposes under two reactions, (39) and (40).  $\text{NH}_3$  from (39) can combine with  $\text{HNCO}$  to produce  $\text{NH}_4\text{NCO}$ , as shown in reaction (33). Some of the UN can undergo to dissociation (reaction (26)) too, but the urea product rearranges itself to origin  $\text{NH}_4\text{NCO}$ .



## 2.1.2. THOR - thermochemical evaluation code

### 2.1.2.1. Introduction

The thermochemical computer code, THOR, was developed to predict combustion and detonation behaviour based in products thermodynamic properties. (Campos, et al., 2007). The difficult of following by experiment, the existing reactions in pyrolysis, combustion or detonation processes, generating intermediary chemical species and compounds, justify the existence of prediction thermochemical codes. (Campos, et al., 2006)

The development was started in 1989 by the Thermodynamic Group from the Mechanical Engineering Department of FCTUC. (Durães, 1999)

THOR was based on theoretical work of Héuze (1985, 1989) (Campos, et al., 2006) (Campos, et al., 2007) (Durães, et al., 1995)-(Durães, et al., 1996) assuming an isobar or an isochoric adiabatic combustion, or a Chapman-Jouguet detonation conditions for the minimum Gibbs free energy. Several thermal equations of state (EoS) can be used on this computer code. (Campos, et al., 2006) (Campos, et al., 2007) The used  $H_L$  EoS is supported by a Boltzmann EoS, based on physical intermolecular potential of gas components, instead of correlations from final experimental results.

Later on the code was enhanced and upgraded to the use of the new polynomial forms of energetic functions, of gas and condensed phases of compounds, proposed by Gordon and McBride, 1994, and the ICT Database of Thermochemical Values, 2005, proposed in ICT (Campos, et al., 2006) (Campos, et al., 2007) (Campos, et al., 2007(2)).

#### 2.1.2.2. General equations

CHNO system is generally known to be a classical reactive system that enables to generate up to  $m$  atomic species and  $n$  chemical components.

To solve this problem (Campos, et al., 2006) (Campos, et al., 2007), is necessary to define the  $m-n$  equilibrium equations. The solution can be determined by Lagrange's multipliers method, or by equilibrium constants. The final calculation for imposed  $P$  (pressure) and  $T$  (temperature) conditions, is then possible by the use of the chemical affinity method (determining the chemical concentrations of  $n$  components). Other way (Campos, 1991) is solving first the system composed by the  $m$  "basic" components, and secondly adding one by one more components, in order to optimize the relative concentration inside the group related to the same atomic species, for the minimum value of global Gibbs free energy (equation (41)).

$$G = \sum x_i \mu_i \quad (41)$$

The Gibbs free energy of each component is defined by  $\mu_i$  (equation (42)).

$$\mu_i = G_{0i}(T) + R T \ln P + R T \ln(x_i) \quad (42)$$

The components selection is dependent of the atoms present at the initial composition. For a classical CHNO system, the equilibrium composition should start with  $CO_2$ ,  $CO$ ,  $H_2O$ ,  $N_2$ ,  $O_2$ ,  $H_2$ ,  $OH$ ,  $NO$ ,  $H$ ,  $N$ ,  $O$ ,  $HCN$ ,  $NH_3$ ,  $NO_2$ ,  $N_2O$ ,  $CH_4$  gases and two types of solid carbon,  $\beta$  and  $\alpha$  (graphite and diamond, respectively). The solution of composition problems, therefore, involves after mass and atomic balance equations:

- The thermodynamic equilibrium for  $G = G_{\min}(P, T, x_i)$ , applying the Tanaka model for the condensed phase (for a CHNO system);
- The thermal equation of state (EoS);
- The energetic equation of state, associated to internal energy (equation (43) with  $e_i(T)$  being calculated initially, for initial THOR versions, from JANAF Thermochemical Tables and polynomial expressions of Gordon and McBride;

$$E = \sum x_i e_i(T) + \Delta e \quad (43)$$

- The combustion condition regime, being  $P_b = P_0$  ( $b$  for burned,  $0$  for initial) constant for isobar adiabatic combustion (equal initial and final total enthalpy  $H_b=H_0$ ), the isochors adiabatic combustion being  $V_b = V_0$  constant (equal initial and final internal energy  $E$ ) and the Chapman-Jouguet condition (mass, momentum and energy balances and equation (44)) for detonation regime, sustained on the assumption that the detonation velocity  $D$  is obtained adding sound velocity  $a_0$  with particular velocity  $u_p$  (equation (45)).

$$\left. \frac{dp}{dV} \right]_s = \frac{P - P_0}{V - V_0} \quad (44)$$

$$D = a_0 + u_p \quad (45)$$

Recently, THOR code was enhanced for any kind of systems of atoms or of molecules, from the existing databases (from institutions like ICT or NASA).

**$H_L$  Thermal Equation of State.** Used  $H_L$  EoS has the general expression shown in (46), where  $V$  represents the volume,  $T$  the temperature and  $X_i$  the mole number of  $i$  compound in reaction gaseous products. The second term,  $\sigma$ , is a fifth order polynome obtained from virial expansion. (Campos, et al., 2006) (Campos, et al., 2007)

$$\frac{PV}{nRT} = \sigma(V, T, X_i) \quad (46)$$

This fifth order polynome,  $\sigma$ , represents very well the behaviour of gaseous mixtures at high temperature and pressure and it is defined by:

$$\sigma(V, T, X_i) = 1 + x + 0.625x^2 + 0.287x^3 - 0.093x^4 + 0.014x^5 \quad (47)$$

With

$$x(V, T, X_i) = \frac{\Omega}{VT^{3/\alpha}} \quad (48)$$

$$\Omega = \sum_{i=1}^s X_i \omega_i \quad (49)$$

$\alpha$  represents the exponent part of the intermolecular potential. Heuzé deduced  $H_9$  and  $H_{12}$  EoS, for  $\alpha=9$  and  $\alpha=12$  respectively, based on theoretical and experimental final correlations. This parameter has great influence on the results and the preceding values are too low to represent the detonation gaseous products, which co-exist in equilibrium at very high pressure. The intermolecular potential function considered in  $H_L$  EoS is the Buckingham  $\alpha^{-6}$  function, where  $\alpha=13.5$ , according to several authors studied for that case.

The  $\omega_i$  values are dependent of each gas component. Making the substitution of (49) in (48):

$$x = \frac{\sum_{i=1}^n X_i \omega_i}{VT^{3/\alpha}} \quad (50)$$

Considering the Boltzmann EoS, is possible to write the equality (51), where  $B_i$  is the covolume of component  $i$  in reaction products.

$$\frac{\sum_{i=1}^n X_i \omega_i}{VT^{3/\alpha}} = \frac{\sum_{i=1}^n X_i B_i}{V} \quad (51)$$

This is valid procedure, because  $H_L$  EoS is reduced to a Boltzmann EoS when, at low densities, the terms of high order (fourth and fifth) in  $\sigma$  expression (47) become negligible.

For the covolume calculation ( $B_i$ ), it was used a simplified rigid sphere model (equation (52)).

$$B_i = \frac{2}{3} \pi r_{0i}^3 N_{AV} \quad (52)$$

$$T = \theta \frac{\varepsilon}{k} \quad (53)$$

Being  $r_{0i}^3$  the intermolecular distance at minimum value of the intermolecular potential and  $N_{AV}$  the Avogadro number. Equation (53) represents temperature evolution. Where  $\theta$  is the adimensional temperature,  $k$  the Boltzmann constant ( $k = 1.380 \times 10^{-23} \text{J/K}$ ) and  $\varepsilon_i/k$  the parameters of Buckingham  $\alpha^{-6}$  intermolecular potential function, for each reaction gaseous product in pure state. For each gas in the products, the values of  $r_{0i}$  and

$\varepsilon_i/k$  parameters are usually obtained by agreement between experimental and theoretical data.

$\theta$  values have great influence on predicted dynamic characteristics of condensed products of reactive mixtures, several of them were evaluated (Durães, et al., 1995) (Durães, et al., 1996) (Durães, et al., 2000). Initially, the value  $\theta=1.4$  has been considered the best-adopted constant value, by comparison with experimental and theoretical results for detonation. Later, the new proposed value was  $\theta=1$ , omitting the referred comparison and meaning that  $\varepsilon_i/k$  is a good measure of each pure compound temperature in shock experimental tests, which is more consistent, theoretically, than taking any other value.

**Energetic Equation of State.** As it was mentioned in the beginning of *General equations*, the energetic ES is related to the internal energy, defined by equation (43). The  $e_i(T)$  are calculated by the polynomial expressions of non-dimensional specific heat, enthalpy and entropy, given by Gordon and McBride polynomials. In the past were used the old Gordon and McBride polynomials (1971) shown by equations (54), (55) and (56), respectively.

$$\frac{Cp_0}{R} = a_1 + a_2T + a_3T^2 + a_4T^3 + a_5T^4 \quad (54)$$

$$\frac{H_0}{RT} = a_1 + \frac{a_2}{2}T + \frac{a_3}{3}T^2 + \frac{a_4}{4}T^3 + \frac{a_5}{5}T^4 + \frac{a_6}{T} \quad (55)$$

$$\frac{S_0}{T} = a_1 \ln(T) + a_2T + \frac{a_3}{2}T^2 + \frac{a_4}{3}T^3 + \frac{a_5}{4}T^4 + a_7 \quad (56)$$

The new formats are the recent Gordon and McBride polynomials (equations (57), (58) and (59)) and they follow the same logic presented above:

$$\frac{Cp_0}{R} = a_1T^{-2} + a_2T^{-1} + a_3 + a_4T + a_5T^2 + a_6T^3 + a_7T^4 \quad (57)$$

$$\frac{H_0}{RT} = -a_1T^{-2} + a_2T^{-1} \ln(T) + a_3 + a_4 \frac{T}{2} + a_5 \frac{T^2}{3} + a_6 \frac{T^3}{4} + a_7 \frac{T^4}{5} + \frac{b_1}{T} \quad (58)$$

$$\frac{S_0}{T} = -a_1 \frac{T^{-2}}{2} - a_2T^{-1} + a_3 \ln(T) + a_4T + a_5 \frac{T^2}{2} + a_6 \frac{T^3}{6} + a_7 \frac{T^4}{4} + b_2 \quad (59)$$

These recent Gordon and McBride polynomials (1994) implied a mathematical and numerical conversion in the modified THOR code achieved in 2008.

The use of the preceding two equations of state (thermal equation of state EoS) and the energetic equation of state (ES) allow the optimization of the final composition of products ( ) always for the minimum value of the Gibbs free energy, calculated for a predefined values of T and P.

**Isobar and Isochor Adiabatic Combustion.** The basic theoretical combustion approach assumes and **isobar adiabatic combustion**, where  $dP = 0$  and  $dQ = 0$  imply  $dH = 0$ , which means that equal initial and final total enthalpy (equation (60)). Equation (60) is equivalent to (61) and also to (62), where the total enthalpy from burned gases is equal to module of the reaction enthalpy. (Campos, et al., 2006) (Campos, et al., 2007)

$$H_b^{T_b} = H_0^{T_0} \quad (60)$$

$$H_b^{T_b} - H_b^{T_0} = -(H_b^{T_0} - H_0^{T_0}) \quad (61)$$

$$H_b|_{T_0}^{T_b} = -\Delta_r^{T_0} H \quad (62)$$

Considering a global isobar adiabatic process, formed by a reactive system enclosed in a non-resistant wall, working like an enthalpy changer of value  $\Delta H$  the equation (62) takes the form of equation (63), where the enthalpy of reaction is distributed to the heated burned gas and the wall, being always  $P=P_0$

$$H_b|_{T_0}^{T_1} + \Delta H = -\Delta_r^{T_0} H \quad (63)$$

As a result, it is possible to consider  $T_0 < T_1 < T_b$ . The corresponding products composition can then be changed from the “basic” chemical components, when  $T_1 = T_0$ , to the final components, when  $T_1 = T_b$ , isobar adiabatic combustion temperature with the preceding condition. The Gibbs free energy, taking its minimum relative value for a (V, T, X<sub>i</sub>) group, is also reduced with increasing values of  $T_1$ , from  $T_0$  to  $T_b$

Thus, the pyrolysis process can now be calculated and justified, like a decomposition process, by the mechanism of heat absorption, from the original adiabatic combustion condition (where are no heat changes). Therefore, the original global isobar adiabatic process, formed by one reactive system enclosed in a non-resistant wall, is modified by the enthalpy value  $\Delta H$ , absorbed from the wall (equation (63)), where the enthalpy of reaction is increased by the heat absorbed from the wall, being always  $P=P_0$ . The Gibbs free energy, taking its minimum relative value for a (V, T, X<sub>i</sub>) group, is also changed (in a similar way) with increasing values of  $T_1$ , from  $T_0$  to final value  $T_b$ .

The **isochor adiabatic combustion** needs the calculation of the internal energy  $E_i^T$ , for a specified  $(V, T, x_i)$ , where  $V$  represents the volume,  $T$  the temperature and  $x_i$  the mass fraction. This  $E_i^T$  can be expressed as a function of the enthalpy,  $H_i^T$ , and of  $PV$  (equation (64)) for the same conditions, as shown in equation (65).

$$PV = \sigma NRT \quad (64)$$

$$E_i^T = H_i^T - \sigma N_i RT_i \quad (65)$$

This expression allows the calculation of values for isochor adiabatic combustion from the obtained values of the corresponding isobar adiabatic combustion, for the same  $P$  and  $T$  conditions, but needs an interactive method to find the solution

**THOR external and internal code structures.** The external structure of Thor is outlined on Figure 19.

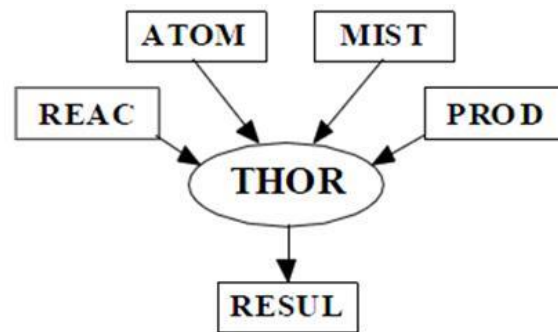


Figure 19: Data access and results output of THOR Code. (Durães, 1999)

The code data access is divided into four files:

- i. **ATOM:** contains the atomic masses of the twenty atomic species for which THOR was programmed for.
- ii. **REAC:** file where it is possible to find the chemical formula, the formation enthalpy at 25°C and 1 atm, the calorific capacity at constant pressure (25°C, 1 atm) and the specific mass at the same conditions (real density), for each one of reactant compound of the chosen mixture.
- iii. **PROD:** is the file where is stored the molecular formula, the formation enthalpy at 25°C and 1 atm and the phase of each reaction product. It is also possible to find in this file, for each gaseous reaction product, the seven high temperature coefficients of Gordon & Mc-Bride polynomials. For condensed species, from the first until the seventh value, the meaning

is: crystal density (theoretical maximum density.- TMS), sound velocity, shock relationship, Gruneisen coefficient, Debye temperature, internal energy of reference and reference entropy. The chosen products are limited to 59, and the condensed phase number is restricted to 29.

- iv. MIST: gives to the program the composition of the reactant mixture (reagent name and its quantities in mol), initial temperature and pressure, type of problem and the chosen equation of state to predict the P-V-T characteristics of gaseous phase. The reactant mixture can contain until seven different reagents and it is mathematically assumed that mixture is homogeneous. It is possible to acquire properties of mixtures with reagents in different phases, because it calculates the average properties for the initial mixture starting from the individual properties of the mixed reagents.

Fortran 77 was the language used to program THOR, converted successively to F90 and MS Fortran. The program does the data treatment and the calculation of the combustion or detonation characteristics. After that, sends the results for RESUL file, under numeric values format and tables. Recently, 2008, it was converted and optimized to Windows© interface.

### ***2.1.2.3. Results and discussion from literature***

**Decomposition path of ammonium nitrate.** Several studies (Durães, et al., 1996(2)) (Durães, et al., 1997) (Durães, et al., 2000) (Morgado, et al., 2002) (Morgado, et al., 2003) (Campos, et al., 2006) were made to determine the decomposition path of ammonium nitrate (AN) using the thermochemical calculation code THOR.

One of them (Durães, et al., 1996(2)) showed the evolution of Gibbs free energy and combustion temperature as a function of absorbed enthalpy,  $\Delta H$ , for AN decomposition (Figure 20); the influence of products selection, as a function of obtained combustion temperature and Gibbs free energy value (vd. Figure 21) show the main decomposition products for AN; and the gas products composition, as function of calculated decomposition temperature (Figure 22).

The theoretical prediction of temperature (Figure 23, graph (a)) and the products composition of the AN thermal decomposition (Figure 23, graph (b)) was also made using THOR code, for knowledge of nitrate additives behaviour (Morgado, et al., 2002) (Morgado, et al., 2003).

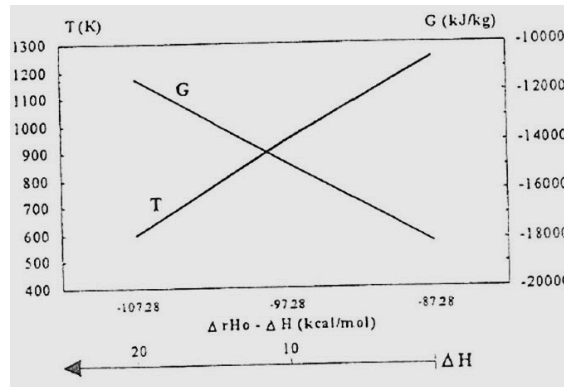


Figure 20: Evolution of Gibbs free energy and combustion temperature as a function of absorbed enthalpy,  $\Delta H$ , for AN decomposition (Durães, et al., 1996(2))

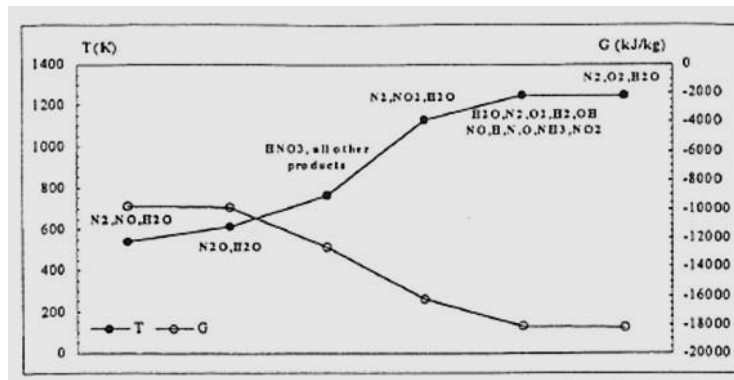


Figure 21: The influence of products selection, as a function of obtained combustion temperature and Gibbs free energy value, for AN (Durães, et al., 1996(2))

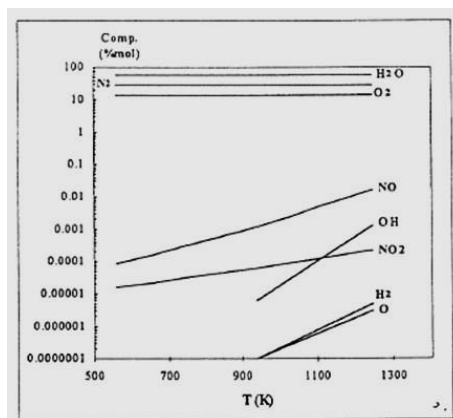


Figure 22: Gas products composition, as a function of calculated decomposition temperature, for AN (Durães, et al., 1996(2))

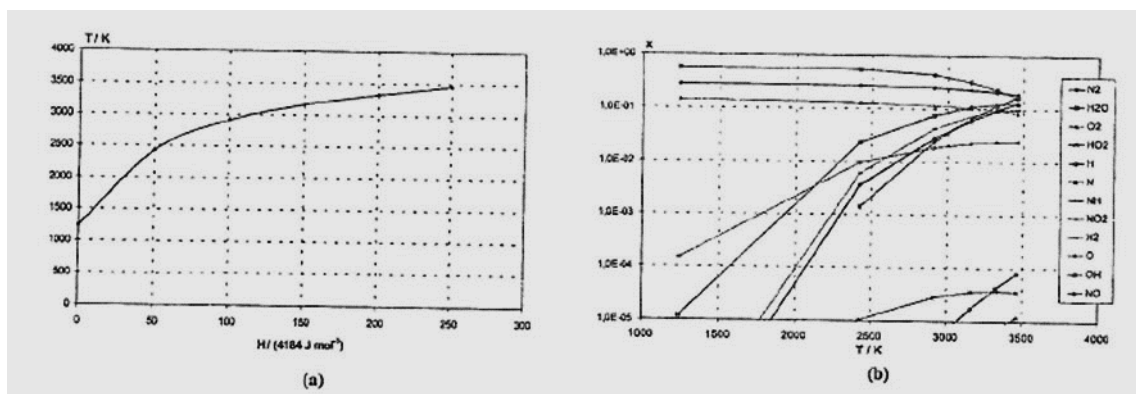


Figure 23: theoretical prediction of (a) temperature and (b) products composition of the thermal decomposition of AN (Morgado, et al., 2002) (Morgado, et al., 2003)

As said in 2.1.1.1, the AN thermal decomposition can be synthesized through reactions which occur for different temperature ranges and heating modes (slowly or quickly). Other studies (Durães, et al., 1997) (Durães, et al., 2000) (Campos, et al., 2006) were made in order to calculate the reaction path of AN decomposition using THOR code. As shown in Tables 4 and 5, it was possible to determine the enthalpy of reaction and internal energy of AN decomposition, respectively, as function of selected products. The theoretical predictions were in a good agreement with AN thermal decomposition described in 2.1.1.1. By order of products appearance on Table 4, it shows the endothermic dissociation above 169°C (reaction (1)), the exothermic elimination of N<sub>2</sub>O on careful heating at 200°C (reaction (2)); the exothermic elimination of N<sub>2</sub> and NO<sub>2</sub> above 230°C (reaction (3)) and the exothermic elimination of N<sub>2</sub> and O<sub>2</sub>, sometimes accompanied by detonation (reaction (4)).

Table 4: Enthalpy of reaction of AN thermal decomposition as function of selected products (Durães, et al., 1997) (Durães, et al., 2000) (Campos, et al., 2006)

| Products of reaction                                 | Reaction in 2.1.1.1.  | $\Delta_r H$ (kJ/mol) |
|--|-----------------------|-----------------------|
| NH <sub>3</sub> + HNO <sub>3</sub>                   | (1)                   | 184.3                 |
| N <sub>2</sub> O + H <sub>2</sub> O                  | (2)                   | - 39.3                |
| N <sub>2</sub> + NO <sub>2</sub> + H <sub>2</sub> O  | (3)                   | - 103.5               |
| N <sub>2</sub> + O <sub>2</sub> + H <sub>2</sub> O   | (4)                   | - 97.4                |
| N <sub>2</sub> + NO + H <sub>2</sub> O               | intermediary products | - 30.5                |
| N <sub>2</sub> + HNO <sub>3</sub> + H <sub>2</sub> O | intermediary products | - 97.4                |

Table 5: Internal energy of reaction of AN thermal decomposition as function of selected products (Durães, et al., 1997) (Durães, et al., 2000) (Campos, et al., 2006)

| Products of reaction                             | Reaction in 2.1.1.1.  | $\Delta_r E$ (kJ/mol) |
|--|-----------------------|-----------------------|
| $\text{NH}_3 + \text{HNO}_3$                     | (1)                   | 179.5                 |
| $\text{N}_2\text{O} + \text{H}_2\text{O}$        | (2)                   | - 46.6                |
| $\text{N}_2 + \text{NO}_2 + \text{H}_2\text{O}$  | (3)                   | - 112.2               |
| $\text{N}_2 + \text{O}_2 + \text{H}_2\text{O}$   | (4)                   | - 129.3               |
| $\text{N}_2 + \text{NO} + \text{H}_2\text{O}$    | intermediary products | - 39.1                |
| $\text{N}_2 + \text{HNO}_3 + \text{H}_2\text{O}$ | intermediary products | - 133.5               |

### 2.1.3. Thermal Analysis

#### 2.1.3.1. Fundamentals of Differential Thermal Analysis (DTA), Differential Scanning Calorimetry (DSC) and Thermogravimetric Analysis (TGA)

According to “*The Analysis of Explosives*” (Yinon, et al., 1981), thermal analysis is an analytical technique where some physical property of the analysed sample is measured as a dynamic temperature function. The types of thermal analysis that have been mainly used for the analysis of explosives are Differential Thermal Analysis (DTA), Differential Scanning Calorimetry (DSC) and Thermogravimetric Analysis (TGA), which will be, succinctly, described below.

The techniques DTA, DSC and TGA have been used mostly to determine explosives thermal properties, as thermal stability, thermal decomposition kinetics and initiation and ignition temperatures. Reaction rates, activation energies and explosion heats are quantitative properties that can be calculated out of the experimentally obtained values.

**Differential Thermal Analysis (DTA).** In DTA the sample, accompanied by a reference sample, is cooled or heated in a furnace at a controlled rate. The temperature furnace, as the temperature difference between the sample and the reference are monitored and recorded to produce a thermogram. (Yinon, et al., 1981)

A differential thermogram consists on a record of the temperature difference between the sample and the reference (differential temperature) plotted as time function, sample temperature, reference temperature or furnace temperature. (Yinon, et al., 1981)

While the sample undergoes reaction, additional heat is absorbed or dissipated producing a temperature rise or decrease when compared to the reference material. The thermogram provides an indication of the occurring reactions and which characterize the sample: the area under the curve is associated to the absorbed or given off energies. The system must be calibrated with reference materials of known heat content, as tin, indium and lead. (Yinon, et al., 1981)

**Differential Scanning Calorimetry (DSC).** In DSC, the reference material and the sample are enclosed on two separate small heaters. The reference material and sample temperatures are simultaneously monitored, and no temperature difference is allowed. The difference in power requirements for the two heaters is measured and recorded as time or temperature function. (Yinon, et al., 1981)

**Thermogravimetric Analysis (TGA).** In TGA, a sample's weight is recorded as temperature or time function, during its heating or cooling at a controlled rate in a controlled atmosphere. The sample can either lose weight to the atmosphere or gain weight by reaction with it.

The Derivative Thermogravimetric Analysis (DTA) measures the rate of weight change by taking the first derivative of the weight change with time. This technique displays more neatly the original curve details and facilitates the kinetic rates calculation.

### ***2.1.3.2. The Arrhenius approach to thermal decomposition***

The combustion involves chemical reactions that occur at finite velocities, which depend on local temperature, reactant species concentrations and, in some cases, pressure. The reaction velocity can be expressed as function of any chemical species properties (reactants or products), which are involved on the reaction. (Almada, 1998) Consequently, an exponential numerical approach can describe its evolution.

**The Arrhenius Equation.** A simple chemical reaction can be described by the following stoichiometric relation:



Where:

$n'_j, n''_j \rightarrow$  Reactants and products stoichiometric coefficients of the reaction, respectively

$M_j \rightarrow$  Arbitrary property common to all species involved in the chemical reaction

$v \rightarrow$  Total number of involved species

As the stoichiometric relation above, the velocity of a chemical reaction can also be expressed by any arbitrary property common to all species involved in the reaction. It is experimentally proved that:

$$\frac{d[M_j]}{dt} = k \prod_{j=1}^v [M_j]^{n'_j} \quad (67)$$

This equation means that the consumption rate of some specie ( $\frac{d[M_j]}{dt}$ ) is proportional to the product of the reactants species concentrations ( $[M_j]^{n'_j}$ ) which exponent is the correspondent stoichiometric coefficient;  $k$  is the proportionality constant known by specific velocity constant. The sum of  $n'_j$  is the reaction order, many times represented by  $n$ .

For a reversible reaction, in equilibrium, both reactions occur at the same velocity, so:

$$k \prod_{j=1}^v [M_j]^{n_j} = k' \prod_{j=1}^v [M_j]^{n'_j} \Leftrightarrow \frac{k}{k'} = \prod_{j=1}^v \frac{[M_j]^{n'_j}}{[M_j]^{n_j}} = K_p \quad (68)$$

$K_p$  is the equilibrium constant.

Van't Hoff concluded that the variation of the equilibrium constant with temperature ( $\frac{d(\ln k)}{dT}$ ) follows the bellow expression, where  $\Delta H^0$  is the enthalpy reaction and  $R$  is the perfect gas constant :

$$\frac{d(\ln k)}{dT} = \frac{\Delta H^0}{RT^2} \quad (69)$$

Integrating (69), the result is:

$$\ln k = -\frac{1}{T} \frac{\Delta H^0}{R} \Leftrightarrow k = e^{-\frac{\Delta H^0}{RT}} \quad (70)$$

As many chemical reactions occur at constant volume (in a limited recipient) or constant pressure (atmospheric pressure), especially the ones associated to combustion, we can consider that the variation of reaction enthalpy is equal to the variation of the internal energy.

Taking these considerations, focusing on (70), **Arrhenius equation** (71) is obtained:

$$k = A e^{-\frac{\Delta E}{RT}} \quad (71)$$

Enhance the following variables:

$\Delta E \rightarrow$  Activation energy (also represented by  $E_a$ ): excess of internal energy of the reactants needed to make the reaction occurs (units: 1/min)

$-\frac{\Delta E}{RT} \rightarrow$  Boltzmann factor: molecules fraction which has the necessary activation energy

$A \rightarrow$  Pre-exponential factor: resultant of the combination of other reaction parameters referred above (units: 1/min)

$R \rightarrow$  Gas constant ( $8.314 \text{ J K}^{-1}\text{mol}^{-1}$ )

$T \rightarrow$  Temperature (units: K)

From Arrhenius equation is important to remember that the reaction velocity increases with the increase of the temperature and, for high  $\Delta E$ , small increments in the temperature can cause high increases in reaction velocity (when ignition point is reached, for example).

**Arrhenius approach to combustion evaluation.** The chemical reactions involved in combustion processes depend on the local temperature, pressure and the reactant species concentrations. They occur at finite velocities. The most of these reactions follows first order kinetic, which means that the time needed to finish a portion of this reaction is independent of the initial concentration of the involved reactant species.

The consumption rate of a reactant specie, or fresh specie ( $f$ ), is equal to the formation rate of the product species, or burned species ( $b$ ), by (66) and (67) it is possible to write:

$$\sum_{j=1}^v n'_j [f] = \sum_{j=1}^v n''_j [b]$$

$$\frac{d [f]}{dt} = \frac{d [b]}{dt} = k \prod_{j=1}^v [b]^{n'_j} = k [b]^n \quad (72)$$

Applying the Arrhenius equation (71) to the formation rate (72) of a burned (or product) specie concentration ( $[b]$ ) in a combustion reaction with a first order kinetic:

$$\frac{d [b]}{dt} = k [b]^n = A e^{-\frac{\Delta E}{RT_b}} [b] \quad (73)$$

The velocity of the formation rate is given by:

$$\frac{dm_b}{dt} = \rho_f \nabla_F A_F \quad (74)$$

$m_b \rightarrow$  Burned species mass

$\rho_f \rightarrow$  Fresh species density

$v_F \rightarrow$  Flame fundamental velocity

$A_F \rightarrow$  Flame area

The concentration of burned species [b], or the mass loss in the reaction ( $\lambda$ ), can be seen as the coefficient between the burned mass ( $m_b$ ) and the total mass present in reaction ( $M_0$ ), which is the sum of the fresh mass ( $m_f$ ) with the burned mass:

$$[b] = \frac{m_b}{m_f + m_b} = \frac{m_b}{M_0} = \lambda \quad (75)$$

Applying (75) to (73):

$$\frac{d[b]}{dt} = \frac{d\lambda}{dt} = \lambda A e^{-\frac{\Delta E}{RT_b}} = Z e^{-\frac{\Delta E}{RT_b}} \quad (76)$$

Where  $Z = \lambda A$

Rearranging equation (75) and making its derived:

$$m_b = \lambda M_0 \Rightarrow \frac{dm_b}{dt} = M_0 \frac{d\lambda}{dt} \quad (77)$$

Making the substitution of (74) and (76) in (77):

$$\rho_f v_F A_F = M_0 Z e^{-\frac{\Delta E}{RT_b}} \quad (78)$$

Rewriting (76) bellow, it is possible to conclude that if you apply the Arrhenius equation the mass loss rate is directly proportional to burned species concentration, to pre-exponential factor A and to  $e^{-\frac{\Delta E}{RT_b}}$ , so the mass loss rate ( $\frac{d\alpha}{dt}$ ) is:

$$\frac{d(\frac{m_b}{M_0})}{dt} = Z e^{-\frac{\Delta E}{RT_b}} = \frac{d\alpha}{dt} \quad (79)$$

Equation (79) is very important experimentally, because it permits the calculation of Z and  $T_b$ . The mathematical method used to do this is applying ln to both side of the equation, which gives:

$$\ln\left(\frac{d\alpha}{dt}\right) = \ln Z - \frac{\Delta E}{RT_b} \quad (80)$$

**Arrhenius approach to DSC/TGA kinetics – Borchardt & Daniels Method.** According with (Rheometric Scientific , 1995), Borchardt & Daniels Method (199), DSC kinetics can be defined two main equations: the Arrhenius expression for the specific rate constant (equation (81), Z and E have the same meaning than A and  $\Delta E$  in equation (71)

and the equation that must be defined relates the reaction progress (or mass loss rate) with time through the use of the rate constant (equation (82)).

$$k(T) = Z e^{-\frac{E}{RT}} \quad (81)$$

$$\frac{d\alpha}{dt} = k (1 - \alpha)^n \quad (82)$$

Where  $\alpha$  is the percent conversion (reaction progress or mass loss rate) and  $n$  the reaction order.

The **Borchardt & Daniels** calculation starts substituting equation (81) for the specific rate constant into equation (82):

$$\frac{d\alpha}{dt} = Z e^{-\frac{E}{RT}} (1 - \alpha)^n \quad (83)$$

Applying the natural logarithm of both sides gives:

$$\ln\left(\frac{d\alpha}{dt}\right) = \ln Z - \frac{E}{RT} + n \ln(1 - \alpha) \quad (84)$$

Combustion reactions follow a first order kinetic and  $\alpha$  varies between 0 and 1, which make the last term negligible, conducting to equation (80). This last referred equation (80) can be associated to the linear equation of type  $y = mx + b$ , where:  $y = \ln\left(\frac{d\alpha}{dt}\right)$ ;  $m = -\frac{\Delta E}{R}$ ;  $x = \frac{1}{T}$ ;  $b = \ln Z$ , which make this equation very useful for experimental numerical approaches.

### 2.1.3.3. Results and discussion from literature

#### 2.1.3.3.1. Ammonium Nitrate (AN)

AN is a quite peculiar crystal because, under ordinary pressure, it presents up to five polymorphic modifications. The study of these phase transitions and how to stabilize them are essential to use AN as energetic oxidant material (Simões, et al., 1998) (Oommen, et al., 1999) (Oommen, et al., 1999(2)) (Portugal, et al., 2000).

Transitions temperatures of various phases are represented on Figure 24.

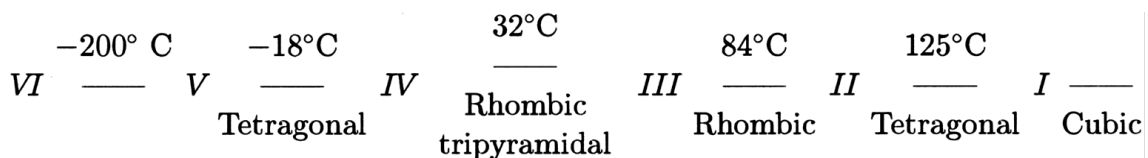


Figure 24: Phase modifications and respectively temperature transitions for ammonium nitrate (Oommen, et al., 1999)

The crystallographic data and stability ranges of each phase are shown on Table 6. Besides those transformations referred on Figure 24 and on Table 6, a metastable transition at 45-50°C was also described. There are also descriptions about modifications under low temperatures (Théorêt, et al., 1964) and at high pressures. Those modifications result on a phase VII below -170°C, and on a transition at high pressures ( $> 9000 \text{ kg/cm}^2$ ) above 160°C.

Table 6: Crystallographic data and stability ranges of the AN phases (Oommen, et al., 1999)

| Phase                     | V   | IV  | III   | II                              | I           |
|---------------------------|---|---|---|---------------------------------|-------------|
| Crystal system            | Orthorh.                                  | Orthorh.                                  | Orthorh.                                    | Tetrag.                         | Cubic       |
| Space group               | <i>Pccn</i>                               | <i>Pmmm</i>                               | <i>Pnma</i>                                 | <i>P4/mbm</i>                   | <i>Pm3m</i> |
| Formula per unit cell (Z) | 8   | 2   | 4   | 2                               | 1           |
| Lattice parameters        | $a = 7.943$<br>$b = 7.972$<br>$c = 9.832$ | $a = 5.745$<br>$b = 5.438$<br>$c = 4.942$ | $a = 7.7184$<br>$b = 5.8447$<br>$c = 7.162$ | $a = 5.7193$<br><br>$c = 4.932$ | $a = 4.366$ |
| Measured at (K)           | 173                                       | 295                                       | 318   | 355                             | 423         |
| Stability ranges (K)      |   |   |   |                                 |             |
| Humid                     | < 255                                     | 255–305                                   | 305–357                                     | 357–398                         | > 398       |
| Dry                       | < 255                                     | 255–328                                   | –   | 328–398                         | > 398       |

Fusion temperature (169.6 °C) and transition temperature at 125°C are well defined, but the temperature transition IV-III is ambiguous and widely debated. This transition is especially important, because it occurs near ambient temperature. The principal founded reasons for the difficulty in stabilizing this transition phase, are moisture, thermal history of the sample, sample weight, mode of crystallization, number of previous transformation and heating mode, purity of sample, stabilization additives, grain size and employed experimental technique.

Literature (Davis, et al., 1996) (Simões, et al., 1998) (Oommen, et al., 1999) (Oommen, et al., 1999(2)) (Portugal, et al., 2000) shows that the phase transitions are dependent of maximum chosen temperature and the water quantity present on the sample.

To better understand the phase transitions behaviours, Oommen et al., 1999, performed thermal cycles (20/150/-50°C) to AN and the obtained results are present on Figure 25 and on Table 7. They founded, besides the transition II-I at 125°C, dry AN suffers the phase transitions IV-II-I-IV-V. If AN is wet, the phase III appears during the heating, but not during the cooling and the followed path is IV-III-II-I-II-IV-V. When the thermal cycle is programmed to reach a maximum temperature of 125°C (avoiding phase transition II-I), the dry AN shows the transitions: IV-II-IV-V, while wet AN follows IV-III-II-II-IV-V phase transitions. These referred phase changes are described

on Table 7, as well as their peaks temperatures and the enthalpies of involved transitions, respectively.

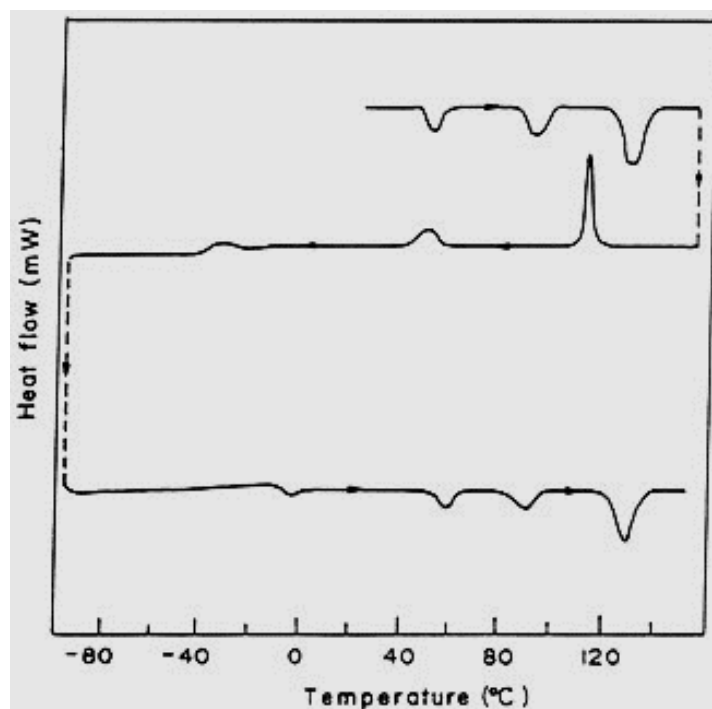


Figure 25: DSC trace of AN on thermal cycling (Oommen, et al., 1999)

Table 7: Heat of phase transitions of AN from Figure 25. (Oommen, et al., 1999)

| Apparent phase change | Peak temperature (°C) | Enthalpy change ( $\Delta H$ , cal/g) |
|-----------------------|-----------------------|---------------------------------------|
| IV-III                | 49                    | 3.68                                  |
| III-II                | 92                    | 3.94                                  |
| II-I                  | 129                   | 11.89                                 |
| I-II                  | 116                   | 10.60                                 |
| II-IV                 | 43.8                  | 4.87                                  |
| IV-V                  | -36.9                 | 1.37                                  |
| V-IV                  | -5                    | 0.89                                  |

The DSC thermogram on Figure 26 (Davis, et al., 1996) is an example of a pure AN sample subjected to a 50°C/min heating rate (fast thermolysis). It is possible to see the transitions IV-II at 51°C, II-I at 124°C. These transitions are in the same temperature range than the described above (deviations 2 and 5°C, respectively). The melting point appears at 124°C (concordant with the 125°C described above) and the endothermic at 257°C corresponds to the AN thermal decomposition.

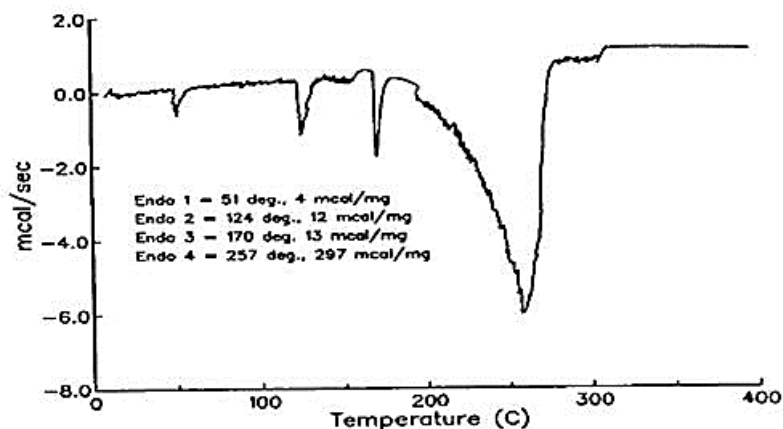


Figure 26: DSC thermogram of pure AN, acquired with a heating rate of 50°C/min (Davis, et al., 1996)

Stabilizing the IV to III phase transition, at room temperature, was a concern of explosives development. The obtained PSAN (Phase Stabilized Ammonium Nitrate) have Ni, Cu or Zn oxides as additives for direct phase change IV-II.

The pure AN and PSAN were compared by DSC analysis (Oommen, et al., 1999(2)) and the results are shown on Figure 27. The first thermogram shows all the reported transitions that can occur from ambient until upper temperatures. Those transitions are: IV-III transition at 40°C, III-II transition at 85°C, and the peak at 125 ° C corresponds to II-I transition, 125°C is the melting point and the endothermic thermal decomposition is present at 260°C. The last referred peak is characteristic of reaction (1).

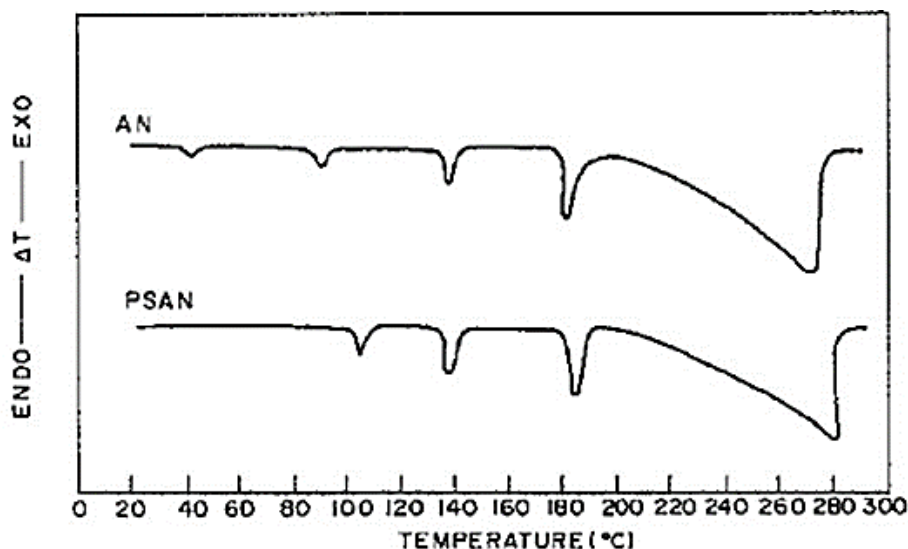


Figure 27: DSC traces of AN and PSAN samples (Oommen, et al., 1999(2))

The only difference between AN and PSAN (vd. Figure 27) is that AN shows the III-II transition phase and PSAN does not. So, to study the thermal decomposition kinetics of AN it can be used AN or PSAN, because the thermal decomposition occurs at the same temperature for both compounds.

Several studies (Almada, 1998) (Simões, et al., 1998) (Portugal, et al., 2000) present the thermal decomposition of PSAN and its kinetic parameters. The thermograms acquired to show the PSAN thermal decomposition are shown in Figures 28 and 29 (Portugal, et al., 2000) (Simões, et al., 1998). The first one shows five different physical solid state phases in the temperature range of  $-18$  until  $125^{\circ}\text{C}$ . The three first peaks, in thermogram, correspond to the following phase changes: solid phase IV directly to solid phase II ( $T \approx 53^{\circ}\text{C}$ ); solid phase II to solid phase I ( $T \approx 125^{\circ}\text{C}$ ); and melting point ( $T \approx 169^{\circ}\text{C}$ ). The fourth peak corresponds to AN thermal decomposition at  $210^{\circ}\text{C}$ , characterized by reactions (1), (2), (3), (6) and (7), (8).

The second one (Figure 29) was acquired to study of the decomposition of PSAN by simultaneous thermal analysis for determination of kinetic parameters (Simões, et al., 1998).

A very similar thermogram was acquired to study the thermal explosion of energetic materials, including PSAN (Almada, 1998). PSAN under a heating rate of  $10^{\circ}\text{C}/\text{min}$ , presents the same four endothermic peaks at  $55.52$ ,  $129.20$ ,  $169.39$  and  $272.73^{\circ}\text{C}$  associated the first two to phase transitions, the third to melting and the fourth to the decomposition reaction. The kinetic parameters obtained on this study are presented at Table 9.

The main thermal decomposition products are  $\text{N}_2\text{O}$  and  $\text{H}_2\text{O}$  result from the exothermic decomposition reaction (2). This has been explained (Simões, et al., 1998) due to the occurrence of the endothermic dissociation reaction (1), which is coupled with the decomposition reaction. This coupling is both kinetic and thermal. The thermal behaviour (endothermic or exothermic) depends on the absence of conditions favorable to the occurrence of an auto-catalytic regime. The heat produced by the exothermic decomposition can then be absorbed by the dissociation reaction - this explain the observed endothermic peaks.

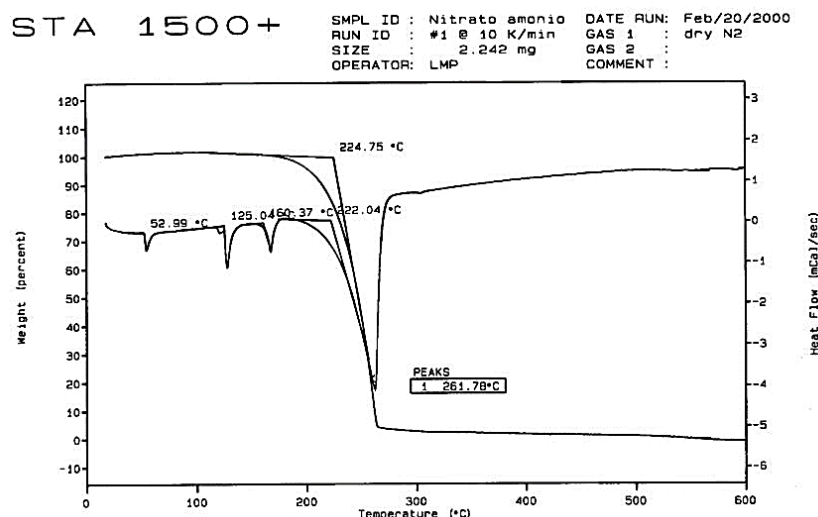


Figure 28: PSAN thermogram acquired by DSC/TGA at an heating rate of 10°C/min (Portugal, et al., 2000)

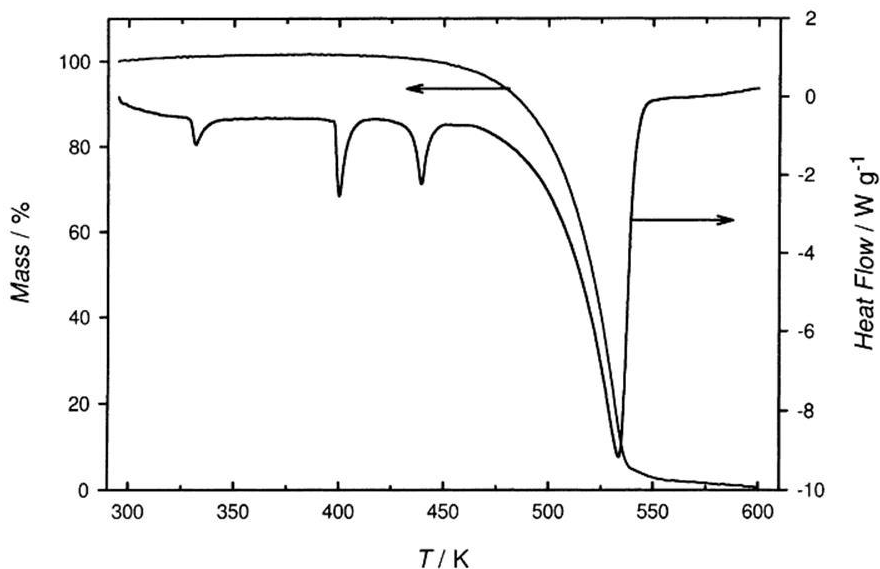


Figure 29: Typical DSC/TGA thermograms for PSAN (Simões, et al., 1998)

Table 8: Endothermic peak temperatures (K) for each phase transition and decomposition of PSAN, where  $\beta$  is the used heating rate.

| $\beta$ (K min <sup>-1</sup> ) | Transformation |           |           |               |
|--------------------------------|----------------|-----------|-----------|---------------|
|                                | IV→II          | II→I      | I→Melt    | Decomposition |
| 2.5                            | 330.1±0.1      | 398.3±0.1 | 437.0±1.4 | 497.0±1.7     |
| 5                              | 330.5±0.4      | 398.7±0.3 | 438.4±0.9 | 515.5±2.3     |
| 10                             | 331.6±0.3      | 399.4±1.9 | 439.2±0.4 | 533.7±0.7     |
| 15                             | 332.0±0.4      | 400.1±0.4 | 439.6±0.2 | 545.5±0.9     |
| 20                             | 332.3±0.3      | 400.6±0.5 | 439.6±0.3 | 551.6±1.4     |

Table 9: Experimental values for activation energy and pre-exponential factor for thermal decomposition kinetics of AN and PSAN

| Reference                 | Compound | Activation energy<br>E (J/mol) | Pre-exponential factor<br>A (1/min) |
|---------------------------|----------|--------------------------------|-------------------------------------|
| (Vyazovkin, et al., 2001) | AN       | 1.14E+05                       | 3.16E+08                            |
| (Vyazovkin, et al., 2001) | AN       | 8.15E+04                       | 1.58E+08                            |
| (Almada, 1998)            | PSAN     | 2.10E+05                       | 3.97E+15                            |

#### 2.1.3.3.2. Urea Nitrate

Urea nitrate (UN) is “similar” to AN, but its molecular structure is quite different. It is interesting to remember that nitrates with an organic cation (carbon and hydrogen sources incorporated on molecule, as UN) are very energetic explosive candidates. (Oxley, et al., 2009) Furthermore, UN does not need a fuel source to generate an explosion.

Figure 30 shows two different DSC thermograms acquired by the same author on different years. (Oxley, et al., 2009) (Oxley, et al., 2013) On both UN thermograms is possible to observe three different thermal events (values refer always first for the left thermogram and second for the right thermogram, on Figure 30): an exothermic peak at 166°C and 162°C, immediately after, a tight exothermic peak at 172°C and 167°C; at the end, an exothermic peak at 403°C and 380°C. These temperature shifts are, probably, due to the different heating rates employed.

As described on 2.1.1.2, UN decomposes in condensed-phase and gaseous species at high temperatures.

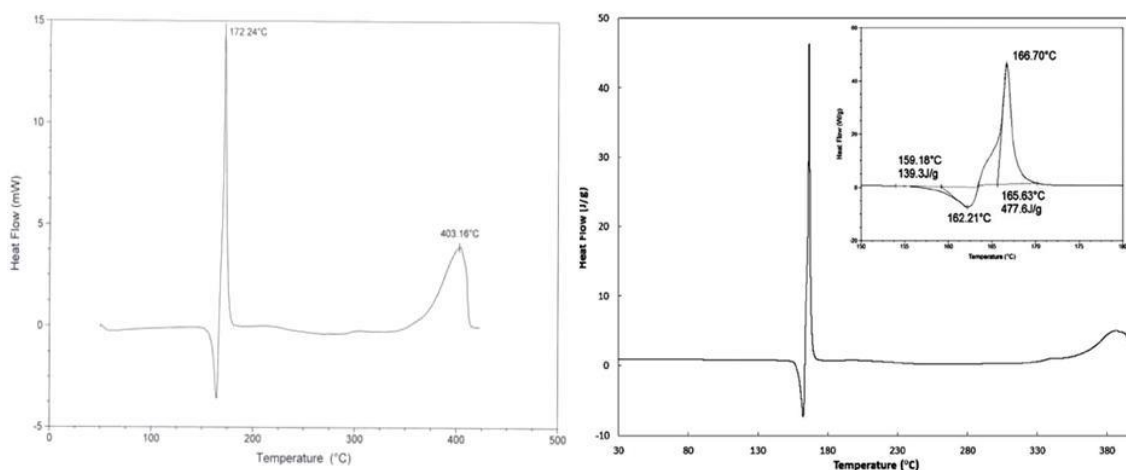


Figure 30: DSC thermograms at 20°C/min (Oxley, et al., 2009) and 10°C/min (Oxley, et al., 2013), respectively

Using different thermogravimetric analysis techniques, the heat flux profiles are also different. (Désilets, et al., 2011(2)) (vd. Figures 30 and 31, or just in Figure 31). The heat flux obtained by the coupled technique DSC/TGA is attenuated, compared with the same heat flux obtained only by DSC. This is, probably, because the sample container (alumina crucibles) is open at on extremity, or due to the high ratio between volumes of DSC/TGA oven/sample container, which makes that decomposition reaction cannot advance to an auto-catalytic stage. Other factor (that contributed for the different heat fluxes) was the competitive endothermic volatilization between the reactive gases, which occurs at DSC/TGA. This fact is verified through the mass losses acquired by TGA.

The TGA result (Désilets, et al., 2011) shows three mass losses which begins at 133, 168 and 276°C, as indicated on Figure 31. The beginning of the first mass loss coincides with the first endothermic peak, continues to rapidly go down until 40% of the mass volatilize, and ends when the endothermic peak turns into the exothermic peak. At 168°C, the maximum of the exothermic peak, takes place the second mass loss, which is responsible for the consumption of 54% of the mass sample. The final mass loss begins at 276°C and ends at 330°C, and corresponds of the final 6% of the remaining mass (the sample container has no residues at the end of the experiment).

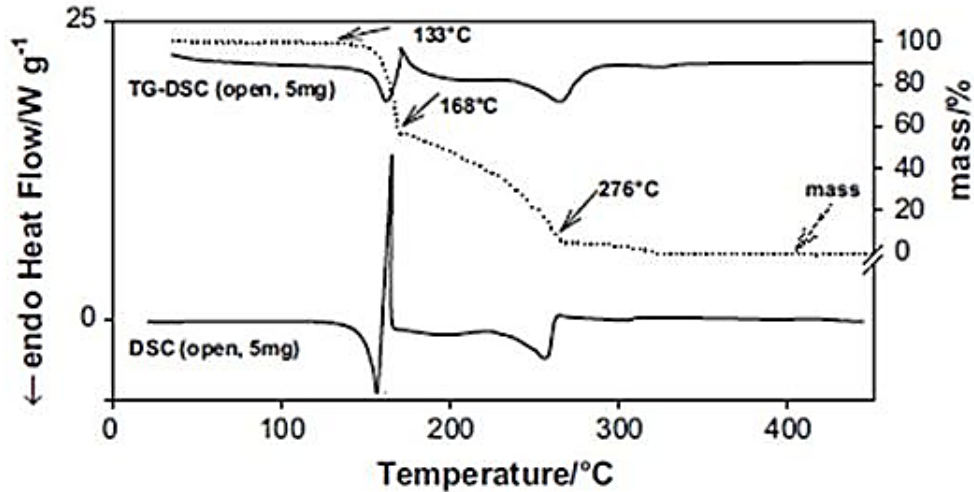


Figure 31: UN thermograms, with a heating rate of 5°C/min. (Désilets, et al., 2011(2))

Oxley et al., 2009, and Désilets et al., 2011(2) calculated the Arrhenius activation energy ( $E_a$ ) and its pre-exponential factor ( $Z$ ). Oxley et al., 2009, used ATSM E 698 method, and Désilets et al., 2011(2) used Kissinger method according to ASTM E698-05. Their results are presented at Table 10 Arrhenius activation energy ( $E_a$ ) and  $Z$  (pre-exponential factor) calculated for Figure 30 and Figure 31.

Table 10 Arrhenius activation energy ( $E_a$ ) and  $Z$  (pre-exponential factor) calculated for Figure 30 and Figure 31, respectively

| Reference                   | Endothermic Peak |                          | Major Exothermic Peak |                          |
|-----------------------------|------------------|--------------------------|-----------------------|--------------------------|
|                             | $E_a$ (kJ/mol)   | $Z$ (min <sup>-1</sup> ) | $E_a$ (kJ/mol)        | $Z$ (min <sup>-1</sup> ) |
| (Oxley, et al., 2009)       | 158              | 1.39E+12                 | 131 ± 13              | 2.66E+09                 |
| (Désilets, et al., 2011(2)) | 225 ± 76         | 31 ± 14                  | 206 ± 13              | 47 ± 4                   |

## 2.1.4. Infra-Red Spectroscopy

### 2.1.4.1. Introduction fundamentals

According to literature (Yinon, et al., 1981), Infra-Red (IR) spectroscopy irradiates the sample with light from the infra-red region with wavelength ( $\lambda$ ) between 2.5 and 15 $\mu$ m (IR frequencies are of the same magnitude order as the molecular vibrational frequencies).

When incident radiation has the same frequencies as molecular vibrational frequencies, the molecule absorbs it while transmits the other frequencies which composes the incident radiation. The amount of energy ( $E$ ) absorbed is given by equation (85) where  $h$  is Planck's constant and  $\nu$  the molecule vibrational frequency.

$$E = h\nu \quad (85)$$

In an IR spectrometer, the sample is irradiated with light throughout the whole IR frequency range. As a result, the IR spectrum plots the sample transmittance as function of wavelength or wavenumber. The wavenumber unit is  $\text{cm}^{-1}$ , where  $1 \text{ cm}^{-1} = 10^4/\lambda$  ( $\mu\text{m}$ ). The transmittance is defined as the ratio of the incident power to the transmitted radiation power.

For analytical applications, the vibrations of organic molecules can be divided in two: vibrations associated with the molecule as a whole and vibrations associated with specific functional groups.

The vibrations associated to the molecule as a whole typically generate absorption bands at wavenumbers bellow  $1300 \text{ cm}^{-1}$ . This region is called "fingerprint region", because the referred absorption bands positions characterize the particular molecule and, hence, they can be used as "fingerprints" to identify unknown samples by comparison with known compounds. Table 11: IR characteristic bands of explosives and some correlations summarizes some spectral correlations in the main groups of explosive compounds, i.e., the vibrations associated to the molecule as a whole.

Table 11: IR characteristic bands of explosives and some correlations (Yinon, et al., 1981)

| Type of Explosive   | Bands ( $\text{cm}^{-1}$ ) | Comments   |
|---|----------------------------|--|
| <i>sym</i> -trinitrocompounds which have the following additional groups: $\text{CH}_3$ , $\text{C}_2\text{H}_5$ , $\text{OCH}_3$ , $\text{OC}_2\text{H}_5$ , $\text{COOH}$ , $\text{OH}$ , $\text{NH}_2$   | 1081                       | The band appears to shift to about $1070 \text{ cm}^{-1}$ in the presence of acidic groups as $\text{COOH}$ or $\text{OH}$                         |
| <i>m</i> -dinitrocompounds which have the following additional groups: $\text{CH}_3$ , $\text{C}_2\text{H}_5$ , $\text{OCH}_3$ , $\text{CHO}$ , $\text{COOH}$ , $\text{OH}$ , $\text{N}=\text{NH}_2$ , $\text{CH}_3\text{NH}$ , $\text{C}_2\text{H}_5\text{NH}$ | 913 - 922                  |  |
| <i>m</i> -dinitrocompounds where other additional groups, if any, were ortho to the nitro   | 830 - 840                  | Not found in <i>sym</i> -trinitrocompounds but present in 2,3,4 and 2,4,5-TNT. Absent in 1,5-dinitrobenzoic acid and 4,6-dinitro- <i>o</i> -cresol |
| Trinitrocompounds   | 909-930                    |  |

|  |                    |   |
|--|--------------------|---|
| <i>o</i> -mononitrocompounds which have one of the following groups ortho to the nitro: CH <sub>3</sub> , C <sub>2</sub> H <sub>5</sub> , CHO, COOH, NH <sub>2</sub> | 781-787            | Not usually found in dinitro or trinitrocompounds |
| <i>p</i> -mononitrocompounds which have one of the following groups ortho to the nitro: CH <sub>3</sub> , C <sub>2</sub> H <sub>5</sub> , CHO, COOH, NH <sub>2</sub> | 1111               | Not usually found in dinitro or trinitrocompounds |
| Nitramines   | 1282               |   |
| Organic nitrates   | 833, 1282,<br>1667 |   |
| Inorganic nitrates   | 833                |   |

The vibrations associated with functional groups generally produce absorption bands in the region above 1300 cm<sup>-1</sup>. These “group frequencies” permit the identification of specific functional groups inside a molecule and play, thus, an important role in structure clarification of unknown compounds. Table 12 is representative of the wave number ranges (1200 cm<sup>-1</sup> to 3100 cm<sup>-1</sup>) and group assignments for spectra features usually observed in explosives IR spectra.

Table 12: Mode assignment and respective wavenumber range, with examples of known explosive types or energetic materials (EM), for spectral features commonly observed in the IR spectra of explosives (McNesby, et al., 2002)

| Mode assignment                    | Example or type of explosive or EM   | Wavenumber (cm <sup>-1</sup> ) |
|------------------------------------|--------------------------------------|--------------------------------|
| NO <sub>2</sub> symmetric stretch  | Nitramine (RDX)                      | 1260 - 1320                    |
| CH <sub>2</sub> bend               | Nitramine (RDX), TNT                 | 1300 - 1450                    |
| NO <sub>2</sub> asymmetric stretch | Nitramine (RDX), TNT                 | 1450 - 1600                    |
| C-H stretch                        | Nitramine (RDX), TNT, nitrocellulose | 2900 - 3100                    |
| C-C stretch                        | TNT                                  | 1620 - 1700                    |
| NO <sub>2</sub> symmetric stretch  | TNT                                  | 1325 - 1375                    |
| NO <sub>2</sub> symmetric stretch  | Nitrocellulose                       | 1200 - 1300                    |
| NO <sub>2</sub> asymmetric stretch | Nitrocellulose                       | 1600 - 1700                    |

The identification of compounds by “fingerprint” comparison and the location of functional groups in unknown compounds have made IR spectroscopy one of the most extensively used analytical techniques for organic compounds identification.

When the samples are in solid state, the methodology employed was the KBr technique, where the sample is milled with potassium bromide (in 1 to 100 ratio) and then mechanically pressed into a pellet which is placed in the IR

Many IR spectra compilations were published. From the particular case of explosives it can be mentioned NICODOM IR Explosives (NICODOM, 2012).

IR spectroscopy was also used for quantitative explosive analysis. Quantitative analysis of known mixtures can be done successfully by using suitable absorption bands which are well separated from each other.

### *2.1.4.2. Results and discussion from literature*

#### *2.1.4.2.1. Ammonium Nitrate*

The main products of the AN thermal decomposition are assumed as  $\text{NH}_3$ ,  $\text{HNO}_3$ ,  $\text{N}_2\text{O}$ ,  $\text{H}_2\text{O}$ ,  $\text{N}_2$ ,  $\text{NO}_2$  and  $\text{NO}$ .

The IR spectra, presented at Figure 32, was acquired to experimentally demonstrate the thermal decomposition of AN (aerosol) at high temperatures (Patil, et al., 1992). Following equation (23), the present products in the referred conditions are  $\text{N}_2\text{O}$ ,  $\text{H}_2\text{O}$ ,  $\text{NH}_4\text{NO}_3$  (AN),  $\text{N}_2$  e  $\text{NO}_2$ .

The reaction products appear on the IR spectra (Figure 32) on the following vibrational modes:  $\text{H}_2\text{O}$  at  $3200\text{ cm}^{-1}$ ; around  $2200\text{ cm}^{-1}$  it is  $\text{N}_2\text{O}$ ; the  $\text{NO}_2$  appears at  $1650\text{ cm}^{-1}$ ; the presence of AN is seen at  $1350\text{ cm}^{-1}$ ;  $\text{NH}_3$  appears around  $850\text{ cm}^{-1}$ . As expected, due to be a bi-atomic molecule with identical atoms,  $\text{N}_2$  vibrational modes are not detected on the IR spectra. The  $\text{N}_2\text{O}$  increase concentration is indicative of extensively decomposition of AN at high pressures.

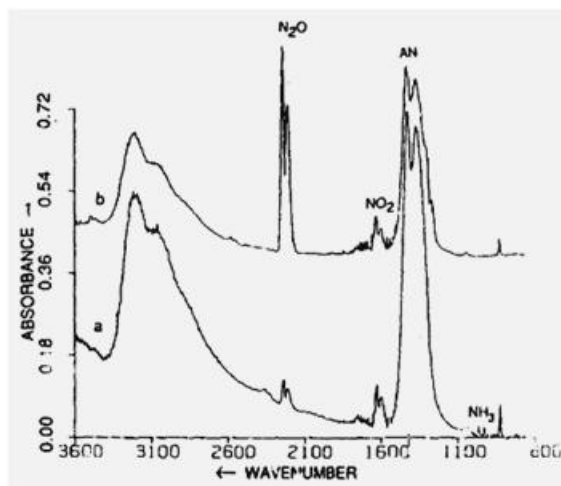


Figure 32: IR spectra of the decomposition products of AN in the gas phase after 10 s at (a) 15 psi, (b) 280 psi of argon. The thermal decomposition was made by DSC/TGA coupled with rapid-scan FT-IR, at a heating rate of 80°C/min

#### 2.1.4.2.2. Urea Nitrate

When the UN thermal decomposition mechanism at low temperatures was studied (Désilets, et al., 2011), it was applied IR spectroscopy to the residue resulting from that thermal decomposition. The acquired spectrum is shown on Figure 33, as well as the characteristic elongations of each detected compound are indicated.

During the UN thermal decomposition at low temperatures (Désilets, et al., 2011), there were acquired two IR spectra, the first one 24h after the exposition of UN at 100°C and the second 48h later. The first acquired spectrum was very similar to the one that will be present on *Chapter 3* (for reactants IV characterization), in Figure 143, which means that UN was slightly decomposed. 48h after the exposure at 100°C, the obtained spectrum is shown at Figure 33 and indicates a strong presence of AN, the presence of urea, as the disappearance of the UN characteristic band at 2410 cm<sup>-1</sup>. During the referred work, there were acquired more IV spectra (but spectra not shown on the article), 72 and 144h after 100°C exposure. The results showed, again, the presence of AN and urea, as well as other similar structures to urea.

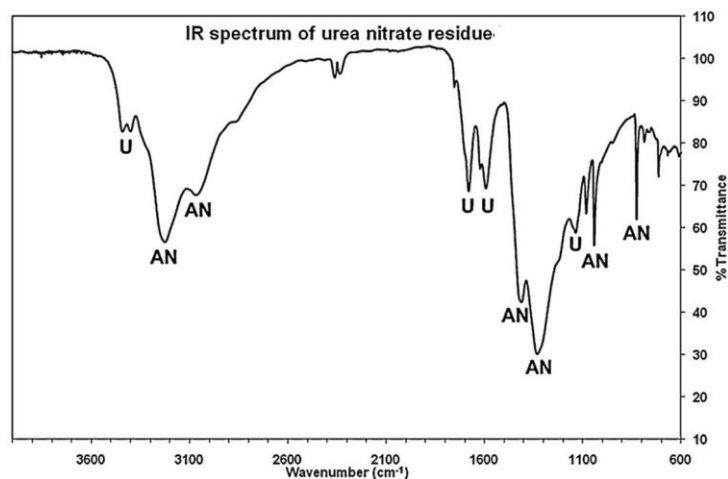


Figure 33: IR spectrum of urea nitrate residue obtained from the UN thermal decomposition at low temperatures (Désilets, et al., 2011).

When the UN thermal decomposition mechanism at high temperatures was studied (Désilets, et al., 2011(2)), there was no possibility of determining, by IR spectroscopy; the liberated gases during the first mass loss (see Figure 31, between 133 and 168°C), due to their rapid volatilization from the sample container. However, it was possible to determine the IR spectra of this thermal decomposition at 143, 150 and 190°C. These spectra are shown on Figure 34, as well as the characteristic elongations of present molecules. The gaseous products formed at 140°C (Figure 34, A spectrum), due to the UN thermal decomposition, were: nitric acid (HNO<sub>3</sub>), carbon dioxide (CO<sub>2</sub>) and nitrous oxide (N<sub>2</sub>O). While temperature was rising until 150°C, near to the melting point, the acquired spectrum (Figure 34, B spectrum) showed the presence of the before referred gases, plus isocyanic acid (HNCO), here detected for the first time. Ammonia (NH<sub>3</sub>) was detected from 170°C. At 190°C, as shown in spectrum C of Figure 34, were detected NH<sub>3</sub>, HNCO, N<sub>2</sub>O e CO<sub>2</sub>.

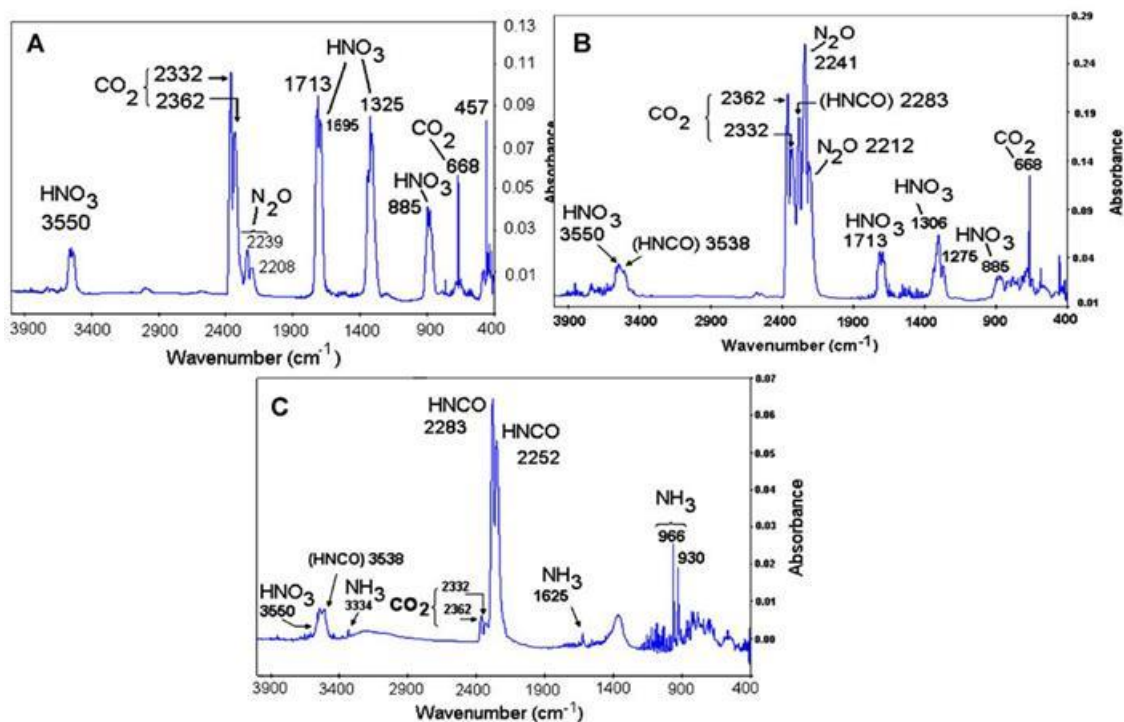


Figure 34: FTIR spectra acquired during the thermal decomposition, made by TGA, of UN at: (A) 143°C, (B) 150°C and (C) 190°C (Désilets, et al., 2011(2)).

In even harsher conditions (Hiyoshi, et al., 2002), were obtained the spectra showed on Figure 35. The gaseous products obtained from UN (T-jump/FT-IR system) heated at 400°C in 8 atm of Ar (Figure 35 (a)) were primarily HCNCO (2281  $\text{cm}^{-1}$ , 2256  $\text{cm}^{-1}$ ),  $\text{CO}_2$  (2359  $\text{cm}^{-1}$ , 2341  $\text{cm}^{-1}$ ),  $\text{N}_2\text{O}$  (2235  $\text{cm}^{-1}$ , 2214  $\text{cm}^{-1}$ ),  $\text{NH}_3$  (966  $\text{cm}^{-1}$ , 930  $\text{cm}^{-1}$ ), and  $\text{H}_2\text{O}$  (rotational structure centered at about 1600 $\text{cm}^{-1}$ ). AN and an unidentified product dominate at longer times. A typical residual spectrum from subtraction of the known products from UN decomposition is shown in Figure 35 (B) which helped the identification of remaining products. The band at 1430  $\text{cm}^{-1}$ , and the broad Fermi resonance triplet at 2950 - 3220 $\text{cm}^{-1}$  were assigned to AN. The multiple bands at 2150 - 2300 $\text{cm}^{-1}$  and 1200 - 1500 $\text{cm}^{-1}$  are assumed to be from  $\text{NH}_4\text{NCO}$ ,  $\text{NH}_4\text{OCN}$ , and species containing  $-\text{C}=\text{N}$  and  $-\text{C}\equiv\text{N}$ , such as cyanamide, dicyandiamide, and related cyclic azines.

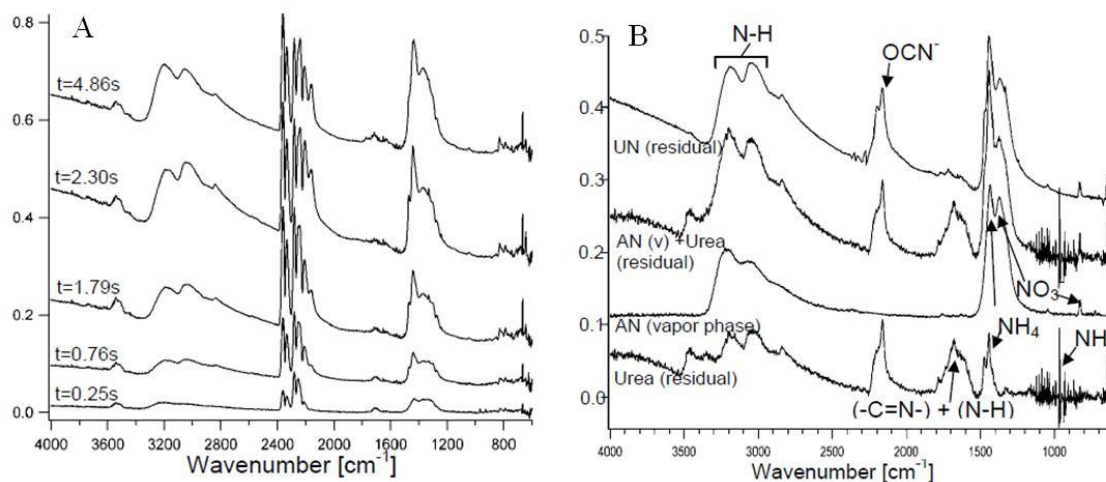


Figure 35: FTIR spectra of (A) time dependence of the IR spectra of decomposition products of UN in Ar, and (B) decomposition products of UN and urea in Ar, both for 8 atm and 400°C (Hiyoshi, et al., 2002)

## 2.2. Predicting calculations

The computational prediction study of the thermal decompositions of AN and UN uses the thermochemical computer code THOR.

All the calculations were performed, for an imposed P and T values, to obtain the chemical products composition for the minimum Gibbs free enthalpy result.

The products compounds were chosen as a combined matrix of reactant atomic species. Possible molecules from combined atoms were proposed by NASA thermobuild. (NASA, 2003)

### 2.2.1. Ammonium nitrate thermal decomposition prediction

#### 2.2.1.1. Methodology and results

Ammonium nitrate ( $NH_4NO_3$ ) is a molecule composed by nitrogen (N), hydrogen (H) and (C) carbon atoms. NASA thermobuild (NASA, 2003) proposed product molecules. From the 40 proposed products molecules it were selected 20.

After several tentative calculations it were selected the best 16 products molecules and composition, always for an isobar adiabatic combustion regime. The used criteria was

the validity of  $\Gamma$  and  $\gamma$  results. It is remembered that (vd. Equation (86)), with  $hdP = 0$ ,  $edV = 0$  and  $\gamma = c_p/c_v$ :

$$\begin{aligned}
 \Gamma = \left. \frac{dH}{dE} \right|_S &\Leftrightarrow \Gamma = \frac{\frac{\delta H}{\delta T} dT + \frac{\delta H}{\delta P} dP}{\frac{\delta E}{\delta T} dT + \frac{\delta E}{\delta V} dV} \Leftrightarrow \\
 &\Leftrightarrow \Gamma = \frac{c_p dT + h dP}{c_v dT + e dV} \Leftrightarrow \\
 &\Leftrightarrow \Gamma = \frac{c_p dt}{c_v dt} \Leftrightarrow \Gamma = \frac{c_p}{c_v} \Leftrightarrow \\
 &\Leftrightarrow \Gamma = \gamma
 \end{aligned} \tag{86}$$

Where the validity of  $\Gamma \approx \gamma$  is applied for no phase transition between combustion products.

The best decomposition products were:  $H_2O$ ,  $H_2$ ,  $N_2$ ,  $O_2$ ,  $H$ ,  $O$ ,  $N$ ,  $NO$ ,  $OH$ ,  $NO_2$ ,  $H_2O_2$ ,  $NH_3$ ,  $HNO_3$  (g),  $NH_2OH$ ,  $NH_2O_2$  and  $N_2H_4$ , because gammas values were always equal between them, on a range from 1.16 to 1.23.

The methodology employed to simulate the thermal decomposition was to vary the formation enthalpy on the thermochemical data base, on a range of -365.1792 to 35.1792 kJ/mol. Thermal decomposition on THOR can be simulated assuming the chosen formation enthalpy of the reactant to be equal to the original enthalpy of reactant, added or subtracted by the value of enthalpy transferred to the environment.

From the 16 selected decomposition products, just 13 appeared with a molar fraction superior to  $10^{-7}$ . They were  $H_2O$ ,  $N_2$ ,  $O_2$ ,  $H_2$ ,  $H$ ,  $O$ ,  $NO$ ,  $OH$ ,  $NO_2$ ,  $H_2O_2$  and  $HNO_3$  (g). The results for products present at thermal decomposition of AN, as a function of temperature, are shown at Figure 36.

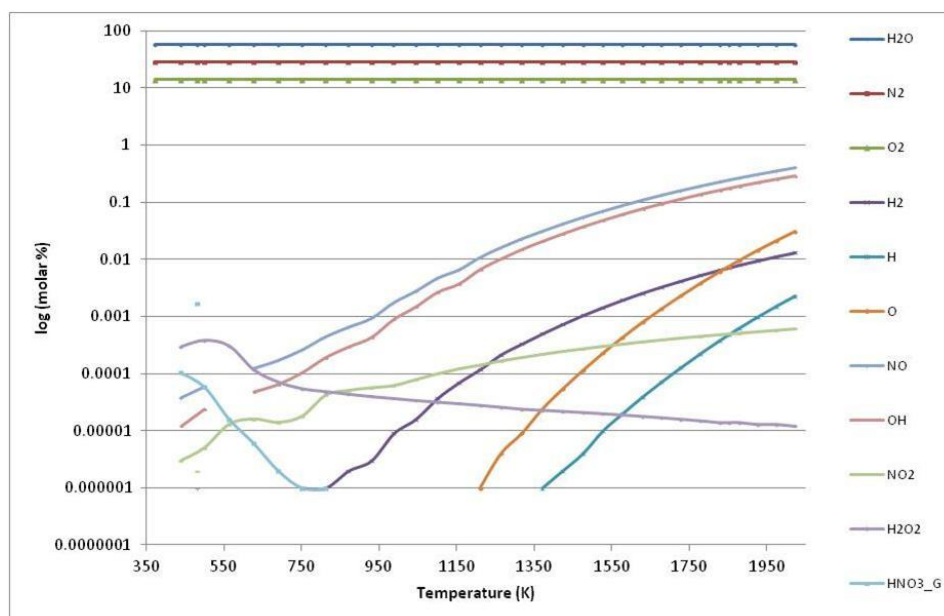


Figure 36 Products decomposition of AN as a function of temperature

### 2.2.1.2. Comparison between experimental results and literature

Thor predicting decomposition species of Ammonium Nitrate, as a function of temperature, presented in Figure 36, show clearly two zones: the first zone is formed by  $\text{H}_2\text{O}$ ,  $\text{N}_2$  and  $\text{O}_2$ , (major equivalent species formed for the same global enthalpy) followed by the others that really shown AN decomposition.

The **AN thermal decomposition mechanism at low temperatures** is observed until around 550 K (temperature near 270°C) (Figure 36). Besides the presence of major equivalent species ( $\text{H}_2\text{O}$ ,  $\text{N}_2$  and  $\text{O}_2$ ), there are also present:  $\text{H}_2\text{O}_2$ , which gets its maximum concentration at 550 K;  $\text{HNO}_3$ , which concentration is continuously decreasing during the referred temperature range;  $\text{NO}_2$  with an unstable concentration until around 950 K;  $\text{NO}$  and  $\text{OH}$ , whose presence stop at 550 K, showing the end of AN thermal decomposition at low temperatures. At this temperature range, according to reactions (1), (6), (7) and (8) (2.1.1.1), the formed species described by literature are;  $\text{HNO}_3$ ,  $\text{H}_2\text{O}$ ,  $\text{NH}_3$  and  $\text{N}_2\text{O}$ . The first two are clearly present on results described above,  $\text{N}_2\text{O}$  is represented by its dissociation (Pieterse, et al., 2005):



$\text{NH}_3$  was counted by THOR, but not appeared on the results, due to its low concentration. Despite of that, THOR gave as result the presence of  $\text{NO}_2$ ,  $\text{OH}$ ,  $\text{NO}$  and  $\text{H}_2\text{O}_2$ , which are species similar to the intermediary ones showed by reactions (6) to (8).

One of the characteristic steps of **AN thermal decomposition at high temperatures** is the  $\text{HNO}_3$  dissociation into  $\text{H}_2\text{O}$ ,  $\text{O}_2$  and  $\text{NO}_2$ . The first two are always present in Figure 36, due to the presented reason in the beginning of this point, but  $\text{NO}_2$  concentration starts stabilizing (presents linear growing) when no more  $\text{HNO}_3$  is present.

According to 2.1.1.1, the predominant decomposition products at high temperatures are  $\text{H}_2\text{O}$ ,  $\text{N}_2$ ,  $\text{O}_2$ ,  $\text{N}_2\text{O}$ ,  $\text{NO}_2$  and  $\text{NO}$ . Again, the presence of the three first ones is clear.  $\text{N}_2\text{O}$  is represented again by its dissociation products (reaction (87)). The species  $\text{H}_2\text{O}_2$ ,  $\text{HNO}_3$  and  $\text{NO}_2$  present at temperature range [500-700 K] are representative of more complex (more than 3 atoms) intermediary species shown on reactions (10) to (25).  $\text{OH}$  and  $\text{NO}$  start to appear, once more, for temperatures bigger than 650K and have always the same ratio concentrations in order to show the decomposition of the intermediary species referred above (Figure 36).  $\text{NO}$  is itself an AN decomposition product when, for example, occurs explosion (reaction (5)). When temperatures are above 1150K, the products  $\text{O}$  and  $\text{H}$  increase their concentration, showing the decomposition of tri-atomic and bi-atomic species into atomic species, which indicates strong energy release, which is typical of explosive oxidizers, as AN.

Comparing the presented obtained results with other studies about thermal decomposition of AN (2.1.2.3) (Durães, et al., 1996(2)) (Morgado, et al., 2002) (Morgado, et al., 2003), where the results are shown in Figure 22 and Figure 23 (b), the similarities are very clear. For both, low (Figure 22) and high temperatures (Figure 23(b)), the same selected species appears with identical behaviour.

## **2.2.2. Urea nitrate thermal decomposition prediction**

### **2.2.2.1. Methodology and results**

Urea nitrate ( $(\text{NH}_2)_2\text{COHNO}_3$ ) is a compound which perfectly fits in a CHNO system (the classical combustion system), due to its atomic composition. The methodology employed to perform THOR calculations about UN thermal decomposition was similar from the shown to AN thermal decomposition.

NASA thermobuild, from the four atoms C, H, N and O, proposed 180 possible molecule compounds. Applying the same choice criteria, 28 molecules were chosen.

The physico-chemical properties of these 28 molecules were confirmed at THOR's thermochemical database.

Performing THOR calculations, the same criteria was used for validation - gammas and temperature stabilities. After several calculations, the species  $\text{CO}_2$ ,  $\text{CO}$ ,  $\text{H}_2\text{O}$ ,  $\text{N}_2$ ,  $\text{O}_2$ ,  $\text{NO}_2$ ,  $\text{N}$ ,  $\text{NH}_3$ ,  $\text{NO}$ ,  $\text{OH}$ ,  $\text{H}$ ,  $\text{H}_2$ ,  $\text{O}$ ,  $\text{C}(\beta)$ ,  $\text{C}(\alpha)$ ,  $\text{C}(\text{g})$  and  $\text{CH}_4$  were selected. The gammas values were always equal and varied between 1.10 and 1.23. The thermal decomposition of UN was simulated, in THOR, by changing the UN formation enthalpy on the thermochemical database, on a range of -632.748 to -182.748 K. From the last 17 selected species, just 12 had molar fraction superior to  $10^{-7}$ :  $\text{CO}_2$ ,  $\text{H}_2\text{O}$ ,  $\text{N}_2$ ,  $\text{CO}$ ,  $\text{O}_2$ ,  $\text{NO}$ ,  $\text{OH}$ ,  $\text{NH}_3$ ,  $\text{H}$ ,  $\text{O}$ ,  $\text{C}(\alpha)$  and  $\text{H}_2$ . The results are shown on Figure 37.

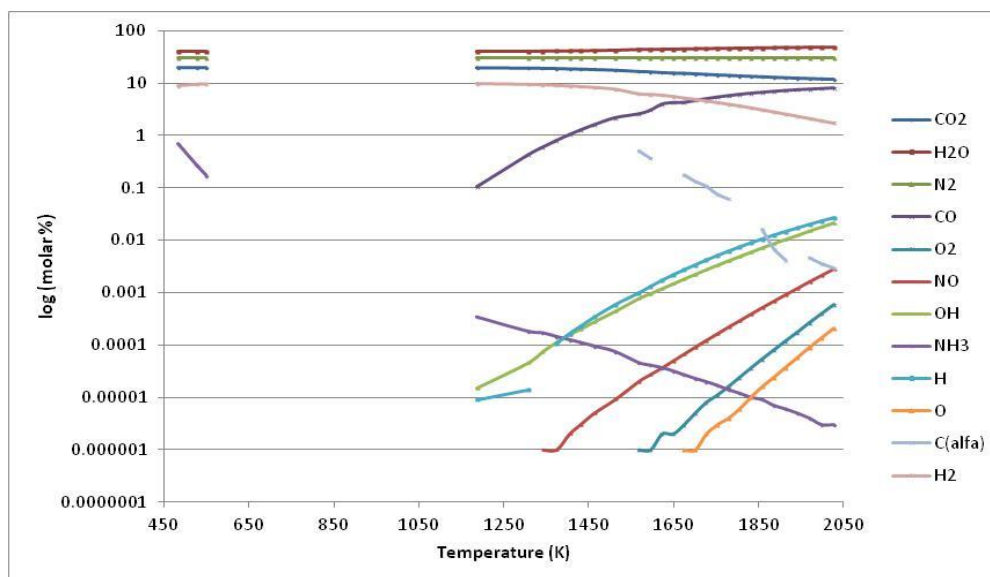


Figure 37: Products decomposition of UN as a function of temperature

#### 2.2.2.2. Comparison between prediction results and literature

In a similar way, Thor thermal decomposition predictions of Urea Nitrate (Figure 37) show clearly two zones: the first zone is formed by  $\text{CO}_2$ ,  $\text{H}_2\text{O}$ ,  $\text{N}_2$  and decreasing values of  $\text{H}_2$  and increasing values of  $\text{CO}$ , followed by the others that really shown Urea Nitrate decomposition.

UN also follows different thermal decomposition mechanisms at low and high temperatures.

At **low temperatures**, which are considered to be below the melting point (until 432 K), the formed decomposition products are  $\text{HNO}_3$ ,  $(\text{NH}_2)_2\text{CO}$ ,  $\text{NH}_3$ ,  $\text{HNCO}$ ,  $\text{C}_2\text{H}_5\text{N}_3\text{O}_2$  and  $\text{NH}_4\text{NO}_3$  (see 2.1.1.2, reactions (26) – (29)). This phase can be seen at Figure 37, on a

temperature range of 484 - 550 K, with the presence of H<sub>2</sub>O, N<sub>2</sub>, CO<sub>2</sub>, H<sub>2</sub> and NH<sub>3</sub>. The only specie found in common was NH<sub>3</sub>, because other decomposition products (shown on literature review) are too complex. HNCO and HNO<sub>3</sub> can decompose through reactions (88) (Fischer, et al., 2002) and (9), which originate the present NH<sub>3</sub>, CO<sub>2</sub> and H<sub>2</sub>O molecules, calculated by



Observing THOR code results for UN (Figure 37). It is possible to see an “empty” zone, where is no compounds presence, in a temperature range of 550 – 1187 K. This fact can be associated to the condensed phase species production described on the **UN thermal decomposition mechanism at high temperatures**, by reactions (30) to (38) (vd. 2.1.1.2). When selected species were just gases, THOR code not found ajustable species for a pre-given global enthalpy values, on the referred temperature range. The pre-selected ones always presented inconsistent values for gammas (sometimes different between them other times with values under 1), and high temperature variations for close enthalpy of reaction values.

It is possible associate the second zone of UN decomposition to UN thermal decomposition (up to 1187 K) above 673 K, which can be related with the harsher conditions linked to high temperatures mechanism. The described formed products in these conditions (reactions (39) and (40) in 2.1.1.2) were NH<sub>3</sub>, HNO<sub>3</sub>, HNCO, N<sub>2</sub>O, CO<sub>2</sub> and H<sub>2</sub>O. NH<sub>3</sub>, H<sub>2</sub>O and CO<sub>2</sub> are significant species on shown results (Figure 37). HNO<sub>3</sub>, HNCO and N<sub>2</sub>O are present in form of their dissociation products (reactions (9) and (87), respectively), O<sub>2</sub>, N<sub>2</sub>, NH<sub>3</sub>, CO<sub>2</sub> and H<sub>2</sub>O. NO, OH, H, O, C ( $\alpha$ ) and H<sub>2</sub> are basic species which can represent, for example, the thermal decomposition of the condensed phase products formed during the UN thermal decomposition.

The difference between the temperature ranges of literature review (2.1.1.2) and the presented computational results (Figure 37) can be justified due to the first ones were been determined by DSC/TGA or T-jump methodologies, whose just have isobaric conditions; while THOR simulation was made under an isobar and adiabatic regime, which justifies the increased temperature ranges.

### 2.2.3. DSC/TGA

#### 2.2.3.1. Ammonium Nitrate

**Experimental methodology and results.** Simultaneous thermal analysis (DSC and TGA) was employed to investigate the thermal decompositions of pure ammonium nitrate (AN) in non-isothermal conditions. The AN used in this study was AN “Poreux” AG from Hydro.

The measurements were carried out using *Rheometric Scientific STA 1500* equipment at two different heating rates, 5°C/min and 10°C/min. Samples weights were between  $13.30 \pm 0.05$  and  $35.40 \pm 0.05$  mg. Four samples were loaded into open alumina crucibles and a dry nitrogen purge flow of 80 ml/min at ambient pressure. This allowed the study of AN phase transitions and the kinetic parameters, as activation energies ( $E_a$ ) and pre-exponential factors ( $Z$ ) of Arrhenius equation. The obtained results are presented in Figures 38 to 41 and in Table 13.

#### DSC/TGA thermograms

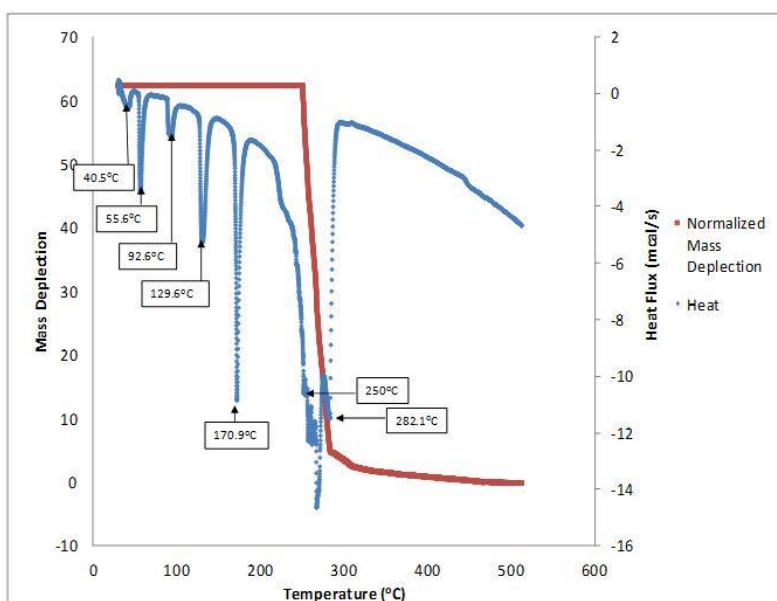


Figure 38: DSC/TGA thermograms for AN (blue and red, respectively) heated at 5°C/min, contained on an open alumina cup ( $M_1 = 34.40$  mg)

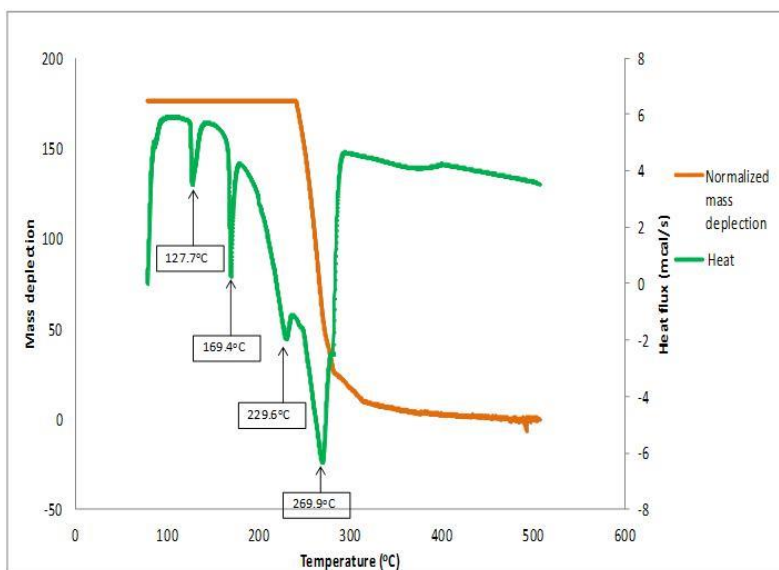


Figure 39: DSC/TGA thermograms for AN (green and orange, respectively) heated at 5°C/min, contained on an open alumina cup ( $M_2 = 13.30$  mg).

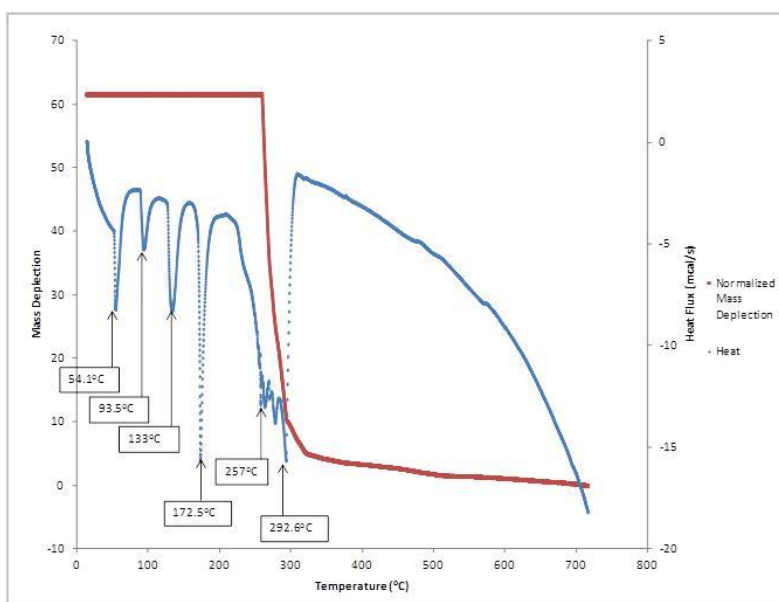


Figure 40: DSC/TGA results for AN (blue and red, respectively) heated at 10°C/min, contained on an open alumina cup ( $M_3 = 35.40$  mg)

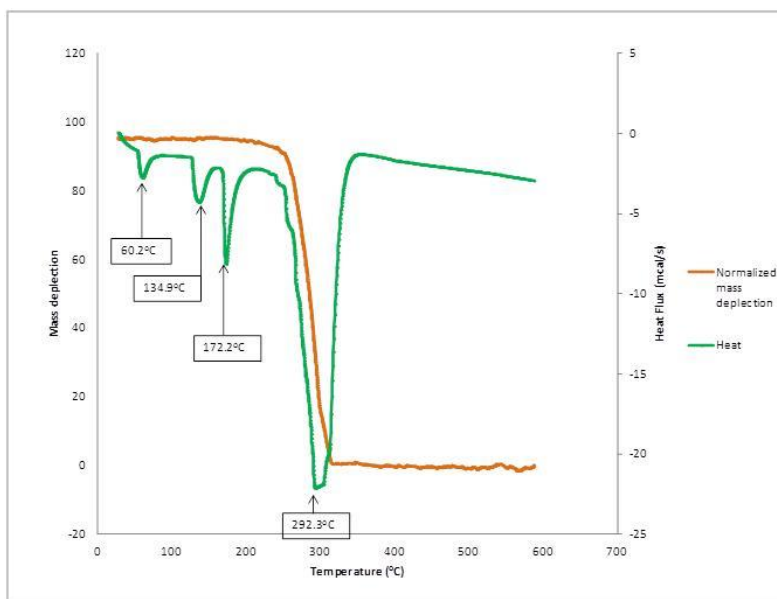


Figure 41: DSC/TGA results for ammonium nitrate (green and orange, respectively) heated at 10°C/min, contained on an open alumina cup ( $M_4 = 20.80$  mg)

**Kinetic parameters calculation and results.** The obtained peak temperatures from DSC thermograms and kinetic parameters based on TGA results are presented on Table 13. The peak temperatures are correspondent to phase transitions, melting point and thermal decomposition of AN. The kinetic parameters ( $E_a$  and  $Z$ ) were obtained through calculations based on Borchardt & Daniels method.

Table 13: DSC Peak temperatures and kinetic parameters obtained from figures 23 to 26. The kinetic parameters were calculated by Borchardt & Daniels method

| Thermograms of figure: | Peak temperature (°C) | Mass Depletion            |                         |             |                           |
|------------------------|-----------------------|---------------------------|-------------------------|-------------|---------------------------|
|                        |                       | $T_{\text{initial}}$ (°C) | $T_{\text{final}}$ (°C) | $E$ (J/mol) | $Z$ ( $\text{min}^{-1}$ ) |
| 38                     | $T_1 = 40.5$ °C       | 256.9                     | 266.3                   | 2.93E+06    | 23.83                     |
|                        | $T_2 = 55.6$ °C       |                           |                         |             |                           |
|                        | $T_3 = 92.6$ °C       |                           |                         |             |                           |
|                        | $T_4 = 129.6$ °C      |                           |                         |             |                           |
|                        | $T_5 = 170.9$ °C      |                           |                         |             |                           |
|                        | $T_6 = 292.4$ °C      |                           |                         |             |                           |
| 39                     | $T_1 = 127.3$ °C      | 240.6                     | 266.0                   | 3.65E+06    | 82.20                     |
|                        | $T_2 = 169.4$ °C      |                           |                         |             |                           |
|                        | $T_3 = 269.1$ °C      |                           |                         |             |                           |

|    |                          |       |       |          |        |
|----|--------------------------|-------|-------|----------|--------|
| 40 | T <sub>1</sub> = 54.1°C  | 260.2 | 266.1 | 3.08E+06 | 75.31  |
|    | T <sub>2</sub> = 93.5°C  |       |       |          |        |
|    | T <sub>3</sub> = 133°C   |       |       |          |        |
|    | T <sub>4</sub> = 172.5°C |       |       |          |        |
|    | T <sub>5</sub> = 292.8°C |       |       |          |        |
| 41 | T <sub>1</sub> = 60.2°C  | 268.9 | 295.8 | 4.86E+06 | 532.72 |
|    | T <sub>2</sub> = 135.2°C |       |       |          |        |
|    | T <sub>3</sub> = 172.8°C |       |       |          |        |
|    | T <sub>4</sub> = 292.6°C |       |       |          |        |

**Physical process discussion.** The first applied heating rate (5°C/min) was performed to simulate a slow combustion, as the case of driven flame. The fast temperature rate (10°C/min) was used to be the double of the previous one.

It was assumed (vd. 2.1.3.3.1), AN presents seven known crystalline modifications. Our results show, implicitly, five of the seven phases. Figure 38 has phase IV (orthorhombic) of AN until 40.5°C (transition of phase IV to phase III); since 40.5 to 55.6 °C is present phase IV and III (both orthorhombic); at 55.6 °C occurs the transition of phase IV to phase II of some AN, which remained stable, this occurrence is described. (Théorêt, et al., 1964) at 50°C; between 55.6 and 92.6 °C are present phases III and II (orthorhombic and tetragonal); the transition of phase III to phase II is described. (Théorêt, et al., 1964) as occurring at 84.5 °C, on our results it appeared at 92.6 °C; between 92.6 and 129.6 °C is present phase II (tetragonal); the transition showed at our results at 129.6 °C is the phase II to phase I transition; at 170.9°C is the melting point of AN; the thermal decomposition of AN occurs at 250°C and it extends to 282.1°C.

The difference of reference temperatures, in presented thermal decomposition, can be justified by the mean particle size of AN. AN is a solid which can change, non-linearly, the molecular geometry and different geometries will have different intra-molecular forces.

Some differences occur when the mass sample is reduced, as shown in Figure 39. The acquisition was programmed to start at higher temperature than the acquisition shown in Figure 38. Due to that, the first transition occurs at 127.7°C and it is correspondent to phase II to phase I transition. The temperature difference between this transition and the same transition in Figure 38 is around 2°C, which means that how much less is the mass

sample, lesser is the temperature needed to achieve the same transition. The same happens for the melting point (Figure 38: m.p.= 170.9°C; Figure 39: m.p.=169.4°C), because it needs less temperature to broke the same chemical links on a minor number of molecules, due to the heat propagation inside of the condensed phase, which dissipates across the molecules.

In Figure 39, the mass loss of thermal decomposition of AN starts between two endothermic peaks (169.4 and 269.9°C), while in Figure 38 the thermal decomposition has a endothermic peak coincident with start of losing mass.

Figure 40 is very similar to Figure 38 with some little deviations, except the transition of phase IV to phase III. It occurs due to the difference between heating rates, the faster heating rate (Figure 41) makes the transitions of phase IV to III and phase IV to II occurring all at the same time. With the slower heating rate (Figure 39) it is possible to clearly see all transitions.

PSAN was tested previously (Davis, et al., 1996) (Simões, et al., 1998) (Oommen, et al., 1999(2)) (Portugal, et al., 2000). The difference between PSAN and presented AN was the five different physical solid state phases in the temperature range of [-18 – 125] °C. PSAN promotes the phase IV changing directly to phase II, avoiding phase III at 32°C. The three first peaks in thermogram of Figure 28 (vd. 2.1.3.3.1) corresponded to the following phase changes: solid phase IV directly to phase II ( $T \approx 53$  °C); solid phase II to solid phase I ( $T \approx 125$  °C); and melting point ( $T \approx 169$  °C). The fourth peak corresponded to AN thermal decomposition at 210 °C. (Portugal, et al., 2000)

All described peaks (Portugal, et al., 2000) are represented in our results (Figure 41), but with some little deviations. Our first four peaks correspond to the following phases, according to other referred study (vd. Figure 29, 2.1.3.3.1): solid phase IV to solid phase III ( $T = 54.1$  °C), solid phase III to solid phase II ( $T = 93.5$  °C), solid phase II to solid phase I ( $T = 133$  °C) and melting point ( $T = 172.5$  °C). The fifth peak corresponds to AN's thermal decomposition at 257°C. Peaks one, three and four were very similar to ones described by Portugal et al., 2000. Comparing our results to those presented by Oommen et al., 1999(2) (vd. Figure 27 and 2.1.3.3.1), beside the referred deviations, it is possible to see the same three peaks on a temperature range of 40 to 140°C.

A DSC test report of AN was presented by NASA (Davis, et al., 1996). Despite the used heating rate, it is possible to observe the peaks previously described and compare with our results. They (Davis, et al., 1996) (vd. Figure 26, 2.1.3.3.1) have phase changes at 51, 124 and 170°C (same point on our results, Figure 39) and a decomposition

endothermic at 257°C (same point on our results, Figure 41). The other phase transitions are at the same temperature range and with small deviations. Although the mass ratio ( $M_3/M_4 \approx 1.7$ ) between Figures 40 and 41 was not so high as for figures 38 and 39 ( $M_1/M_2 \approx 2.6$ ), it is possible to see that is a factor that also affects our DSC measurements (Figures 40 and 41). Though  $M_3/M_4$  is smaller than  $M_1/M_2$ , it is still enough to show different transitions: in Figure 40 is possible to see the endothermic transitions of phase IV to phase III ( $T=54.1$  °C), phase III to phase II ( $T=93.5$  °C), phase II to phase I ( $T=133$  °C); while in Figure 41 the transition of solid phase III ( $T=60.2$ °C) goes directly to solid phase I ( $T=134.9$ °C). The mass effect is also observable at the decomposition's endothermic peaks range of 257 to 292.6°C of Figure 40, which shows the absorbed heat by decomposition chemical reactions (DSC result) while sample is losing mass (TGA result). In Figure 41 this endothermic peaks range disappear and became in only one peak, which means that DSC just detect the global heat consumed in all reactions of thermal decomposition, because the masses (in this case) are too small. A mass ratio of 1.7 (Figures 40 and 41) does not cause so large deviations on temperature range of the DSC peaks, as a mass ratio of 2.6 (Figures 38 and 39). In Figures 40 and 41, the melting point peaks ( $T_3=172.5$ °C and  $T_4=172.2$ °C, respectively) and the thermal decompositions peaks appear at the same temperature, with a deviation of 0.3°C, almost ten times less than 2°C deviation on Figures 38 and 39 ( $T_3=292.6$ °C and  $T_4=292.3$ °C, respectively). So, the concordance between DSC assays is bigger when the sample mass ratio between them is 1. This can be observed comparing Figure 38 with 39 (bigger mass ratio), Figures 40 and 41 (minor mass ratio).

**Reaction processes discussion.** *Literature review (2.1.1.1)* clarify that reaction (1), due to AN's endothermic dissociation above 169°C, corresponds to a proton transfer reaction; reaction (2) represents the exothermic elimination of N<sub>2</sub>O on careful heating at 200°C; reaction (3) corresponds to exothermic elimination of N<sub>2</sub> and NO<sub>2</sub> above 230°C; reaction (4) is representative of exothermic elimination of nitrogen and oxygen, sometimes accompanied by detonation; and reaction (5) has been suggested when AN undergoes explosion

Reaction 1 is clearly represented in all our results (Figures 38 to 41) on a range of 169.4 to 172.5°C. Reactions (2), (3), (4) and (6) are implicit on results shown at Figures 38 and 40 (results acquired for bigger masses), on a temperature range of 250 to 2962.6°C. For small masses (Figures 39 and 41), the endothermic peak, which occurs

simultaneously with the mass loss, is well defined. It occurs because, at that temperature, the dissociation velocity of remaining AN (reaction (1)) is bigger than the reaction velocity of other referred reactions ((2), (3), (4) and (6) to (25)) and, for this, the global reaction heat is given by reaction (1), which is endothermic and detectable by DSC. The endothermic dissociation is much more significant than exothermic thermal decomposition. For bigger masses, the exothermic reactions are not negligible, because the present mass seems to be enough to saturate reactions (1), (6) (7) and (8) i.e., the bulk decomposition saturation (and still remains mass enough to other reactions occur on a detectable scale of DSC).

**Kinetic parameters discussion.** The results presented on this work present a quite good correlation between them. The activation energy ( $E_a$ ) varied between 2.93E+06 and 4.86E+06 J/mol and the pre-exponential factor ( $Z$ ) varied between 23.83 and 532.72.

The  $E_a$  and  $Z$  are bigger when the applied heating rate is higher (Table 13, comparison between Figures 40 and 41 with Figures 38 and 39) and when the mass sample is smaller (Table 13, comparison between Figures 39 and 41 with Figures 38 and 40).

The mass sample also affects  $E_a$  and  $Z$  When mass samples are bigger, the  $E_a$  and  $Z$  are smaller because AN undergoes to a surface decomposition, which means that solid AN decomposes by “slices”. For smaller masses, the solid AN suffers bulk decomposition, i.e., decomposes itself all at the same time, which needs more energy to achieve all mass (the input energy is uniformly absorbed).

### 2.2.3.2. Urea Nitrate

**Experimental methodology and results.** To study of the thermal decomposition of UN in non-isothermal conditions was used pure UN purchased from *SelectLab Chemicals, GmbH*. Once again, the measurements were carried out using *Rheometric Scientific STA 1500* equipment. There were used two different heating rates 5°C/min and 10°C/min. Samples weights were between  $7.69 \pm 0.05$  and  $41.0 \pm 0.05$  mg. Five samples were loaded, again, into open alumina crucibles and a dry nitrogen purge flow, of 80 ml/min at ambient pressure, was used. This study allowed the determinations of melting point, thermal decomposition and the kinetic parameters characteristics from UN. The

acquired thermograms are presented on Figures 42 to 45 and the calculated kinetic parameters are shown on Table 14.

### DSC/TGA thermograms

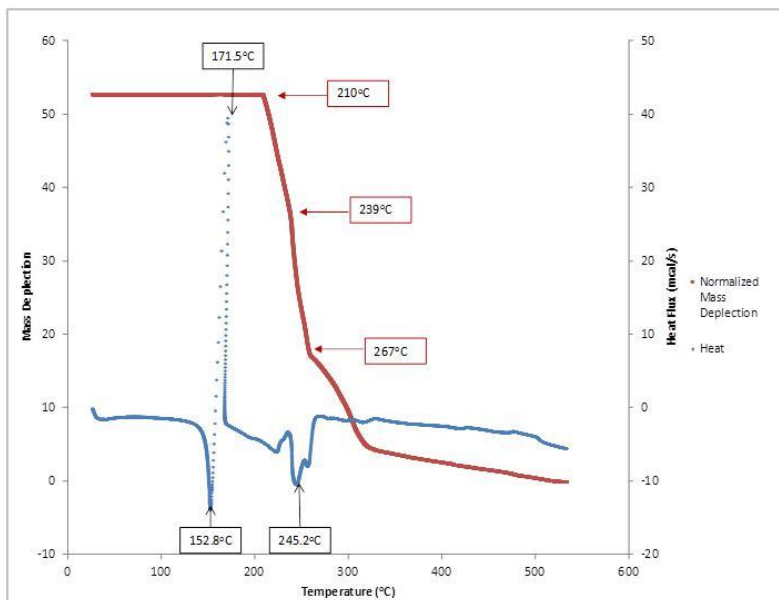


Figure 42: DSC/TGA results for urea nitrate (blue and red, respectively) heated at 5°C/min, contained on an open alumina cup ( $M_1 = 41.0$  mg)

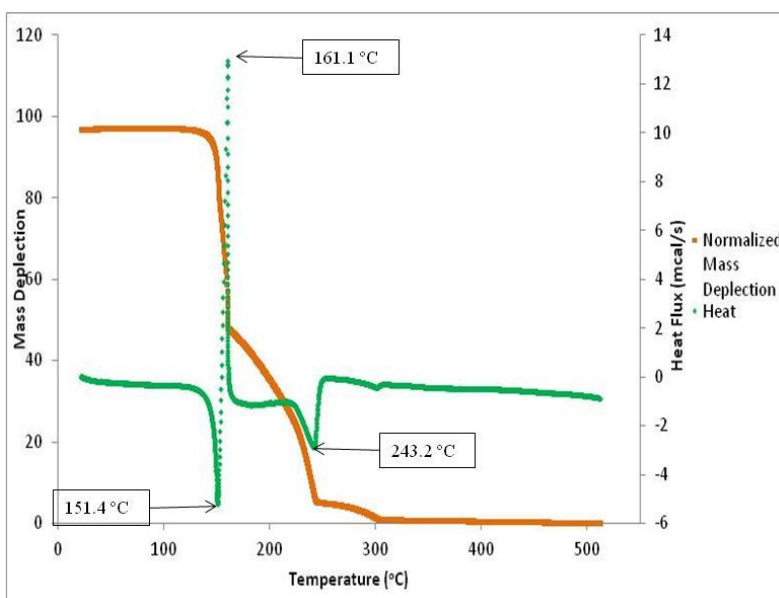


Figure 43: DSC/TGA results for urea nitrate (green and orange, respectively) heated at 5°C/min, contained on an open alumina cup ( $M_2 = 9.28$  mg)

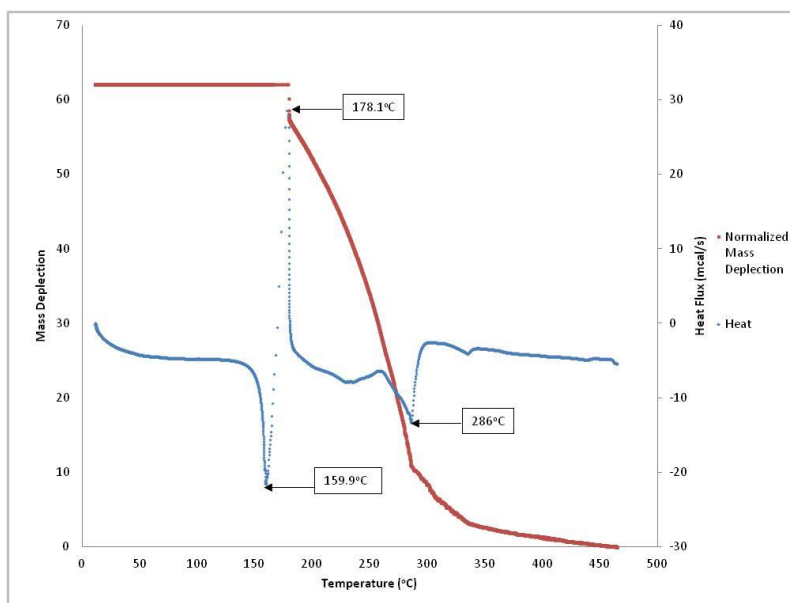


Figure 44: DSC/TGA results for urea nitrate (blue and red, respectively) heated at 10°C/min, contained on an open alumina cup ( $M_3 = 34.50$  mg)

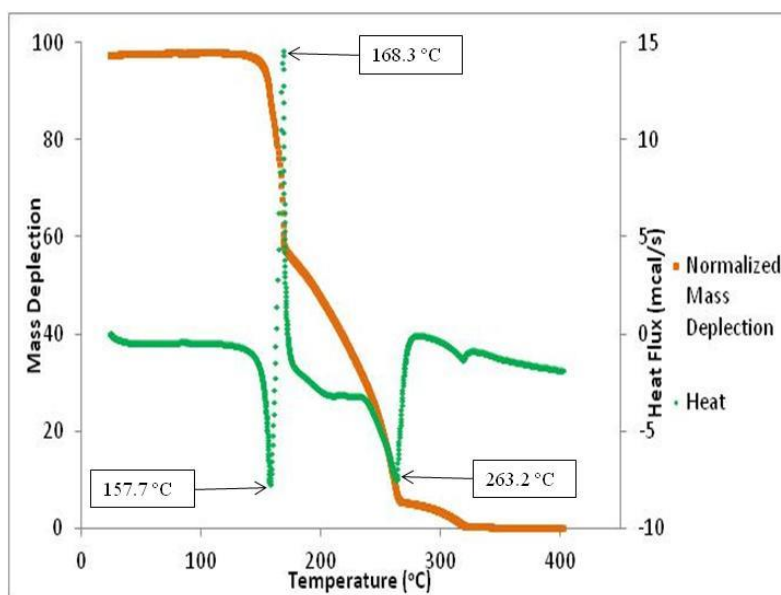


Figure 45: DSC/TGA results for urea nitrate (green and orange, respectively) heated at 10°C/min, contained on an open alumina cup ( $M_4 = 7.69$  mg)

**Kinetic Parameters.** The obtained peak temperatures from DSC thermograms and kinetic parameters based on TGA results are presented on Table 14. The peak temperatures are correspondent to melting point (first one) and thermal decomposition of UN (the last two). The kinetic parameters ( $E_a$  and  $Z$ ) were obtained through calculations based on Borchardt & Daniels method.

Table 14: DSC Peak temperatures and kinetic parameters obtained from Figures 42 to 45.

| Thermograms of<br>Figure: | Peak<br>temperature (°C)        | Mass Depletion            |                         |           |                        |
|---------------------------|---------------------------------|---------------------------|-------------------------|-----------|------------------------|
|                           |                                 | T <sub>initial</sub> (°C) | T <sub>final</sub> (°C) | E (J/mol) | Z (min <sup>-1</sup> ) |
| 42                        | T <sub>1(endo)</sub> = 152.8 °C | 212.4                     | 232.6                   | 1.615E+06 | 2.721                  |
|                           | T <sub>2(exo)</sub> = 171.5 °C  | 240.1                     | 244.5                   | 1.887E+06 | 4.727                  |
|                           | T <sub>3(endo)</sub> = 245.2 °C | 268.9                     | 307.208                 | 3.889E+06 | 5.874                  |
| 43                        | T <sub>1(endo)</sub> = 151.4 °C | 151.2                     | 161.3                   | 6.133E+06 | 1.593E+13              |
|                           | T <sub>2(exo)</sub> = 161.1 °C  | 164.1                     | 222.7                   | 7.220E+05 | 5.169                  |
|                           | T <sub>3(endo)</sub> = 243.2 °C | 269.7                     | 301.3                   | 1.022E+06 | 164.120                |
| 44                        | T <sub>1(endo)</sub> = 159.6 °C | 209.8                     | 284.7                   | 1.543E+06 | 1.722                  |
|                           | T <sub>2(exo)</sub> = 178.1 °C  |                           |                         |           |                        |
|                           | T <sub>3(endo)</sub> = 286 °C   |                           |                         |           |                        |
| 45                        | T <sub>1(endo)</sub> = 157.7 °C | 155.9                     | 165.0                   | 9.939E+06 | 1.656E+20              |
|                           | T <sub>2(exo)</sub> = 168.3 °C  | 174.5                     | 262.2                   | 1.236E+06 | 1.238                  |
|                           | T <sub>3(endo)</sub> = 263.2 °C | 278.7                     | 319.8                   | 7.249E+06 | 189.294                |

**Physical processes discussion.** Our DSC results are relatively similar to those ones described on *Literature Review* (Oxley, et al., 2009) (Oxley, et al., 2013) (Désilets, et al., 2011(2)).

Comparing our results (Figures 44 and 45) to those presented on Figure 31 (2.1.3.3.2), it can be observed their similarity for temperatures less than 250°C. Figure 31 has other exothermic peak at 403°C and 380°C and we just get endothermic peaks after the exothermic one (values indicated on Figure 42). These facts probably occur due to the different temperature rates used in each experiment. Ours experiments were performed with a rate of 10°C/min, while their experiment was performed at 20°C/min. These different temperature rates can change the degradation mechanism, and mechanisms rate.

Making the comparison between our results (Figures 42 and 43) with those presented on Figure 32 (2.1.3.3.2) it is possible to see many similarities: the endothermic and exothermic peaks appear on same range temperatures and there are no two exothermic peaks. Also, the TGA thermograms had the same profile. Like it was exposed for AN, different mass samples of UN and different applied heating rates have different contributions for DSC/TGA results (Figures 42 to 45). These influences are few

detected on melting point, but they have larger influence on thermal decomposition temperatures. Bigger masses and higher heating rates increase the melting temperature, but in few Celsius degrees. In first case, the maximum difference is 2.2°C (comparison between Figures 42 and 43 and between Figures 44 and 45). In second case, the maximum difference temperature is 7.1°C (comparison between Figures 42 and 44 and between Figures 43 and 45). These considerations, once again, mean that are needed higher temperatures to melt and thermal decompose higher masses, and molecular movements follow easier slow heating rates than higher ones, because the “thermal choke” is smaller. These considerations are more notable for the exothermic and endothermic peaks of UN thermal decompositions

**Reaction processes discussion.** Presented DSC results are very similar to those described on *Literature Review*. (Hiyoshi, et al., 2002) (Oxley, et al., 2009) (Oxley, et al., 2013) (Désilets, et al., 2011(2))

The first endothermic peak at, approximately, 150°C (all results), which is the melting point of UN, corresponds to the dissociation of urea nitrate (reaction 26) and to the decomposition of urea (reaction (27)). The exothermic peak, for us near 170°C (results of Figures 42 and 44) or near 160°C (for Figures 43 and 45) and in *Literature Review* (2.1.1.2) between 166.7 and 172°C, is due to the occurrence of three reactions: biuret formation (reaction (28)), ammonium nitrate formation (reaction (29)) or ammonium isocyanate formation (reaction (33)). From 190°C to 250°C, urea continues to degrade while biuret starts to decompose (reversed reaction (28)). Production of cyanuric acid and ammelide is accelerated and new compounds slowly appear in low amount: ammonium isocyanate (reaction (33)), ammeline and melamine (reactions (34) to (36)). In our results, these degradations, decompositions and productions are characterized by the endothermic peaks at 245.2 °C (Figure 42), 243.2°C (Figure 43), 286°C (Figure 44) and 263.2°C (Figure 45).

According to literature, at 250°C, only cyanuric acid, ammelide, ammeline and melamine were present in appreciable amounts, while urea and biuret were completely decomposed. Approximately at this temperature we have an endothermic peak (256.5°C, Figure 42), which probably means that the previous reactions are still occurring and the new compounds are forming in high amounts.

From 250 °C to 360 °C, all material started to decompose essentially by the reverse reaction to generate isocyanic acid and ammonia (reactions (1), (2), (37) and (38)). This can be proved in our results, by the TGA results, where the last mass loss starts on a range of 246 to 280°C and ends at a range of 300 to 328°C. Our alumina cup has no mass inside when experiment ended, which means that all UN were pyrolysed into gases.

**Kinetic parameters discussion.** To determine the kinetic parameters of thermal decomposition of UN, it was calculated the activations energies ( $E_a$ ) and pre-exponential factors ( $Z$ ). Our results are based on the same expressions described at 2.1.3.2 and they are shown on Table 14.

Oxley et al., 2009 calculated Arrhenius activation energy ( $E_a$ ) for UN and its pre-exponential factor, based on a DSC performed at 10°C/min to a mass of 0.36 mg, but using a different calculation methodology. They used the ATSM E 698 method and we used the Borchardt & Daniels methodology. They obtain an  $E_a = 1.58E+05$  J/mol with a  $Z = 1.39E+12$  min<sup>-1</sup> for the endothermic peak, and  $E_a = 1.31E+05$  J/mol with an  $Z = 2.66E+09$  min<sup>-1</sup> (Table 10).

Désilets et al., 2011(2), performed a DSC at 20°C/min to a mass of 5 mg of UN and determined the activations energies and pre-exponential factors based on the first endothermic and exothermic peaks. They reported an activation energy of 2.06E+05 J/mol with pre-exponential factor  $Z = 3.850$  min<sup>-1</sup> for the major exothermic peak: For the endothermic peak they determined an activation energy of 2.25E+05 J/mol with a pre-exponential factor  $Z = 3.434$  min<sup>-1</sup> (Table 10).

Our results are different from those ones, probably due to the chosen temperature range. They made their calculations assuming, as reference, endothermic and exothermic peaks, while our results were based in the linear zone at TG measurements. So, different temperature ranges means different zones of reaction.





## CHAPTER 3 – EXPERIMENTAL TESTING OF SELECTED COMPOSITIONS

### 3.1. Mixtures compositions - Thermodynamic Properties

It were studied two series of mixtures compositions, shown on Tables 15 and 16. Table 15 is a selection of Table 16, where mixtures 3.1 and 3.2 are equivalent in mass percentage of oxidant/binder/additive to mixtures 4.1 and 4.2, mixtures 3.3 and 3.4 are equivalent in richness to 4.1 and 4.2.

Table 15: First serie of mixtures – composition in mass percentage

|                                 | Mixture n°. | PU (%) | AN (%) | UN (%) | Al (%) | MT (%) |
|---------------------------------|-------------|--------|--------|--------|--------|--------|
| 1. Mixtures based on AN oxidant | 1.1         | 24     | 76     | 0      | 0      | 0      |
|                                 | 1.2         | 23     | 71     | 0      | 6      | 0      |
|                                 | 1.3         | 21     | 69     | 0      | 10     | 0      |
|                                 | 1.4         | 23     | 71     | 0      | 0      | 6      |
|                                 | 1.5         | 21     | 69     | 0      | 0      | 10     |
|                                 | 1.6         | 12     | 88     | 0      | 0      | 0      |
|                                 | 1.7         | 11     | 83     | 0      | 6      | 0      |
|                                 | 1.8         | 9      | 81     | 0      | 10     | 0      |
|                                 | 1.9         | 11     | 83     | 0      | 0      | 6      |
|                                 | 1.10        | 9      | 81     | 0      | 0      | 10     |
| 2. Mixtures based on UN oxidant | 2.1         | 24     | 0      | 76     | 0      | 0      |
|                                 | 2.2         | 23     | 0      | 71     | 6      | 0      |
|                                 | 2.3         | 21     | 0      | 68     | 11     | 0      |
|                                 | 2.4         | 23     | 0      | 71     | 0      | 6      |
|                                 | 2.5         | 21     | 0      | 68     | 0      | 11     |
|                                 | 2.6         | 12     | 0      | 77     | 11     | 0      |
|                                 | 2.7         | 12     | 0      | 77     | 0      | 11     |
|                                 | 2.8         | 12     | 0      | 88     | 0      | 0      |
|                                 | 2.9         | 11     | 0      | 83     | 6      | 0      |
|                                 | 2.10        | 9      | 0      | 80     | 11     | 0      |
|                                 | 2.11        | 11     | 0      | 83     | 0      | 6      |
|                                 | 2.12        | 9      | 0      | 80     | 0      | 11     |

PU – PolyUrethane; AN – Ammonium Nitrate; UN – Urea Nitrate; Al – aluminium powder; MT – Magnesium / Teflon mixture

Table 16: Second serie of mixtures – composition in mass percentage

|                                 | Mixture n°. | PU (%) | AN (%) | UN (%) | AI (%) | MT (%) |
|---------------------------------|-------------|--------|--------|--------|--------|--------|
| 3. Mixtures based on AN oxidant | 3.1         | 7.32   | 83.59  | 0      | 0      | 9.09   |
|                                 | 3.2.        | 7.32   | 83.58  | 0      | 9.10   | 0      |
|                                 | 3.3.        | 17.43  | 73.49  | 0      | 0      | 9.08   |
|                                 | 3.4.        | 17.43  | 73.49  | 0      | 9.08   | 0      |
| 4. Mixtures based on UN oxidant | 4.1         | 7.31   | 0      | 83.59  | 0      | 9.10   |
|                                 | 4.2         | 7.31   | 0      | 83.60  | 9.09   | 0      |

The thermodynamic properties of used reactants components are shown on Tables 17 to 22.

Table 17: Thermodynamic properties of Ammonium Nitrate (ICT, 2005) (Jolkkonen, 2012)

|   |  |
|---|--|
| <b>Molecular Formula</b>                        | NH <sub>4</sub> NO <sub>3</sub>            |
| <b>Molar Mass</b>                               | 80.043 g/mol                               |
| <b>Phase</b>                                    | Solid                                      |
| <b>Density</b>                                  | 1.725 g/cm <sup>3</sup>                    |
| <b>Enthalpy of Formation</b>                    | -344.26 kJ/mol                             |
| <b>Entropy of Formation</b>                     | 151.1 J.mol <sup>-1</sup> .K <sup>-1</sup> |
| <b>Boiling point</b>                            | 210°C                                      |
| <b>Heat of combustion/ Enthalpy of Reaction</b> | 210.47 kJ/mol                              |
| <b>Cp</b>                                       | 139.3 J.mol <sup>-1</sup> .K <sup>-1</sup> |

Table 18: Thermodynamic properties of Urea Nitrate (ICT, 2005) (Oxley, et al., 2013)

|   |  |
|---|--|
| <b>Molecular Formula</b>                        | (NH <sub>2</sub> ) <sub>2</sub> COHNO <sub>3</sub> |
| <b>Molar Mass</b>                               | 123.068 g/mol                                      |
| <b>Phase</b>                                    | Solid  |
| <b>Density</b>                                  | 1.67 g/cm <sup>3</sup>                             |
| <b>Enthalpy of Formation</b>                    | -546.47 kJ/mol                                     |
| <b>Entropy of Formation</b>                     | Not found  |
| <b>Melting point</b>                            | 157-160°C  |
| <b>Heat of combustion/ Enthalpy of Reaction</b> | 552.24 kJ/mol                                      |
| <b>Cp</b>                                       | Not found  |

Table 19: Thermodynamic properties of PolyUrethane (ICT, 2005)

|                          |   |
|--------------------------|---|
| <b>Molecular Formula</b> | C <sub>10</sub> H <sub>18.711</sub> N <sub>0.273</sub> O <sub>3.294</sub> |
| <b>Molar Mass</b>        | 195.495 g/mol   |
| <b>Phase</b>             | Solid   |

|   |                     |
|---|---------------------|
| <b>Density</b>                                  | 1 g/cm <sup>3</sup> |
| <b>Enthalpy of Formation</b>                    | - 679.52 kJ/mol     |
| <b>Entropy of Formation</b>                     | Not found           |
| <b>Boiling point</b>                            | 250°C               |
| <b>Heat of combustion/ Enthalpy of Reaction</b> | Not found           |
| <b>Cp</b>                                       | Not found           |

Table 20: Thermodynamic properties of Aluminium (ICT, 2005) (Jolkkonen, 2012)

|   |   |
|---|---|
| <b>Molecular Formula</b>                        | Al  |
| <b>Molar Mass</b>                               | 26.982 g/mol                              |
| <b>Phase</b>                                    | Solid                                     |
| <b>Density</b>                                  | 2.702 g/cm <sup>3</sup>                   |
| <b>Enthalpy of Formation</b>                    | 0 kJ/mol                                  |
| <b>Entropy of Formation</b>                     | 28.3 J.mol <sup>-1</sup> .K <sup>-1</sup> |
| <b>Boiling point</b>                            | 2518°C                                    |
| <b>Heat of combustion/ Enthalpy of Reaction</b> | 838.41 kJ/mol                             |
| <b>Cp</b>                                       | 24.4 J.mol <sup>-1</sup> .K <sup>-1</sup> |

Table 21: Thermodynamic properties of Magnesium (ICT, 2005)

|   |  |
|---|--|
| <b>Molecular Formula</b>                        | Mg   |
| <b>Molar Mass</b>                               | 24.305 g/mol                                 |
| <b>Phase</b>                                    | Solid  |
| <b>Density</b>                                  | 1.740 g/cm <sup>3</sup>                      |
| <b>Enthalpy of Formation</b>                    | 0 kJ/mol                                     |
| <b>Entropy of Formation</b>                     | 148.616 J.mol <sup>-1</sup> .K <sup>-1</sup> |
| <b>Boiling point</b>                            | 1107°C                                       |
| <b>Heat of combustion/ Enthalpy of Reaction</b> | 601.64 kJ/mol                                |
| <b>Cp</b>                                       | 32.552 J.mol <sup>-1</sup> .K <sup>-1</sup>  |

Table 22: Thermodynamic properties of Teflon (ICT, 2005)

|   |  |
|---|--|
| <b>Molecular Formula</b>                        | C <sub>2</sub> F <sub>4</sub>              |
| <b>Molar Mass</b>                               | 100.016 g/mol                              |
| <b>Phase</b>                                    | Solid                                      |
| <b>Density</b>                                  | 2.310 g/cm <sup>3</sup>                    |
| <b>Enthalpy of Formation</b>                    | 820.482 kJ/mol                             |
| <b>Entropy of Formation</b>                     | 9414 J.mol <sup>-1</sup> .K <sup>-1</sup>  |
| <b>Thermal degradation point</b>                | 370°C                                      |
| <b>Heat of combustion/ Enthalpy of Reaction</b> | Not Found                                  |
| <b>Cp</b>                                       | 101.6 J.mol <sup>-1</sup> .K <sup>-1</sup> |

## 3.2. Thermochemical properties predictions for studied mixtures

### 3.2.1. Mixtures based on Ammonium Nitrate

#### 3.2.1.1. Free Gibbs enthalpy and temperatures of combustion predictions

Prediction of isobar adiabatic combustion temperature, as function of the equivalent ratio ( $r$ ) of the mixture, gives an evaluation information of reaction effectiveness. This value must be couple with Gibbs free energy result for the same  $r$ . An example, Ammonium Nitrate (AN)/Polyurethane (PU) reaction, is shown in Figure 46, presenting the evolution of calculated Gibbs Free Enthalpy and an isobar adiabatic “combustion” temperature  $T_b$  as a function of equivalence ratio  $r$ . The maximum  $T_b$  value is always for  $r$  greater than 1. The presence of  $C_\beta$  modifies this maximum  $T_b$  value. (Quaresma, et al., 2013)

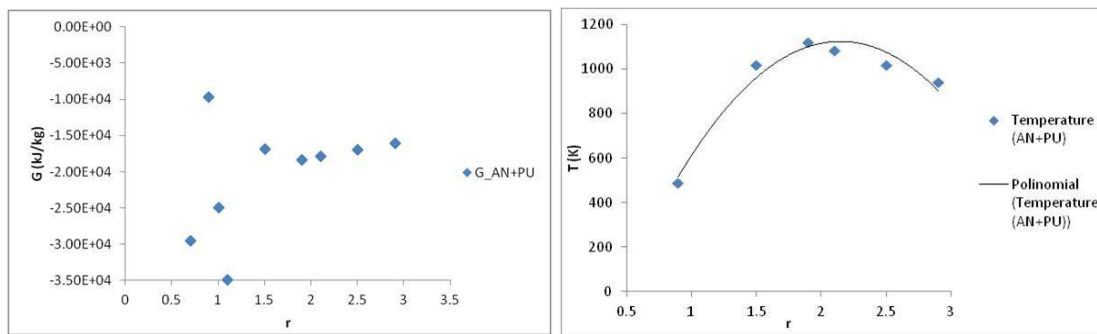


Figure 46: Evolution of predicted Gibbs Free Enthalpy (left) and combustion temperature  $T_b$  (right) of isobar adiabatic reaction of Ammonium Nitrate – PolyUrethane, as a function of equivalence ratio  $r$  (adimensional) (Quaresma, et al., 2013)

For richness near 1 (Figure 46, left), the predicted Gibbs Free Enthalpies have discrepant values. This fact is due to the change of fundamental species,  $CO_2$ ,  $H_2O$ ,  $O_2$  and  $N_2$ , for poor mixtures into  $CO_2$ ,  $H_2O$ ,  $H_2$  and  $N_2$ , for rich mixtures.

The second graph (right) shown on Figure 46 shows that the maximum predicted temperature of combustion is 1121.5 K for a mixture with  $r = 1.9$ .

#### 3.2.2.2. Prediction of temperature combustion as a function of additives concentration

To study the influence of additives in mixtures composed by AN (as oxidant) and PU (as binder) were made several calculations for a composition of PU/AN with  $r=1.9$ ,

which was the composition with higher temperature of combustion. The results, obtained in the study of the influence of mass percentage of MT and Al at temperature of combustion in mixtures composed by AN and PU, are presented on Figure 47 and Figure 48.

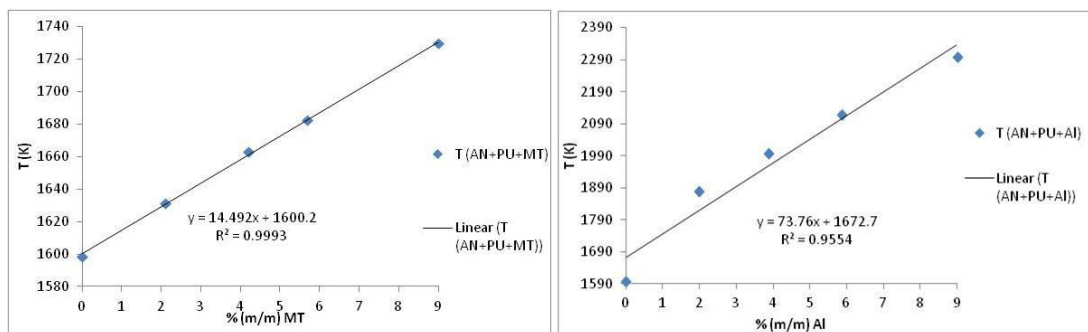


Figure 47: Influence of mass percentage of MT (left) and Al (right) at temperature of combustion in a mixture composed by AN and PU (for % (m/m) additives = 0: 76% AN + 24%PU)

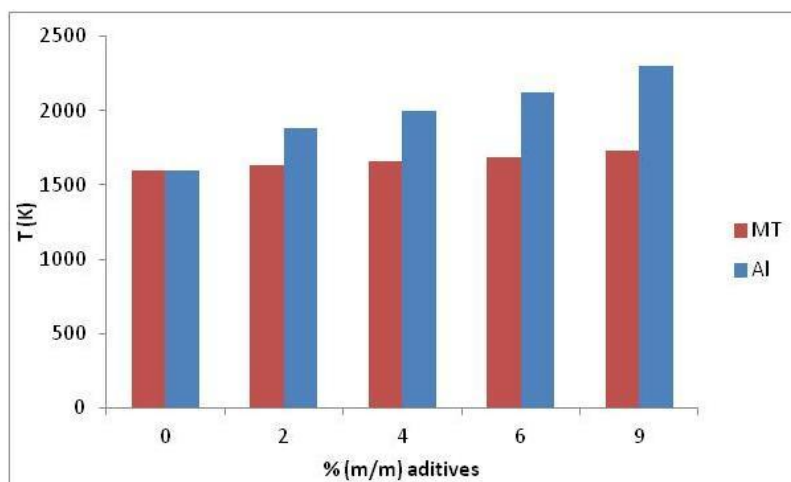


Figure 48: Comparison between the influences of mass percentages of additives in mixtures composed by AN and PU (for % (m/m) additives = 0: 76% AN + 24%PU)

From Figure 47 and Figure 48 it is possible to conclude that for the same percentage of each additive, Al is the one who reaches higher temperatures on the predicted mixtures. It is also possible to observe that, for both additives, the increase of the concentration of the additive in the mixture increases its temperature of combustion.

## 3.2.2. Mixtures based on Urea Nitrate

### 3.2.2.1. Free Gibbs enthalpy and predictions of combustion temperatures

Some similarities are found changing AN to UN. Predicting results of urea nitrate-polyurethane reaction, shown in Figure 49. The maximum  $T_b$  value is also always for  $r$  greater than 1, assuming condensed  $C_\beta$  formation. (Quaresma, et al., 2013)

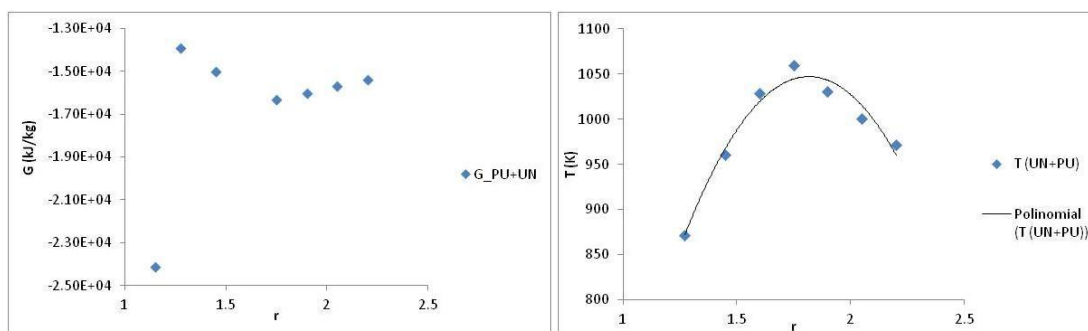


Figure 49: Evolution of predicted Gibbs Free Enthalpy (left) and combustion temperature  $T_b$  (right) of isobar adiabatic reaction of Urea Nitrate – PolyUrethane, as a function of equivalence ratio  $r$  (adimensional) (Quaresma, et al., 2013)

The lowest value of predicted Gibbs Free Enthalpy is for  $r=1.15$ , which is the value of the richness of UN without any binder. With UN, the stoichiometric condition  $r=1$  is never reached. On the presence of PU, the lowest value for Free Gibbs Enthalpy is for UN/PU mixture is  $r = 1.75$ . The maximum temperature of combustion predicted is 1060 K, for a mixture of UN/PU with  $r=1.75$ .

### 3.2.2.2. Combustion temperature prediction as a function of additives concentration

The influence of additives in UN plus PU mixtures was studied. All calculations were made for a mixture of UN and PU with  $r=1.75$ . The results of thermochemical calculations are presented on Figure 50 and Figure 51.

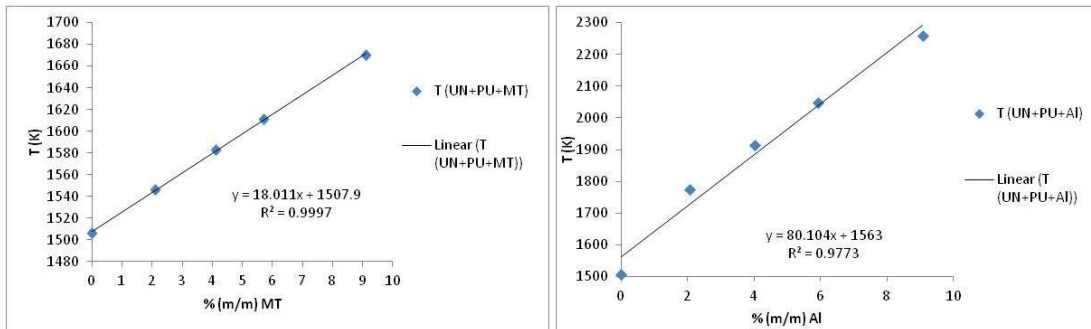


Figure 50: Influence of mass percentage of MT (left) and Al (right) at temperature of combustion in a mixture composed by UN and PU (for % (m/m) additives = 0: 86% UN + 14%PU)

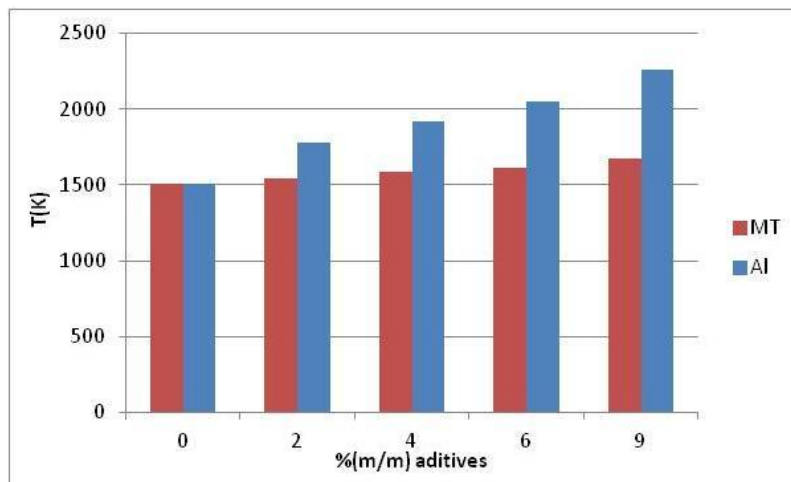


Figure 51: Comparison between the influences of mass percentages of additives in mixtures composed by UN and PU (for % (m/m) additives = 0): 86% UN + 14%PU)

The predicted results for the combustion temperature as a function of additives for UN were very similar to those ones with AN. Al gives to the mixture higher temperatures of combustion. All calculations were made for a mixture of UN and PU with  $r = 1.75$ .

### 3.3. Combustion experimental study

#### 3.3.1. Introduction

The definition of combustion, although it has been extensively studied, is not clear. (Kubota, 2002) The basis of combustion theory is related to gaseous reaction phase.

The combustion of gaseous materials produces heat accompanied by emission from the luminous reaction products. Chemical reactions occur between the molecules of the reactive gas, when it is heated by an external energy source. This reaction belongs to a reaction initiation process, which is exothermic and forms high temperature products. This process, a part of the combustion phenomena, is known as **ignition**. When the heat produced by this exothermic reaction heats up the unreacted portion of the reactive gas, a successive ignition process is established without external heating. This process is known as **self-sustaining combustion**. The ignited region between the unburned and burned regions is called **combustion wave** and it propagates toward the unburned zone (Kubota, 2002).

Although ignition and combustion of energetic solid materials have additional physicochemical processes, such as phase transitions, it is fundamentally the same as the ignition and combustion of reactive gases (Kubota, 2002).

When the heat is transferred to the surface of an energetic material, the surface and the subsurface temperatures are increased simultaneously. When the surface (zone I - Figure 52) reaches the decomposition or gasification temperature, the endothermic and/or exothermic reactions occur on and above the surface (zone II - Figure 52). The decomposition gases react to form reaction products accompanied by a great heat release, and the temperature in the gas phase increases (zone III - Figure 52). If this reaction process occurs even after the heat given to the surface is removed, combustion is established. On the other hand, if the exothermic and gasification reactions are terminated after the heat given to the surface has been removed, ignition has failed and combustion is not established. (Kubota, 2002)

External heating is needed for ignition. Successive heating is needed from the high-temperature burned portion to the low-temperature unburned portion for **combustion**. (Kubota, 2002)

### 3.3.2. Simplified combustion model – cigar burning approach

It can be assumed, for energetic solid materials, a simplified combustion phenomena when (1) is a one-dimension burning model, and (2) it is a steady-state burning at constant pressure, which implies mass conservation. Generically, the mass conservation can be expressed in function of the mass burning rate of the material ( $\dot{m}$ ), its density ( $\rho$ ), the velocity of mass consumption ( $u$ ) and the area ( $A$ ) of the burning surface:

$$\dot{m} = \frac{dm}{dt} = \rho u A \quad (89)$$

The velocity of mass consumption ( $u$ ) is the sum of the propagation velocity ( $D$ ) of the heat in the “fresh” materials and the fundamental flame velocity ( $V$ ), responsible for the heat released during the reactions (equation 90).

$$u = D + V \quad (90)$$

The mass burning rate of the materials can be expressed by equation (91), which relates the reaction advancement degree ( $\lambda$ ) with the formation of the burned material ( $m_b$ ) and the total mass present in the combustion ( $M_0$ ).

$$\lambda = \frac{m_b}{M_0} \quad (91)$$

Where

$$M_0 = m_f + m_b \quad (92)$$

Assuming the mass rate of the burned material ( $\frac{dm_b}{dt}$ ), applying equation (91):

$$\begin{aligned} m_b &= \lambda M_0 \\ \frac{dm_b}{dt} &= M_0 \frac{d\lambda}{dt} \end{aligned} \quad (93)$$

The boundary conditions for  $\lambda$  are 0 when  $t = t_0$  (and  $M_0 = m_f$ ) and 1 when  $t = t_b$  (and  $M_0 = m_b$ ).  $t_0$  is the instant when only fresh material is present,  $t_b$  is the instant when all fresh material was converted into burned one. The formation of the fresh material ( $m_f$ ), due to the burning of the previous one can be expressed as:

$$m_f = 1 - \lambda M_0 \quad (94)$$

Assuming equation (93), equation (89) can be now rewritten as:

$$M_0 \frac{d\lambda}{dt} = \rho u A \quad (95)$$

To understand the behavior of this parameters in combustion, this simplified combustion phenomena is schematized on Figure 52 for our test samples (cigars).

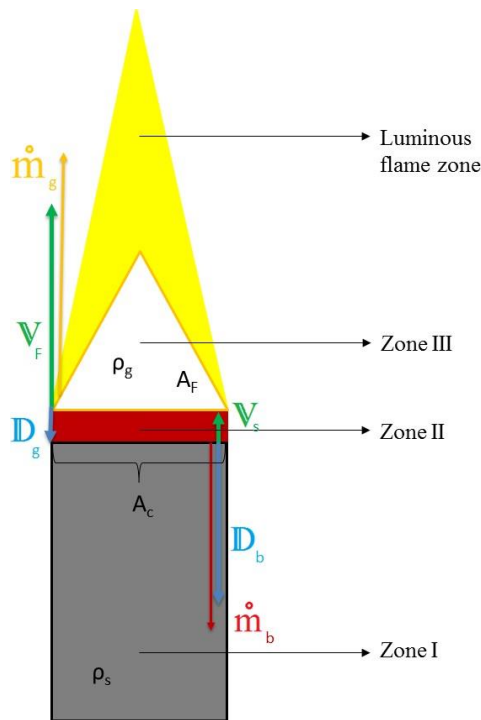


Figure 52: Scheme of the simplified combustion phenomena for cigar burning test. Zone I is the condensed-phase zone, zone II the condensed-phase reaction zone and zone III is the gas phase reaction zone.

The fresh solid mass consumption rate ( $\dot{m}_b$ ) between zone I and II, assuming the mass conservation equation (89), is dependent of the density of: the condensed-phase, which is correspondent to the number of the present solid species per volume unit ( $\rho_s$ ); the burning surface, which is the area where it is possible to occur heat flux between the burning surface and the non-burning subsurface ( $A_c$  – in Figure 52 is associated to a circle); and the velocity of mass consumption ( $u$ ).

Equation (89) takes the form:

$$\dot{m}_b = \frac{dm_b}{dt} = \rho_s D_b A_c \quad (96)$$

The left side of the equation can be seen as what is happening in zone II and the right side as what is happening at zone I.

In this case, the velocity of mass consumption ( $u_b$ ) it is equal to the propagation velocity ( $D_b$ ), because just phase transitions are occurring and flame is not produced ( $V_s \approx 0$ ). Propagation velocity, due to be a physical characteristic can be directly measured:

$$\mathbb{D}_b = \frac{dx}{dt} \quad (97)$$

Where  $dx$  is the displacement when fresh mass turns into burned mass and  $dt$  the time interval when it occurs.

While the fresh solid mass is consumed, degasification occurs at zone II. This means that a volume of fresh gases are formed while solid mass is burning. Due to mass conservation, the mole number of the burned material is equal to the mole number of the formed gases. Applying the Perfect Gases equation (98), which can be applied for rates, it is possible to have a relationship between the fresh solid mass consumption rate ( $\dot{m}_b$ ) and the volume of the fresh gases formation rate ( $\dot{V}$ ) (equation (99)):

$$PV = nRT \quad (98)$$

$$\begin{aligned} P\dot{V} &= \frac{\dot{m}_b}{M} RT \Leftrightarrow \\ \Leftrightarrow \dot{V} &= \frac{\dot{m}_b}{M} \frac{RT}{P} \end{aligned} \quad (99)$$

Where  $\dot{V}$  is the volume of the fresh gases formation rate,  $\dot{m}_b$  is the fresh solid mass consumption rate,  $M$  is the molar mass of the formed gases multiplied by their molar fraction ( $M = x_i M_i$ ),  $R$  the perfect gas constant,  $P$  the atmospheric pressure and  $T$  the decomposition temperature, which is the phenomena that occurs at the burning surface (zone II).

The volume of the fresh gases formation rate ( $\dot{V}$ ) is directly related with their consumption rate ( $\dot{m}_g$ ) at zone III, because all volume of formed gases are surrounded by a reaction zone, between zone III and luminous flame zone, which confines it and mass conservation is applied. For this, zone III can be called has gases reaction zone. Mathematically this is expressed by relations of equations (91) (92) and (93) between fresh ( $m_f \rightarrow \dot{V}$ ) and burned material ( $m_b \rightarrow \dot{m}_g$ ), which have all the same advancement degree ( $\lambda$ ), considering the boarder of these two different zones.

In zone III, due to reactions, the luminous flame zone is formed, so exists a fundamental flame velocity. The propagation velocity ( $\mathbb{D}_g$ ) is negligible, because chemical reactions are occurring, instead of phase transitions. So  $u = V_F$  (see equation (100)).

Propagation velocity, due to be a physical characteristic can be directly measured (equation (96)), but fundamental flame velocity cannot be, because it is a chemical

characteristic (not observable). So, to find fundamental flame velocity ( $V_F$ ) equation (89) can be applied and takes the form:

$$\dot{m}_g = \frac{dm_g}{dt} = \rho_g V_F A_F \quad (100)$$

Where  $\rho_g$  is the density of the burning gases and  $A_F$  is the area of the flame (burning surface) which, in Figure 52, can be associated to a triangle. Making the analogy between equation (100) and Figure 52, the left part is what is happening on periphery of zone III and the right part, what is happening between zone II and zone III.

The density of the burning gases can be given by:

$$\rho_g = \frac{\dot{m}_g}{\dot{V}} \quad (101)$$

Substituting (101) in (100), is possible to get the fundamental flame velocity equation, expression that gives the final value of  $V_F$  (102):

$$\begin{aligned} \dot{m}_g &= \frac{\dot{m}_g}{\dot{V}} V_F A_F \\ V_F &= \frac{\dot{V}}{A_F} \end{aligned} \quad (102)$$

### 3.3.3. Experimental testing

#### 3.3.3.1. Reactants

Energetic mixtures, presented at Table 15 Table 16, use Ammonium Nitrate ( $\text{NH}_4\text{NO}_3$  “Poreux” AG from *Hydro*) and Urea Nitrate ( $((\text{NH}_2)_2.\text{COHNO}_3)$  from *SelectLab Chemicals, GmbH*) particles as fillers. PolyUrethane, from *Simões de Carvalho, Ltd*, was a formulated commercial product of two liquid solutions, one containing the prepolymer and the other the diisocyanate solution. It is assumed global compositions of these materials according to ICT Database, 2005 (Quaresma, et al., 2013). Thermodynamic properties and global values of used components were presented in Table 17, Table 22 Table 19.

Urea nitrate was bought as wet crystals, so it was needed to dry it. There was needed more than 5h (cycles of 30 min) to dry it at a temperature below 80 °C. Both ammonium and urea nitrates were micronized and stored on sealed containers. To AN was added DMF, in very small concentrations, in order to reduce its hygroscopicity.

Aluminum particles (Al “black 000 India” from *Carob*), Magnesium (delivered from pyrotechnics industry *CAROB Industries*, assuming 92 to 95% purity) and Teflon (delivered by *Goodfellows*, purity was accepted to be up to 98%) were also assumed according to ICT Database, 2005. Magnesium/Teflon (MT) mixture has a fixed Mg/Teflon percentage (in mass) of 55/45% (Quaresma, et al., 2013) (Campos, et al., 2007). Table 23 presents some physical properties of the used Aluminium (vd. Durães, et al., 2006) that is usually applied for pyrotechnic proposes. Its appearance is dark grey and it has a greasy coating to protect it against water attack during storage. The aluminium particles melting point was measured as  $\approx 670$  °C by Simultaneous Thermal Analysis (Rheometrics STA 1500), 10 °C above the value for pure aluminium. The difference may be due to some partial oxidation of aluminium surface by air during storage (Quaresma, et al., 2013) (Durães, et al., 2006).

Table 23. Aluminium physical properties (experimentally measured)

|  | Particle size,<br>$d_{\text{mean}} ; d_{50}$<br>and $d_{90}-d_{10}$ ( $\mu\text{m}$ ) | Density,<br>$\rho$<br>( $\text{kg m}^{-3}$ ) | BET surf. area,<br>$A_s$<br>( $\text{m}^2 \text{kg}^{-1}$ ) | Aver. pore diameter,<br>BET, BJHdesorp.<br>( $\text{Å}$ ) | Purity<br>(%) |
|--|---|--|---|---|---------------|
| Al black 000 India<br>( <i>Carob</i> ) | 18.6 ; 11.8<br>47.7 – 1.6   | $2700.0 \pm 2.8$                             | $4475.2 \pm 299$  | 238 ; 190   | 89.3          |

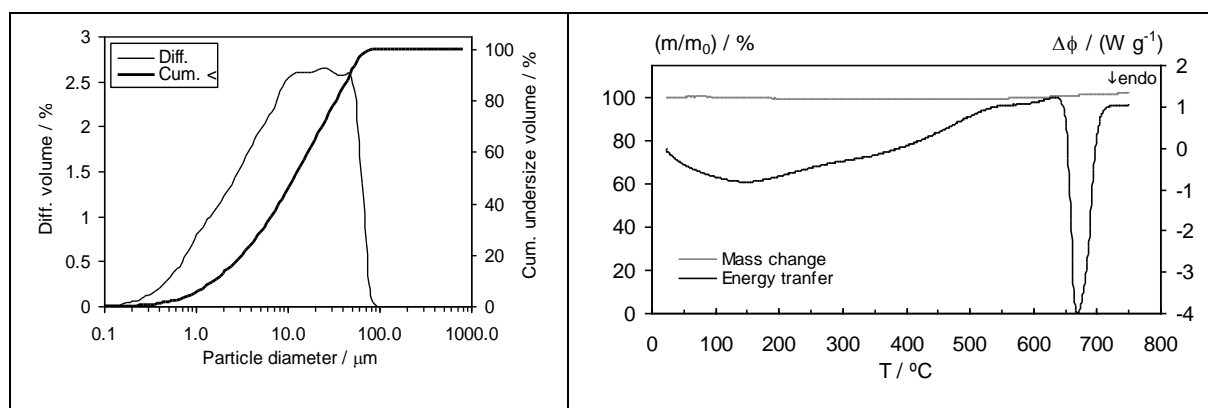


Figure 53. Aluminum (Al black 000 India - Carob) particle size distributions obtained by Laser Diffraction Spectrometry (left figure) and Simultaneous thermal analysis (DSC/TG) of Al black 000 India (Carob), in Ar/H<sub>2</sub>(48%) atmosphere and heating rate of 40°C/min (right figure).

Magnesium was considered to have 92 to 95% purity and granulometric size between 3 and 15  $\mu\text{m}$ . The measure density was 1.60 to 1.67, i.e. less than the approved value cited in ICT Tables, 1974, showing that these Mg particles could be coated with some polymeric or organic material. Teflon material was the granulometric mean size

between 6 to 9  $\mu\text{m}$ . The purity was accepted to be up to 98% (Quaresma, et al., 2013). Thermodynamic properties and global values of used components were presented in Table 20 Table 22.

### **3.3.3.2. *Mixing Procedure***

The experimental mixtures were mixed using homemade (improvised) mixing systems to simulate terrorist conditions. For small quantities (until 8 g), an one screw mixing system – screwdriver – was used (similar to a single screw extruder system). The mixing container was a PVC cylinder, with six holes of two different diameters. For larger quantities (upper to 50 g), a double twin mixing system (kitchen mixer) was used. The mixer container was used as mixing container.

Three different orders of addition of the reactants on the mixing procedure were:

1. Oxidizer, polyol solution, additive and diisocyanate solution.
2. Diisocyanate solution firstly added to the oxidizer, additive and polyol solution.
3. The used one on the optimized mixtures was: oxidizer, polyol solution, diisocyanate solution and the additive was the last component to be added.

The mixing time, for small samples, was around one hour. For larger samples, at least 3 hours were needed. These times could vary, because the most important parameter during the mixing time was the observable homogeneity between reactants. The mixing process was stopped when, apparently, bigger homogeneities were reached.

### **3.3.3.3. *Preparation of the samples***

**Cigar Burning Test.** For cigar burning tests, syringes were used as sample container. They have 10 mm of diameter, 70 mm of length, a PolyMethylMethAcrylate (PMMA) wall (1 mm of thickness) and a piston with 70 mm of length made of PMMA and with an extremity of polybutadiene rubber. This kind of container had two configurations: with and without the tip (Figure 54).

Cigars were prepared by two ways:

1. Injecting the mixtures inside them in a conventional way, which was pressing them through the mixture. Then, the mixture inside the cigar was manually pressed, added more mixture, and pressed again. This pressing methodology was only used when the syringe tip has been cut.

2. When syringes was with their tip (10 mm of length and 4 mm of diameter), mixture was pressed in a press, using a special apparatus developed exclusively for this propose. These king of samples were pressed until they get a pre-defined volume, during one minute.

Preparations were storage from one day to one week before use at room temperature. Samples had the look shown on Figure 54.



Figure 54: Cigar burning test samples

**Disk Burning Test.** The disk, which was the sample container, is composed by a PolyVinyl Chloride (PVC) container and a PolyMethylMethAcrylate (PMMA) lid. (Durães, et al., 2006) Its design is shown on Figure 55.

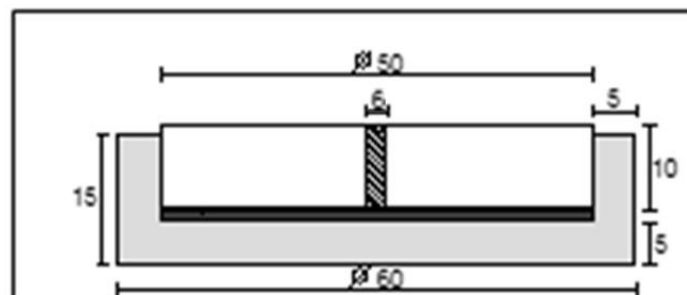


Figure 55: Disk test samples (all dimensions in millimeters). Adapted from Durães, et al., 2006.

For disk burning tests, the mixture was injected and pressed manually, inside the PVC container. After put the PMMA cylinder, disk samples were pressed by two different ways:

1. Disks were put between two steel plates and pressed with a vise, remaining for one week. The polymerization of PU occurred during that time.

2. Disks were pressed in a press, over one minute at 10 tons. The polymerization of PU occurred due to exposure to 80 °C in a oven.

Samples were tested after one day to one week of storage at room temperature and they looked like as shown on Figure 56, respectively. The hole in the center was made before experiments.



Figure 56: disk samples

#### 3.3.3.4. *Experimental set-ups*

**Cigar Burning Test.** To execute this kind of test, two holes were made on the samples, spaced between them of 5 mm and with 5 mm of profundity. The distance between the top of the sample and the first hole was between 10 and 25 mm.

The sample was collocated above a metal cylinder, two Cr/Al thermocouples (Thermocoax TKI 10/10/NN) were put inside the two holes, as shown on Figure 57. These thermocouples were connected to an electronic amplifier for thermocouples (having an integrated circuit for cold junction), allowing measurements of flame temperature. The amplified signal was recorded by a digital signal analyzer (Tektronix TDS 320) and results were printed by a *Desk Jet 550C HP* printer (Figure 58). Independently, a video-crono-photography (Casio Excilim), having recording speed up to 1000 fps (frames per second), allowed the real time flame records. Recording speed was usually 30 fps, implying a time delay of 1/30 s for two successive frames. This camera was collocated in front of the sample.

The graph paper was used as reference for flame displacement, during the tests. The aluminum paper was used to collect the burnt mixture (Figure 57).



Figure 57: Experimental set-up for cigar burning tests

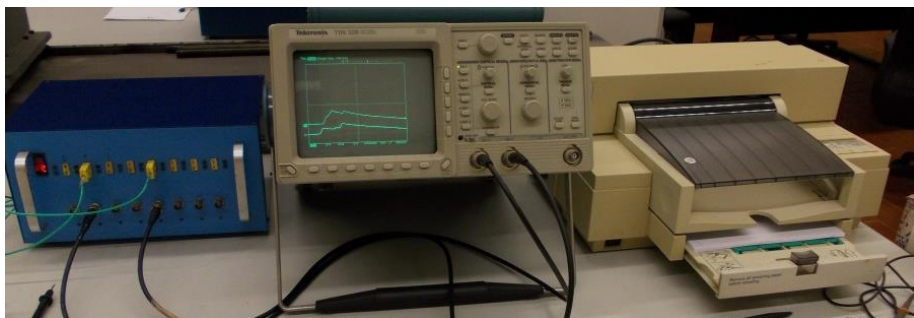


Figure 58: Recording equipment

**Disk Burning Tests.** Disk burning tests were performed in two experimental set-ups. In the first one, disk was put in the horizontal position, sustained by a laboratory claw, a mirror was placed above the disk with an angle around  $45^\circ$ , in order to be possible to film the combustion of the mixture through the PMMA surface (Figure 59). All this apparatus was sustained by a laboratory support.



Figure 59: horizontal experimental set-up for disk burning test

The second experimental set-up used on these tests was in the vertical position. Once again, the disk was held by a laboratory claw, but no mirror was necessary. The camera was put 1 m away from the disk, due to safety aspects for the machine. This set-up is presented on Figure 60.



Figure 60: vertical experiment set-up for disk burning test

#### ***3.3.3.5. Thermocouples and time delay calibrations***

Calibration of the thermocouples, temperature and time measurements, was done using a pyrotechnical cord having standard flame velocities of  $1 \text{ cm.s}^{-1}$  (Figure 61). This procedure allows confirming the measurement of flame velocity, based in time delay between the two thermocouples (Figure 62).



Figure 61: Thermocouples assembly for calibration of temperature equipment

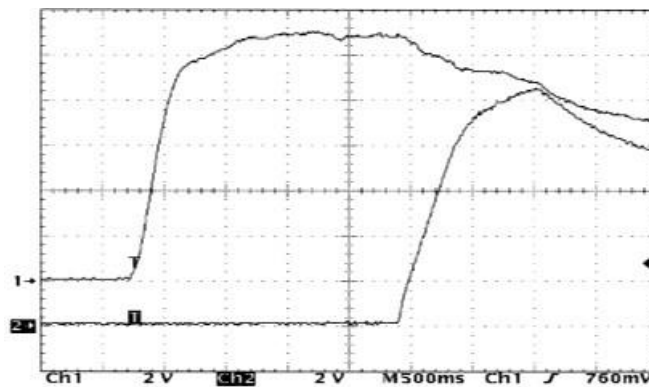


Figure 62: Temperature records showing thermocouples delay allowing flame velocity measurement (2 V/div↔ 200 °C/div.) as a function of time (500 ms/div.)

Between experiments, thermocouples were tested with a lighter flame to ensure that no one was damaged. Figure 63 is exemplificative of that kind of calibration. These kind of calibration consisted on heating of thermocouples during 5 s, with an interval of 15 s between the heating of each thermocouple.

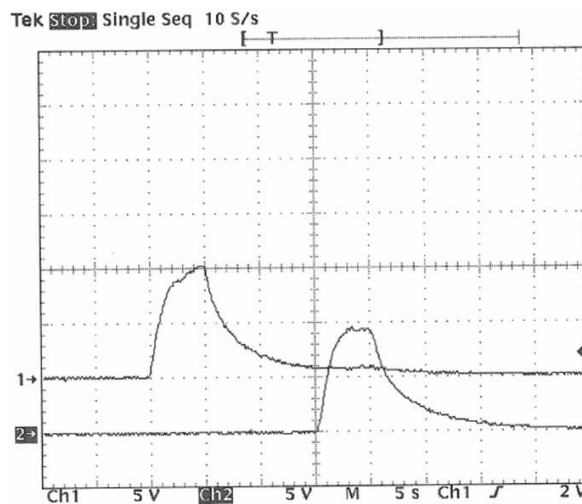


Figure 63: Temperature record in function of time of 5 s of lighter flame in each thermocouple. Between the heating of two thermocouples, 15 s elapsed.

### 3.3.3.6. Typical testing procedure

**Cigar Burning Tests.** These kind of tests were performed quite close to isobaric combustion conditions. Before tests, the recording equipment was programmed for measurements. Temperature measurement records (an example is showed on Figure 64), had selected parameters for digital signal analyzer: 5 V/div, 5s/div and trigger varied between 1 and 3 V. For real time flame records the selected parameters were: 30 fps, HD mode and autofocus for details. Samples were weighed and all relevant lengths (height, width, thermocouples positions and diameter) were measured. Cigar burning tests consisted on ignite the cigar, on the upper part, with a lighter or with a blowtorch. When it was needed, more than one ignition was made. During the combustion of the sample, temperatures were acquired by the thermocouples and all combustion behavior were recorded by the camera. To study closer the combustion phenomena, a magnifying glass was place between the camera and the sample (closer to the sample) (Figure 65). When combustion was extinct, the burnt residues were collected, weighed and packed for further IR analysis.

With the recorded movies, it was possible to study: the propagations of the driven flames of PMMA, the mixture and the explosions; flame velocities and the analysis of the appearance of the flame (reaction zones).

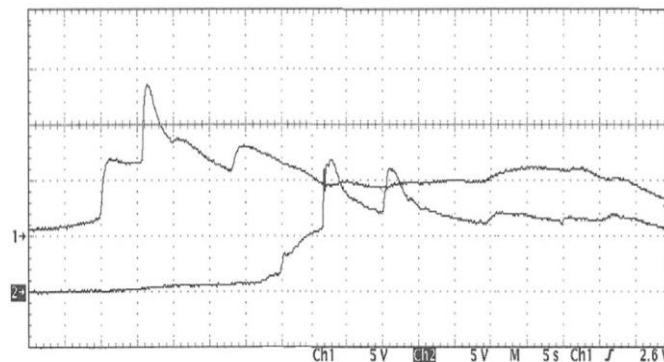


Figure 64. Example of experimental temperature record of AN/PU mixture with MT (5 V/div  $\leftrightarrow$  500 °C/div.) as a function of time (5 s/div.)



Figure 65: Visualization of the combustion of a cigar with the help of a magnifying glass

**Disk Burning Tests.** These kind of tests were performed more close to adiabatic combustion conditions (due to the existing insulating walls). Before disk burning tests, the samples were weighed and mixture thickness was measured. After preparing the camera with the same definitions than referred above and collocate the disk on the vertical position, the disk burning tests started with the ignition of the sample. That was made with a blowtorch at the back part (PVC) of the sample. Sometimes, when ignition by the back was ineffective, it was tried at the front part (PMMA). After combustion, disks were weighed, opened and the burnt mixture was collected and packed to IR analysis.

With the recorded movies was possible to study the areas of two different explosions, time needed by the mixture to acquire that area and all combustion behavior of the samples.

**Studied parameters.** The parameters studied during this work, for cigar burning tests, were: densities of the fresh mixtures; maximum temperature acquired by the thermocouples, during the combustion of the samples; velocity of propagation of the flame in PMMA; velocity of propagation of the flame in one explosion; velocity of propagation of the flame in the mixture and flame velocity in the mixture.

For disk burning tests, the studied parameters were: densities of the fresh mixtures; time elapsed since there was no hot points until the appearance of one that originates explosion; area of the chosen hot point. For the measurements of the hot points there were chosen two different hot points.

All results will have a general description about what was observed during the combustion and relevant facts about measurements will be described. All results will be accompanied by the reference photos that allowed the measurements.

The results will be present by the order and with the numbers presented on Table 15 and Table 16.

**Mathematical expressions used for the treatment of the results.** The density ( $\rho$ ) of the fresh mixture was calculated based on the follow equation:

$$\rho = \frac{m}{V} \quad (103)$$

Where  $m$  is the weighed mass,  $V$  is the volume of the mixture, which was calculated through equation (104).

$$V = \pi \cdot r^2 \cdot l \quad (104)$$

With  $r$  being the radius of the PMMA lid and  $l$  the thickness of the sample.

All velocities of propagation of the different flames ( $\mathbb{D}$ ) were calculated using equation (105):

$$\mathbb{D} = \frac{\Delta x}{\Delta t} \quad (105)$$

Where  $\Delta x$  is the displacement or the length (in the case of the explosions) of the flames during the interval of time,  $\Delta t$ .  $\Delta x$  was measured through chosen frames, where were made relationships between the length shown on figures and the diameter of the syringe or the diameter of the PMMA lid.  $\Delta t$  was the time elapsed between the chosen frames.

The flame velocity ( $\mathbb{V}$ ) was measured through the equation (106):

$$\mathbb{V} = \frac{\mathring{V}}{A_F} \quad (106)$$

$\mathring{V}$  → volume flow of the producted gases

$A_F$  → area of the flame.

The volume flow ( $\mathring{V}$ ) was calculated with basis on the bellow equation:

$$\mathring{V} = \frac{\mathring{m} R T}{P M} \quad (107)$$

Where  $\mathring{m}$  is the mass flow of the burning mixture,  $R$  is the constant for perfect gases,  $T$  is the average temperature of decomposition acquired by DSC/TGA,  $P$  is the atmospheric pressure and  $M$  is molar mass of the predicted produced gases (by THOR

calculations) multiplied by their molar fraction,. The area of the flame ( $A_F$ ) was measured approximating the shape of the flame to a geometrical figures and by the correlations of the lengths of that with the diameter of the cigar (which is known the real value).

The mass flow ( $\dot{m}$ ) was calculated by equation (108):

$$\dot{m} = \rho D A_{F \rightarrow B} \quad (108)$$

$A_{F \rightarrow B}$  is the area of the surface of the mixture which was being burning, which is all the same and is given by the equation (109):

$$A_{F \rightarrow B} = \pi r^2 \quad (109)$$

For the disk burning tests, the area of the chosen hot point was measured through correlations between the measured area and the PMMA lid on the image, which real value was known.

### 3.3.4. Experimental results

#### 3.3.4.1. Mixture n° 1.2 - heterogeneous mixture based on AN, PU and Al

100 g of mixture constituted by 72% AN, 22 % PU and 6% Al (m/m) were prepared using the mixing procedure described on section 3.3.3.2. The disk was prepared using the methodology described in 3.3.3.3, and used after one week of storage.

**Disk burning test.** The density of the disk was  $1600 \text{ kg/m}^3$ . At Figure 66 the aspect of the disk before and after combustion are presented.



Figure 66: Disk of mixture n°. 1.2. Image on the right shows the fresh mixture on the disk. Image on the left shows the disk after the partial combustion of the mixture.

This test was performed with the disk on horizontal position. During this experiment five different ignition modes were tested: with a lighter on the hole of the PMMA face of the disk, this PMMA combustion took more than 3 minutes and mixture not burnt; with a paper impregnated with commercial ethanol placed on the hole in the center of the PMMA face, not even PMMA burnt; with gunpowder and cord fuse placed on the hole; with dried paper and with a burning PMMA stick, both placed on central hole of the disk.

Combustion was reached, after 1 minute, the center of the mixture turned incandescent. The beginning of the incandescence was not recorded. In the end of the ignition with gunpowder and fuse cord there was no incandescence on the mixture, but in the next movie, elapsed one minute and a half, the incandescence was present. Between these two movies elapsed one minute and a half. Two little spark was seen during this ignition time. The incandescence were accompanied by grey smoke, which became stronger during the movies. After 1 minute and 10 seconds, the self-combustion was observed, as it can be seen on Figure 67. Two last referred ignitions were tried before the combustion. Never happened explosions.

On the flame shown on Figure 67, it can be seen 4 colored zones: the transparent one, which corresponds to degasification of the mixture; an orange translucent - ignition zone of the gases released by the mixture; orange - combustion and reaction of the gases with Al; and the white zone, which corresponds to the combustion products of the reaction between Al and the gases released by the mixture.



Figure 67: Combustion of the disk with mixture n°. 1.2.

### ***3.3.4.2. Mixture n° 1.4 - heterogeneous mixture based on AN, PU and MT***

Mixture n°. 1.4 was composed by 72% AN, 22 % PU and 6% MT (m/m). There were made 100 g of mixture through process 2 described on 3.3.3.2. Just disk burning test was made with this composition.

**Disk burning test.** Figure 68 shows the aspect of the sample before it was experimented.



Figure 68: Disk of mixture n°. 1.4 before its combustion

During this experiment, three ignition with the blow torch were tried and two movies were recorded. They lasted 30 seconds, 16 seconds and 6 seconds, respectively.

On the first movie, beside the three ignitions, occurred one explosion 20 seconds after the stop of the last ignition. During this time no incandescence on mixture was seen. Explosion lasted 1 minute, originated a thin orange flame, which had 2 seconds of

duration. It was possible to see the decrease of the light emitted by the flame. Mixture was apparently extinguished during, at least, 7 seconds.

Auto-ignition occurred between movies, because second movie starts with the described flame (but more intense and with a yellow zone). It was auto-ignition, because there was no time between movies to do another ignition with the blowtorch. It started with combustion and not with explosion, because explosions lasted, at least, 1 seconds and the time elapsed between movies was less than that.

This flame can has several reasons: degasification with expansion was always occurring, the flame appeared when that gases reached their temperature of ignition, due to the increase of pressure from combustion of MT mixture; the increase of temperature, due to gas expansion, was high enough to make an exothermic decomposition of AN; the mixture is apparently extinguished until suffers auto-combustion, due to the smolder combustion of PU, which reaches enough temperatures to occur thermal decomposition of Mg and gas expansion due to combustion of Teflon, which originates the flame.

The mixture was apparently extinct during 5 seconds and then occurred one explosion. During this auto-combustion, occurred 5 explosions, always followed by the described flame and the extinction. Mixture was always burning from 4<sup>th</sup> explosion until the end of the last movie. These was observed sometimes on the front part of the disk, other times, just in the back (here sometimes was just luminosity, flame was not visible due to the disk position).

The experiment described above was performed with the disk on horizontal position. Table 24 shows the obtained results. The density was calculated by equation (103). The measurement of the areas of explosion one ( $A_1$ ) and two ( $A_2$ ) were made approaching the incandescent area to a circle and to two ellipses, respectively. The measurements were made comparing the perimeter of the PMMA (see Figure 55) with the perimeters of the burning areas shown on Figure 69 Figure 70, respectively. Time ( $\Delta t$ ) was the elapsed time between frames records of each explosion. The subscript values on A and  $\Delta t$  are referent to the studied explosion and they are associated to the indicated figure. Explosions one and two corresponds to explosions 2 and 5 in the movies. One minute passed between them.

Table 24: Results obtained from the combustion of mixture n°. 1.4.

| $\rho$ (kg/m <sup>3</sup> ) | $\Delta t_1$ (s) | $A_1$ (m <sup>2</sup> ) | Fig. | $\Delta t_2$ (s) | $A_2$ (m <sup>2</sup> ) | Fig. |
|-----------------------------|------------------|-------------------------|------|------------------|-------------------------|------|
|-----------------------------|------------------|-------------------------|------|------------------|-------------------------|------|

|      |      |          |              |      |          |              |
|------|------|----------|--------------|------|----------|--------------|
| 2104 | 0.07 | 2.29E-05 | Figure<br>69 | 0.07 | 3.21E-04 | Figure<br>70 |
|------|------|----------|--------------|------|----------|--------------|

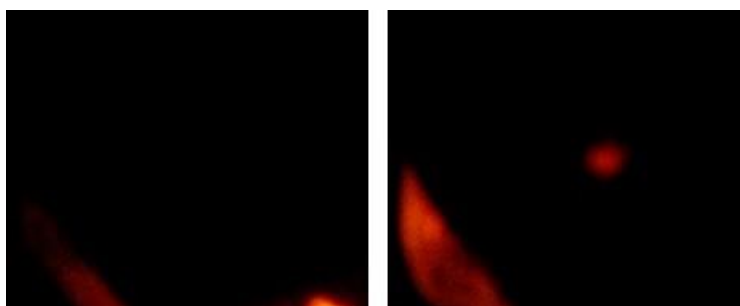


Figure 69: Frames which shows the moment before explosion one (at left) and the first appearance of explosion one (at right). The measurement of the area was made at right image.

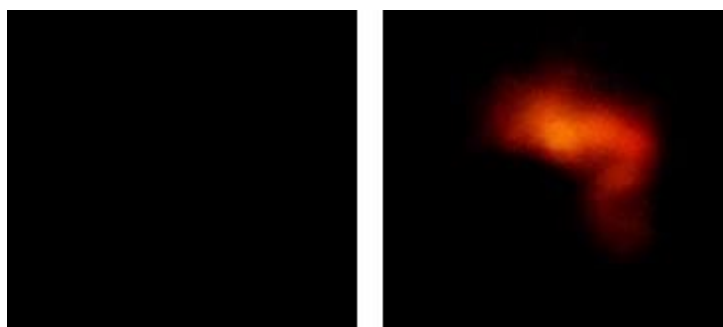


Figure 70: Frames which shows the moment before explosion two (at left) and the first appearance of explosion two (at right). The measurement of the area was made at right image.

#### **3.3.4.3. Mixture n° 1.5 - heterogeneous mixture based on AN, PU and MT**

The composition of this mixture was 69% AN, 21% PU and 10% MT (m/m). There was made 50 g of this mixture and that was used methodology 2 described on 3.3.3.2. Both tests were performed with this mixture.

**Cigar Burning Test.** The sample was prepared by methodology 1, for cigar burning test, described on 3.3.3.3. Figure 71 shows the cigar before and after combustion.

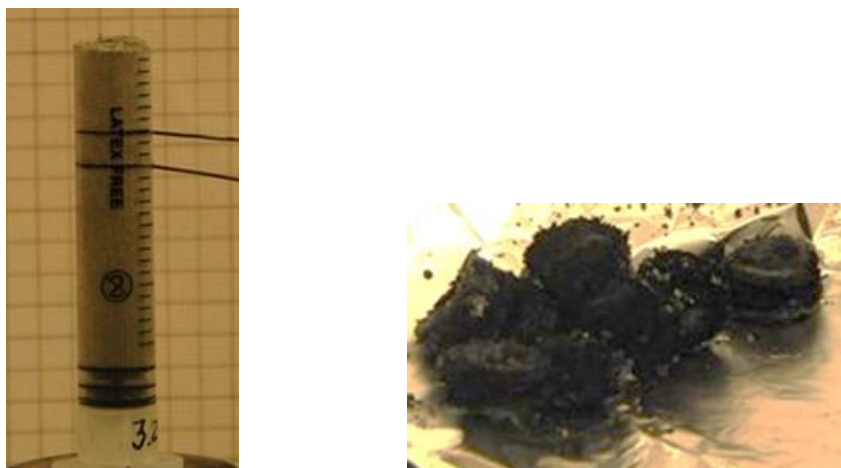


Figure 71: Mixture n°. 1.5 prepared for a cigar burning test (left) and its residues after combustion (right)

On this experiment, the trigger was made manually. 14 explosions occurred during 1 minute and 51 seconds, with different intensities and durations. There was no significant light changes before explosions, but after them, the flames lost their light intensities (sometimes, just was possible to see an orange thin perimeter - Figure 74, the right one). This fact occurred probably due the strong gas expansion caused by MT mixture.

During all experiment was possible to see the bubble of the mixture and the porosity of burnt material, which proves degasification. This is also possible to see in some shown images (Figure 72, Figure 73, Figure 75). The gas expansion was also seen, because the volume of the burnt material was higher than the fresh one, during the combustion process.

Analysing the flame shown on Figure 72, it is possible to observe the three zones: the almost transparent orange, which corresponds to degasification; the orange zone, which is the ignition of the formed gases; and the yellow zone, which is correspondent to the combustion of the ignited gases. It is also possible to see the combustion of MT mixture by the white trace in the orange hollow zone. The colours of this flame are quite different from those which has Al as additive. This fact can be due to the radiative formed products, which not get such higher temperatures as the ones formed with Al, and / or due to less formation of black carbon, showing a minor pyrolysis from PU.

The results obtained from the analysis of this experiment are summarized on Table 25.



Figure 72: Flame of combustion of mixture n°.1.5 on a cigar burning test.

Table 25: Results obtained from the combustion of mixture n°. 1.5 on cigar burning test. There was studied: density of the fresh mixture ( $\rho$ ), maximum temperatures acquired by thermocouples ( $Th_1$  is the upper one and  $Th_2$  is the downer), velocities of flame propagation of PMMA, explosion, mixture and fundamental flame velocity.

|                                    |           |
|------------------------------------|-----------|
| $\rho$ (kg/m <sup>3</sup> )        | 1377.2    |
| Maximum temperature – $Th_1$ (°C)  | 1300      |
| Maximum temperature – $Th_2$ (°C)  | 1350      |
| $D_{PMMA}$ (m/s)                   | 2.00E-04  |
| Studied images for $D_{PMMA}$      | Figure 73 |
| $D_{explosion}$ (m/s)              | 5.00E-03  |
| Studied images for $D_{explosion}$ | Figure 74 |
| $D_{mixture}$ (m/s)                | 1.06E-04  |
| Studied images for $D_{mixture}$   | Figure 75 |
| $V_{Flame}$ (m/s)                  | 1.43E-01  |
| Studied image for $V_{Flame}$      | Figure 72 |

For calculation of the velocity of flame propagation of PMMA ( $D_{PMMA}$ ) it was used equation (105). The baseline for position measurement was the liquid PMMA, shown on Figure 73. The delay time was measured between frame time references.

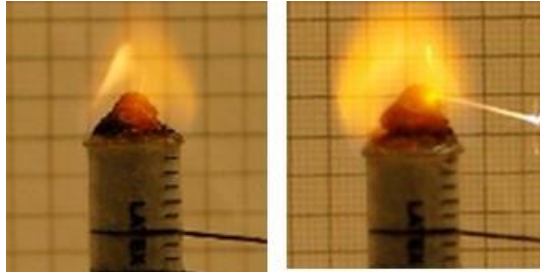


Figure 73: Frames used to study the velocity of flame propagation of PMMA. The initial position is image on the left, final position the image on the right.

Equation (105) was used to calculate the velocity of the propagation of the explosion ( $D_{\text{explosion}}$ ) and measurement were made on the left image shown on Figure 74. The measurement of the burnt distance was the length of the incandescent part. The time was measured as described above.

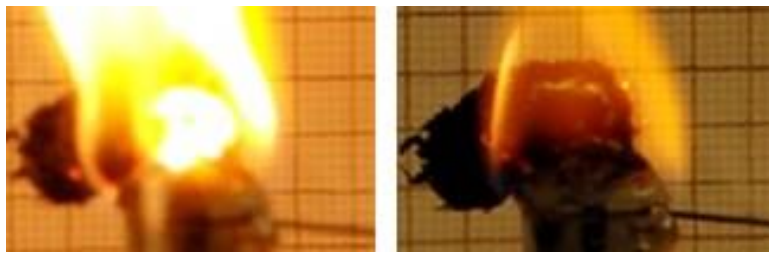


Figure 74: Frames used to study the velocity of propagation of explosion in mixture n°. 1.5. The frame of the left shows the bigger burning area of this explosion and the frame of the right shows the end of the explosion (when no more incandescence on the mixture was seen).

Once again, equation (105) was used to calculate the velocity of propagation of the mixture ( $D_{\text{mixture}}$ ), based on measurements made on Figure 75. The baseline for position measurements was the incandescent bubble on both frames. The delay time was measured between frame time references.

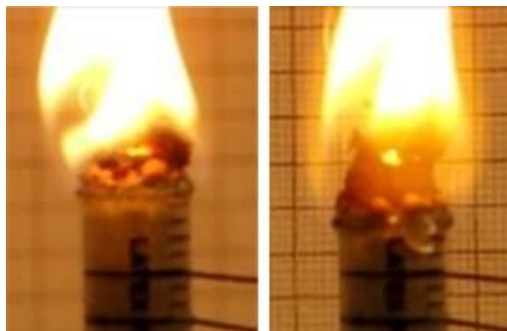


Figure 75: Frames used to study the velocity of propagation of the mixture n°. 1.5. The frame at the left is correspondent to the initial position, and the frame at right, the final position.

To calculate the flame velocity ( $V_{\text{Flame}}$ ), equation (106) was used. The area of the flame was measured in Figure 72, approximating the shape of the flame's area to a triangle and by the correlations of the lengths of the triangle with the diameter of the cigar (which is known the real value). The base of the triangle was coincident with the last line which is possible to see in the hollow zone. There was also considered the area of a rectangle which height was from bubbles of burning mixture until the base of the triangle. The width considered was the vanished yellow limit.

**Disk Burning Test.** This sample was prepared by methodology 1 described at 3.3.3.2, for disk burning tests. Figure 76 shows the aspect of the sample before it was experimented.



Figure 76: Disk of mixture n°. 1.5 before its combustion

This experiment was performed with the disk on a vertical position. During almost 1 minute, three attempt of ignition were made. The first one was for short time, but the

next two were longer. Two more ignitions, always with a blowtorch, were tried. The last ignition, which lasted 26 seconds, finally turned into combustion.

During 2 minutes and 3 seconds, 16 explosions occurred. Explosions 8, 9, 10, 11 and 12 were extinguished with a blowing. . Between explosions there was no possibility to see burning mixture, due to PMMA flames. It just was possible to see on shown images of studied explosions 1 and 2, which corresponds on reality to explosions 11 and 15.

Every explosions generated light as shown on left frame of Figure 77. The kind of flames shown on Figure 78 corresponds to mixture's combustion, without explosion. PMMA flames are more yellow than white, when compared with those ones.

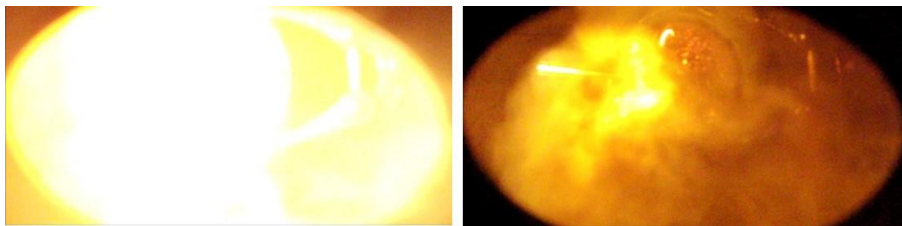


Figure 77: Flames generates by explosion. Frame of the left shows the maximum intensity of light during explosions. Frame of the right shows the flame on the end of the explosion.

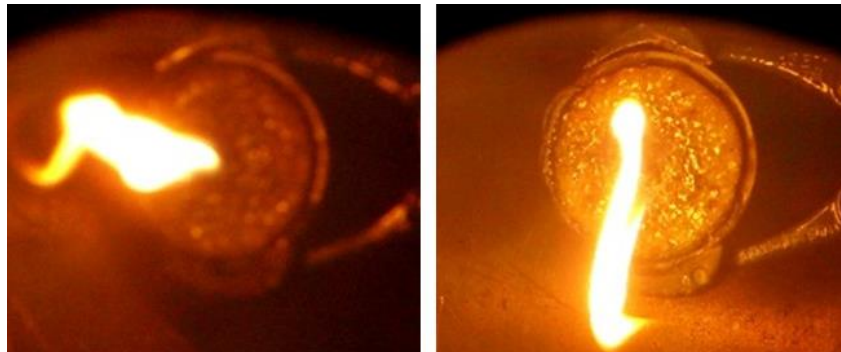


Figure 78: Combustion flames generated by the burning of mixture n°.1.5

The studied parameters on this test were the same referred on 3.3.3.2. The results are presented on Table 26.

Table 26 Results obtained from the disk burning test of mixture n°. 1.5.

| $\rho$ (kg/m <sup>3</sup> ) | $\Delta t_1$ (s) | $A_1$ (m <sup>2</sup> ) | Fig.      | $\Delta t_2$ (s) | $A_2$ (m <sup>2</sup> ) | Fig.      |
|-----------------------------|------------------|-------------------------|-----------|------------------|-------------------------|-----------|
| 1775.0                      | 0.07             | 7.39E-05                | Figure 79 | 0.07             | 7.99E-06                | Figure 80 |

The measurements were made taking in account the area of both incandescent parts (the most yellow ones) shown on Figure 79 Figure 80. They were approximated to circles. In case of explosion two, the sum of the two circles was made. This explosions corresponds to self-ignition of the mixture. The Figure 79 Figure 80 were acquired after self-extinction and during auto-ignition.

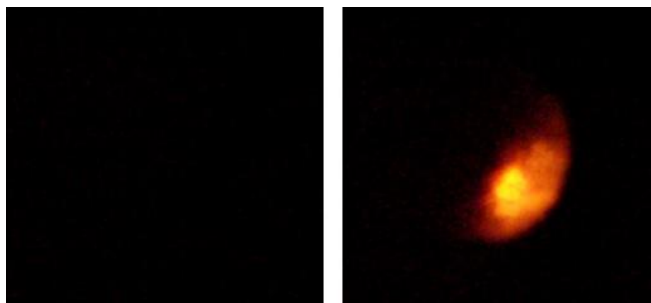


Figure 79: Frames which shows the moment before explosion one (at left) and the first appearance of explosion one (at right). The measurement of the area was made at right image.

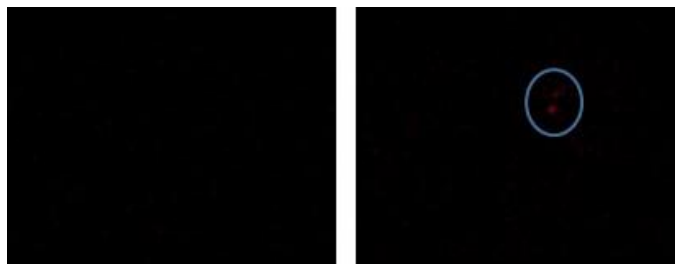


Figure 80: Frames which shows the moment before explosion two (at left) and the first appearance of explosion two (at right). The measurement of the area was made at frame of the right.

#### ***3.3.4.4. Mixture n° 1.8 - heterogeneous mixture based on AN, PU and Al***

The chemical composition of this mixture was 69% AN, 21% PU and 10% Al (m/m). 50 g of mixture were made with procedure 2 (3.3.3.2). Both tests were realized with this mixture.

**Cigar Burning Test.** The sample was prepared by methodology 1, for cigar burning test, described on 3.3.3.3. Figure 81 shows the cigar before and after combustion. The part of the mixture which is outside of the syringe appeared during the curing time, which indicates that the mixture expands during the curing time.

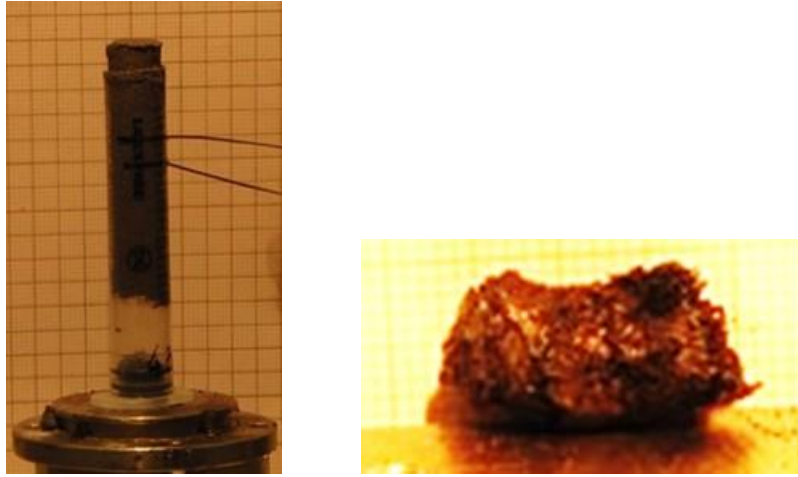


Figure 81: cigar of the fresh mixture n°.1.8 (left) and its residues of combustion (right)

During the film measurement (2 minutes and 57 seconds) occurred two explosions. Just one ignition (with lighter) was necessary and mixture started the combustion without the help of the PMMA flame. The ignition was made directly on the mixture, on the upper part of cigar (see Figure 81 – the left one), and the combustion was auto-sustained until it arrives to PMMA surrounding material.

There was gas expansion, because the volume of the burnt material was higher than the fresh one. This fact is also observable at Figure 82, by the hollow part on the showed flame. On that figure in also possible to see an inclination on burning surface, as well as on flame position. It indicates the heterogeneities of the mixture, which different concentrations on same area produces different burning conditions, forming a slant on effective surface of combustion.

Analysing the flame (Figure 82), is possible to see three different zones: the hollow one, due to gas expansion; the orange one, due to the ignition of the produced gases; and the white one, due to combustion of the referred gases. The white colour is due to the radiance of black carbon. There is also possible to see some sparks, probably due to higher concentrations of Al particles on that surface.

The explosions occurred probably due to the presence of even higher Al concentrations on that surface, which was used to increase the temperature of combustion on mixtures, and it was effective. The heterogeneity saw on combustion process is directly related with the heterogeneity of the studied mixture. The results obtained from the analysis of this test are presented on Figure 27.



Figure 82: Flame of combustion of mixture n°. 1.8 on a cigar burning test

Table 27: Results obtained from the combustion of mixture n°. 1.8 on cigar burning test. There was studied: density of the fresh mixture ( $\rho$ ), maximum temperatures acquired by thermocouples ( $Th_1$  is the upper one and  $Th_2$  is the downer), velocities of flame propagation of PMMA, explosion, mixture and fundamental flame velocity.

|                                    |           |
|------------------------------------|-----------|
| $\rho$ (kg/m <sup>3</sup> )        | 1249.8    |
| Maximum temperature – $Th_1$ (°C)  | 850       |
| Maximum temperature – $Th_2$ (°C)  | 1250      |
| $D_{PMMA}$ (m/s)                   | 1.61E-04  |
| Studied images for $D_{PMMA}$      | Figure 83 |
| $D_{explosion}$ (m/s)              | 7.16E-03  |
| Studied images for $D_{explosion}$ | Figure 84 |
| $D_{mixture}$ (m/s)                | 1.11E-04  |
| Studied images for $D_{mixture}$   | Figure 85 |
| $V_{Flame}$ (m/s)                  | 3.93E-01  |
| Studied image for $V_{Flame}$      | Figure 82 |

The reference for the measurement of the velocity of propagation of flame in PMMA ( $D_{PMMA}$ ) was the upper part of the liquid PMMA (Figure 83). Equation (105) was used for the calculation of this parameter. The methodology employed to record distance and time was the same along all this work (images from delay).

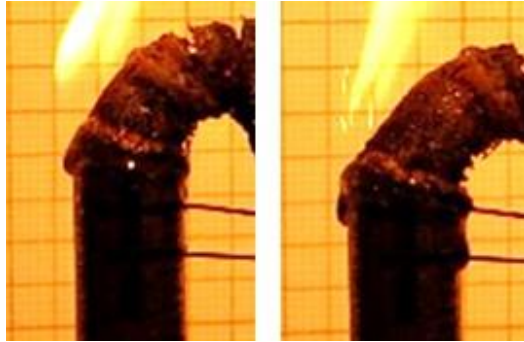


Figure 83: Frames used to study the velocity of the propagation of the flame on PMMA. The initial position is image on the left, final position the image on the right

The measurement of the velocity of propagation of the explosion ( $D_{\text{explosion}}$ ) was made in a similar way than described for mixture n°. 1.5. Due to the reaction of Al with the products of combustion of mixture n°.1.8, the length of the burnt residues (the incandescent ones on both frames of Figure 84) increased. That length was taken as displacement. The initial position was the base of the incandescent part on left frame. The final position was the upper part of the incandescent residues on the right frame of Figure 84.

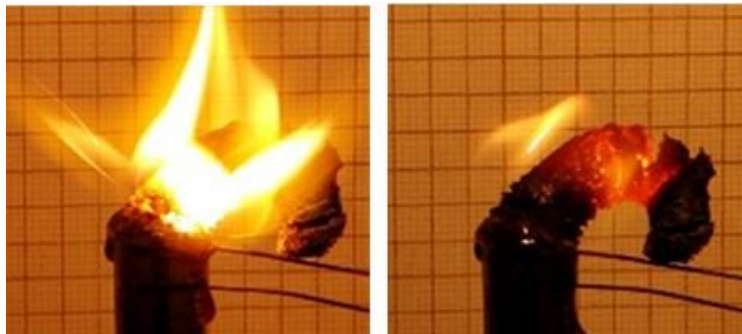


Figure 84: Frames used to study the velocity of propagation of explosion in mixture n°. 1.8.

The measure of the velocity of propagation of the flame ( $D_{\text{mixture}}$ ) in mixture n°. 1.8 was acquired between two explosions. The baseline for position measurements was the separation between PMMA and the burnt mixture (Figure 85). The methodology employed was the correlations between real and photographic distances and equation (105).

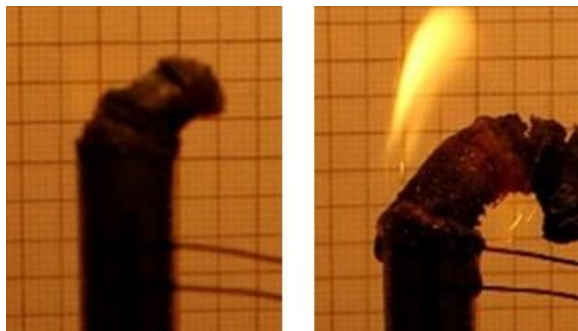


Figure 85: Frames used to study the velocity of propagation of the mixture n°. 1.8. The frame at the left is correspondent to the initial position, and the frame at right, the final position.

For measurements of fundamental flame velocity ( $V_{\text{Flame}}$ ) there was constructed a triangle which perimeter was coincident with the separation between the orange and the yellow zone of the flame of Figure 82. The base of this triangle was coincident with the middle part of the burnt mixture. Correlations between real and photographic distances were made. The calculation was based on equations (106) to (109).

**Disk Burning Test.** This sample was prepared by methodology 1 described at 3.3.3.3, for disk burning tests. Figure 86 shows the aspect of the sample before it was experimented. No pictures were taken to the burnt sample.

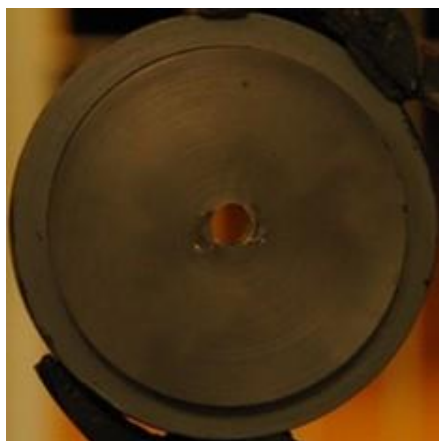


Figure 86: Disk of mixture n°. 1.8 before its combustion

This experiment was performed with the disk on a vertical position. There were needed approximately 4 minutes to get ignition of the mixture in the disk.

Ignition was made with a blowtorch, at the back part of the disk (PVC) and that was not constant during the 4 minutes (some stops were made to see if ignition was already happening).

During 2 minutes and 11seconds of film occurred 10 explosions, with different durations and intensities. To count explosions, the reference were: the burning mass and the intensity / colour of the light of the flame emitted by the mixture.

When there was mass consumption, which was possible to see as represented on Figure 87, the emitted flame was yellow, almost white. When, apparently, there was no mass consumption, the flame was orange, almost transparent, with some sparks (Figure 87, the right one). This transparency was due to degasification of the mixture and the sparks due to Al's reaction with gaseous combustion products. When the mass consumption was higher, longer was the duration of the yellow flame. These descriptions show the mixture heterogeneity. This heterogeneity was also seen due to the propagation of the mass consumption, which was no linear. Sometimes, just a little area burnt, other times were possible to see the incandescence propagates through the mixture.

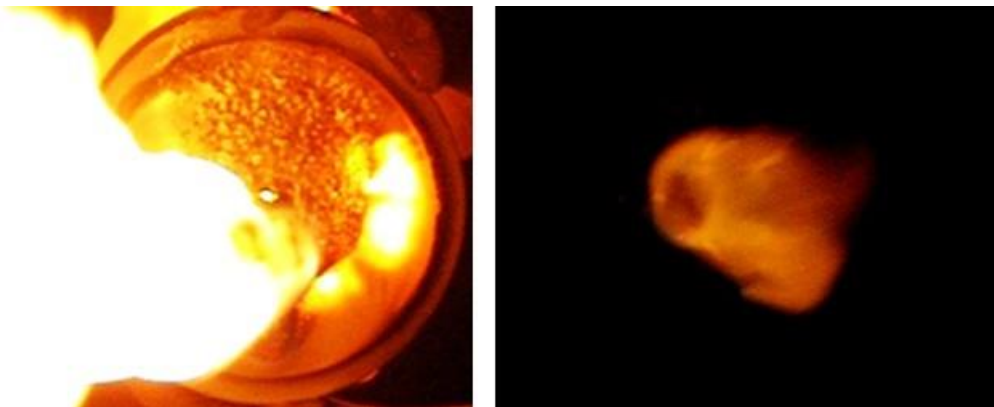


Figure 87: Flames of combustion of mixture n°.1.8 when it had mass consumption (at left) and when there was no mass consumption (at right).

The results presented on Table 28 were calculated from equation (109).

Table 28 Results obtained from the disk burning test of mixture n°. 1.8.

| $\rho$ (kg/m <sup>3</sup> ) | $\Delta t_1$ (s) | $A_1$ (m <sup>2</sup> ) | Fig.      | $\Delta t_2$ (s) | $A_2$ (m <sup>2</sup> ) | Fig.      |
|-----------------------------|------------------|-------------------------|-----------|------------------|-------------------------|-----------|
| 2080.1                      | 0.07             | 8.17E-05                | Figure 88 | 0.03             | 6.16E-06                | Figure 89 |

The measurements of areas were made comparing the perimeter of the PMMA (which was measured before combustion) with the perimeters of the burning areas shown on Figure 88 and Figure 89, which were approximated to circles. The delay time was measured between frame time references.



Figure 88: Frames which shows the moment before explosion one (at left) and the first appearance of explosion one (at right). The measurement of the area was made at right image.

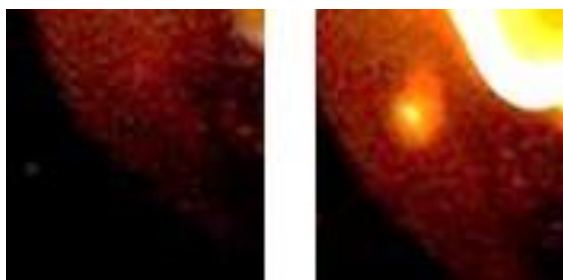


Figure 89: Frames which shows the moment before explosion two (at left) and the first appearance of explosion two (at right). The measurement of the area was made at frame of the right.

### ***3.3.4.5. Mixture n° 2.6 - heterogeneous mixture based on UN, PU and Al***

This mixture had, as composition, 77% UN, 12% PU and 11% Al (m/m). The used mixing procedure was the 2, referred on 3.3.3.2, and 50 g of mixture were produced. Just cigar burning test was experimented.

***Cigar Burning Test.*** Sample was prepared according to methodology 1 presented on *Preparation of the samples*, for cigar burning test. Figure 90 shows the look of the mixture n° 2.6 before and after its combustion.

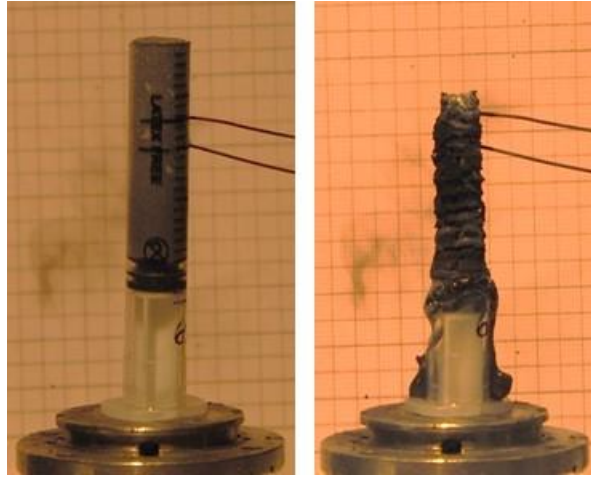


Figure 90: Mixture n°. 2.6 prepared for a cigar burning test (left) and its residues after combustion (right)

At the beginning of this test, the burning mixture suffered self-extinction. Movie was recorded immediately after the second ignition with lighter. It was recorded other self-extinction of the flame. These extinctions can be explained by the heterogeneity of the mixture, high gas production and low temperature flames of PMMA, whose conciliation not promote the combustion of the mixture.

Combustion is reached by driven flame due to self-combustion of PMMA at zones where heterogeneity is not so high, and the temperature of the PMMA flame (plus its slow burning rate) is enough to keep the driven flame of the mixture. In zones where the additive concentration is higher, explosions occurs.

Driven-flame process, from PMMA surrounded cylinder, was very important to sustain flame progression in the mixture.

Analysing the flame of combustion (Figure 91), this degasification is observable, it is the hollow zone between the ashes and orange part of the flame. After degassing, the formed gas reacts with oxygen from air, suffering ignition (orange zone of the flame) and posterior combustion. The yellow (almost white) zone of the flame corresponds to the emission of light from gaseous combustion products, which had gases as reactants. This colour corresponds to the emission of black carbon, when exposed to high temperatures.

Table 29 summarize the results achieved on the treatment of this experiment.



Figure 91: Flame of combustion of mixture n°. 2.6 on a cigar burning test

Table 29: Results obtained from the combustion of mixture n°. 2.6 on cigar burning test. There was studied: density of the fresh mixture ( $\rho$ ), maximum temperatures acquired by thermocouples ( $Th_1$  is the upper one and  $Th_2$  is the downer), velocities of flame propagation of PMMA, explosion, mixture and fundamental flame velocity.

|                                    |           |
|------------------------------------|-----------|
| $\rho$ (kg/m <sup>3</sup> )        | 1345.4    |
| Maximum temperature – $Th_1$ (°C)  | 1300      |
| Maximum temperature – $Th_2$ (°C)  | 1800      |
| $D_{PMMA}$ (m/s)                   | 2.41E-04  |
| Studied images for $D_{PMMA}$      | Figure 92 |
| $D_{explosion}$ (m/s)              | 6.00E-03  |
| Studied images for $D_{explosion}$ | Figure 93 |
| $D_{mixture}$ (m/s)                | 1.75E-04  |
| Studied images for $D_{mixture}$   | Figure 94 |
| $V_{Flame}$ (m/s)                  | 2.45E-01  |
| Studied image for $V_{Flame}$      | Figure 91 |

The baseline for the measurement of  $D_{PMMA}$  was the lower part of the liquid PMMA, for both images of Figure 92. The expression (105) was used to this calculation. The delay time was measured between frame time references.

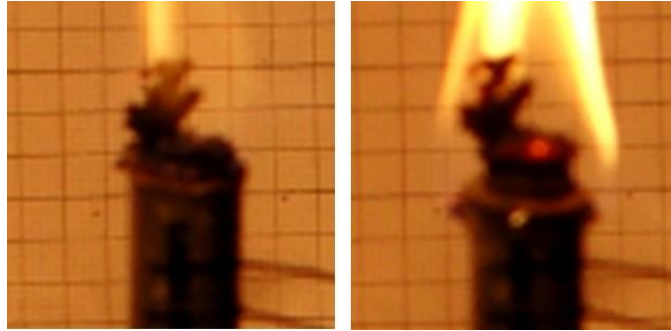


Figure 92: Frames used to study the velocity of the propagation of the flame on PMMA. The initial position is image on the left, final position the image on the right.

To calculate  $D_{\text{explosion}}$  equation (105) was used and there was measured the height of the incandescent part of the mixture (right image of Figure 93). That was made relating the distances of the photo with the real ones, like the width of the cigar. Time was measured as referred above.

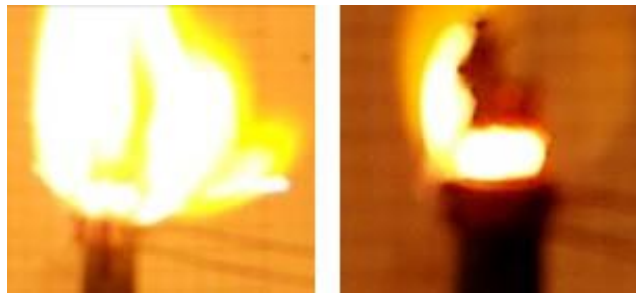


Figure 93: Frames used to study the velocity of propagation of explosion in mixture n°. 2.6.

For calculation of  $D_{\text{mixture}}$  equation (105) was used. Initial position was determined immediately on the beginning of sustained combustion (without external source), and final position was determined by the last incandescent point on the video. The reference frames are shown on Figure 94. Time was recorded by the video. During this measurements occurred two explosions.

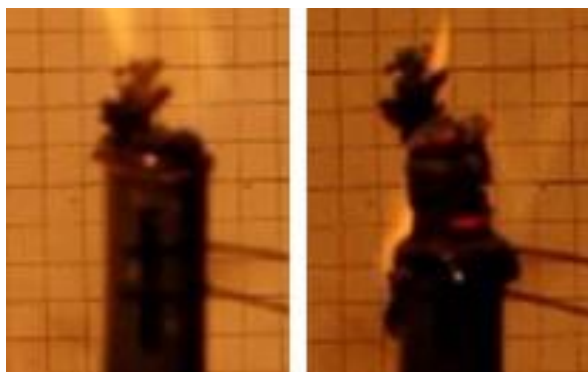


Figure 94: Frames used to study the velocity of propagation of the mixture n°. 2.6. The frame at the left is correspondent to the initial position, and the frame at right, the final position.

The fundamental flame velocity ( $V_{\text{Flame}}$ ) was measured through the calculation using expressions (106) to (109) and with base on flame showed on Figure 91. The area of the flame was measured approximating the shape of the flame to a triangle and by the correlations of the lengths of the triangle with the diameter of the cigar (which is known the real value).

#### **3.3.4.6. Mixture n° 2.7 - heterogeneous mixture based on UN, PU and MT**

Mixture n°. 2.7 was composed by 77% UN, 12%PU and 11%MT (m/m). The employed mixing procedure was the 2 on 3.3.2.2. 50 g of mixture were prepared.

This mixture never was collocated on disks or on syringes, because it suffered self-ignition 10 minutes after its preparation.

After its preparation, mixture was stored on a plastic cup covered with aluminium paper. In less than 10 minutes, it was possible to see the formation of dense gases, with a green dark colour near the mixture and with white colour near the aluminium paper.

Since this observation until self-ignition occurred few seconds passed. The aluminium paper was projected, a white and very brilliant flame was formed, which had the diameter of the cup, around 1 meter of height. The colour of the flame was very similar to that one showed on left image of Figure 77, typical from combustion of the MT mixture.

A fire extinguisher was used to extinguish this combustion.

#### **3.3.4.7. Mixture n° 3.1 - heterogeneous mixture based on AN, PU and MT**

The chemical composition of this mixture was 84% AN, 7% PU and 9% MT (m/m). 50 g of mixture were made with procedure 3 (3.3.3.2). Both tests were realized with this mixture.

**Cigar Burning Test.** The sample used in this experiment was prepared according methodology 2 described on 3.3.3.3, for cigar burning tests. The preparation of the sample was made one month after mixture's preparation. Temperature measurement was performed with only a thermocouple.

Figure 95 shows the aspect of the mixture before and after its combustion on a cigar burning test.

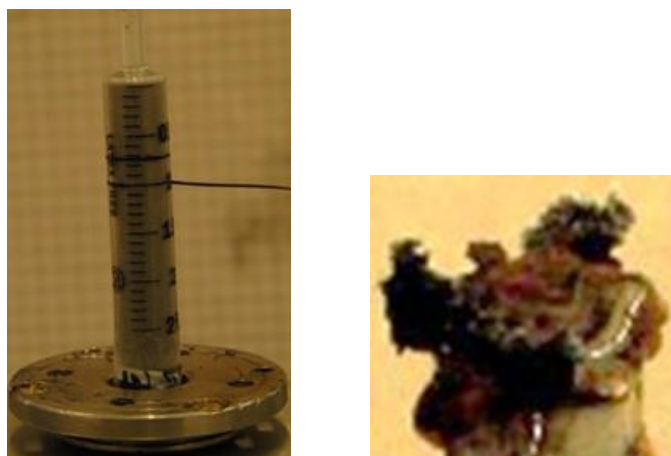


Figure 95: Mixture n°. 3.1 prepared for a cigar burning test (left) and its residues after combustion (right).

During the combustion was possible to see the expansion of the burnt mixture and the outflow of the liquid mixture (visible at Figure 98 and Figure 99). This outflow, coupled with large gas expansions during explosions, caused the inclination of the burning mixture (visible at Figure 96).

There occurred 60 explosions during 3 minutes and 54 seconds, with different durations and intensities. After one of the explosions, there were burning mixture that jumped away and continued to burning outside the cigar. At this point, the PMMA flame was enough to cause other explosion which extinguished the combustion, showing the large gas expansion. This phenomena was seen a couple of times.

During 1 minute and 19 seconds of ignition (after one explosion that extinguished the combustion of the mixture), the lighter flame was enough to cause bubble of the mixture

and 5 explosions, without combustion get to a PMMA driven-flame combustion. When driven-flame combustion was reached, mixture continued the combustion during 2 minutes and 34 seconds, always with explosions happening.

The flame of this mixture was also very irregular between explosions, as described above. At Figure 96, is possible to see the PMMA combustion (blue zone), gas expansion (bubble and hollow zone of the flame), gas ignition (orange zone), gas combustion (yellow zone) and the presence of high temperature on the burning mixture (incandescent parts in the mixture). The explosions caused by MT mixture have much more luminosity than the ones caused by Al, and that is the reason to use MT compositions on flares.

The results of the analysis of this test are presented on Table 30.



Figure 96: Flame of combustion of mixture n°. 3.1 on a cigar burning test

Table 30: Results obtained from the combustion of mixture n°. 3.1 on cigar burning test. There was studied: density of the fresh mixture ( $\rho$ ), maximum temperatures acquired by thermocouples ( $Th_1$  is the upper one and  $Th_2$  is the downer), velocities of flame propagation of PMMA, explosion, mixture and fundamental flame velocity.

|                                    |           |
|------------------------------------|-----------|
| $\rho$ (kg/m <sup>3</sup> )        | 1332.6    |
| Maximum temperature – $Th_1$ (°C)  | 1250      |
| Average temperature – $Th_1$ (°C)  | 900       |
| $D_{PMMA}$ (m/s)                   | 2.00E-04  |
| Studied images for $D_{PMMA}$      | Figure 97 |
| $D_{explosion}$ (m/s)              | 2.89E-03  |
| Studied images for $D_{explosion}$ | Figure 98 |
| $D_{mixture}$ (m/s)                | 5.00E-05  |

|   |                               |
|---|-------------------------------|
| Studied images for $D_{\text{mixture}}$ | Figure 99                     |
| $V_{\text{Flame}}$ (m/s)                | $4.451\text{E-}01 \pm 0.0005$ |
| Studied image for $V_{\text{Flame}}$    | Figure 96                     |

To calculate  $D_{\text{PMMA}}$  it was used equation (105). The baseline for positions in this measurement of was the separation between liquid PMMA and liquid mixture, on both frames showed on Figure 97. The delay time was measured between frame time references.



Figure 97: Frames used to study the velocity of the propagation of the flame on PMMA. The initial position is image on the left, final position the image on the right.

According to equation (105) to calculate  $D_{\text{explosion}}$ , the measurement of the burnt distance was based on the left frame of Figure 98 and was the length of the incandescent part. The delay time was measured between frame time references.



Figure 98: Frames used to study the velocity of propagation of explosion in mixture n°. 3.1.

The measurement for  $D_{\text{mixture}}$  was made between explosions, according to equation (105). The baselines for positions were the bubble part of the mixture, for both frames on Figure 99. The time was measured as referred above.



Figure 99: Frames used to study the velocity of flame propagation in the mixture n°. 3.1. The frame at the left is correspondent to the initial position, and the frame at right, the final position.

For calculations of  $V_{\text{Flame}}$ , equations (106) to (109) were used. The baseline for this area measurement was the hollow triangle, surrounded by yellow flame (Figure 96). The rectangle area correspondent to the burnt products (which are visible on the hollow part) was subtracted of triangle's area.

**Disk Burning Test.** This sample was prepared by methodology 2 described at 3.3.3.3, for disk burning tests. The preparation of the sample was made one month after mixture's preparation. Figure 100 shows the aspect of the sample before and after it was experimented.



Figure 100: Disk of mixture n°. 3.1. Image on the left shows the fresh mixture on the disk. Image on the right shows the disk after the combustion.

This test was performed on the vertical position. During this test were recorded one movie with 6 minutes and 18 seconds. Three ignitions were tried, always with a blowtorch and at the back of the sample. The first lasted 8 seconds, the other two lasted around 30 seconds.

On first ignition, 7 explosions occurred. The mixture appeared always incandescent between explosions and, sometimes, it was possible to see its increase and decrease. When blowtorch was off, mixture just sustain the combustion for 1 minute and a half. Total time of combustion was 1minute and 8 seconds.

During the second ignition occurred 6 explosions and the incandescence between explosions were not so notable. Sometimes, there were any incandescence between explosions. Once again, after blowtorch was off, the combustion just sustained itself during 1 minute and a half.

Third ignition lasted 30 seconds and occurred 7 explosions. After blowtorch was off, was possible to see a blue flame. Self-sustained combustion (without flame) and PMMA driven flame combustion (blue flame) lasted 3 minutes and 14 seconds. During this time occurred 78 explosions. The blue flame was not present between explosions in most of the time, but sometimes it reappeared. One time, when mixture was apparently extinguished, a blow was enough to promote an explosion.

Due to the back part the sample container was almost totally destroyed, when explosions occurred, it was possible to observe a yellow/white flame emerge, but it was extinguished in the end of explosions. Some explosions were enough to propagate other explosions. Just the explosions which come from extinguished mixture were counted. It was possible to observe that, for maintain self-combustion which occurred just on the end of the third ignition, mixture had to be incandescent on the centre.

The fact that was possible to see the mixture totally extinguished between explosions is, probably, due to the gas expansion from MT. The increase of pressure originated the explosions, and probably not the increase of temperature. Other hypothesis for these pulsed explosions can be the non-linearity of heat transfer along the mixture, due to heterogeneities. Explosions could occurred when heat reached zones of higher concentrations of MT mixture. The facts of there were no incandescence between explosions and there happened heat transfer could be due to the smoulder combustion of PU. This can also explain combustion due to increase of pressure and not of temperature, because PU is formulated for not burn (safety aspects on its uses).

The results presented on Table 31 were calculated from equation (109).

Table 31 Results obtained from the disk burning test of mixture n°. 3.1.

| $\rho$ (kg/m <sup>3</sup> ) | $\Delta t_1$ | $A_1$ (m <sup>2</sup> ) | Fig. | $\Delta t_2$ | $A_2$ (m <sup>2</sup> ) | Fig. |
|-----------------------------|--------------|-------------------------|------|--------------|-------------------------|------|
|-----------------------------|--------------|-------------------------|------|--------------|-------------------------|------|

|        |      |          |            |      |          |            |
|--------|------|----------|------------|------|----------|------------|
|        | (s)  |          |            | (s)  |          |            |
| 1933.7 | 0.07 | 5.41E-06 | Figure 101 | 0.07 | 6.52E-04 | Figure 102 |

This experiment was performed with the disk on a vertical position. The measurement of the areas of explosion 1 and 2 were made approaching the incandescent area to two circles and to an ellipse (Figure 101 and Figure 102), respectively. The calculation was made as previously was described. The first explosion happened during second ignition. Explosion 2 occurred with self-ignition or driven flame ignition

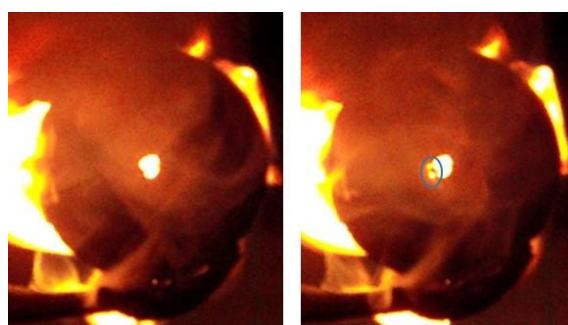


Figure 101: Frames which shows the moment before explosion one (at left) and the first appearance of explosion one (at right). The measurement of the area was made at right image, on area surrounded by blue.



Figure 102: Frames which shows the moment before explosion two (at left) and the first appearance of explosion one (at right). The measurement of the area was made at right image.

#### 3.3.4.8. Mixture n° 3.2 - heterogeneous mixture based on AN, PU and Al

This mixture was constituted by 84% AN, 7% PU and 9% Al (m/m). The mixing procedure used on this mixture was the 3 presented on 3.3.3.2 and 50 g were made. Both tests were experimented with this mixture.

**Cigar Burning Test.** The sample was prepared by methodology 2, for cigar burning test, described on 3.3.3.3. The preparation of the sample was made one month after mixture's preparation. Figure 103 shows the cigar before its combustion and the respective residues in the end of the combustion.



Figure 103: Mixture n°. 3.2 prepared for a cigar burning test (left) and its residues in the end of the combustion (right).

During 4 minutes and 59 seconds occurred 34 explosions, with different intensity and durability. The most of them occurred from the third minute, probably because heat transfer was more stabilized after some time of combustion and the pressure, due to gas expansion, increased inside the fresh mixture, which made zones with more concentration of Al get into explosion, what not occurred in the beginning.

It was observable that, before explosions, some parts of the burning area got more and more incandescent until their get their maximum of intensity and transform into explosion, which is the reverse process used for measurement of velocity of propagation of explosion in the mixture. What was observable is the burning of Al (responsible for colour changing of the incandescent parts) and showed the increase of temperature needed by mixture to arrive to explosion.

The mixture never suffered auto-extinction and ignition was made with a lighter. On this mixture was also possible to see the phase transitions of the mixture, solid to liquid and liquid to gas (due to bubble).

On Figure 104, is possible to see degasification (hollow zone), gases ignition (orange zone) and gases combustion (white/yellow zone) of the burning mixture. The blue zone of the presented flames is due to PMMA combustion and it is the flame responsible for

the drive-flame combustion of the mixture. The incandescent parts shows that, during the combustion, mixture reaches high temperatures.

Figure 104 is a good example of the reaction of Al with gaseous products (from mixture's combustion) and with oxygen (from air), because of the sparks above the homogeneous yellow part of the flame. At the end, ashes had a very porous look.

Table 32 summarizes the results acquired from this experiment.



Figure 104: Flame of combustion of mixture n°.3.2 on a cigar burning test.

Table 32: Results obtained from the combustion of mixture n°. 3.2 on cigar burning test. There was studied: density of the fresh mixture ( $\rho$ ), maximum temperatures acquired by thermocouples ( $Th_1$  is the upper one and  $Th_2$  is the downer), velocities of flame propagation of PMMA, explosion, mixture and fundamental flame velocity.

|                                    |            |
|------------------------------------|------------|
| $\rho$ (kg/m <sup>3</sup> )        | 1206.6     |
| Maximum temperature – $Th_1$ (°C)  | 800        |
| $D_{PMMA}$ (m/s)                   | 3.26E-04   |
| Studied images for $D_{PMMA}$      | Figure 105 |
| $D_{explosion}$ (m/s)              | 2.46E-03   |
| Studied images for $D_{explosion}$ | Figure 106 |
| $D_{mixture}$ (m/s)                | 1.79E-04   |
| Studied images for $D_{mixture}$   | Figure 107 |
| $V_{Flame}$ (m/s)                  | 2.66E-01   |
| Studied image for $V_{Flame}$      | Figure 104 |

For measurement of  $D_{PMMA}$ , the baseline for positions was the middle point of the liquid PMMA (on the upper part of PMMA combustion). The delay time was measured

between frame time references (Figure 105). Equation (105) was used for calculation of this velocity.

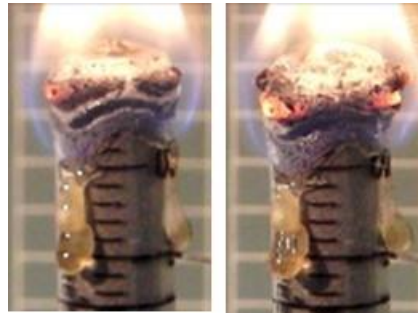


Figure 105: Frames used to study the velocity of the propagation of the flame on PMMA. The initial position is image on the left, final position the image on the right.

To measure  $D_{\text{explosion}}$ , Figure 106 was the reference and equation (105) was used. The measure was made immediately after the first explosion. The positions measurement was based on the height of the burnt part on right frame of Figure 106 (height of blue rectangle). Correlations between image length and real length were made. Time measurements were performed as described above.



Figure 106: Frames used to study the velocity of propagation of explosion in mixture n°. 3.2.

The measurement of  $D_{\text{mixture}}$  was made after the second explosion until the beginning of the third one. Between explosions it is considered zones of bigger homogeneity. Equation (105) was used and the reference for position measurement was the middle point of the liquid mixture (approximately the middle point of the burnt mixture – Figure 107).

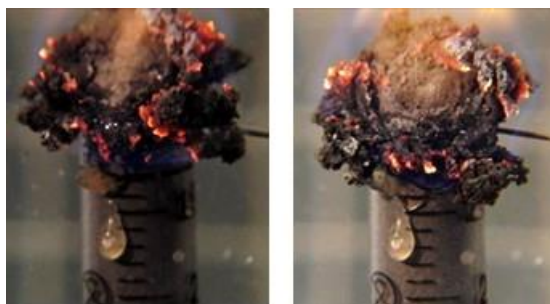


Figure 107: Frames used to study the velocity of flame propagation in the mixture n°. 3.2. The frame at the left is correspondent to the initial position, and the frame at right, the final position.

The methodology employed on the measurement of  $V_{\text{Flame}}$  was the use of equations (106) to (109) and the construction of a triangle which perimeter was coincident with the separation between the orange and the yellow zone of the flame. The baseline for the base of the triangle was the most above incandescent part of the mixture (Figure 104).

**Disk Burning Test.** This sample was prepared by methodology 2 described at 3.3.2.3, for disk burning tests. The preparation of the sample was made one month after mixture's preparation. Figure 108 shows the aspect of the sample before and after it was experimented.



Figure 108: Disk of mixture n°. 3.1. Image on the right shows the fresh mixture on the disk. Image on the centre shows the disk after combustion. Image on the left shows the mixture after the combustion (disk without the PMMA lid).

This experiment was performed with the disk on a vertical position. During 1 minute and 50 seconds, there were tried four ignitions, with a blowtorch, at back of the disk. No one started the combustion of the mixture and the last one was quite long (46 seconds). Two more ignitions with the blowtorch were tried, but now on PMMA face of the disk.

PMMA continued its combustion after second ignition, during 27 seconds, but still not enough to get combustion of the mixture.

After, there was tried to make the ignition directly to the mixture and, when PMMA lid was removed, it was possible to see that all mixture remained fresh. Two attempts were made. Initially, the blowtorch was with no oxygen on the flame and was possible to observe the bubble of the mixture, but just on the peripheral area of the disk hole, and some drops fell down of the mixture. These drops could be due to polyol or diisocyanate which were not polymerized, or water, due to decompositions at low temperatures.

When oxygen was added to the blowtorch's flame, it was possible to see a more intense bubble in all area that were in contact with the flame. The flame reflected by the sample (blowtorch's flame plus some flame from mixture), on this point, had spark in it, which indicates the presence of Al. Beside these, in this ignition, was also possible to observe the colour of the reflected flame changing. Sometimes this flame got whiter and bigger, conciliated with incandescence of the burning mixture, which indicate that mixture needed high temperatures during a long time to react. Self-combustion was reached during almost 3 seconds, followed by auto-extinction.

Table 33 summarizes the results acquired from this experiment and from equation (109).

Table 33 Results obtained from the disk burning test of mixture n°. 3.2.

| $\rho$ (kg/m <sup>3</sup> ) | $\Delta t_1$ (s) | $A_1$ (m <sup>2</sup> ) | Fig.       | $\Delta t_2$ (s) | $A_2$ (m <sup>2</sup> ) | Fig.       |
|-----------------------------|------------------|-------------------------|------------|------------------|-------------------------|------------|
| 2086.5                      | 0.03             | 4.16E-06                | Figure 109 | 0.04             | 2.55E-06                | Figure 110 |

The measurements were made comparing the perimeter of the PMMA (which was measured before combustion) with the perimeters of the burning areas shown on bottom Figure 109 and Figure 110. The delay time was measured between frame time references.

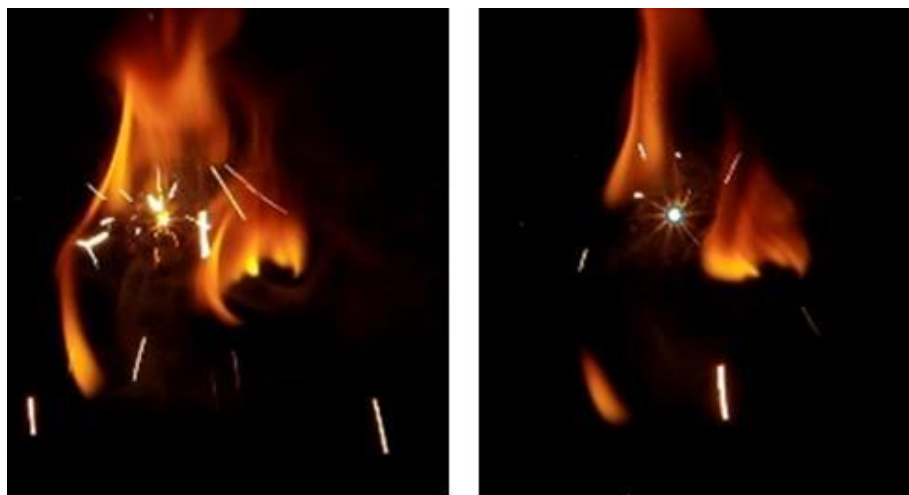


Figure 109: Frames which shows the moment before explosion one (at left) and the first appearance of explosion one (at right). The measurement of the area was made at right image, on area surrounded by blue.



Figure 110: Frames which shows the moment before explosion two (at left) and the first appearance of explosion one (at right). The measurement of the area was made at right image surrounded by a blue circle.

### ***3.3.4.9. Mixture n° 3.3 - heterogeneous mixture based on AN, PU and MT***

The chemical composition of this mixture was 74% AN, 17% PU and 9% MT (m/m). 50 g of mixture were made with procedure 3 (3.3.3.2). Both tests were realized with this mixture.

**Cigar Burning Test.** The sample was prepared by methodology 2, for cigar burning test, described on 3.3.3.3. Sample was prepared and tested as mixtures n°. 3.1 and n°.

3.2. Figure 111 shows the cigar before and its residues after combustion. Just one thermocouple was used on this experiment.



Figure 111: Mixture nº. 3.2 prepared for a cigar burning test (left) and its residues in the end of the combustion (right).

During this test occurred 37 explosions. Some of those explosions were so strong that, sometimes, some part of the burnt mixture were projected away from cigar. For two times, there were projection of burning mixture which continued the burning far away from cigar. This probably can prove self-combustion of the mixture.

The second explosion as so strong that extinguished the combustion of the mixture. These facts, plus the porosity of the burnt residues, proves the large gas expansion caused by MT mixture, when present in higher concentrations.

During the burning process was possible to see the expansion of the burning mixture, because burnt residues had more volume than the fresh mixture, and bubble. During combustion was possible to see some spark due to the mixture's heterogeneity.

The flame of this mixture was very heterogeneous, sometimes had the colours of the shown figures, but other times it was almost transparent. Figure 112 shows the four colours characteristic to reactions already described on other mixtures. Those colours are: yellow, orange, transparent and blue.

The results acquired from this experiment are presented on Table 34. The temperature of this sample had a quite different behaviour, because it was possible to record two peaks of temperature and two constant temperatures.



Figure 112: Flame of combustion of mixture n. 3.3 on a cigar burning test

Table 34: Results obtained from the combustion of mixture n. 3.3 on cigar burning test. There was studied: density of the fresh mixture ( $\rho$ ), maximum and average temperatures acquired by thermocouple, velocities of flame propagation of PMMA, explosion, mixture and fundamental flame velocity.

|  |            |
|--|------------|
| $\rho$ (kg/m <sup>3</sup> )                    | 1393.1     |
| Maximum temperature (1) – Th <sub>1</sub> (°C) | 900        |
| Average temperature (1) – Th <sub>1</sub> (°C) | 500        |
| Maximum temperature (2) – Th <sub>1</sub> (°C) | 1150       |
| Average temperature (2) – Th <sub>1</sub> (°C) | 800        |
| $D_{PMMA}$ (m/s)                               | 3.57E-04   |
| Studied images for $D_{PMMA}$                  | Figure 113 |
| $D_{explosion}$ (m/s)                          | 7.46E-03   |
| Studied images for $D_{explosion}$             | Figure 114 |
| $D_{mixture}$ (m/s)                            | 2.47E-04   |
| Studied images for $D_{mixture}$               | Figure 115 |
| $V_{Flame}$ (m/s)                              | 1.90       |
| Studied image for $V_{Flame}$                  | Figure 112 |

The baseline for position measurement to calculate  $D_{PMMA}$  was the base of the liquid PMMA. The delay time was measured between frame time references (Figure 113). Calculations were based on equation (105).

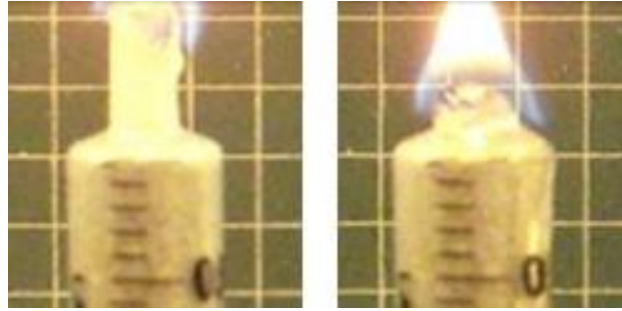


Figure 113: Frames used to study the velocity of the propagation of the flame on PMMA. The initial position is image on the left, final position the image on the right.

The measure of distance for calculation of  $D_{\text{explosion}}$  was measured based on the incandescent part on the left frame of Figure 114. Time was measured as described before. Equation (105) was used to perform the calculation.

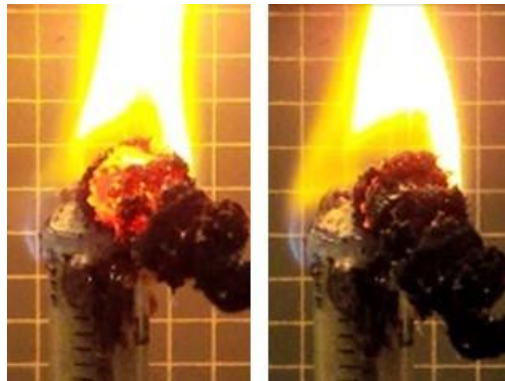


Figure 114: Frames used to study the velocity of propagation of explosion in mixture n°. 3.3.

The baseline for measurement of  $D_{\text{mixture}}$ , for positions, was the upper part of the bubble of the mixture, on Figure 115. The delay time was measured between frame time references. Equation (105) was used.

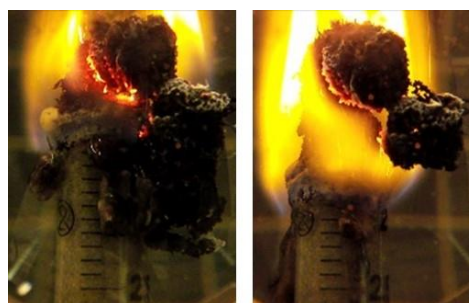


Figure 115: Frames used to study the velocity of flame propagation in the mixture n°. 3.3. The frame at the left is correspondent to the initial position, and the frame at right, the final position.

For calculation of  $V_{\text{Flame}}$ , was analysed Figure 112. The measurement of the area of the triangle was made at the same way as described above for other mixtures, but there were also subtracted the area of the triangle which involves the incandescent part of the burning mixture. Equations (106) to (109) were used.

**Disk Burning Test.** This sample was prepared by methodology 2 described at 3.3.3.3, for disk burning tests. The disk was prepared and tested on time like the previous disk. Figure 116 shows the aspect of the sample before and after it was experimented.



Figure 116: Disk of mixture n. 3.3. Images on the top shows the fresh mixture on the disk. Images on the bottom shows the disk after combustion.

This test was performed on the vertical position. During this test were recorded three movies. On the first one, 25 seconds of ignition on PVC container (back part of the sample) by blowtorch was tried, but without reaching the combustion. On second movie, 1 minute of ignition was tried by the same way that was as previously described. Here, it was possible to observe that mixture suffered some explosion, near the area of the central hole, and stayed incandescent for a while. An incandescent point was visible during the time between the stop of the ignition and the beginning of the explosion, which lasted 2 seconds and then suffered auto-extinction. It shows that is needed the temperature of the flame of the blowtorch to reach combustion. The temperature of PVC flame is not enough to start the ignition, but it is enough to sustain the combustion. On last movie, ignition lasted 20 seconds and occurred 3 explosions during that time. During the combustion of the sample occurred 27 explosions, which lasted almost 5

seconds (each one). Between explosions several occurrences were observed. It was possible to see complete extinction between some of them, between others just an incandescent point was observed. Sometimes, before explosions, it was possible to see the incandescent part increase and decrease its area. After all explosions, continuous incandescence on mixture was observed.

Explosions had always emitted white light. There was quite difficult to count explosions, because sometimes one explosion generates other explosions, which occurred simultaneously. Just were counted explosions which not happened due to the propagation of other explosions. Besides the heterogeneity, the behaviour of the combustion was rather radial, from the centre to the periphery, and top to bottom. This behaviour showed that mixture needed the oxygen flame to rise ignition (radial behaviour) and PVC flame was just enough to keep the combustion, which has an ascendant behaviour.

Due to that mixture was mostly heated on the upper half, which originated downwards heat propagation through the mixture. Gas expansion of MT, which raised the pressure inside the sample container, contributed for the downward propagation.

During the test, in periods of extinction of the mixture, was possible to see burnt and fresh areas. The irregularities during the combustion, which lead to explosions, can have several reasons: the critical thickness for homogeneous propagation of combustion was not reached, the heterogeneity of the mixture, which leads to a heterogeneous heat transfer (hotspots were observable, as described above), the PVC flame not had enough temperature to sustain a constant driven-flame combustion.

The large gas expansion, from MT mixture, was proved again, due to the deformation of the PMMA on the end of the experiment (see Figure 116, the right one, at the bottom).

The results acquired from this experiment are presented on Table 35 and equation (109) was used to do the calculations.

Table 35 Results obtained from the disk burning test of mixture nº. 3.3.

| $\rho$ (kg/m <sup>3</sup> ) | $\Delta t_1$<br>(s) | $A_1$ (m <sup>2</sup> ) | Fig.          | $\Delta t_2$<br>(s) | $A_2$ (m <sup>2</sup> ) | Fig.          |
|-----------------------------|---------------------|-------------------------|---------------|---------------------|-------------------------|---------------|
| 1979.0                      | 0.07                | 7.37E-05                | Figure<br>117 | 0.07                | 7.26E-05                | Figure<br>118 |

The measurement of the areas of explosion 1 and 2 were made approaching the incandescent area to a trapezium (Figure 117) and to an ellipse (Figure 118), respectively. Between the two shown explosions elapsed more than 3 minutes.

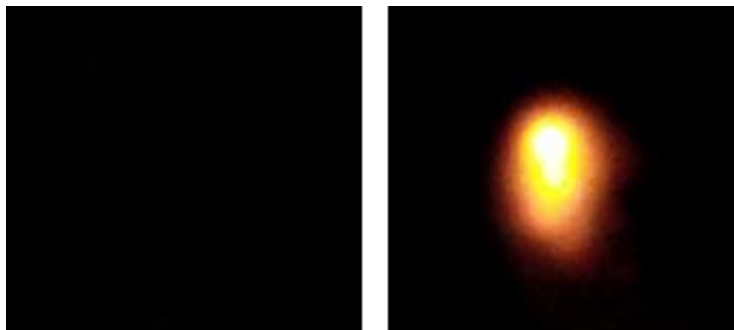


Figure 117: Frames which shows the moment before explosion one (at left) and the first appearance of explosion one (at right).

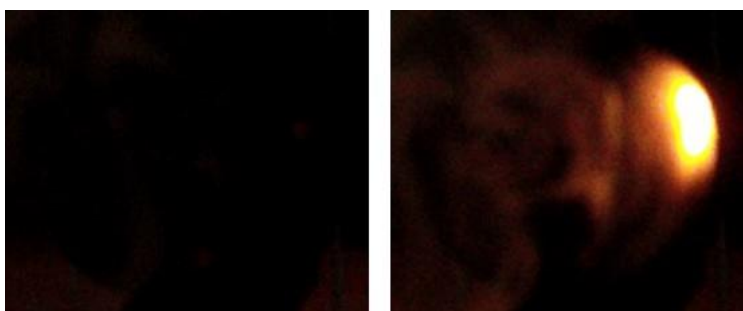


Figure 118: Frames which shows the moment before explosion two (at left) and the first appearance of explosion two (at right).

### ***3.3.4.10. Mixture n° 3.4 - heterogeneous mixture based on AN, PU and Al***

This mixture had, as composition, 74% AN, 17% PU and 9% Al (m/m). The used mixing procedure was the 3, referred on 3.3.3.2, and 50 g of mixture were produced. Both tests were performed with this mixture.

***Cigar Burning Test.*** Sample was prepared according to methodology 2 presented on *Preparation of the samples (3.3.3.3)*, for cigar burning test. The sample was prepared and tested in the same periods as the previous mixture. Figure 119 shows the look of the mixture n° 3.4 before and after its combustion.



Figure 119: Mixture n°. 3.4 prepared for a cigar burning test (left) and its residues of combustion (right).

In this experiment, just one thermocouple was used. During the experiment, the trigger was manual (not automatic as programmed). Due to that, the only peak temperature appeared on the beginning of the measurement and probably its maximum was not recorded.

During 6 minutes and 19 seconds, 6 explosions occurred. During the combustion was very usual to see the liquid mixture bubble, which proves the degasification of the mixture and it is supported by the hollow zone on the flame. These two facts are observable on Figure 120 and Figure 123.

The incandescent part of the mixture on both images proves the high temperatures present on mixture's combustion. It was also possible to see that, after explosions, the degasification was higher than in constant burning, due to the hollow zone formed between the mixture and the radiative part of the flame. On Figure 120 and Figure 123, is possible to see the four zones of reaction, already described on 3.3.4.8 – hollow, orange, white/yellow and blue zones.

Figure 120 is a good example of the reaction of Al with gaseous products (from mixture's combustion) and with oxygen (from air), because of the sparks above the homogeneous yellow part of the flame. Looking carefully, is possible to see that those spark have different colours (between orange, yellow and white), which proves the different stages of Al's combustion. At the end, ashes had a very porous look.

The results acquired from the analysis of this test are synthetized on Table 36.



Figure 120: Aspect of the flame during the combustion of the mixture n°. 3.4 on a cigar burning test

Table 36: Results obtained from the combustion of mixture n°. 3.4 on cigar burning test. There was studied: density of the fresh mixture ( $\rho$ ), maximum and average temperatures acquired by thermocouple, velocities of flame propagation of PMMA, explosion, mixture and fundamental flame velocity.

|  |            |
|--|------------|
| $\rho$ (kg/m <sup>3</sup> )                | 1316.6     |
| Maximum temperature – Th <sub>1</sub> (°C) | 1150       |
| Average temperature – Th <sub>1</sub> (°C) | 700        |
| $D_{PMMA}$ (m/s)                           | 3.98E-04   |
| Studied images for $D_{PMMA}$              | Figure 121 |
| $D_{explosion}$ (m/s)                      | 3.05E-03   |
| Studied images for $D_{explosion}$         | Figure 122 |
| $D_{mixture}$ (m/s)                        | 1.20E-04   |
| Studied images for $D_{mixture}$           | Figure 123 |
| $V_{Flame}$ (m/s)                          | 4.30E-01   |
| Studied image for $V_{Flame}$              | Figure 124 |

The reference frames for measurements of  $D_{PMMA}$  are presented on Figure 121 and the used equation was (105). The baseline for positions used for this measurement was the zone, of liquid PMMA, immediately below the blue part of the flame. The delay time was measured between frame time references.



Figure 121: Frames used to study the velocity of the propagation of the flame on PMMA. The initial position is image on the left, final position the image on the right.

The positions measurement, for calculation of  $D_{\text{explosion}}$  (equation (105)) was based on the height of the incandescence on left frame of Figure 122. The delay time was measured between frame time references



Figure 122: Frames used to study the velocity of propagation of explosion in mixture n°. 3.4.

To calculate  $D_{\text{mixture}}$  was used equation (105) and Figure 123 presents the studied frames. The baseline for the measurement of the positions was the bubble part of the burnt mixture. Time was the acquired as referred above. Correlations that were made were the same that was already described.

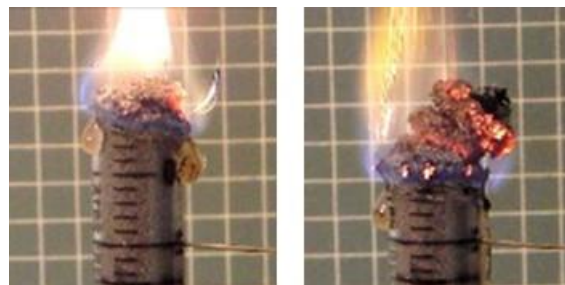


Figure 123: Frames used to study the velocity of flame propagation in the mixture n°. 3.4. The frame at the left is correspondent to the initial position, and the frame at right, the final position.

The methodology employed on the measurement of  $V_{\text{Flame}}$  was by a triangle which perimeter was coincident with the separation between the hollow and the yellow zone of

the flame (Figure 124). The base of this triangle was coincident with the middle part of the burnt mixture. The calculation was made using equations (106) to (109).



Figure 124: Flame of combustion of mixture n°. 3.4 used for measurements of fundamental flame velocity.

**Disk Burning Test.** The pressing methodology employed was the 2 (3.3.3.3) and it was prepared as described on previously mixture. Figure 125 shows the aspect of the sample before and after it was experimented.



Figure 125: Disk of mixture n°. 3.4. Image on the left shows the fresh mixture on the disk. Image on the right shows the disk after the combustion.

This experiment was performed with the disk on a vertical position. There were made 11 ignitions to this disk, always with blowtorch. They were made directly in the mixture (there was no PMMA lid), and not in the back of the disk, as usual.

On the first three ignitions, the mixture did not burn. Just in fourth attempt occurred combustion. It was possible to see the combustion, due to the incandescence on the mixture, bubble, expansion (some part of the burnt mixture was projected away from disk) and extinction.

After flame extinction, the burnt part of the mixture still was incandescent. The next three ignitions were made to sustain the flame. The mixture extinguished the combustion, so other attempt was necessary. The mixture burnt, but quickly it extinguished again. Three other ignition were made, one to sustain and the other to relight the mixture, but at the last ignition mixture were totally burnt.

Mixture stopped totally the combustion at 3 min and 22 seconds of film. As said before, it is possible to say that there happened no explosions, just combustion, because the flame pattern was not so different on three combustions. The only observable difference was the increase of light intensity, but it was simultaneously with bigger areas of combustion. So, the heterogeneity of the mixture was the only responsible for that pattern and for irregular mass combustion. The analysis of this experiment is synthetized on Table 37 and was made based on equation (109).

Table 37 Results obtained from the disk burning test of mixture n°. 3.4.

| $\rho$ (kg/m <sup>3</sup> ) | $\Delta t_1$ (s) | $A_1$ (m <sup>2</sup> ) | Fig.       | $\Delta t_2$ (s) | $A_2$ (m <sup>2</sup> ) | Fig.       |
|-----------------------------|------------------|-------------------------|------------|------------------|-------------------------|------------|
| 1983.2                      | 0.03             | 1.00E-05                | Figure 126 | 0.03             | 7.55E-06                | Figure 127 |

The measurements were made at the same way than described above. For  $A_1$ , the incandescent area was approximated to a rectangle (on blue at Figure 126, right) and, for  $A_2$ , the area was approximated to a circle (on blue at Figure 127).



Figure 126: Frames which shows the moment before appearance of  $A_1$  (at left) and the first appearance of  $A_1$ .



Figure 127: Frames which shows the moment before  $A_2$  (at left) and the first appearance of  $A_2$  (at right).

#### 3.3.4.11. Mixture n° 4.1 - heterogeneous mixture based on UN, PU and MT

The chemical composition of this mixture was 84% UN, 7% PU and 9% MT (m/m). 50 g of mixture were made with procedure 3 (3.3.3.2). Both tests were realized with this mixture.

**Cigar Burning Test.** The sample used in this experiment was prepared according methodology 2 described on 3.3.3.3, for cigar burning tests. The preparation of the sample was made one month after mixture's preparation-

Figure 128 shows the aspect of the mixture before and after its combustion on a cigar burning test.

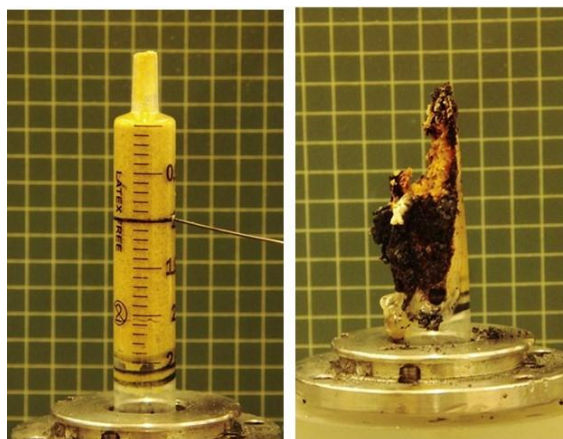


Figure 128: Mixture n°. 4.1 prepared for a cigar burning test (left) and its residues after combustion (right).

As shown in all presented photos (bellow and the above one at the right), the mixture just burnt peripherally. The flame was mainly produced by PMMA combustion.

The influence of the mixture in the flame is not clear. The most effect of temperature on this mixture was the expansion of the burnt material.

In this mixture the extinction was much more frequent, at least 3 additional ignitions were necessary. 3 temperature measurements were acquired, the maximum temperature presented in Table 38: Results obtained from the combustion of mixture n°. 4.1 on cigar burning test. There was studied: density of the fresh mixture ( $\rho$ ), maximum and minimum temperatures acquired by thermocouple, velocities of flame propagation of PMMA, explosion, mixture and fundamental flame velocity. is, probably, the temperature of the PMMA flame and the minimum temperature is the higher temperature acquired in the centre of the mixture.

The heat transmission by PMMA flame to the mixture, once again, was not enough to sustain the driven-flame combustion of the mixture. But worse than in the mixture n°. 4.2.

The photo of the burnt mixture (Figure 128) show that the inside part of the mixture did not burnt. The Figure 129 shows hotspots (incandescent zones) and the shape of the ashes indicate, once again, high temperatures on mixture and gas release, respectively. There was no explosions during this cigar burning test.

The frame shown for the flame of the mixture (Figure 131) shows again the 3 colours of the flame (blue, orange and white), which is a mixture from PMMA and mixture gases of combustion. Due to the lack of orange zone, the flame shown is probably most due to PMMA combustion. The hollow zone between mixture and white flame is not due to gas release from mixture, because it not has the orange or blue zone between them, which shows that there is no ignition of the released gases, which confirms the previous sentence.

The results acquired from this experiment are summarized on Table 38.



Figure 129: Aspect of the mixture n°. 4.1 during its combustion on a cigar burning test

Table 38: Results obtained from the combustion of mixture n°. 4.1 on cigar burning test. There was studied: density of the fresh mixture ( $\rho$ ), maximum and minimum temperatures acquired by thermocouple, velocities of flame propagation of PMMA, explosion, mixture and fundamental flame velocity.

|  |              |
|--|--------------|
| $\rho$ (kg/m <sup>3</sup> )                | 1934.6       |
| Maximum temperature – Th <sub>1</sub> (°C) | 300          |
| Minimum temperature – Th <sub>1</sub> (°C) | 100 ± 0.5    |
| $D_{PMMA}$ (m/s)                           | 1.74E-04     |
| Studied images for $D_{PMMA}$              | Figure 130   |
| $D_{explosion}$ (m/s)                      | -            |
| Studied images for $D_{explosion}$         | Not occurred |
| $D_{mixture}$ (m/s)                        | 4.91E-04     |
| Studied images for $D_{mixture}$           | Figure 131   |
| $V_{Flame}$ (m/s)                          | 3.10         |
| Studied image for $V_{Flame}$              | Figure 132   |

For calculation of  $D_{PMMA}$  equation (105) was used and Figure 130 was the reference for measurements. The base line for distance measurement was the lower part of the blue flame from PMMA, for both frames. The delay time was measured between frame time references

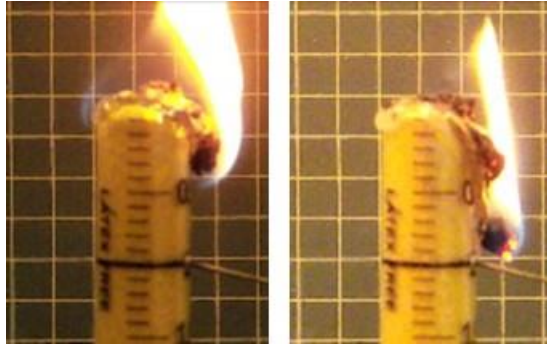


Figure 130: Frames used to study the velocity of the propagation of the flame on PMMA. The initial position is image on the left, final position the image on the right.

The measurement of distance, for calculation of  $D_{\text{mixture}}$  (equation (105)), was made through correlations of the length between two frames (Figure 131) and with the real diameter of the cigar. Time was measured as described above.

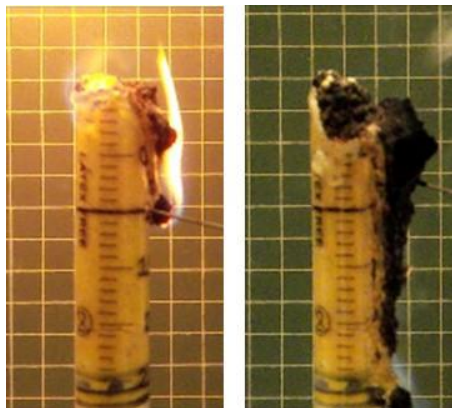


Figure 131: Frames used to study the velocity of flame propagation in the mixture n°. 4.1. The frame at the left is correspondent to the initial position, and the frame at right, the final position.

To calculate  $V_{\text{Flame}}$ , equations (106) to (109) were used. The methodology used was the same than described in 3.3.1.10. The base of the triangle was measured between the end of the hollow zone of the flame and the burnt PMMA, in Figure 132.



Figure 132: Flame of combustion of mixture n. 4.1 on a cigar burning test

**Disk Burning Test.** This sample was prepared by methodology 2 described at 3.3.3.3, for disk burning tests. The preparation of the sample was made one month after mixture's preparation and it was tested two days after sample's preparation. Figure 133 shows the aspect of the sample before and after it was experimented.



Figure 133: Disk of mixture n. 4.1. Image on the left shows the fresh mixture on the disk. Image on the right shows the disk after the combustion.

This experiment was performed with the disk in vertical position. During this test, combustion was not reached. 5 ignitions with blowtorch were tried, at the back part of the disk. Ignitions lasted between 47 seconds and 7 seconds. Other ignition was tried, but at the front part of the disk. The PMMA entered into combustion, but it not affected the sample. PMMA combustion lasted 25 seconds and it was extinct with a blow.

#### **3.3.4.12. Mixture n° 4.2 - heterogeneous mixture based on UN, PU and Al**

This mixture was constituted by 84% UN, 7% PU and 9% Al (m/m). The mixing procedure used on this mixture was the 3 presented on 3.3.3.2 and 50 g were made. Both tests were experimented with this mixture.

**Cigar Burning Test.** The sample was prepared by methodology 2, for cigar burning test, described on 3.3.3.3. The preparation of the sample was made one month after mixture's preparation. Figure 134 shows the cigar before its combustion and the respective residues in the end of the combustion.



Figure 134: Mixture n°. 3.2 prepared for a cigar burning test (left) and its residues of combustion (right).

This mixture barely suffered combustion. Just lateral combustion, due to PMMA. It was used a blowtorch, but after the signal acquisition (after the PMMA flame passed through the thermocouple).

Mixture suffered extinction three times. Its ignition was very difficult, there was necessary between 25 and 30 seconds for each ignition, with blowtorch and with lighter, respectively. 20 seconds with lighter were not enough to make the ignition.

The left frame of Figure 135 shows one frame of ignition with blowtorch. There is possible to see that the area of combustion increased (combustion was occurring on a slant), showing the erosion that oxygen flow makes to the mixture surface. The sharp incandescent spots and the bubbles show the high local temperatures and the expansion of the gases, when mixture passes from liquid to gaseous phase. The right image of Figure 135 shows the weak flame produced during the driven-flame combustion of the

mixture. That kind of flame just ensured the transition of solid to liquid phase (mistletoe on the upper part of the right frame in Figure 135 and right frame of Figure 138).

Due to the bubbles on liquid phase and the porous ashes, it is possible to conclude that gases were released. But two hypothesis could happen for self-extinction: gases were produced in lower quantities, or the reactions between the produced gases and oxygen from air not produced radiant species and, consequently, produce low temperatures.

The temperature acquired by the thermocouple shows that heat flux is not well transmitted along the mixture. Analyzing the flame shown on right frame of Figure 135 upward, the blue zone corresponds to the formation of the gases, due to the combustion of PMMA (transparent blue), and to their ignition (more opaque blue) - also visible on left frame of Figure 135; the white zone is the combustion of the gaseous products from PMMA's combustion. Upper to this white zone, it is possible to see an orange zone, which shows the ignition of the gases released during the combustion of the mixture. The upper white zone, which corresponds to the combustion of the PMMA and the mixture, is surrounded by an orange "line", closer to the burnt mixture, showing that there is only combustion of the mixture, with few gas release. The bubbles just occur when there is contact between the flame and the mixture.

When the flame extinguishes, the gas release stops. Never occurred explosions.

A good example of a driven flame in this combustion is Figure 138. It is possible to see the blue zone from PMMA combustion; the transparent zone, due to the release of gases during the combustion of the mixture; the orange zone that is the ignition of released gases; and the white zone, which is correspondent to the combustion of the gases released by the combustions of the PMMA and the mixture, due to the oxygen present in air.

Table 39 summarizes the results obtained from this experiment.

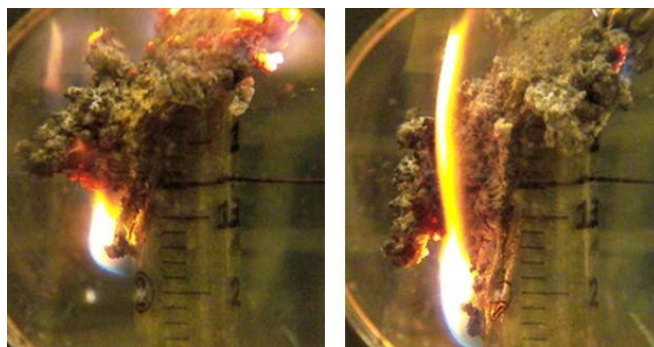


Figure 135: Aspect of the mixture n°. 4.2 and its flames during its combustion on a cigar burning test

Table 39: Results obtained from the combustion of mixture n°. 4.2 on cigar burning test. There was studied: density of the fresh mixture ( $\rho$ ), maximum temperature acquired by thermocouple, velocities of flame propagation of PMMA, explosion, mixture and fundamental flame velocity.

|  |              |
|--|--------------|
| $\rho$ (kg/m <sup>3</sup> )                | 1902.8       |
| Maximum temperature – Th <sub>1</sub> (°C) | 100          |
| $D_{PMMA}$ (m/s)                           | 1.74E-04     |
| Studied images for $D_{PMMA}$              | Figure 136   |
| $D_{explosion}$ (m/s)                      | -            |
| Studied images for $D_{explosion}$         | Not occurred |
| $D_{mixture}$ (m/s)                        | 4.91E-04     |
| Studied images for $D_{mixture}$           | Figure 137   |
| $V_{Flame}$ (m/s)                          | 3.10         |
| Studied image for $V_{Flame}$              | Figure 138   |

The measurement of  $D_{PMMA}$  was made considering equation (105) and Figure 136. The baseline for distance measurement was the lower part of the blue flame from PMMA, for both frames. The delay time was measured between frame time references



Figure 136: Frames used to study the velocity of the propagation of the flame on PMMA. The initial position is image on the left, final position the image on the right.

The measurement of distance, for calculation of  $D_{mixture}$  (equation (105)), was made through correlations of the length between two frames shown on Figure 137, and with the real diameter of the cigar. The delay time was measured between frame time references.

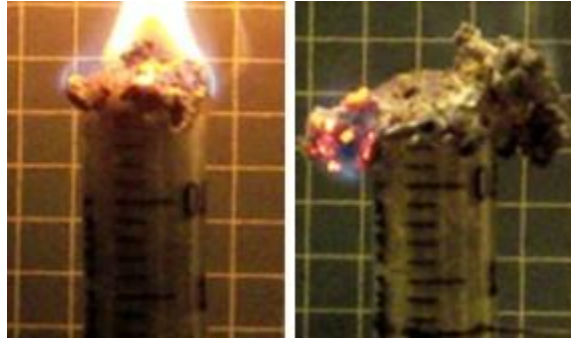


Figure 137: Frames used to study the velocity of flame propagation in the mixture n°. 4.2. The frame at the left is correspondent to the initial position, and the frame at right, the final position.

To calculate  $V_{\text{Flame}}$ , equations (106) to (109) were used. The area of the flame was measured approximating the shape of the flame to a triangle and by the correlations of the lengths of the triangle with the diameter of the cigar (which is known the real value).

Figure 138 was used for measurements.



Figure 138: Flame of combustion of mixture n°. 4.2 on a cigar burning test

**Disk Burning Test.** This sample was prepared by methodology 2 described at 3.3.3.3, for disk burning tests. The preparation of the sample was made one month after mixture's preparation. Figure 139 shows the aspect of the sample before and after it was experimented.

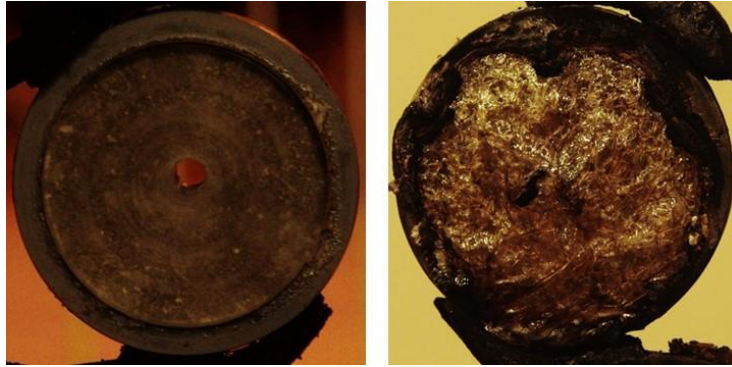


Figure 139: Disk of mixture n°. 4.2. Image on the left shows the fresh mixture on the disk. Image on the right shows the disk after the combustion.

This experiment was performed with the disk in vertical position. During this test, combustion of the mixture was not reached.

2 ignitions with blowtorch were tried, at the back and at the front part of the disk. The first lasted 1 minute and 20 seconds and the second one lasted 22 seconds, respectively. On first ignition, nothing happened. After second ignition, just PMMA suffered combustion, which lasted 2 minutes and 28seconds, and was extinct with a blow.

During and after this ignition on PMMA's face, it was possible to see the mixture emerging from the periphery of the PMMA and bubble. During the combustion of PMMA it was possible to observe several incandescent point on the emerged mixture (Figure 140)



Figure 140: Combustion of disk with mixture n°. 4.2 where it is possible to see the PMMA's flame and hotspots of the mixture.

### 3.4. Infra-Red Spectroscopy

The Infra-Red (IR) spectra present during this thesis were acquired using a *FTIR Thermo Scientific Spectrometer, 6700 Nicolet* model, with a *DTGS KBr* as detector. The acquisition was programmed in transmittance mode, with a resolution of 4, with 32 scan per run and in a wavenumber range of 400 to 4000  $\text{cm}^{-1}$ .

All the pills were made in proportions of 1 mg of each studied compound / mixture for 100 mg of Potassium Bromide (KBr), pressed less than 10 ton during 10 minutes.

The spectra of pure reactants, the collection of the main characteristics in table and the comparison with theoretical values and experimental data collected from literature are presented in this point.

#### 3.4.1. Reactants

In order to attempt the identification of the reactants in explosive mixtures, before and after their combustion, the IR spectra of reactants were acquired. The main bands of each reactant, as well as their intensity and correspondent wavenumbers will be described in function of their correspondent molecular vibrational modes.

##### 3.4.1.1. Ammonium Nitrate

The IR spectrum of pure ammonium nitrate (AN) which was one of the oxidants used in our explosive mixtures is presented at Figure 141. At Table 40 the spectrum characteristics, namely, maximum wavenumber of the band and band type, as well as the attribution of the vibration mode are collected.

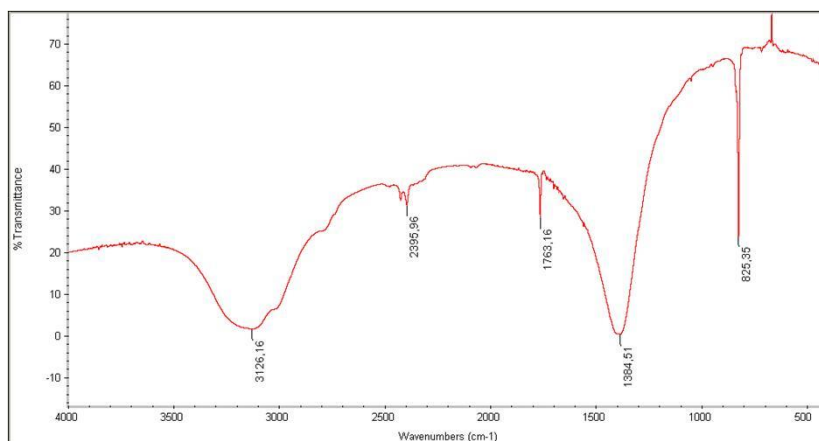


Figure 141: IR spectrum of pure Ammonium Nitrate

Table 40: IV spectra band types, wavenumber ranges of appearance and characteristic vibrational modes for pure ammonium nitrate. The assignment of vibrational modes to the spectrum bands were made comparing with early reports. (Théorêt, et al., 1964) (Silverstein, et al., 1998) (Chattopadhyay, 1996)

| Band type and range                                     | Peak band Wavenumber (cm <sup>-1</sup> ) | Vibrational mode  |
|---|--|---|
| Strong band; [3300 - 2800] cm <sup>-1</sup>             | 3126                                     | NH <sub>4</sub> <sup>+</sup> asymmetric stretch and deformation   |
| Weak and thin band; [2450 - 2380] cm <sup>-1</sup>      | 2425; 2396                               | AN's paraffinic coating   |
| Weak band; at approximately, 1700 cm <sup>-1</sup>      | 1763                                     | combination of NO <sub>3</sub> <sup>-</sup> symmetric stretch and NO <sub>3</sub> <sup>-</sup> in-plane deformation |
| Strong band ;[1500 – 1250] cm <sup>-1</sup>             | 1384                                     | overlap of NH <sub>4</sub> <sup>+</sup> asymmetric deformation and NO <sub>3</sub> <sup>-</sup> asymmetric stretch  |
| Strong but thin; at, approximately, 800cm <sup>-1</sup> | 825                                      | NO <sub>3</sub> <sup>-</sup> out-of-plane deformation   |

The acquired IR spectrum of pure AN was concordant to those ones founded on literature.

A small quantity (3 % m/m) of dimethylformamide (DMF) was added to pure AN in order to reduce its hygroscopicity, after the micronization and during the storage. The IR spectra of AN with DMF is presented on Figure 142. It was acquired to study the influence of DMF on the IR spectra of pure AN. Both spectra were plotted together (Figure 142) to found the differences between them.

The AN with DMF spectra (Figure 142) was also acquired to make possible the identification of AN in our explosive mixtures and in their combustion products. This will be the spectrum used to evaluate the presence of AN.

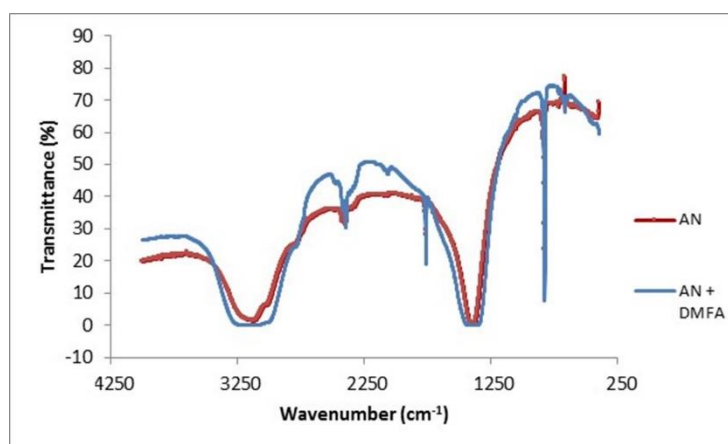


Figure 142: Overlap of AN (red) and AN with DMF (blue) spectra

Comparing both spectra (Figure 142) it is possible to see that 3 % (m/m) of DMF has no significant influence on IR spectrum of AN. It is possible to see saturation of some bands: the large band at around  $3300$  to  $3000$   $\text{cm}^{-1}$  has the influences of  $\text{NH}_4^+$  asymmetric stretch and deformation from AN, and N-H axial deformation of a primary amide from DMF; the band at  $1425$  to  $1335$   $\text{cm}^{-1}$  has the influences of overlap of  $\text{NH}_4^+$  asymmetric deformation and  $\text{NO}_3^-$  asymmetric stretch from AN, and the C – N axial deformation from DMF.

The appreciable difference is the increase of signal at  $\approx 2300$   $\text{cm}^{-1}$ , due to the vibration of the methyl groups of DMF.

One interesting fact is that the double peaked band at, around  $2400$   $\text{cm}^{-1}$ , is potentiated by DMF. Probably it is due to R – C – N bounds between AN and DMF or between AN and the paraffin used to produce the AN prills, which can be a derivate from stearic acid. (Chattopadhyay, 1996)

#### 3.4.1.2. Urea Nitrate

The IR spectrum of pure urea nitrate, also used as oxidant during this work, is presented at Figure 143. The most relevant are collected at Table 41.

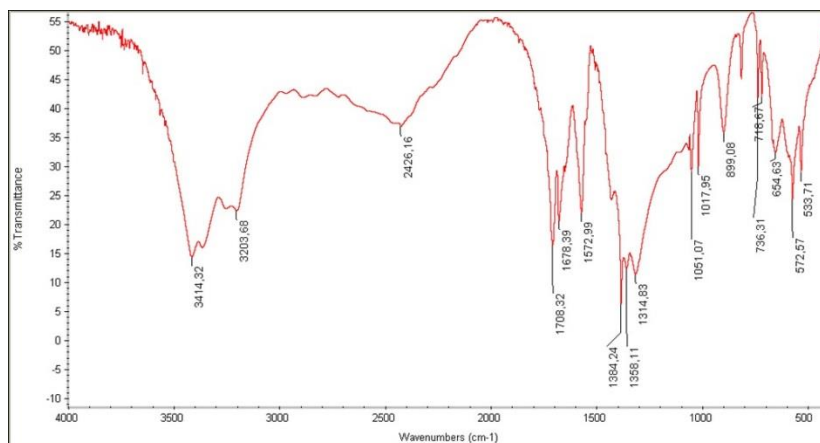


Figure 143: IR spectrum of pure Urea Nitrate

Table 41: Most relevant band types, wavenumber ranges of appearance and characteristic vibrational modes of pure urea nitrate. The assignment of vibrational modes to the spectrum bands were made comparing with early reports. (Oxley, et al., 2013) (Désilets, et al., 2011)

| Band type and range                                     | Peak band Wavenumber (cm <sup>-1</sup> ) | Vibrational modes   |
|---|--|---|
| Strong band (double peak); [3500-3200] cm <sup>-1</sup> | 3414 (minimum)                           | NH <sub>2</sub> asymmetric stretch                                  |
| Strong band (double peak); [3500-3200] cm <sup>-1</sup> | 3204 (minimum)                           | NH <sub>2</sub> symmetric stretch                                   |
| Medium and large band; [2330 - 2550] cm <sup>-1</sup>   | 2426                                     | C=O···H···ONO <sub>2</sub> symmetric stretch (most typical from UN) |
| Strong but thin band                                    | 1708                                     | C=O symmetric stretch   |
| Strong but thin band                                    | 1573                                     | N – H angular deformation   |
| Strong band (four peaks) ;[1500 – 1250]cm <sup>-1</sup> | 1384 (minimum)                           | NO <sub>3</sub> <sup>-</sup> asymmetric stretch                     |
| Medium and thin band                                    | 816                                      | NO <sub>3</sub> <sup>-</sup> out-of-plane deformation               |

The acquired IR spectrum for UN was concordant with those ones described at literature, which proves that our reactant was really UN in pure state.

### 3.4.1.3. PolyUrethane

The acquired IR spectrum of PU is presented at Figure 144 and its more relevant bands are presented at Table 43. Even being a commercial product, the exact composition was unknown, so the comparisons were made with some spectra of different kinds of PU presented on literature (Neves, 2010) and by the correlation with typical vibrational modes, also founded in literature (Silverstein, et al., 1998).

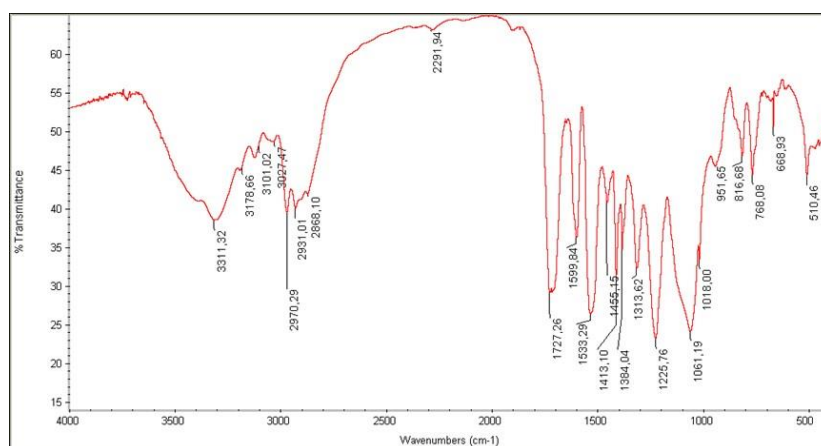


Figure 144: IR spectrum of commercial PolyUrethane

Table 42: Most relevant band types, wavenumber ranges of appearance and characteristic vibrational modes of the used commercial PU. The assignment of vibrational modes to the spectrum bands were made comparing with early reports. (Silverstein, et al., 1998) (Neves, 2010)

| Band type and range  | Peak band Wavenumber (cm <sup>-1</sup> ) | Vibrational modes   |
|--|--|---|
| Strong band; [3500-3250] cm <sup>-1</sup>                  | 3311 (minimum)                           | O – H stretch characteristic of intermolecular hydrogen bond                            |
| Strong band (multiple peaks); [3000-2800] cm <sup>-1</sup> | 2970 (minimum)                           | C – H symmetric and asymmetric stretches  |
| Strong but thin band                                       | 1727                                     | C=O stretch characteristic of ester bound   |
| Medium and thin band                                       | 1600                                     | C=C stretch from a di-substituted benzene   |
| Strong but thin band                                       | 1533                                     | Band overlap: C-N stretch and N-H elongation typical from urethane group                |
| Strong but thin band                                       | 1225                                     | C(=O)-O axial deformation characteristic of ester bound                                 |
| Strong band; [1170 – 1030]cm <sup>-1</sup>                 | 1061                                     | Bands overlap: C –O-C symmetric and asymmetric axial deformations, typical from ethers. |
| Weak and large band; [720 – 620] cm <sup>-1</sup>          | 669                                      | N-H out-of-plane symmetric angular deformation, typical from amides                     |

The PU used in this work presents a vibrational band at 1384 cm<sup>-1</sup>, not assigned to any structural characteristic of this product that could be a problem for the identification of products intended in this work, because it is coincident with one of the bands characteristic of the NO<sub>3</sub><sup>-</sup> species.

#### 3.4.1.4. Aluminium

Aluminium (Al) was used in our experiments as additive for our mixtures, in order to rise combustion temperatures (Quaresma, et al., 2013). Due to the used Al has a greasy coating to protect it against water attack during storage, the IR spectrum was made to see if that had vibrational modes on IR region of light. The result (Figure 145) shows that this greasy coating has no significant vibrational modes that can identify fresh aluminium in our mixtures, before and after combustion.

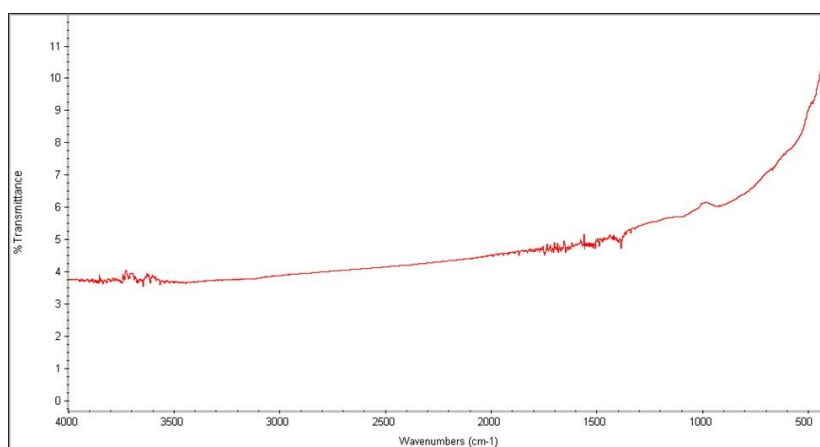


Figure 145: IR spectrum of aluminium lined with a greasy coat

#### 3.4.1.5. Magnesium and Teflon mixture

The Magnesium/Teflon (MT) mixture was used in our mixtures to increase the gas expansion during the combustion (Quaresma, et al., 2013). Teflon is a  $\text{CF}_2$  polymer commercialized by *Dupon* as powder. The correspondent IR spectrum is presented at Figure 146 and Table 43 contents the description of main parameters. As expected, the IR spectra just shows the vibrational modes of Teflon because, as Al, Mg not have vibrational modes.

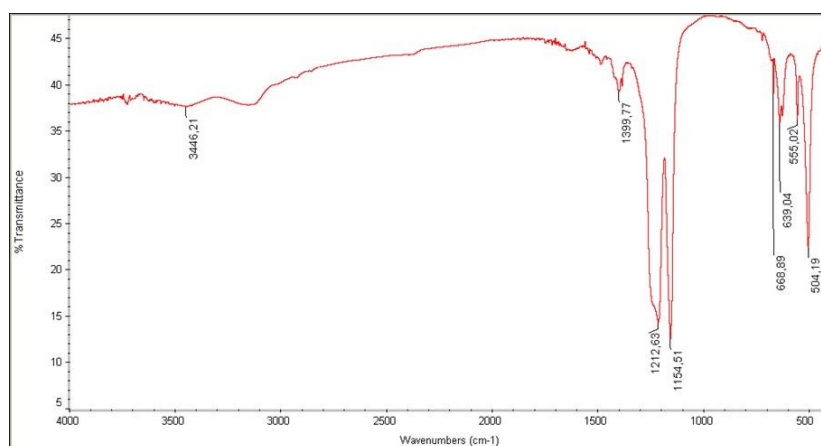


Figure 146: IR spectrum of Magnesium and Teflon (MT) mixture

Table 43: Most relevant band types, wave number ranges of appearance and characteristic vibrational modes of Teflon. The assignment of vibrational modes to the spectrum bands were made comparing with early reports. (Silverstein, et al., 1998) (Hopp, et al., 2007)

| Band type and range                                       | Peak band Wavenumber (cm <sup>-1</sup> ) | Vibrational modes                   |
|---|--|-------------------------------------|
| Strong band (three peaks); [1400 – 1000] cm <sup>-1</sup> | 1400                                     | C – F axial deformation             |
|   | 1213                                     | CF <sub>2</sub> typical elongations |
|   | 1154                                     |                                     |
| Medium and thin band                                      | 640                                      | Chain stretching and wagging modes  |
| Strong band (two peaks); [550 – 502] cm <sup>-1</sup>     | 555                                      | Bending and rocking modes           |
|   | 504                                      |                                     |

### 3.4.2. Studied Mixtures

#### 3.4.2.1. Mixture n° 3.1 - heterogeneous mixture based on AN, PU and MT

Mixture 3.1 was composed by AN (84% (m/m)), PU (7% (m/m)) and MT mixture (9% (m/m)), as described on Table 16.

#### Fresh mixture characterization

To study the influence of PU on AN and their possible products of reaction after the curing, was acquired the IR spectrum of AN with PU (Figure 147 (b)). Using the same mass content but without additive, obtaining a mass percentage of 92% for AN and 8% of PU in the mixture.

Figure 147 (a) shows the overlap of AN (with DMFA) spectrum (Figure 142) with PU spectrum (Figure 144).

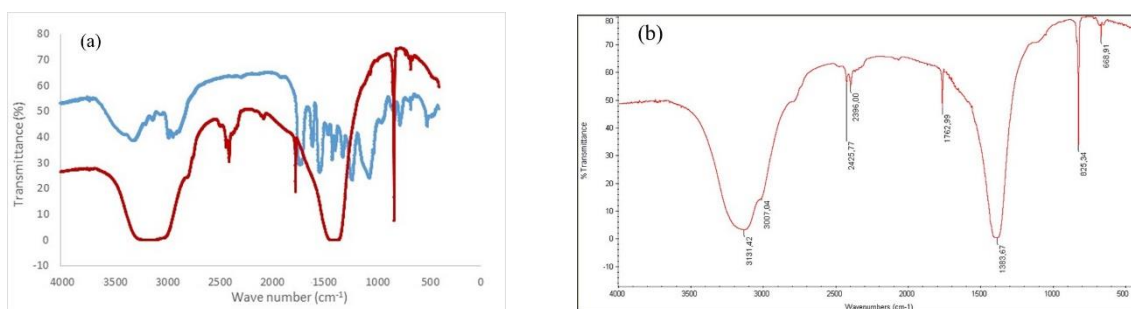


Figure 147: (a) Overlap of IR spectra of AN with DMF (red) and PU (blue) and (b) the acquired IR spectrum for AN with PU mixture.

The IR spectrum of the mixture AN/PU is very similar with the AN' IR spectrum (Figure 141). It was already expected, because AN was the major constituent of the mixture. PU was only 8% of the total mixture mass percentage, which makes that its own spectrum had been covered by the AN's spectrum.

For characterization of global mixture composition, the same methodology was employed. Figure 148 shows (a) the overlap of IR spectrum of AN / PU mixture (same as Figure 147 (b)) with the IR spectrum for MT mixture; and (b) the acquired IR spectrum for fresh mixture n°. 3.1. Table 44 shows the analysis of the presence of the reactants used in mixture.

There is no new peaks that can only be associate to the mixture AN/PU/MT. Once again, the IR spectrum of this mixture was correspondent to spectrum of the majority component, which was the AN.

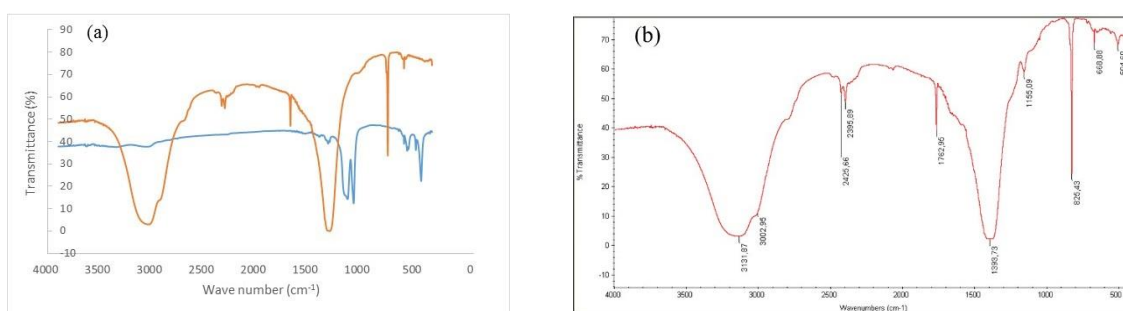


Figure 148: (a) overlap of IR spectra of AN / PU (orange) mixture and MT mixture (blue); (b) IR spectrum for mixture 3.1 (84%AN/ 7%PU/ 9%MT)

## HOMEMADE EXPLOSIVES BASED ON AMMONIUM AND UREA NITRATES

Table 44: Analysis of the presence of reactants in fresh mixture 3.1 by compound, typical peak band wavenumber from Table 40, Table 42 and Table 43, new wavenumber of the typical peak in Figure 148 (b) and respective presence.

| Compound         | Typical Peak band Wavenumber (cm <sup>-1</sup> ) | Peak band Wavenumber on Figure 148 (b) (cm <sup>-1</sup> ) | Vibrational modes  | Presence in fresh mixture |
|------------------|--|--|--|---------------------------|
| Ammonium Nitrate | 2425 / 2396                                      | 2426 / 2396  | AN coating   | Yes                       |
|                  | 1384   | 1394   | overlap of NH <sub>4</sub> <sup>+</sup> asymmetric deformation and NO <sub>3</sub> <sup>-</sup> asymmetric stretch | Yes                       |
| Polyurethane     | 1533   | (1394)   | Band overlap: C-N stretch and N-H elongation typical from urethane group   | No – overlapped by AN     |
|                  | 669  | 669  | N-H out-of-plane symmetric angular deformation, typical from amides  | Yes                       |
| MT mixture       | 1155   | 1155   | CF <sub>2</sub> typical elongations  | Yes                       |
|                  | 505  | 505  | fingerprint zone of Teflon, elongation characteristic of bending and rocking modes                                 | Yes                       |

### Burnt mixture characterization

As referred at 3.3.3.4, there were used two experimental test configurations: vertical cylindrical set-up (or “cigar” burning test) and horizontal thin layer circular box (or “disk” test).

**“Cigar” burning test.** In order to know if there was the presence, or not, of fresh material in the end of this kind of test, two IR spectra were compared. Figure 149 shows both spectra used on these comparisons: (a) IR spectrum of burnt material from the combustion of mixture 3.1 (experimental isobaric conditions). and (b) the overlap of spectrum (a), in orange, with the spectrum (b) of Figure 148 (fresh mixture), displayed in blue.

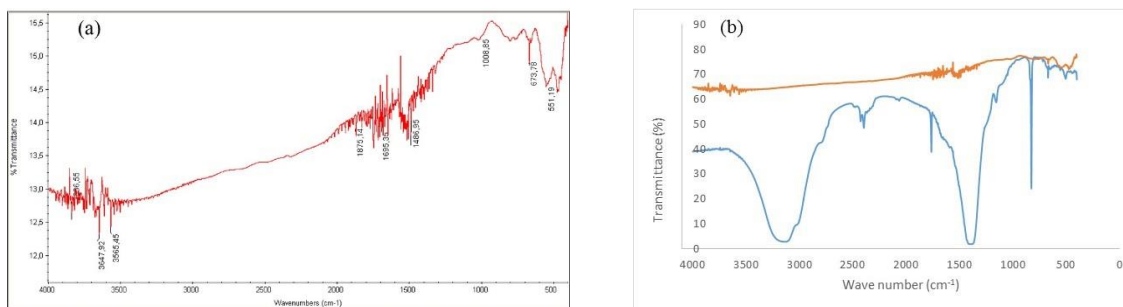


Figure 149: IR spectra of: (a) burnt mixture n°3.1 in experimental isobaric conditions; (b) overlap of spectra of burnt material (orange) and fresh mixture n°3.1 (blue). The transmittance of burnt mixture, in (b) was increased 5 times, in order to be possible the visualization of its characteristic bands.

The IR spectrum of burnt material from mixture n°. 3.1 is almost linear when compared with the one from the fresh mixture (Figure 149 (b)). This indicates that mixture n°.3.1 mainly produces  $\beta$  – carbon, which has no IR spectrum, during its combustion. This fact was visible during the experiments, on ashes formation. Table 45 shows the presence of reagents on burnt mixture, according to IR spectrum at Figure 149 (a).

Table 45: Analysis of the presence of reactants in burnt mixture 3.1 (cigar test burning) by compound, typical peak band wavenumber from Table 40, Table 42 and Table 43, new wavenumber of the typical peak at Figure 149 (a).

| Compound         | Typical Peak band Wavenumber (cm <sup>-1</sup> ) | Peak band Wavenumber on Figure 149 (cm <sup>-1</sup> ) | Vibrational modes  | Presence in burnt mixture - cigar |
|------------------|--|--|--|-----------------------------------|
| Ammonium Nitrate | 2425 / 2396                                      | -  | AN coating   | No                                |
|                  | 1384   | -  | overlap of NH <sub>4</sub> <sup>+</sup> asymmetric deformation and NO <sub>3</sub> <sup>-</sup> asymmetric stretch | No                                |
| Polyurethane     | 1533   | -  | Band overlap: C-N stretch and N-H elongation typical from urethane group   | No                                |
|                  | 669  | -  | N-H out-of-plane symmetric angular deformation, typical from amides  | No                                |
| MT mixture       | 1155   | -  | CF <sub>2</sub> typical elongations  | No                                |
|                  | 505  | -  | fingerprint zone of Teflon, elongation characteristic of bending and rocking modes                                 | No                                |

Typical products of combustion of a MT mixture were also found. The more notable bands (Figure 149 (a)), at 466 and 551 cm<sup>-1</sup>, are correspondent to MgF<sub>2</sub> and to Mg-C-F unit elongations, respectively. These bands are described in literature as appearing at 459 and 565 cm<sup>-1</sup> (Koch, 2002).

The large but weak band that appears on wave number range of 640 to 710  $\text{cm}^{-1}$  can be attributed to the products of combustion of this kind of mixture as: primary and secondary amines, more concretely to N–H out-of-plane angular and symmetric deformations (typical wave number range: [930 – 666]  $\text{cm}^{-1}$ ), C–H out-of-plane angular deformation characteristic from alkenes (typical wave number range: [1000 – 650]  $\text{cm}^{-1}$ ); O – H out-of-plane deformation from alcohols (typical wave number range: [770 – 650]  $\text{cm}^{-1}$ ) (Silverstein, et al., 1998). Probably, this band is largely affected by the products of combustion of PU, because those kind of products are described in literature (Chattopadhyay, et al., 2009) and the characteristic peak of PU at 669  $\text{cm}^{-1}$  disappears to origin this new band. It can be also products of the reaction of PU and AN, because all reaction products of AN are gaseous and PU produces solid products which can react with the gaseous ones, to origin bounds like the ones described before. As there is no presence of the characteristic bands of AN, neither of PU, which means that all of them suffered combustion.

Due to lack of information about the combustion of these kind of mixture, there is no possibility to attribute these last referred peaks to compounds in concrete.

By spectral comparison, only combustion residues of PU and MT were identifiable, there was no presence of AN, PU or MT on these combustion products, which means that all fresh mixture was consumed on experimental isobaric combustion conditions.

**“Disk” burning test.** The same methodology referred above was made to discover the presence of fresh material at burnt mixture n°. 3.1, in experimental adiabatic conditions. The acquired IR spectrum for burnt material of mixture n°.3.1 is shown at Figure 150 (a). The overlap of IR spectra of fresh and burnt material of the referred mixture is shown at Figure 150(b).

At Table 46, the comparison between spectra was analysed.

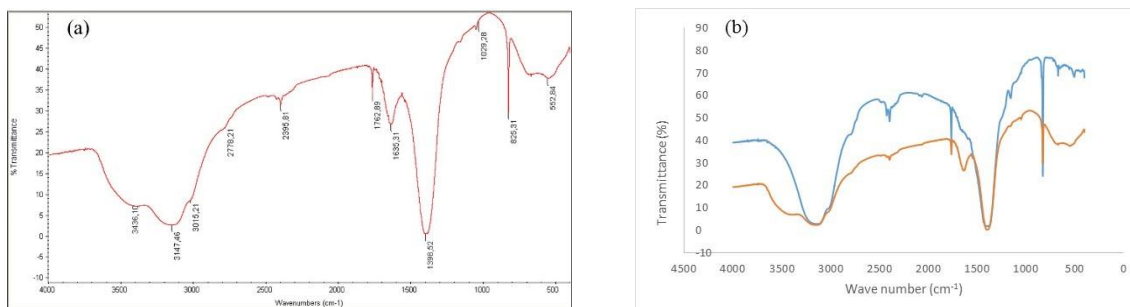


Figure 150: IR spectra of: (a) burnt mixture n°3.1 in experimental adiabatic conditions; (b) overlap of spectra of burnt (orange) and fresh (blue) materials of mixture n°3.1.

Table 46 Analysis of the presence of reactants in burnt mixture 3.1 (disk test burning) by compound, typical peak band wavenumber from Table 40, Table 42 and Table 43, new wavenumber of the typical peak in Figure 150 (a).

| Compound         | Typical Peak band Wavenumber (cm <sup>-1</sup> ) | Peak band Wavenumber at Figure 150 (a) (cm <sup>-1</sup> ) | Vibrational modes  | Presence in burnt mixture - disk |
|------------------|--|--|--|----------------------------------|
| Ammonium Nitrate | 2425 / 2396                                      | 2426 / 2397  | AN coating   | Yes                              |
|                  | 1384   | 1398   | overlap of NH <sub>4</sub> <sup>+</sup> asymmetric deformation and NO <sub>3</sub> <sup>-</sup> asymmetric stretch | Yes                              |
| Polyurethane     | 1533   | (1398)   | Band overlap: C-N stretch and N-H elongation typical from urethane group   | No – overlapped by AN            |
|                  | 669  | 669  | N-H out-of-plane symmetric angular deformation, typical from amides  | Yes                              |
| MT mixture       | 1155   | 1160   | CF <sub>2</sub> typical elongations  | Yes                              |
|                  | 505  | -  | fingerprint zone of Teflon, elongation characteristic of bending and rocking modes                                 | No                               |

As for the combustion products found at “cigar burning test” described above, here are also found the Mg-C-F unit elongations at 553 cm<sup>-1</sup> (from MT mixture combustion); the large but weak band, attributed to the products of combustion of PU, that appears on wave number range of 640 to 710 cm<sup>-1</sup>, with the one of the characteristic PU peaks

having relevance inside this range ( $669\text{ cm}^{-1}$ ). This means that still existed fresh PU in our burnt mixture.

Two bands were found to be associated exclusively with this experimental burning conditions: the band present between  $3310$  and  $3650\text{ cm}^{-1}$ , which indicates the presence of O – H axial deformation in intermolecular bounds, which can be associated to water, alcohols produced during the combustion reactions of PU, or AN/PU combustion products which have O–H bounds (AN has O – H groups in its products of thermal decomposition, see 2.1.1.1), or any O–H intermolecular bound of products formed due to the reaction between the four reactants; and the strong but thin band at  $1635\text{ cm}^{-1}$ , which can belong: to vibrations of the skeleton of mononuclear aromatic rings (substituted or not), to  $\text{NO}_2$  asymmetric stretch from nitro compounds in cyclic chain composed by C and N atoms. The appearance of these two last bands indicates de production of more molecules, which functional groups has now relevance in IR spectrum, such alcohols and smaller compounds with aromatic rings or cyclic chains. This production can be achieved or by reaction between reactants, or due to breaking bounds of PU.

The mixture AN/PU suffered some combustion, because it characteristic band has its intensity reduced. The consumption of AN can also be proved by the decrease of the intensity of its characteristic bands.

There was almost total consumption of the additive (MT mixture), due to the appearance of typical bands of MT combustion products and to the vanishing almost complete of the band at  $1160\text{ cm}^{-1}$ .

**Correlation between both tests.** Experimental isobaric conditions allows the complete combustion of the sample, because there was no fresh reactants on the analysed burnt material. In experimental adiabatic conditions, the combustion process was not complete, because all reactants were identified on burnt sample.

Although, there were present compounds which came from the thermal decomposition and/or further reactions of the reactants. This was proved by the appearance of characteristic bands of possible combustion products, which not appeared on IR spectrum of the fresh mixture 3.1. These are: strong and large band between  $710$  and  $640\text{ cm}^{-1}$ , which can be associated to the overlap of primary and secondary amines and alkenes elongations; medium and thin band at  $1635\text{ cm}^{-1}$  (at Figure 149(a) this band is a turbulent zone), that can be correspondent to the vibrations of the skeleton of

mononuclear aromatic rings (substituted or not) and NO<sub>2</sub> asymmetric stretch from nitro compounds in cyclic chain composed by C and N atoms; and the large and strong band between 3650 and 3310 cm<sup>-1</sup> (at Figure 149 (a) this band is also a turbulent zone) that can be associated to O – H axial deformation in intermolecular bounds, characteristic of polymeric structures with OH group or/and water. The first two referred peaks can also be associated to unreacted PU, because the PU used on this work is hardly inflammable, while our oxidants have a low thermal decomposition temperatures (when compared with PU). When thermal decomposition temperatures of the oxidants are reached, some of them decomposes into gases and unreacted or barely burned PU is now detectable by IR spectroscopy.

The above referred vibrational modes would be related to combustion products of the studied mixture after some further work. It will be necessary to repeat the experiment, at least, three times to have reproducibility of the results. It will be essential to the smallest and thin bands, because that kind of bands can be also associated to baseline modifications of the spectrometer, or to the environmental laboratory conditions.

IR spectra from those different kind of combustion conditions are very different. Isobaric conditions produces an almost liner spectrum, due to the presence of β-carbon. Adiabatic experimental burning conditions produces water, while isobaric combustion do not. Some products of combustion were the same, or very similar between them, for both combustion types, as Mg – C –F unit, primary and secondary amines, carbon dioxide and alkenes.

#### ***3.4.2.2. Mixture n° 3.2 - heterogeneous mixture based on AN, PU and Al***

Mixture 3.2 was composed by AN (87% (m/m)), PU (7% (m/m)) and Al (9% (m/m)), as described on Table 16. This mixture has the same mass portions than the previous one, the only change is the additive.

##### *Fresh mixture characterization*

As shown on 3.4.1.4, Al has no characteristic IR spectrum, due to be a monoatomic compound. To see if that has any reactivity with our AN/PU mixture, the IR spectrum of mixture 3.2 was acquired. The result is the spectra shown on Figure 151(a). The overlap of IR spectrum of (a) with the IR spectrum of mixture AN/PU (already presented on Figure 147(b)) is presented on Figure 151(b).

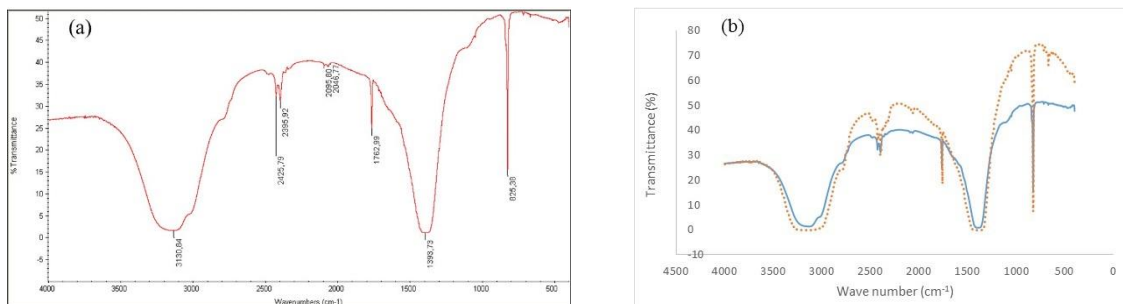


Figure 151: (a) IR spectra of fresh mixture 3.2 (b) Overlap of IR spectrum of: fresh mixture 3.2 (same as (a) – blue) and of mixture AN/PU (same as figure 44 (b) – dashed orange)

As it was expected, Al has no influence on vibrational modes of AN/PU mixture (see Figure 145).

### Burnt mixture characterization

Al increases the temperature reaction on explosive mixtures due to its post-reaction with common combustion products, as  $O_2$ . As it was seen before, Al has no significant influence on IR spectrum of fresh mixture 3.2. So, the main objective of this analysis is to demonstrate if Al combustion products are identifiable by IR spectroscopy, in order to prove the use of Al in the explosive mixture.

**“Cigar” burning test.** The IR spectrum of combustion products of mixture 3.2 is shown on Figure 152 (a). In order to analyse the similarities and the differences between the fresh and burnt material from mixture 3.2, the last referred IR spectrum was compared with the IR spectrum of fresh mixture (already presented on Figure 151), and this spectra comparison is present on Figure 152 (b).

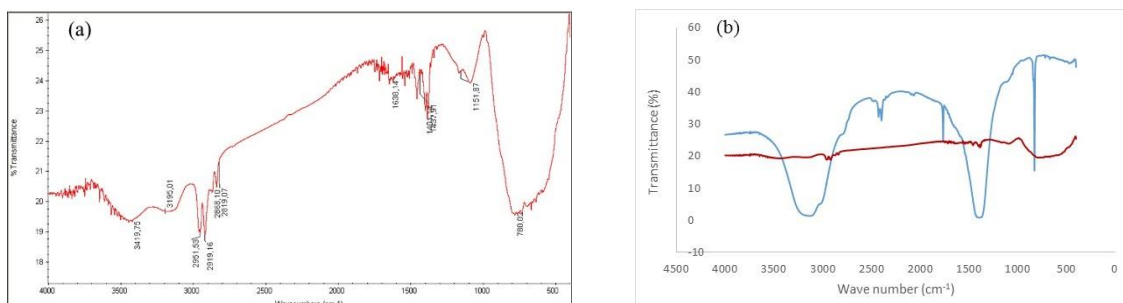


Figure 152: (a) IR spectrum of combustion products of mixture 3.2., burnt at isobaric conditions; (b) overlap of IR spectra of fresh (blue) and burnt material (red) from mixture 3.2.

Table 47: Analysis of the presence of reactants in burnt mixture 3.2 (cigar test burning) by compound, typical peak band wavenumber from Table 40 and Table 42, new wavenumber of the typical peak in Figure 152 (a).

| Compound         | Typical Peak band Wavenumber (cm <sup>-1</sup> ) | Peak band Wavenumber on Figure 152 (cm <sup>-1</sup> ) | Vibrational modes  | Presence in burnt mixture - cigar |
|------------------|--|--|--|-----------------------------------|
| Ammonium Nitrate | 2425 / 2396                                      | -  | AN coating   | No                                |
|                  | 1384   | -  | overlap of NH <sub>4</sub> <sup>+</sup> asymmetric deformation and NO <sub>3</sub> <sup>-</sup> asymmetric stretch | No                                |
| Polyurethane     | 1533   | -  | Band overlap: C-N stretch and N-H elongation typical from urethane group   | No                                |
|                  | 669  | -  | N-H out-of-plane symmetric angular deformation, typical from amides  | No                                |

As happened in mixture 3.1, in the same kind of test, there is a linear IR spectrum, which probably indicates, again, the total or almost total combustion.

The most characteristic new band is the large one that appears on a wave number range of 1150 to 400 cm<sup>-1</sup>. It probably belongs to aluminium oxide (Al<sub>2</sub>O<sub>3</sub>) species, which has its IR absorption band between 1100 and 350 cm<sup>-1</sup>, and which are predicted species of aluminium's combustion (Kuzik, et al., 1999) (Ryczkowski, 2001)

The weak band, with multiple peaks, that appears on a range of 2800 to 3600 cm<sup>-1</sup> can be associated to O – H axial deformation in intermolecular bounds, which can be associated to water, alcohols, or any O–H intermolecular or intramolecular bound of products formed due to the reaction between the four reactants. Aluminium hydroxide (Al(OH)<sub>3</sub>) is also one of the predicted products that can vibrate on this wave number range.

The weak band, with multiple peaks, that appears on a range of 1400 to 1600 cm<sup>-1</sup> could be associated to the skeleton vibrations of aromatic rings, which can be connected (or not) with secondary amines, of PU. But it was still unidentified.

**“Disk” burning test.** When the combustion of mixture 3.2 was made in experimental adiabatic conditions, its products of reaction were collected and analysed. But, as demonstrate of 3.3, this composition barely burnt in this conditions. The Figure 153(a) is the IR spectra of the referred combustion products, and Figure 153 (b) is the IR spectra for fresh mixture.

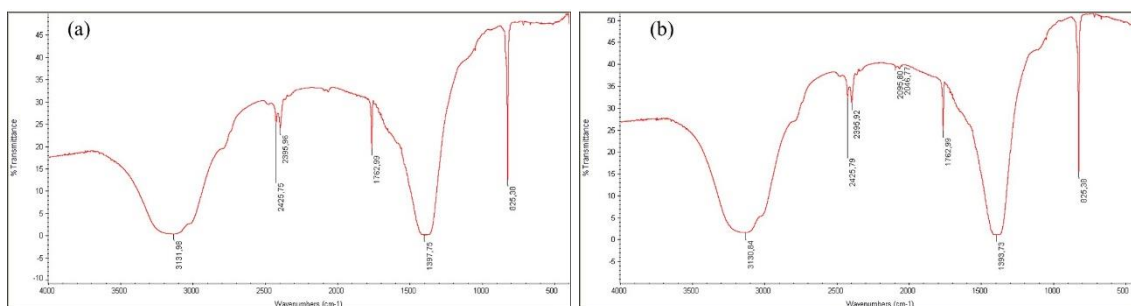


Figure 153: (a) IR spectrum of the collected residues after “disk” test had been employed to mixture 3.2; (b) IR spectrum of fresh mixture 3.2 (also shown in Figure 151 (a))

As expected, both spectra are identical, because combustion did not occur, at least, in detectable quantities.

**Correlation between both tests.** Once again, to find the spectroscopic differences and similarities between the two presented combustion processes, the overlap of two IR spectrum for different burning conditions was made. The IR spectra overlapping is not presented because it is exactly the same that is present on Figure 152 (b).

In “cigar” burning test, the combustion occurred and consumed all the mixture, and it is proved by the absence of fresh material in the combustion material. Otherwise, in “disk” burning test, this mixture did not undergo to combustion and just fresh material were present.

### ***3.4.2.3. Mixture n° 4.1 - heterogeneous mixture based on UN, PU and MT***

Mixture 4.1 was composed by UN (87% (m/m)), PU (7% (m/m)) and MT mixture (9% (m/m)), as described at Table 16. It was exactly the same mass proportion than mixture 3.1, the only change is the oxidant.

#### **Fresh mixture characterization**

In order to study the influence of PU on UN and their possible products of reaction after de curing, was acquired an IR spectrum of UN with PU, which is shown at Figure 154 (b). Figure 154 (a) shows the overlap of IR spectrum of UN (Figure 143) with IR spectrum of PU (Figure 144).

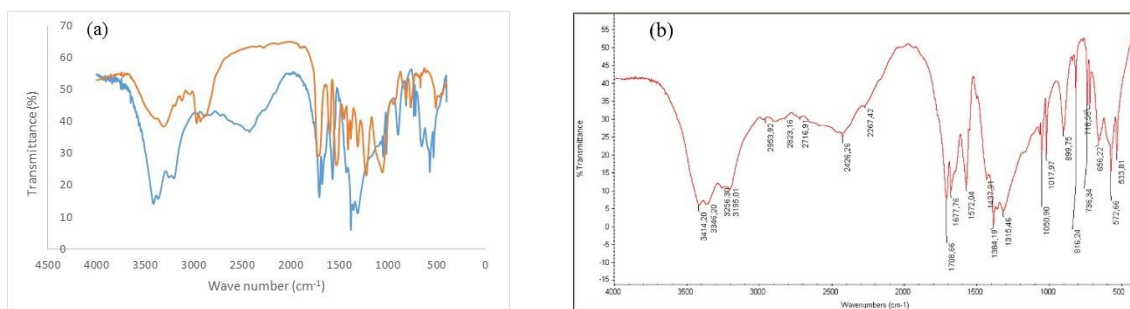


Figure 154: (a) Overlap of IR spectra of pure UN (blue) and PU (orange) and (b) the acquired IR spectrum for pure UN with PU mixture

It is very difficult to attribute more than one band to each compound, because they have very coincident IR spectra, as seen in Figure 154 (a). Although PU has more different functional groups than UN, UN is in bigger quantity and has very similar vibrational modes to PU, as C=O, N – H and NO<sub>3</sub><sup>-</sup> stretches.

The only band that can identify the presence of PU in our mixture is the weakest one, in a wavenumber range of 3000 to 2800 cm<sup>-1</sup>, having its maximum at 2974 cm<sup>-1</sup>, which belongs to C – H symmetric and asymmetric stretches.

UN can be identified by its most typical band, in a range of 2360 to 2550 cm<sup>-1</sup>, having its minimum at 2426 cm<sup>-1</sup>, where C=O···H···ONO<sub>2</sub> symmetric stretch is present.

One characteristic of this mixture (UN/PU) is that the bands characteristic of NH<sub>2</sub> symmetric and asymmetric stretches, in a range of 3500 to 3200 cm<sup>-1</sup>, get larger and less well-defined.

For IR characterization of global mixture composition, the methodology employed was identical. Figure 155 shows (a) the overlap of IR spectrum of UN / PU mixture (same as Figure 154 (b)) with the IR spectrum for MT mixture (also presented at Figure 146); and (b) the acquired IR spectrum for fresh mixture n<sup>o</sup>. 4.1. Table 48 shows the analysis of IR spectrum of fresh mixture 4.1, with basis in previous analysis.

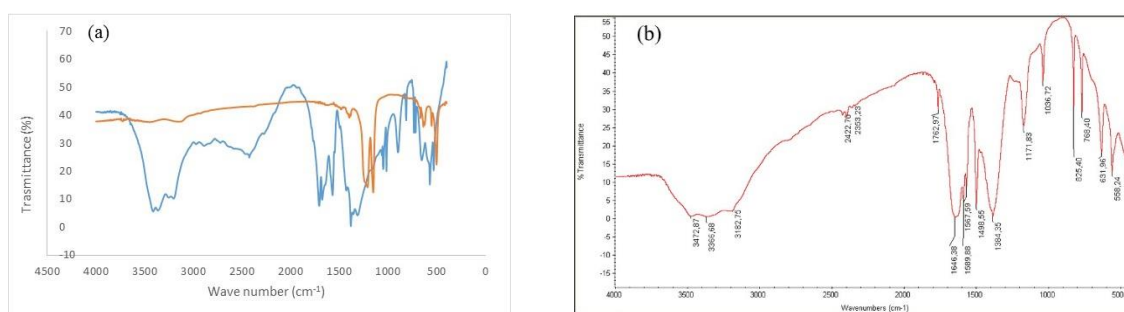


Figure 155: (a) overlap of IR spectra of UN / PU mixture (blue) and MT mixture (orange); (b) IR spectrum for mixture 4.1 (84% UN / 7% PU / 9% MT)

Table 48: Analysis of the presence of reactants in fresh mixture 4.1 by compound, typical peak band wavenumber from Table 41 to Table 43 and Figure 154 (b), new wavenumber of the typical peak in Figure 155 (b) and respective presence.

| Compound      | Typical Peak band Wavenumber (cm <sup>-1</sup> ) | Peak band Wavenumber on Figure 155(b) (cm <sup>-1</sup> ) | Vibrational modes  | Presence in fresh mixture |
|---------------|--|---|--|---------------------------|
| Urea Nitrate  | 2426   | 2426  | C=O...H...ONO <sub>2</sub> symmetric stretch (most typical from UN)              | Yes                       |
| Polyurethane  | 2970   | 2806  | Band overlap: C-N stretch and N-H elongation typical from urethane group         | Yes                       |
| MT mixture    | 1155   | 1172  | CF <sub>2</sub> typical elongations  | Yes                       |
| UN/PU mixture | 3414 / 3346                                      | 3473 / 3367 / 3183  | overlap of NH <sub>2</sub> symmetric and asymmetric stretches and water presence | Yes                       |
|               | 3256 / 3195                                      |   |  |                           |

As shown on Table 48, the most characteristic alteration for spectrum in Figure 154 (b) is the extension of the band in the range of 3200 to 3500 cm<sup>-1</sup>. This enlargement is probably due to water formation/absorption during the mixing and curing time, or due to the free OH groups which came from the polyol.

The peak at 2426 cm<sup>-1</sup>, from UN, has less intensity when MT mixture is present. This indicates the dissolution on UN, probably due to the mixing with the polyol (from PU) before adding the diisocyanate.

#### Burnt mixture characterization

The procedure used to study the combustion products of mixtures based on UN, as oxidant, PU as binder and MT mixture as additive, was the same already described on 3.4.2.1. Once again, there were study experimental isobar (“cigar” burning test) and adiabatic (“disk” burning test) combustion regimes.

**“Cigar” burning test.** Two IR spectra were compared, in order to know if there was the presence of fresh material in the end of this burning test. Figure 156 (a) shows IR spectrum of burnt material from the combustion of mixture 4.1 (experimental isobaric conditions). Figure 156 (b) represents the overlap of spectrum (a), with the spectrum (b) of Figure 155 (fresh mixture).

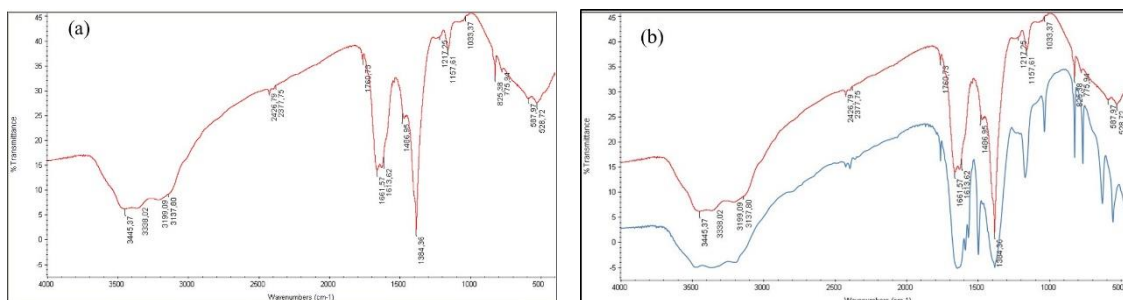


Figure 156: IR spectra of: (a) burnt mixture n°4.1 in experimental isobaric conditions; (b) overlap of spectra of burnt (red) and fresh material (blue) from mixture n°4.1 (the last one is also present at Figure 155 (b))

The biggest difference in spectra of fresh and burnt mixture is, again, the extension and definition of the band inside the range of  $3200$  to  $3500\text{ cm}^{-1}$ . It is more defined (more similar to Figure 153 (b)) probably due to the evaporation of water. There are, again, thermal decomposition products of MT mixture, as  $\text{MgF}_2$  and  $\text{Mg} - \text{C} - \text{F}$  unit elongations at  $529\text{ cm}^{-1}$  and  $588\text{ cm}^{-1}$ .

There is possible to see that some fresh material suffered combustion, because the bands of the burnt mixture are less intense, but still characteristic of the fresh mixture. The combustion was barely enough to form products with different and detectable vibrational modes than the ones present in the fresh mixture. The only difference that can be associated to the products of combustion of this kind of mixture are, again, the products of thermal decomposition of MT.

**“Disk” burning test.** Combustion in experimental adiabatic conditions was also tried for mixture n°. 4.1. The acquired IR spectrum for burnt material of mixture n°.4.1 is shown in Figure 157 (a). The overlap of IR spectra of fresh and burnt material of the referred mixture is shown on Figure 157 (b).

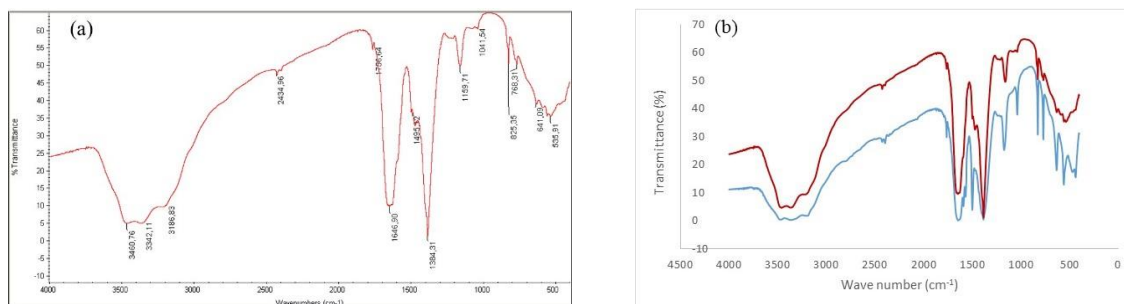


Figure 157: (a) IR spectrum of combustion products of mixture 4.1, burnt at adiabatic conditions; (b) overlap of IR spectra of fresh (blue) and burnt material (red) from mixture 4.1.

As in previous test, adiabatic burning conditions also produces the consumption of reactants and water, but in less quantities (bands intensity are closer than in isobaric experimental conditions),

Once again, the only identifiable combustion products are the ones which comes from the MT mixture. Now,  $\text{MgF}_2$  and  $\text{Mg} - \text{C} - \text{F}$  unit elongations appears at 448 and 557  $\text{cm}^{-1}$ , respectively.

**Correlation between both tests.** As it is possible to observe at Figure 156 and Figure 157, the pattern of combustion on both regime types are very similar. The biggest difference is that in “cigar” burning test there are more consumption of fresh material, as well as water, than in “disk” burning test.

#### ***3.4.2.4. Mixture n° 4.2 - heterogeneous mixture based on UN, PU and Al***

Mixture 4.2 was composed by UN (87% (m/m)), PU (7% (m/m)) and Al (9% (m/m)), as described at Table 16. It has the same mass percentage of same compounds (only changed the oxidant) than mixture 3.2.

##### **Fresh mixture characterization**

As shown on 3.4.2.1, Al has no characteristic IR spectrum and neither affects the IR spectrum of AN / PU mixture (Figure 151 (a)). To see if that has any reactivity with UN/PU mixture, the IR spectrum of mixture 4.2 was acquired. The result is the spectrum shown on Figure 158 (a). The overlap of IR spectrum of (a) with the IR spectrum of mixture UN/PU (already presented on Figure 154 (b)) is presented on Figure 158 (b).

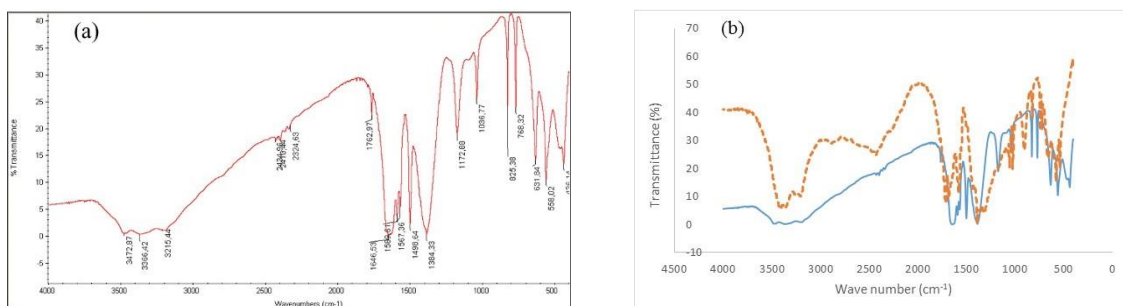


Figure 158: (a) IR spectra of fresh mixture 4.2; (b) Overlap of IR spectrum of: fresh mixture 4.2 (same as (a) – blue) and of mixture UN/PU (same as Figure 154 (b) – dashed orange)

As occurred for AN/PU mixture, Al has few influence on the characteristic peaks of UN and PU in mixture 4.2. They appear on the same range of wavenumber, with similar overlaps, when compared to the IR spectrum of the mixture without the additive. The only observable difference is the new peak at  $436\text{ cm}^{-1}$ . It probably belongs to an  $\text{Al}_2\text{O}_3$  specie (typical bands in a range of  $1100\text{ to }350\text{ cm}^{-1}$ ) that can be formed during the mixing or curing time.

Once again, the dissociation of UN occurs, due to the reaction with the water and the polyol (this mixture spent more time without the adding of diisocyanate than the previous one). Its characteristic band ( $2426\text{ cm}^{-1}$ ) is very thin, when compared to the mixture without additive.

Due to the high level of bands overlapping, between UN and PU, just one band for each compound will be taken as reference for its presence on burnt mixtures.

Urea nitrate will be characterized by its characteristic band at  $2426\text{ cm}^{-1}$ , PU by its band  $1590\text{ cm}^{-1}$ , which characteristic of C=C stretch from a di-substituted benzene (see Table 43), and the fresh mixture 4.2 by its peak at  $436\text{ cm}^{-1}$ .

### Burnt mixture characterization

**“Cigar” burning test.** For characterization of burnt compounds and the presence of fresh material on mixture n°. 4.2, after its burning on experimental isobaric conditions, an IR spectrum of its residues was made. The result is presented at Figure 159 (a). To make the referred characterization, the overlap of the IR spectrum of fresh mixture (showed at Figure 158 (a)) with the IR spectrum of burnt material (same as presented at

Figure 159 (a) was analysed and it is shown on Figure 159 (b). Figure 49 summarizes the referred analysis.

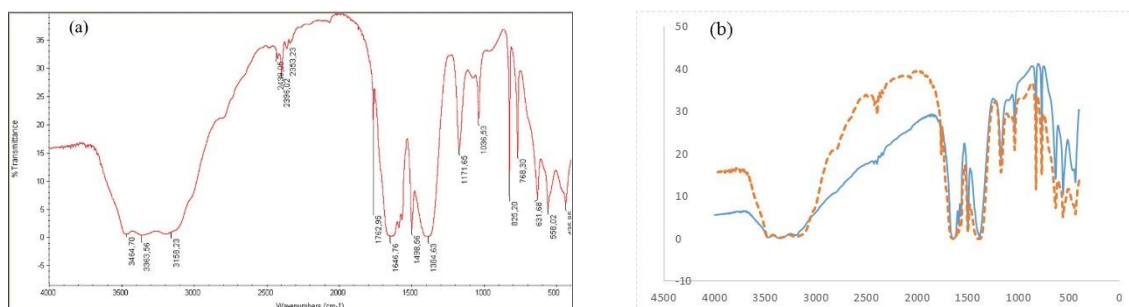


Figure 159: IR spectra of: (a) burnt mixture n°4.2 in experimental isobaric conditions; (b) overlap of spectra of burnt (dashed orange) and fresh material (blue) from mixture n°4.2 (same as presented at Figure 154 (b))

Table 49: Analysis of the presence of reactants in burnt mixture 4.2 (cigar burning test) by compound, typical peak band wavenumber from Table 41 to Table 43, new wavenumber of the typical peak in Figure 159 (a).

| Compound         | Typical Peak band Wavenumber (cm <sup>-1</sup> ) | Peak band Wavenumber on Figure 159(a) (cm <sup>-1</sup> ) | Vibrational modes   | Presence in burnt mixture - cigar |
|------------------|--|---|---|-----------------------------------|
| Urea Nitrate     | 2426   | 2426  | C=O···H···ONO <sub>2</sub> symmetric stretch (most typical from UN) | Yes                               |
| Polyurethane     | 1590   | 1589  | C=C stretch from a di-substituted benzene                           | Yes                               |
| UN/PU/Al mixture | 436  | 436   | Al – O stretching   | Yes                               |

Although the spectra shown of Figure 159 (b) are very similar, some differences are possible to see in the intensity and definition of the peaks.

The bands between 3500 and 3100 cm<sup>-1</sup> are now well-marked, which means that the water presence was reduced and now it is possible to see vibrational modes that can belong to NH<sub>2</sub> symmetric and asymmetric stretches, to primary or secondary amine salts elongations, which can be also products of reaction (from reaction of PU/UN, or from PU's decomposition, for example) or just the presence of fresh material with this kind of bonding (both UN and PU has this kind of bonds in their composition). The very thin peak at 2978 cm<sup>-1</sup> shows the presence of C – H symmetric and asymmetric stretches, which was not observable on fresh mixture.

Now the presence of urea nitrate is clear, because its characteristic band is well-marked. If there is no heating, UN can dissociate in a reversible reaction into nitric acid and urea.

Probably, with the low temperature (below the needed one to make the UN dissociation irreversible) acquired by this composition during the burning, these two compounds reacted again to form UN and that why its presence is so notable on IR spectrum of burnt mixture 3.2.

The intensity of the bands associated to  $\text{NO}_3^-$  out-of-plane deformation ( $825 \text{ cm}^{-1}$ ) and to  $\text{Al}_2\text{O}_3$  species elongations ( $436 \text{ cm}^{-1}$ ) are now bigger, which could indicate the formation of more compounds with these structures after the burning, or when some UN is burned it allows the visualisation of the bands of the other reactants, which were covered by the UN characteristic vibrational modes.

**“Disk” burning test.** Combustion in experimental adiabatic conditions was made for mixture n°. 4.2. The acquired IR spectrum for burnt material of mixture n°.4.2 is shown at Figure 160 (a). The overlap of IR spectra of fresh and burnt material of the referred mixture is shown at Figure 160 (b). The analysis made between the fresh mixture and the combustion residues is summarized at Table 50.

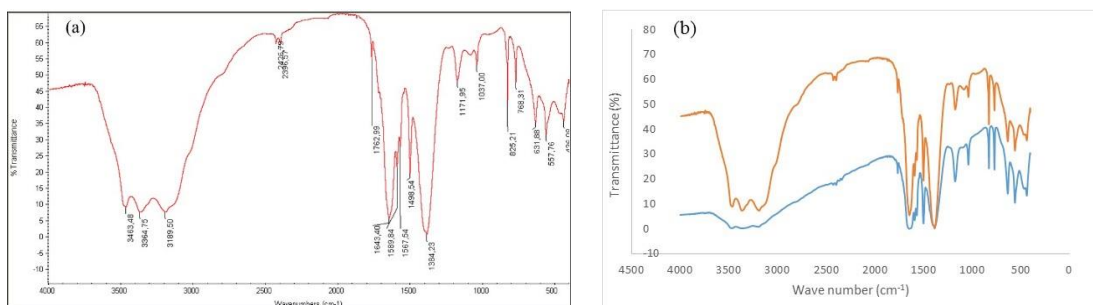


Figure 160: (a) IR spectrum of combustion products of mixture 4.2, burnt at adiabatic conditions; (b) overlap of IR spectra of fresh (blue) and burnt material (orange) from mixture 4.2.

Table 50: Analysis of the presence of reactants in burnt mixture 4.2 (disk burning test) by compound, typical peak band wavenumber from Table 41 to Table 43, new wavenumber of the typical peak at Figure 160 (a).

| Compound     | Typical Peak band Wavenumber (cm <sup>-1</sup> ) | Peak band Wavenumber on Figure 160 (a) (cm <sup>-1</sup> ) | Vibrational modes   | Presence in burnt mixture - disk |
|--------------|--|--|---|----------------------------------|
| Urea Nitrate | 2426   | 2427   | C=O···H···ONO <sub>2</sub> symmetric stretch (most typical from UN) | Yes                              |
| Polyurethane | 1590   | 1590   | C=C stretch from a di-substituted                                   | Yes                              |

|                  |     |     |                   |     |
|------------------|-----|-----|-------------------|-----|
|                  |     |     | benzene           |     |
| UN/PU/Al mixture | 436 | 436 | Al – O stretching | Yes |

As occurred in experimental isobaric conditions, the presence of water in the burnt material decreased and some characteristic vibrational modes showed up again. These are shown again by the definition of the bands in a wavenumber range of 3500 – 3200  $\text{cm}^{-1}$ , the well-marked characteristic band of UN and the thinly appearance of the band at 2798  $\text{cm}^{-1}$ .

There were also the consumption of fresh material and it is visible by the reduction of the intensity of the bands present at a wavenumber range of 1300 to 400  $\text{cm}^{-1}$ .

**Correlation between both tests.** For find the spectroscopic differences and similarities between the two presented combustion processes, the overlap of two IR spectrum for different burning conditions was made and it is presented on Figure 161. The analysis of these two spectra are synthetized on Table 51.

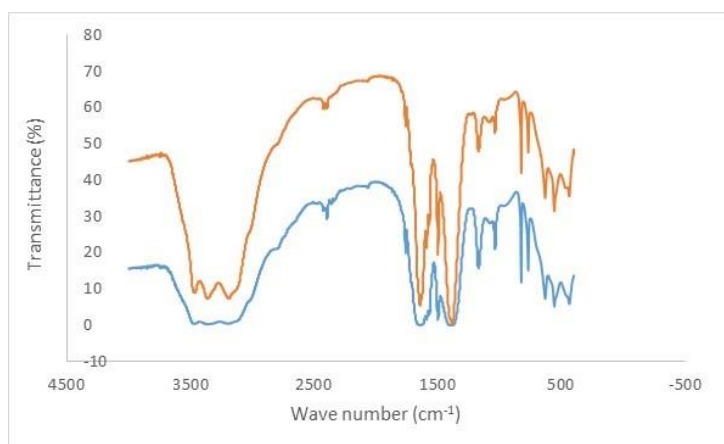


Figure 161: Overlap of IR spectra of burnt material, from mixture 4.2. The blue spectrum shows IR spectrum of burnt mixture on the “cigar” burning test (Figure 159 (a)), and the orange one shows the burnt material IR spectrum of “disk” burning test (Figure 160 (a)).

Table 51: Analysis of the presence of reactants and common combustion products in burnt mixture 4.2 in experimental isobaric (cigar) and adiabatic (disk) conditions by compounds, typical peak band wave number from tables 42 to 44, new wave number of the typical peak in Figure 159 (a) and Figure 160 (a).

| Compound | Typical Peak band Wave number ( $\text{cm}^{-1}$ ) | Vibrational modes | Presence in burnt mixture - cigar | Presence in burnt mixture - disk |
|----------|--|-------------------|-----------------------------------|----------------------------------|
|----------|--|-------------------|-----------------------------------|----------------------------------|

|  |                                |   |     |     |
|--|--------------------------------|---|-----|-----|
| Urea Nitrate   | 2426                           | C=O...H...ONO <sub>2</sub> symmetric stretch (most typical from UN)   | Yes | Yes |
| Polyurethane   | 1590                           | C=C stretch from a di-substituted benzene   | Yes | Yes |
| MT mixture   | 1155                           | CF <sub>2</sub> typical elongations   | Yes | Yes |
| UN/PU/Al mixture (both for fresh and burnt mixtures) | 436                            | Al – O stretching   | Yes | Yes |
|  | [3500 – 3100] cm <sup>-1</sup> | Overlap of NH <sub>2</sub> symmetric and asymmetric stretches and primary or secondary amine salts elongations (for fresh mixture has water presence) | Yes | Yes |
|  | 825                            | NO <sub>3</sub> <sup>-</sup> out-of-plane deformation   | Yes | Yes |

By the analysis made between these two spectra, the only notable difference between them is that experimental adiabatic combustion regime consumes more water than the isobaric one. Probably it is possible to say the same about the UN's consumption, due to the lower intensity and high definition of the bands peaks at adiabatic burning test. This can show that when UN and H<sub>2</sub>O are consumed in combustion, it allows the appearance of the characteristic peaks from other components in the mixture.

## CHAPTER 4 - RESULTS DISCUSSION

### 4.1. Ammonium and Urea Nitrates Thermal Decompositions

#### 4.1.1. THOR prediction

The results acquired from thermochemical calculations, using THOR code, for prediction of thermal decomposition species of ammonium and urea nitrates had quite similar behaviour (vd. Figure 162 and Figure 163, respectively). They show two zones: the first zone is formed by major equivalent species formed for the same global enthalpy, followed by the others that really show AN and UN decompositions.

According to literature, UN thermal decomposition shows formation of solid species. THOR predicted this fact, because it shows an empty zone, where there are no products formation (Figure 163). The chosen species for calculations, besides the  $C(\alpha)$ , were all gases. It is difficult to find exactly the products composition founded experimentally in bibliography. Predictions keep high temperature conditions and experimental compositions are detected after a cooling process.

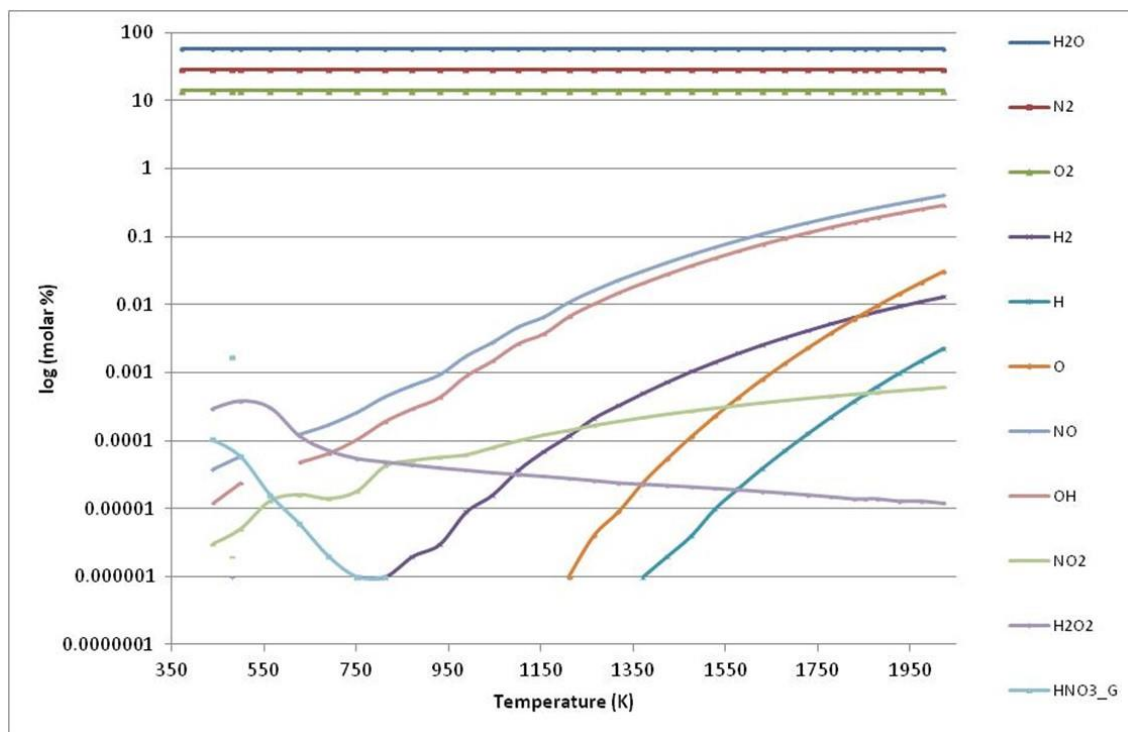


Figure 162: Thor predicted decomposition species of AN in function of temperature.

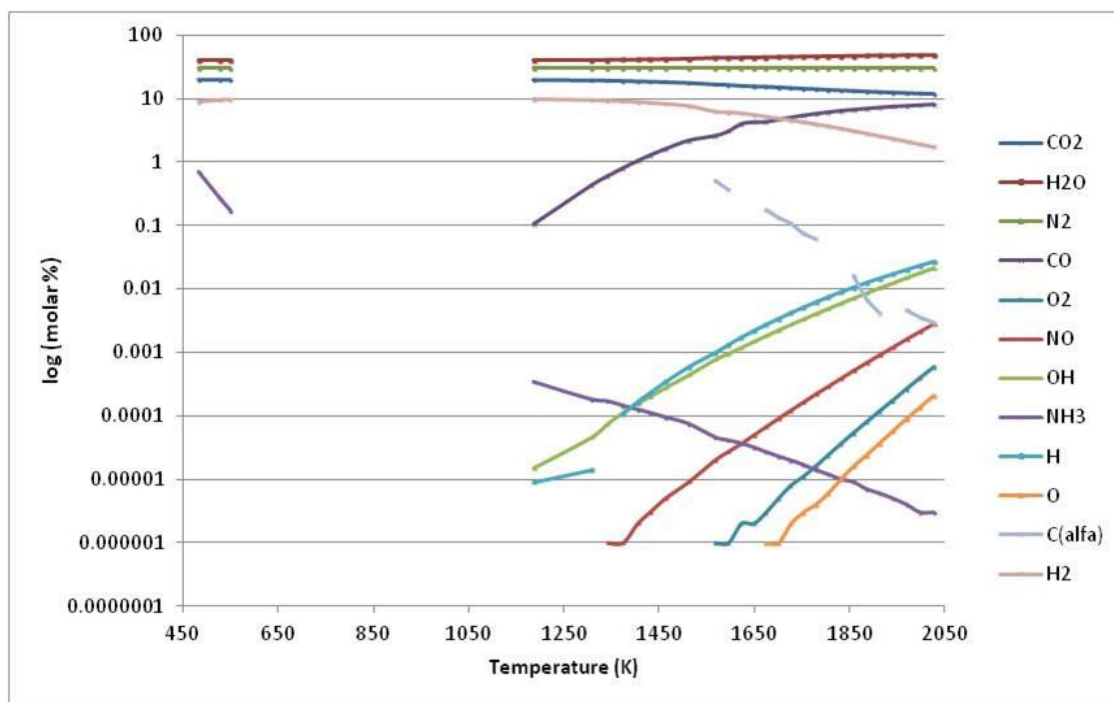


Figure 163: Thor predicted decomposition species of UN in function of temperature.

## 4.1.2. DSC/TGA

### 4.1.2.1. Ammonium Nitrate

At 2.2.2.1, four DSC/TGA thermograms were presented. Two of them were performed with a heating rate of 5°C/min and showed five phase transitions on the predicted temperature range - the averaged acquired melting point was 170.2°C and the averaged thermal decomposition temperature acquired was 268.0°C. The other two DSC/TGA thermograms were performed with a heating rate of 10°C/min and showed four phase transition on the predicted temperature range - the averaged acquired melting point was 172.4°C and the averaged thermal decomposition temperature acquired was 292.7°C. All thermograms present phase transitions, the melting point was similar, but the thermal decomposition temperatures acquired had significant deviations.

The different number of phase transitions acquired on the different thermograms, as well as their temperatures, and the significant deviations acquired for the thermal decomposition temperatures of AN were attributed to the samples weights, which affect the heat transfer along the solid. Samples with little weight, the exothermic reactions had no influence on the DSC result, because the heat released by them is not significant

for DSC acquisition, but higher weights promote more reactions and exothermic reactions occurs on a detectable way. Higher masses seems to promote bulk decomposition saturation.

The kinetic parameters presented on this work were concordant between them. The activation energy ( $E_a$ ) varied between  $2.93E+06$  and  $4.86E+06$  J/mol and the pre-exponential factor ( $Z$ ) varied between 23.83 and  $532.72 \text{ min}^{-1}$ .

The activation energy and the pre-exponential factor  $Z$  are dependent of the applied heating rate and of the sample's weight. They increase with the increase of the heating rate and with the decrease of the sample's weight.

### ***4.1.2.2. Urea Nitrate***

It was also acquired four DSC/TGA thermograms to study the thermal decomposition of UN. They were presented on 2.2.2.2. All thermograms showed three main peaks, two endothermic and one exothermic. Except in one case, all peaks appeared associated with mass losses.

For the two thermograms acquired with a heating rate of  $5^\circ\text{C}/\text{min}$ , the averaged melting point (first endothermic peak) acquired was  $158.7^\circ\text{C}$ , the averaged decompositions temperatures for exothermic and second endothermic peaks were  $166.3^\circ\text{C}$  and  $244.2^\circ\text{C}$ , respectively. For the other two thermograms, acquired with a heating rate of  $10^\circ\text{C}/\text{min}$ , the averaged melting point (first endothermic peak) was  $152.1^\circ\text{C}$ , the averaged decompositions temperatures for exothermic and second endothermic peaks were  $173.2^\circ\text{C}$  and  $274.6^\circ\text{C}$ , respectively.

As happened for AN, different weight of samples and different applied heating rates at UN have different contributions for DSC/TGA results, which reflects on different temperatures for the same step of mass loss.

The results presented on 2.2.2.2 were similar to the ones showed on Literature Review, which means that it is possible to associate the described thermal decomposition mechanisms of UN (2.1.1.2) to our DSC/TGA results.

In relation to the kinetic parameters, the activation energy ( $E_a$ ) varied between  $7.22E+05$  and  $9.94E+06$  J/mol and the pre-exponential factor ( $Z$ ) varied between 1.72 and  $1.66E+20 \text{ min}^{-1}$ . The calculated activation energies were all in the same magnitude order, but the pre-exponential factor varied largely. For bigger masses, this parameters

was on the same magnitude order, but for small masses it varied according to the studied mass loss step. The first mass loss step, which is coincident with the first endothermic had the highest Z, the other two mass loss steps had values on the same magnitude order for the equivalent mass loss step, but one hundred times higher between the second mass loss step and the third mass loss step.

## **4.2. Development and detection of studied mixtures**

Mixtures compositions, by mass percentage, were described on 3.1, as well as the thermodynamic properties of all reactants used on them. The parameters used to characterize the thermodynamic properties of the reactants were: molecular formula, molar mass, phase, density, enthalpy and entropy of formation, boiling point, heat of combustion/ enthalpy of reaction and specific heat capacity.

### **4.2.1. THOR predictions of combustion products properties**

#### ***4.2.1.1. Free Gibbs enthalpy and temperatures of combustion, for oxidants (AN and UN) and binder (PU) mixtures***

The minimum free Gibbs enthalpy and the maximum combustion temperatures, for mixtures based on AN and UN as oxidants and PU as binder, were found for richness values of 1.9 and 1.75, respectively. Free Gibbs Enthalpies varied between  $-1.83E+04$  and  $-1.60E+04$  kJ/kg and the considered range for these variations was with r between 1.5 and 2.9.

The  $r = 1.9$  corresponds to a mixture of 72% AN and 28% PU (m/m), and  $r = 1.75$  corresponds to a mixture of 86% UN and 14% PU (m/m), respectively.

#### ***4.2.1.2. Predicted temperature of combustion as function of additives for previous mixtures (AN and UN with PU)***

There were added 2, 4, 6 and 9% (m/m) of additives - Al and MT mixture - on the mixtures described above, for  $r = 1.9$  (AN/PU) and for  $r = 1.75$  (UN/PU).

For mixtures composed by different oxidants and same additive, the results were identical: how higher was the concentration of the additive, higher was the predicted temperature of combustion of the respective mixture.

The presence of Al in the mixtures increased more their temperature of combustion than the presence of the MT mixture.

The mixtures of AN/PU/Al reached temperatures of combustion between 1595.9 K (Al% = 0) and 2329.2 K (Al% = 9) and the ones with MT mixture varied between 1595.9 K (MT% = 0) and 1716.7 K (MT% = 9).

The mixtures of UN/PU/Al reached temperatures of combustion between 1500 K (Al% = 0) and 2250 K (Al% = 9) and mixtures of UN/PU/MT, the temperatures of combustion varied between 1500 K (MT% = 0) and 1666.7 K (MT% = 9).

### 4.2.2. Combustion experiments

Two types of combustion conditions were performed: cigar and disks burning tests. The first type of test was more close to isobaric, at ambient pressure, conditions. The second type, having PMMA disks as confinements, was more close to adiabatic conditions.

The only parameter studied for both tests was the density of the fresh mixture ( $\rho$ ) present on both confinements.

For cigar burning tests, the studied combustion parameters were: temperatures of mixtures combustions (T); the propagation velocities of the heat on PMMA ( $D_{PMMA}$ ), on explosions ( $D_{explosion}$ ), on the burning mixture ( $D_{mixture}$ ); and the fundamental flame velocity ( $V_{Flame}$ ), which is product of the exothermic reactions between the gases formed during the combustion of the mixture and the oxygen present in air.

For disk burning tests, the studied parameters, beside density, were: the area of two explosions, by deflagration, of the mixture (A) and the time ( $\Delta t$ ) needed to occurs the deflagration in the fresh mixture.

#### 4.2.2.1. Densities of the fresh mixtures

To have a general idea about the densities of the studied mixtures, for each test, their densities were plotted all together, as shows Figure 164.

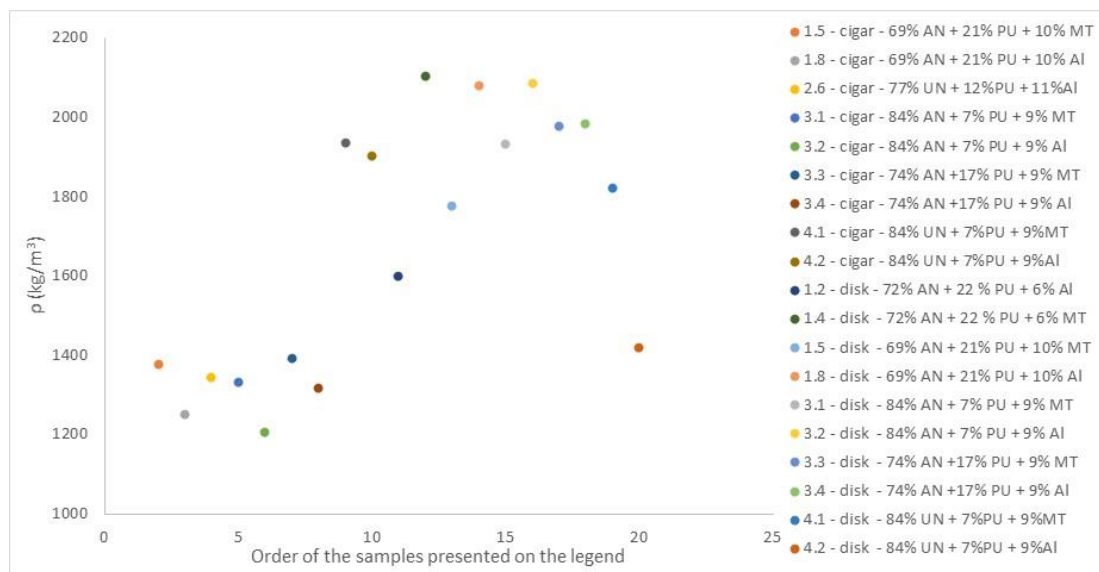


Figure 164: Densities of all studied mixtures, for each test.

Figure 165 shows the results for the densities measured for the cigar burning tests (left) and for disk burning tests (right), separately.

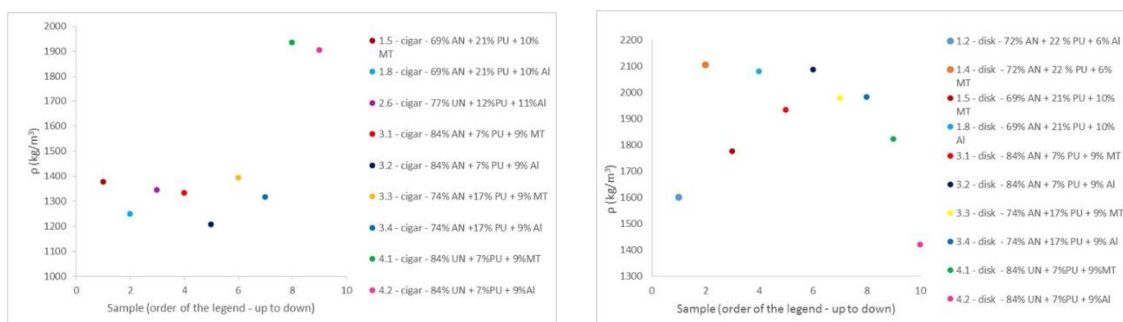


Figure 165: densities of the mixtures separated by tests. At left are presented the densities of the mixtures on cigars. At right, the densities of the same mixtures, but in disks. Mixtures 1.2 and 1.4 just were performed in disks burning tests.

For cigars burning tests (Figure 165, left), the densities of mixtures composed by AN, PU and MT, varied between 1332.6 and 1393.1  $\text{kg/m}^3$ . The averaged density for these mixtures was  $1367.6 \pm 0.5 \text{ kg/m}^3$ . For same mixtures, but varying the additive for AI, the densities varied between 1206.6 and 1316.6  $\text{kg/m}^3$  and the averaged density was  $1257.7 \pm 0.5 \text{ kg/m}^3$ . Globally, the mixtures of AN had an averaged density of  $1312.6 \pm 0.5 \text{ kg/m}^3$

For mixtures composed by UN (Figure 165, left), the density range varied more, because of the quantity of the mass used of this oxidant. The density of these mixtures

varied between 1345.4 and 1934.6 kg/m<sup>3</sup> and the averaged density was 1727.6 ± 0.5 kg/m<sup>3</sup>.

As expected, higher is the molar masses of the used reactants, higher will be the density of the mixture. MT has a higher mass than Al, the mixtures with MT has higher masses than mixtures with Al. UN has a higher molar mass than AN, mixtures with UN has higher densities than the ones with AN.

For disk burning tests (Figure 165, right), the mixtures of AN/PU/MT varied their densities between 1775.0 and 2103.8 kg/m<sup>3</sup> and the averaged density was 1947.9 ± 0.5 kg/m<sup>3</sup>. Same mixtures, changing the additive for Al, had densities that varied between 1600.5 and 2086.5 kg/m<sup>3</sup>, and the averaged density was 1937.6 ± 0.5 kg/m<sup>3</sup>. Globally, on disks, the mixtures of AN had an averaged density of 1942.7 ± 0.5 kg/m<sup>3</sup>.

Mixtures composed by UN, for disk burning tests, had densities of 1420.4 ± 0.5 kg/m<sup>3</sup> (for Al) and 1822.5 ± 0.5 kg/m<sup>3</sup> (for MT mixture). The averaged value for this densities is 1621.4 ± 0.5 kg/m<sup>3</sup>.

Mixtures of AN had similar behaviour for both additives, which means that for high pressures (disks were pressed with higher pressure than cigars), the major contribution for the density of the mixture is the component in higher quantity, in this case, the AN. The influence of the mass of the additive is notable, but not relevant (MT mixture produces mixtures with higher densities than Al).

For mixtures of UN, the presence of the additive is more relevant, but two samples are not enough to quantify this relevance.

The difference between the averaged densities for mixtures of AN and for mixtures of UN shows that smaller molecules have higher power of compression and this is why AN samples had higher densities than UN samples.

#### ***4.2.2.2. Temperature profiles of mixtures in cigar burning tests***

The study of the temperature profile of the mixtures in cigar burning test was made in function of the used additive. Figure 166, at left shows the temperature profile of the mixtures with MT as additive, and at right shows the temperature profile of the mixtures with Al.

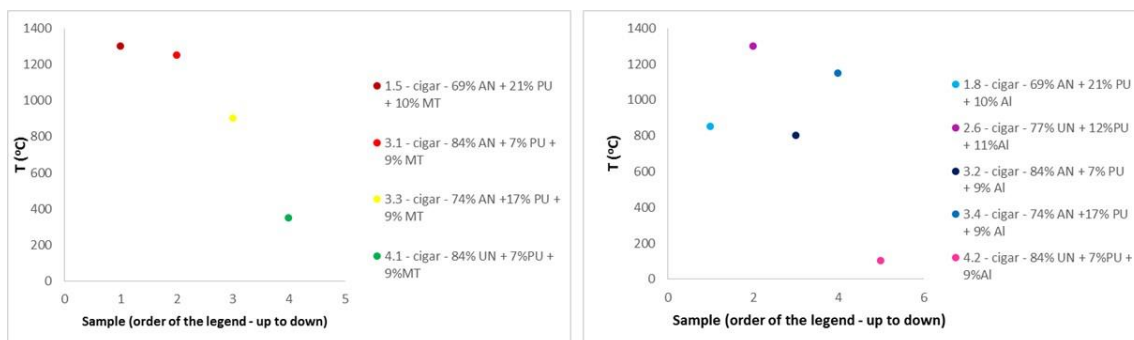


Figure 166: Temperature profiles of the studied mixtures. Left image is correspondent to samples which has MT mixture as additive. Right image corresponds to mixtures with Al as additive.

For the temperature profile of samples with MT in their composition (left image on Figure 166), it is possible to observe that higher temperature was acquired for the sample with higher concentration of MT and for the smaller concentration of AN (sample 1.5). For the same concentration of MT (samples 3.1 and 3.3), the higher temperature was acquired for the one which had higher concentration of AN, as expected.

As it is possible to observe in Figure 166 (left), the samples 1.5, 3.1 and 3.3 has smaller differences on MT mixture concentration (just 1%), the expected was that the dark red point (sample 1.5) appears below the yellow one (sample 3.3), because of the concentration of the AN. This probably occurred due to the using of different mixing procedures. The order of the addition of the reactants was very different from procedure 2 (3.3.2.2) used in mixture 1.5, to procedure 3 (3.3.2.2.) used in mixtures 3.1 and 3.3. It is not possible to say which the factor (on the mixing procedure) that altered the temperature profile of the samples. To study that it will be need to do two set of mixtures that just change one reactant in the order of addition in each set. From procedure 2 to procedure 3, two changes on the order of the addition of the reactants were made.

The mixture with UN (4.1) was the one that had worst conductivity and combustion not occurred on the position of the temperature acquisition.

On mixtures with AN, the concentration of the oxidant increased the temperature (see mixtures 3.1 and 3.3 at left image of Figure 166). These temperatures varied between 900 and 1300 °C. THOR code predicted temperatures around 1600 K, which means a good prediction.

For samples with Al as additive (Figure 166, right image), the profile temperature was not conclusive. Mixtures 3.2 and 3.4 were prepared by procedure 3 and mixture 1.8 was prepared according procedure 2 (3.3.3.2). Mixtures 3.2 and 3.4 were the extremes, which probably means that, in this procedure (3 of 3.3.3.2), the contribution of the PU rises the temperature profile of the mixture. Mixture 1.8 has higher concentration of PU than mixture 3.4 (mixture with higher concentration of PU and with AN as oxidant) but has lower temperature profile.

Samples of UN had also an inconclusive profile of temperature, because just more 2% of Al raised the temperature more than 1000°C, for minor quantities of UN. The temperature profile of the samples with UN/PU/Al varied between 100 and 1330°C. This profile has an explanation that needs to have more study on that. The mixing procedure here was determinant, because polyol hydrolyses the UN and diisocyanate not. Diisocyanate and UN promote more bounds which breaks are more exothermic. Besides the high temperature acquired by mixture 1.8 during the combustion, mixture 2.7 (76% UN + 12%PU + 12%MT) which was prepared by the same mixing procedure than sample 1.8, suffered auto-combustion.

When polyol was added first (by mixing procedure 3) the mixture 4.2, as well as 4.1, not burned. The hydrolysis of UN reduces its hazards. These facts means that mixing procedure (2) promotes the hazards of these mixtures of UN.

The study about the influence of the mixing procedure, i.e, the influence of the order of the addition of the reactants, the curing time and pressing mode in our mixtures needs to be further to understand these temperature profiles, on cigar burning tests.

### ***4.2.2.3. Velocity of propagation of PMMA***

Due to the combustion achieved on our cigar burning tests were driven-flame combustion, it is important to see the contribution of the self-combustion of the PMMA on our mixtures, by the study of the velocity of propagation of heat on the PMMA ( $D_{PMMA}$ ). Figure 167 shows the general behaviour of the velocity of propagation of heat on the PMMA, in cigar burning tests.

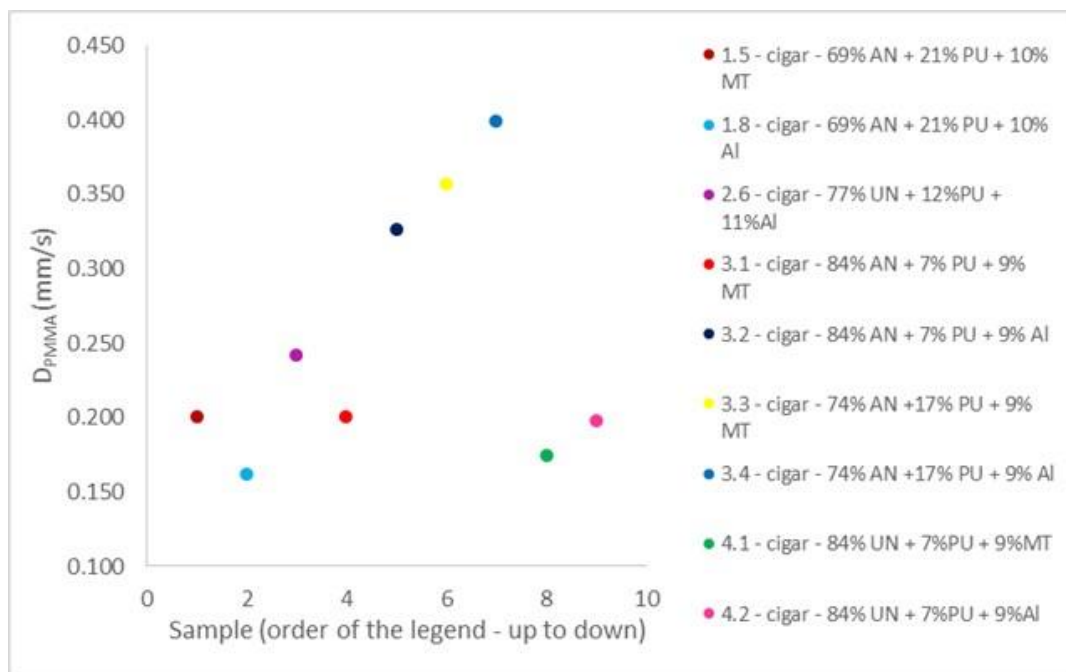


Figure 167: Velocities of the flame propagation on PMMA for each studied sample, on cigar burning tests

Analysing Figure 167, there is possible to see a linear distribution of the samples between 0.15 and 0.25 mm/s, which gives an averaged value for  $D_{PMMA}$  of  $0.196 \pm 0.005$  mm/s. This proves that, for the majority of the samples, the flame of the PMMA was the responsible for a continuous driven-flame that ensures total combustion of the sample.

The three samples (3.2, 3.3 and 3.4), which presented  $D_{PMMA}$  higher than 0.25 mm/s (Figure 167), were samples of AN/PU which richness was closest from  $r = 1.9$  (richness founder for the highest temperature of combustion for mixtures of AN/PU).

Mixtures 3.3 and 3.4 had the same composition ( $r = 1.9$  for AN/PU), the additive was the only different between them. The higher  $D_{PMMA}$  was acquired for the one which had Al (3.4). Mixtures 3.1 and 3.2 were in the same situation, but with  $r > 1.9$  for AN/PU, and just the one with Al (3.2) raised the value of  $D_{PMMA}$ . This shows the influence of the reactions between Al and higher concentrations of AN, proving that Al not reacts directly with AN, but with its combustion products when present in higher quantities, as expected. This not occurs for the MT mixture, which combustion products not have reactivity with the combustion products of the AN, and that why that  $D_{PMMA}$  had is value inside the expected range.

**4.2.2.4. Flame velocity propagation jumps on explosions**

The study of the flame velocity propagation jumps on explosions ( $D_{\text{explosion}}$  - deflagration, to be more correct) was considered the combustion of the pre-expanded gaseous products of the burning mixture. This combustion was observed by the emission of light on the burnt material, which was characterized by incandescence, as shown in figures along 3.3.4.

The results for  $D_{\text{explosion}}$  are presented on Figure 168, and not all mixtures presented these kind of explosions. The  $D_{\text{explosion}}$  is an indicative of self-sustained combustion with flame velocity jumps.

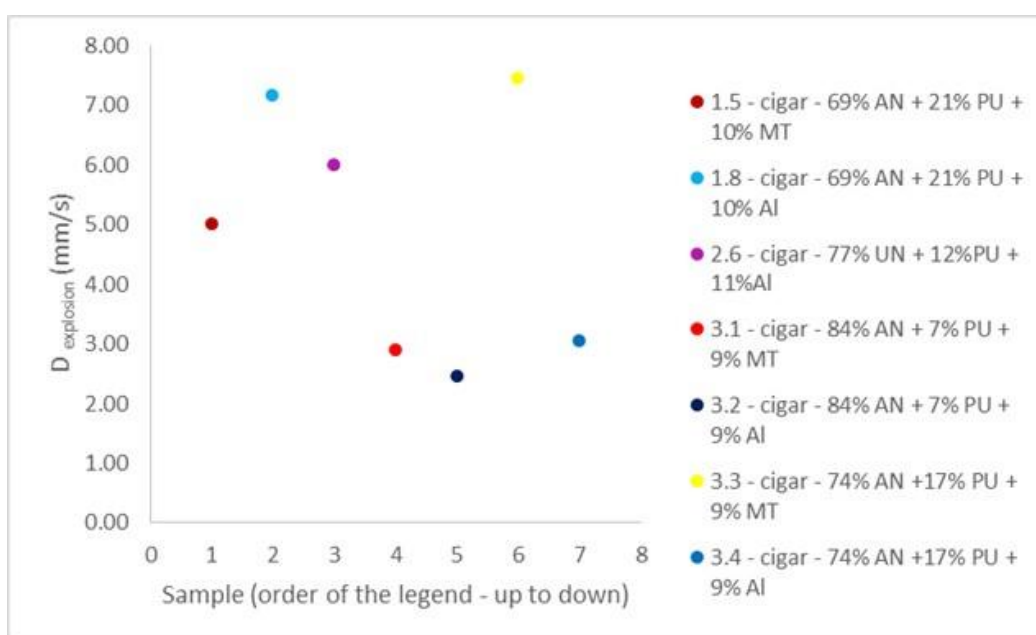


Figure 168: Velocities of the flame propagation on explosions ( $D_{\text{explosion}}$ ) in cigar burning tests. Mixtures 4.1 and 4.2 are not present because they not presented this kind of combustion.

The velocities of the flame propagation on explosions ( $D_{\text{explosion}}$ ) on studied samples varied between 2.46 and 7.46 mm/s. They not had a pattern, but their velocity range was small (5 mm/s).

The mixture with MT which reached higher  $D_{\text{explosion}}$  was the one with AN/PU with  $r = 1.9$  (0.49 mm/s), and the one which reach the lower  $D_{\text{explosion}}$  was the one with higher concentration of AN (0.05 mm/s), which means that MT mixture and AN, and their reactions products, not make reactions that produce high amounts of energy. In the right stoichiometry of AN/PU, MT mixture promotes this velocity due to its large gas expansion.

The mixtures with Al which reach higher  $D_{\text{explosion}}$  were the ones with higher concentration of Al, 10 % in the case of AN/PU (7.16 mm/s) and 11% in the case of UN/PU (6 mm/s).

#### 4.2.2.5. Velocity of the flame propagation on the studied mixtures

The velocity of the flame propagation on the studied mixtures ( $D_{\text{mixture}}$ ) was studied by the observation of the mixtures, when they were passing from their solid state to liquid and gaseous states (all mixtures bubbled). This is the velocity that mixtures needs to change their phases and to produce reactions.

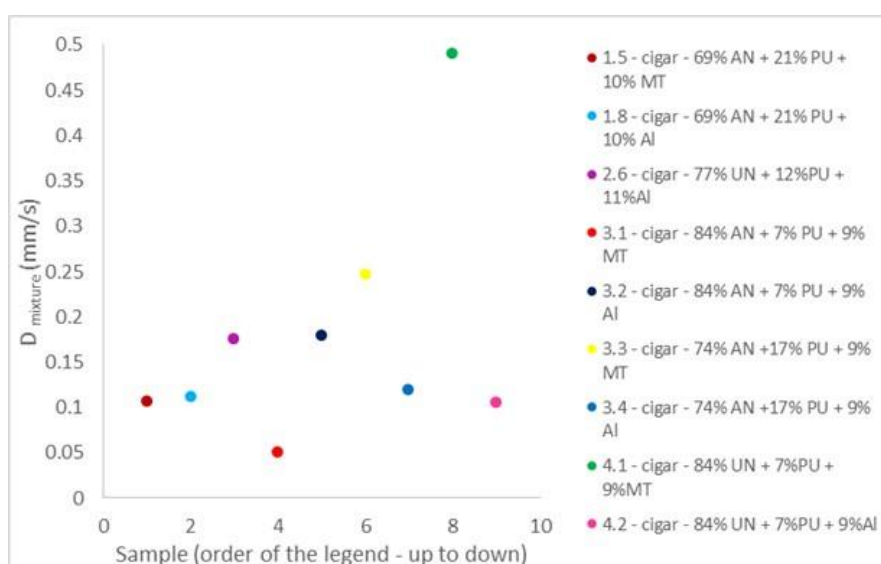


Figure 169: velocities of the flame propagation on the studied mixtures ( $D_{\text{mixture}}$ ) in cigar burning tests.

Analysing Figure 169, besides the sample 4.1, the velocity of the propagation of the heat on the studied mixtures ( $D_{\text{mixture}}$ ) had similar behaviours, because their velocity range was tight ([0.05 – 0.25] mm/s).

These extremes belongs to MT mixtures, the higher one is for AN/PU mixture with  $r = 1.9$ , and the lower one is for the higher concentration of AN in AN/PU mixture, again. This proves that MT mixture, as additive, is just effective when the mixture AN/PU has the best stoichiometry. Its gas expansion promotes  $D_{\text{mixture}}$  when it is not big enough to extinguish the combustion.

For mixtures with Al as additive, the velocity of the propagation of the heat on the studied mixtures ( $D_{\text{mixture}}$ ) is proportional to the presence of oxidant. Higher is the concentration of the oxidant, higher is the  $D_{\text{mixture}}$ . This is due to the reactions of Al

with the oxygen from the burned mixture. Their range of variation is from 0.11 to 0.18 mm/s.

Although the number of the samples are not enough to have accurate results, for UN mixtures it happens the same: the MT mixture is effective on the best stoichiometry of UN/PU and Al effectiveness is dependent of the oxidant quantity.

#### 4.2.2.6. Fundamental flame velocities

The fundamental flame velocity ( $V_F$ ) is an approximated measure of the chemical combustion process of the formed gases. This is directly related with the volume consumption of the formed gases ( $\dot{V}$ ) and the area of the degasification formed by their production ( $A_F$ ) by equation (106) (see 3.3.3.6). The results obtained for this parameter of combustion are synthetized on Figure 170.

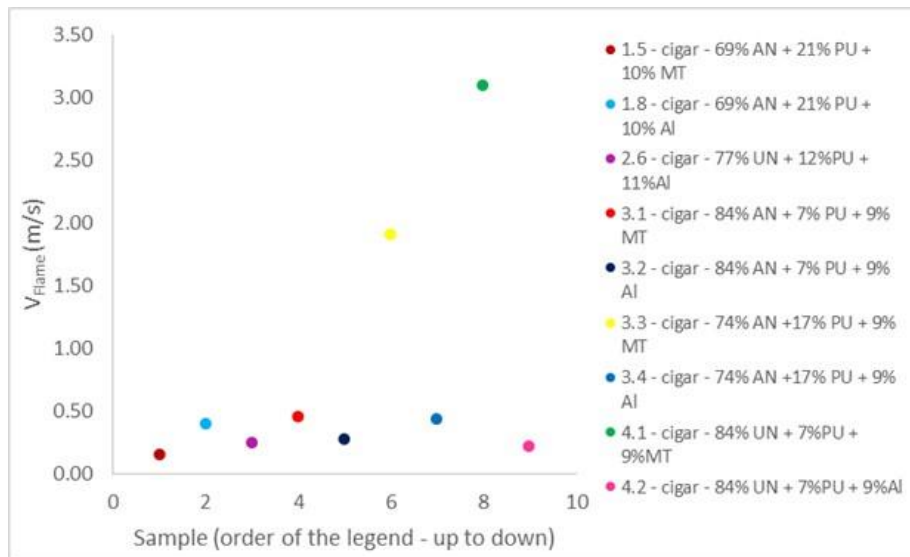


Figure 170: fundamental flame velocities ( $V_{Flame}$ ) for studied mixtures, in cigar burning tests.

Higher flames velocities were achieved for mixtures with MT mixture as additive, with oxidant and the binder in proportion of best richness, which means in stoichiometric proportions to achieve the best combustion temperatures. For mixture AN/PU/MT ( $r = 1.9$  for AN/PU),  $V_F$  was 1.9 m/s, and for mixture UN/PU/MT ( $r = 1.75$  for UN/PU),  $V_F$  was 3.1 m/s. These results were predictable, due to large expansion of MT mixture, which indicated higher volume rates.

The other mixtures varied their  $V_F$  on a range of 0.14 to 0.45 m/s, with an averaged value for fundamental flame velocity of  $0.30 \pm 0.01$  m/s.

The  $V_F$  of the mixtures with Al as oxidant had the same behavior previously described. Higher was the concentration of the oxidant, higher was the  $V_F$ . Once again, this parameters is also a hazard one, due to the combustion power that those mixture can have, if subjected to a proper ignition.

Generally, MT mixture promoted more all the studied velocities, due to its gas expansion which revealed to be a physical factor that has great effect on the combustion of the studied mixtures, on isobaric conditions. This pressure parameter is more effective how close the mixture, of the oxidant and the binder, is in the ideal stoichiometry for achieve the highest temperature of combustion.

The hazards of the Al additive on the studied mixtures are not higher than the ones due to MT mixture, but they can be achieved easier when ideal stoichiometry of oxidant, binder and additive are unknown.

#### ***4.2.2.7. Local explosions areas and time delay in disk combustion samples***

Beside densities, the areas of the explosions by deflagration of the studied mixtures, and the time needed to reach the respective explosion were the parameters calculated for combustion on disk tests, approaching adiabatic conditions.

There are no results for UN mixtures because they not suffered combustion.

Figure 171 and Figure 172 shows the obtained results for the time ( $\Delta t$ ).and for areas (A), respectively.

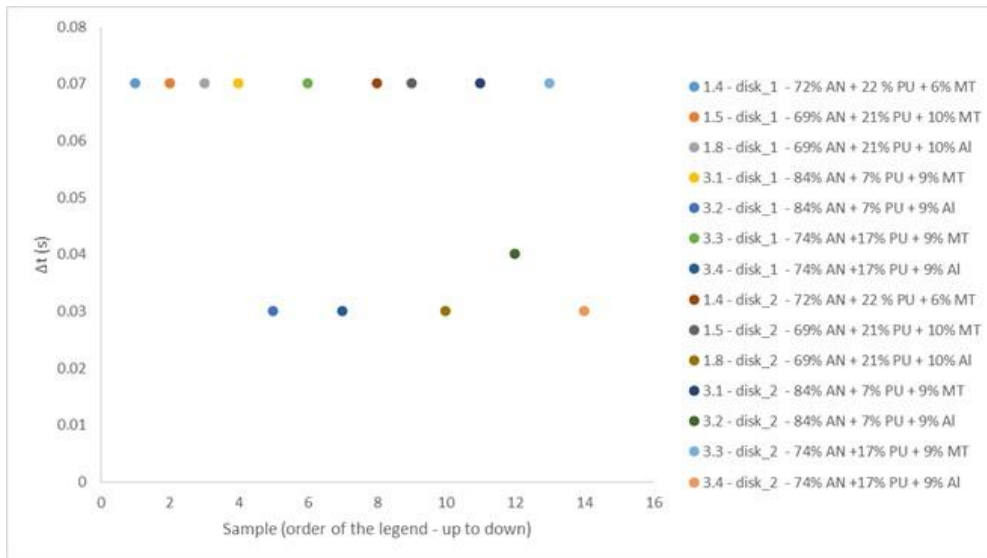


Figure 171: Time needed by each mixture to reach explosion by deflagration. On the legend, the number after the underscore means the number of the studied explosion.

All mixtures with Al in their composition, except sample 1.8 in first explosion, last between 0.3 and 0.4 s to reach explosions by deflagration. All mixtures with MT mixture as additive and sample 3.4 (first explosion) needed 0.07 seconds to reach the explosions.

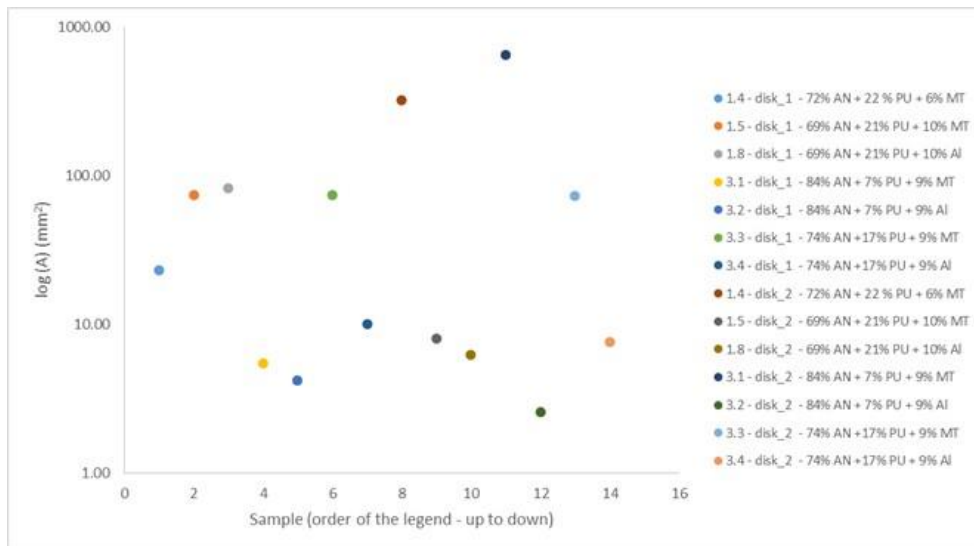


Figure 172: Areas (A) of explosion by deflagration of each mixture in logarithmic scale. On the legend, the number after the underscore means the number of the studied explosion.

The pattern of the areas (log(A)) of explosion are not so clear as their time of appearance (Δt), although it is possible to see two regions of areas, one above log(A) = 10 and other bellow.

The areas below  $\log(A) = 10$  are from mixtures with Al in their composition which needed minor times to reach explosions. Once again, mixture 1.8 was an exception. The areas above  $\log(A) = 10$  belonged to mixtures which had MT mixture as additive, but there were two exceptions, mixtures numbers 1.5 (second explosion) and mixture 3.1 (first explosion).

These results, from Figure 171 and Figure 172, show that the mixtures with MT mixture as additive, needs more time to reach explosions by deflagration than the ones with Al, but their areas of deflagration are bigger than the Al ones.

Both additives increase the hazards on studied mixtures, but MT mixture is worst due to gas expansion, which promotes the bigger areas of combustion.

### **4.2.3. Infra-Red Spectroscopy**

The main objective of the use of the IR spectroscopy on this work was to characterize the studied mixtures, before and after its combustion. The analysis was performed using the optimized mixtures described on Table 16. The mixtures with lower concentration of AN were not characterized, because their mass percentage, in relation to the others, were not significant for big changes on the IR spectra. AN mixtures of lower concentrations had a similar combustion behaviour than the higher ones.

To characterize the studied mixtures by IR spectroscopy was necessary, firstly, to analyse the IR spectra of the reactants, in order to detect their presence on the mixture and to evaluate the formation of new bounds, with different functional groups, on the mixtures.

Mixtures were analysed after and before their combustion (3.4.2), to evaluate the profile of the combustion, to know if there was formation of new solid compounds and to evaluate the presence of the fresh mixture in the burnt residues.

#### **4.2.3.1. Reactants IR characterization**

To characterize the presence of the reactants in the mixtures, there were chosen some characteristic bands of the IR spectrum of each reactant. Table 52 shows the chosen

bands for each reactants, as well as their characteristics, typical wavenumber for each peak and corresponding vibrational modes.

Table 52: Chosen bands and respective bands intensities, ranges and peaks wavenumbers for characterization of the reactants in the mixtures, before and after their combustion.

| Reactant         | Typical Peak band Wavenumber (cm <sup>-1</sup> ) | Band intensity and range   | Vibrational modes  |
|------------------|--|--|--|
| Ammonium Nitrate | 2425 / 2396                                      | Medium and thin band [2385 – 2450] cm <sup>-1</sup>              | AN coating   |
|                  | 1384   | Strong band ;[1500 – 1250] cm <sup>-1</sup>                      | overlap of NH <sub>4</sub> <sup>+</sup> asymmetric deformation and NO <sub>3</sub> <sup>-</sup> asymmetric stretch |
| Urea Nitrate     | 2426   | Medium and large band; [2330 - 2550] cm <sup>-1</sup>            | C=O···H···ONO <sub>2</sub> symmetric stretch (most typical from UN)  |
| Polyurethane     | 2970   | Strong band (multiple peaks) peak); [3000-2800] cm <sup>-1</sup> | Band overlap: C-N stretch and N-H elongation typical from urethane group   |
|                  | 1590   | Strong but thin band   | C=C stretch from a di-substituted benzene  |
|                  | 1533   | Strong but thin band   | Band overlap: C-N stretch and N-H elongation typical from urethane group   |
|                  | 669  | Weak and large band; [720 – 620] cm <sup>-1</sup>                | N-H out-of-plane symmetric angular deformation, typical from amides  |
| MT mixture       | 1155   | Strong band (two peaks); [1200 – 1000] cm <sup>-1</sup>          | CF <sub>2</sub> typical elongations  |
|                  | 505  | Strong band (two peaks); [550 – 502] cm <sup>-1</sup>            | fingerprint zone of Teflon, elongation characteristic of bending and rocking modes                                 |
| Aluminium        | -  |  | Not has IR spectrum due to be a monoatomic compound  |

#### 4.2.3.2. IR characterization of fresh mixtures

There was found one IR band which can be associated to the mixture of UN and PU. That band has a wavenumber range of [3500 – 3100] cm<sup>-1</sup> and can be associated to Overlap of NH<sub>2</sub> symmetric and asymmetric stretches and primary or secondary amine salts elongations.

The addition of the additives to the studied mixtures not changed their IR spectra, just added some typical peaks, in case of the MT mixture. Those peaks were at 1155 cm<sup>-1</sup> and at 505 cm<sup>-1</sup>.

The results for the analysis of the mixtures of AN and PU are presented on Table 53. The results for mixtures which UN was the oxidizer are presented on Table 54.

Table 53: Analysis of the presence of reactants in fresh mixtures 3.1 and 3.2 (AN as oxidant) by compound and typical peak band wavenumbers (see tables above). ✓ used to “yes”, ✗ used to “no”.

| Compound         | Typical Peak band Wavenumber (cm <sup>-1</sup> ) | Presence in fresh mixture 3.1 (AN/PU/MT) | Presence in fresh mixture 3.2 (AN/PU/Al) |
|------------------|--|--|--|
| Ammonium Nitrate | 2425 / 2396                                      | ✓  | ✓  |
|                  | 1384   | ✓  | ✓  |
| Polyurethane     | 1533   | ✗  | ✗  |
|                  | 669  | ✓  | ✓  |
| MT mixture       | 1155   | ✓  | ✗  |
|                  | 505  | ✓  | ✗  |

Table 54: Analysis of the presence of reactants in fresh mixtures 4.1 and 4.2(UN as oxidant) by compound and typical peak band wavenumbers (see tables above). ✓ used to “yes”, ✗ used to “no”.

| Compound      | Typical Peak band Wavenumber (cm <sup>-1</sup> ) | Presence in fresh mixture 4.1 (UN/PU/MT) | Presence in fresh mixture 4.2 (UN/PU/Al) |
|---------------|--|--|--|
| Urea Nitrate  | 2426   | ✓  | ✓  |
| Polyurethane  | 2970   | ✓  | ✓  |
| MT mixture    | 1155   | ✓  | ✗  |
| UN/PU mixture | 3414 / 3346                                      | ✓  | ✗  |

The mixtures were well characterized and were founded enough characteristic peaks to identify, by IR spectroscopy, all fresh compounds (except Al) used on these mixtures. A general overview about the IR spectra of the studied mixtures showed that, in all spectra, the major component of the mixture was the best visualized. The presence of MT mixture, in some cases, was also well seen.

#### 4.2.3.3. IR characterization of burned mixtures

There were also found some typical IR bands for combustion products of the studied mixtures, which are presented on Table 55. Table 56 and Table 57 shows the IR analysis made to the burned mixtures of AN/PU and UN/PU, respectively.

Table 55: Chosen bands and respective peaks wavenumbers for characterization of the mixtures after combustion.

| Combustion products of | Typical Peak band Wavenumber (cm <sup>-1</sup> ) | Vibrational modes   |
|------------------------|--|---|
| MT mixture             | 466  | MgF <sub>2</sub> elongations  |
|                        | 551  | Mg – C – F unit elongations   |
| AN/PU/MT mixture       | Band [3310 – 3595]                               | O – H axial deformation in intermolecular bounds, characteristic of polymeric structures with OH group; water   |
| AN/PU/Al mixture       | [1150 – 400] cm <sup>-1</sup>                    | Al – O stretching from Al <sub>2</sub> O <sub>3</sub> species   |
|                        | [3600 – 2800] cm <sup>-1</sup>                   | O – H axial deformation in intermolecular bounds, which can be associated to alcohols, water or to Al(OH) <sub>3</sub>                                |
| UN/PU/MT mixture       | [3500 – 3100] cm <sup>-1</sup>                   | Overlap of NH <sub>2</sub> symmetric and asymmetric stretches and primary or secondary amine salts elongations (for fresh mixture was water presence) |
| UN/PU/Al mixture       | 436  | Al – O stretching   |
|                        | 3500 – 3100] cm <sup>-1</sup>                    | Overlap of NH <sub>2</sub> symmetric and asymmetric stretches and primary or secondary amine salts elongations (for fresh mixture was water presence) |

Table 56: Analysis of the presence of reactants and combustion products in burned mixtures 3.1 and 3.2 (AN as oxidant) by compound and typical peak band wave numbers (see tables above). ✓ used to “yes”, ✗ used to “no”.

| Compounds                         | Typical Peak / band Wave number (cm <sup>-1</sup> ) | Presence in burnt sample 3.1 |      | Presence in burnt sample 3.2 |      |
|-----------------------------------|---|------------------------------|------|------------------------------|------|
|                                   |   | Cigar                        | Disk | Cigar                        | Disk |
| Ammonium Nitrate                  | 2425 / 2396   | ✗                            | ✓    | ✗                            | ✓    |
|                                   | 1384  | ✗                            | ✓    | ✗                            | ✓    |
| Polyurethane                      | 1533  | ✗                            | ✗    | ✗                            | ✓    |
|                                   | 669   | ✗                            | ✓    | ✗                            | ✓    |
| MT mixture                        | 1155  | ✗                            | ✓    | ✗                            | ✗    |
|                                   | 505   | ✗                            | ✗    | ✗                            | ✗    |
| Combustion products of MT mixture | 466   | ✓                            | ✗    | ✗                            | ✗    |
|                                   | 551   | ✓                            | ✓    | ✗                            | ✗    |

|   |                              |   |   |   |   |
|---|------------------------------|---|---|---|---|
| Combustion Products typical from AN/PU/MT formulation | [640 – 710]                  | ✓ | ✓ | ✗ | ✗ |
|   | 1635                         | ✗ | ✓ | ✗ | ✗ |
|   | [3310 – 3595]                | ✗ | ✓ | ✗ | ✗ |
| Combustion Products typical from AN/PU/Al formulation | [1150–400] cm <sup>-1</sup>  | ✗ | ✗ | ✓ | ✗ |
|   | [3600–2800] cm <sup>-1</sup> | ✗ | ✗ | ✓ | ✗ |

Table 57: Analysis of the presence of reactants and combustion products in burned mixtures 4.1 and 4.2 (UN as oxidant) by compound and typical peak band wavenumbers (see tables above). ✓ used to “yes”, ✗ used to “no”.

| Compound                                | Typical Peak band Wavenumber (cm <sup>-1</sup> ) | Presence in burnt sample 4.1 |      | Presence in burnt sample 4.2 |      |
|---|--|------------------------------|------|------------------------------|------|
|   |  | cigar                        | disk | cigar                        | disk |
| Urea Nitrate                            | 2426   | ✓                            | ✓    | ✓                            | ✓    |
| Polyurethane                            | 2970   | ✗                            | ✓    | ✗                            | ✗    |
|   | 1590   | ✗                            | ✗    | ✓                            | ✓    |
| MT mixture                              | 1155   | ✓                            | ✓    | ✗                            | ✗    |
| UN/PU mixture                           | 3473 / 3367 / 3183                               | ✓                            | ✓    | ✓                            | ✓    |
| Combustion products of MT mixture       | 448  | ✓                            | ✓    | ✗                            | ✗    |
|   | 557  | ✓                            | ✓    | ✗                            | ✗    |
| Combustion products of UN/PU/Al mixture | 436  | ✗                            | ✗    | ✓                            | ✓    |

The burned mixtures with AN as oxidant (Table 57) were well characterized in relation of the presence of fresh material, as well as in relation of the typical combustion products of each mixture.

The sample 3.1 burned on both conditions, but in cigar burning test there was no presence of fresh material in ashes from its combustion. The sample 3.2 on the disk burning test not suffered combustion and, due to that, was not possible to characterize the IR spectrum of this mixture at adiabatic conditions. On the opposite side was sample 3.2 on cigar burning test that completely burned and fresh material was not present in its residues.

The profile of the burned samples of mixtures based on UN as oxidant (Table 57) had closest profiles, because no one of the mixtures totally burned. All mixtures had visible presence of fresh and materials and IR spectroscopy confirmed those presences.

In general, when fresh mixtures (before combustion) are analysed by IR spectroscopy, just the vibrational modes of their principal component are observed. This means that reactants with less than 10% (m/m) in mixture's composition are not analysable by this technique.

After combustion, it was possible to analyse the presence of new components when the combustion was incomplete. When combustion was total, the IR spectrum is plane and there is nothing to analyse. But even when combustion of the mixture is not total, it just will be possible to observe new components on IR spectrum if some kind of separation would be applied to the combustion products, because if those products are produced on percentages less than 10% of the raw material (non-burned) it will be not analysable by this technique.



## CHAPTER 5 – SYNTHESIS AND CONCLUSIONS

Homemade explosives (HME) and Improvised Explosives Devices (IED) are the preferred tool on bombing events. HME and IED can also be applied in disturbances in normal supply chains.

Supply chain security is very important for international transporters, operators and authorities, in order to guarantee that all essential needs are covered, import and export safely and on time. Then, it was tried to follow the steps which a terrorist could be follow to choose and perform a terrorist attack using open market products.

Ammonium and Urea Nitrates were the selected oxidants to produce explosives for several reasons: historical know-how from previous accidents and terrorist attacks, explosive properties, easy acquisition and transportation for large quantities.

Besides all incidents, ammonium nitrate (AN) is a good reference to study explosive properties and combustion phenomena. It is also a compound very present on daily life - fertilizers, cleaning products, civil explosive applications, relatively safe to manage and store.

Urea nitrate (UN) was an elected oxidant essentially due to its explosive potentialities. The fact of being an original oxidant molecule with a carbon content in its structure, makes it a promisor explosive molecule, which not need the addition of a combustible (that is the case of fuel-oil for AN).

The worst problems seen for both oxidants were their hygroscopicity and their high solubility in polar solvents, as polyol solution of the polyurethane (PU) binder. This last effect was more notable for UN.

Mixtures of AN and UN with PU solution, as binder, were tested, with aluminium (Al) and a mixture of Magnesium/Teflon (MT) as additive. Decomposition of reactants, as a function of temperature, was predicted using THOR code. Combustion temperatures were also theoretical predicted in order to define tested compositions. THOR code was also used to predict the Free Gibbs enthalpy for mixtures composed by the oxidants and the binder, and to predict the temperature combustion as a function of the additive in the previous mixtures. For original mixtures, the Free Gibbs Enthalpies varied between  $-1.83E+04$  and  $-1.60E+04$  kJ/kg, richness (r) between 1.5 and 2.9. Temperatures varied between 1227 and 2630 °C.

DSC/TGA thermograms of reactants help to define composition and show levels of decomposition. AN and UN thermograms show some significant differences between them, showing an exothermic peak of UN in quite low temperatures. This exothermic peak of UN, not defined in AN, proves the potential capacities of this oxidant when used in explosive compositions. The acquired results were concordant with those founded on the literature.

Experimental tests used two configurations: cigar and disk burning tests. This last sample was pressurized in order to keep propellant mixture at high levels of compaction and ensuring quite adiabatic conditions in flame progression. Cylindrical samples were tested before cylindrical boxes, verifying burning properties.

Fresh mixtures varied their averaged densities between 1313 and 1943 kg/m<sup>3</sup> for AN mixtures, and between 1728 and 1621 kg/m<sup>3</sup> for UN mixtures. The coupled values corresponds to samples for cigar burning tests and for disk burning tests, respectively.

For atmospheric pressure conditions, on cigar burning tests, the combustion with additives, Al or MT mixture, show an increasing flame temperature on the levels of 1300 °C, for both oxidants.

It was possible to measure three flame velocities in a single experiment: on PMMA, which was responsible for driven-flame combustion; on explosions, that was generated from deflagration of the gaseous products, on the heterogeneous mixtures, which was the reference velocity to pass from fresh to burned materials. All obtained velocity values were in the order of mm/s, being the propagation velocities of PMMA and of the mixtures ten times lesser that the propagation flame velocity in the explosions.

Measured fundamental flame velocities presented an averaged value of 0.30 s.

Disk burning test present an experimentally approach to adiabatic conditions. It was observed spontaneous explosions, due to the fast heat propagation, inside the mixture, and the consequent gas expansion. MT additive seems to present an increased contribution to the expansion.

It was observed the self-ignition of one of the UN/PU compositions with MT, during curing time. It seems to be due to complex phenomena of production of gas, from UN. The addition of diisocyanate to the UN, followed by the addition of the MT and, at least, the addition of polyol, create physical and chemical conditions to occur gas production and self-ignition of the mixture. When polyol is firstly added to UN, UN is solubilized and the followed addition of diisocyanate and the additive is no more dangerous. These reactions needs further studies to be completely clarified

The infrared analysis study here presented is enough to evaluate the presence of the reactants (except Al), as well as the presence of some typical compounds associated to the fresh and burned mixtures. There were founded typical bands for each situation.

The most relevant conclusions about the IR spectroscopic study performed on this work were that the IR spectra of the mixtures shows, mainly, the presence of the components present in quantities higher than 10% (m/m). To evaluate the presence of the compounds in lesser quantities, it would be needed separation techniques and further IR analysis. To have knowledge and to characterize the formation of new compounds before and after burning the mixtures, it would be necessary the employment of other analytical techniques as, for example, gas or liquid chromatography (GC or LC, respectively) coupled with mass spectrometry (MS).

The high hygroscopicity of AN and UN is a factor that have to be controlled for a successful combustion of these mixtures. Another factor that needs special attention on further studies is the mixing procedure.

As further work, it can also be considered the application of the DSC/TGA technique to the fresh mixtures in more large quantities. To study their behaviour when submitted to controlled fast heating rates. This will be advantageous to have knowledge about relevant phase transitions, melting points, thermal decomposition temperatures, kinetic parameters and thermal instabilities of the developed mixtures.

Spectrometric studies have to be done to have more data about the structure and the bounds formed on these heterogeneous mixtures. More depth studies on IR spectroscopy, which can include Raman and ATR/FTIR spectroscopy, will be useful to evaluate the typical compounds present on mixtures (before and after combustion) that just correspond to these mixtures and no other, with reactants with similar functional groups and/or structures. It also be useful employ mass spectrometry and RMN to fresh and burned mixtures. It will give much more useful forensic data for detection and identification of the chosen compounds and mixtures.

The last, but maybe the more important to further studies, is the deflagration – detonation transition (DDT) properties of these mixtures. They will confirm bomb capabilities and their critical mass and sizes.



## BIBLIOGRAPHIC REFERENCES

**Akira. 1998.** The Terrorist's Handbook. *Akira's Home Page*. [Online] 1998. <http://www.capricorn.org/~akira/home/terror.html>.

**Almada, Sara de Jesus de Vidigal e. 1998.** *Explosão Térmica de Materias Energéticas*. LEDap : Departamento de Engenharia Mecânica da Faculdade de Ciências e Tecnologia da Universidade de Coimbra, 1998.

**Almog, Joseph, et al. 2007.** Recovery and Detection of Urea Nitrate in Traces. *J Forensic Sci.* 2007, pp. 1284-1290.

**BBC. 1993.** 1993: IRA bomb devastates City of London. *On This Day 1950 - 2005*. [Online] BBC Home, 24 April 1993. [http://news.bbc.co.uk/onthisday/hi/dates/stories/april/24/newsid\\_2523000/2523345.stm](http://news.bbc.co.uk/onthisday/hi/dates/stories/april/24/newsid_2523000/2523345.stm).

**Bureau of Alcohol Tobacco Firearms and Explosives; Federal Bureau of Investigation. 2007.** *Indicators and Warnings for Homemade Explosives*. s.l.: Technical Support Working Group, 2007.

**Caldwell, John. 2011.** *Understanding the Basis of Improvised Explosive Devices (IED)*. Norfolk : Civil-Military Fusion Center, 2011.

**Campos, J. 1991.** Thermodynamic calculation of solid and gas combustion pollutants using different equation of state. *Proceeding of 1st International Conference on Combustion Technologies for a Clean Environment*. 1991, Vol. 1, pp. 30.4-1 - 30.4-11.

**Campos, J., et al. 2007(2).** Decomposition path of pyrolysis and combustion of thermite/nitrate/metal compositions. *International Annul Conference of ICT*. 38th, 2007(2).

**Campos, J., et al. 2006.** Decomposition path of pyrolysis and combustion of energetic materials. *I Conferência Nacional de Métodos Numéricos em Mecânica dos Fluidos e Termodinâmica*. 2006, pp. 1-15.

## BIBLIOGRAPHIC REFERENCES

**Campos, José, et al. 2007.** Predicting Combustion and Detonation Properties Using Thermodynamic Code THOR. *4th Workshop on Pyrotechnic Combustion Mechanisms - ICT*. 2007, pp. 1-20.

**Carvalho, P., Campos, J. and Gadiot, and G. 1995.** Burning Rate Modifiers for NA/HTPB-IPDI Composite Solid Propellants for Gas Generators. *International Annual Conference of ICT*. 1995, Vol. 26th, pp. 69.1-69.14.

**Chattopadhyay, Arun K. 1996.** *Coating for ammonium nitrate prills. 5,567,910* United States, 22 October 1996.

**Chattopadhyay, D. K. and Webster, Dean C. 2009.** Thermal stability and flame retardancy of polyurethanes. *Progress in Polymer Science*. 2009, Vol. 34, pp. 1068-1133.

**Davis, Dennis D. and Dee, Louis A. 1996.** *Chemical Characterization and Reactivity Testing of Fuel-Oxidizer Reaction Product*. USA : National Aeronautics and Space Administration, 1996.

**Deen, Thalif. 2005.** Inter Press Service - News Agency. *IPS*. [Online] 25 July 2005. <http://www.ipsnews.net/2005/07/politics-un-member-states-struggle-to-define-terrorism/>.

**Désilets, Silvan, et al. 2011(2).** Analyses of the thermal decomposition of urea nitrate at high temperature. *Thermochimica Acta* 5. 2011(2), pp. 59– 65.

**Désilets, Sylvain, et al. 2011.** Degradation mechanism and thermal stability of urea nitrate below the melting point. *Thermochimica Acta* 521. 2011, pp. 176-183.

**Doherty, Ruth. 2009.** *Detection of Homemade Explosives (HMEs)*. s.l. : U.S. Department of Homeland Security, Science and Technology (S&T) Directorate , 2009.

**Durães, L., Campos, J. and Gois, J. C. 1996.** New Equation of State for the Detonation Products of Explosives. *Proc. of 1995 APS Topical Conference on Shock Compression of Condensed Matter*. 1996, pp. 385-388.

**Durães, L., Campos, J. and Góis, J.C. 1995.** Deflagration and Detonation Using a New Equation of State. *24th International Annual Conference of ICT*. 1995, pp. 1-12.

**Durães, L., Campos, J. and Portugal, A. 2006.** Radial Combustion Propagation in Iron(III)Oxide/ Aluminum Thermite Mixtures. *Propellants, Explosives and Pirotechnics*. 31, 2006.

**Durães, L., Campos, J. and Portugal, A. 1997.** Reaction path of energetic materials using THOR codes. *American Institute of Physics*. 1997, pp. 341-344.

**Durães, L., Campos, J. and Portugal, A. 1996(2).** Thermal Decomposition of Energetic Materials Using THOR Code. *Proc. of the Twenty Second International Pyrotechnics Seminar*. 1996(2), pp. 497-508.

**Durães, L., Campos, J. and Portugal, A. 2000.** Thermodynamical Prediction of Combustion and Detonation Properties Using Modified Thor Code. *Proc. of the 31st International Annual Conference of ICT*. 2000, pp. 1-11.

**Durães, Luísa Maria Rocha. 1999.** *Composição e Propriedades Termodinâmicas dos Produtos de Detonação e de Deflagração*. Coimbra : Departamento de Química da FCTUC, 1999.

**Fischer, Gerd, et al. 2002.** Synthesis, Properties and Dimerization Study of Isocyanic Acid. *Z. Naturforsch.* 2002, pp. 19–24.

**Foldvary, Fred E. 2001.** The Progress Report - Editorial. *Ammonium Nitrate: regulate it*. [Online] 2001. <http://www.progress.org/fold226.htm>.

**FP-25/30 anos. 2010.** DN Portugal. *Surgimento das FP-25 fez sentido. Não tenho de que me arrepende*. [Online] Lusa, 19 April 2010. [http://www.dn.pt/inicio/portugal/interior.aspx?content\\_id=1548271&page=-1](http://www.dn.pt/inicio/portugal/interior.aspx?content_id=1548271&page=-1).

**FPNEM. 2013.** *Technical Report 5*. s.l. : Project Group FPNEM - Formulation and Production of New Energetic Materials, 2013.

## BIBLIOGRAPHIC REFERENCES

**Glenn D. Roberstson, Jr. 1953.** *Some physic-chemical properties of the system nitric acid – nitrogen dioxide – water.* Pasadena, California : California Institute of Technology, 1953.

**Headquarters, Department of the Army United States Marine Corps. 2005.** *IMPROVISED EXPLOSIVE DEVICE DEFEAT.* Washington, DC : Marine Corps Information Publication, 2005.

**History.com. 1996-2013.** Feb 26, 1993: World Trade Center bombed. *This day in History.* [Online] A&E Television Networks, LLC, 1996-2013. <http://www.history.com/this-day-in-history/world-trade-center-bombed>.

**Hiyoshi, Reiko I., et al. 2002.** Experimental and computational study of the thermal decomposition of uronium nitrate (urea nitrate). *12th International Detonation Symposium.* 2002, pp. 1-8.

**Hopp, B., et al. 2007.** Femtosecond pulsed laser deposition of biological and biocompatible thin layers. *Applied Surface Science.* 2007, Vol. 253, 19, pp. 7806–7809.

**ICT. 2005.** *Database of Thermochemical Values.* Fraunhofer-Institut für Chemische Technologie, Germany : s.n., 2005.

**Infopédia. 2003 - 2013.** FP 25 (Forças Populares 25 de abril). *Infopédia - Enciclopédia e Dicionários Porto Editora.* [Online] Porto Editora, 2003 - 2013. [http://www.infopedia.pt/\\$fp-25-%28forcas-populares-25-de-abril%29;jsessionid=VsO9NtzR0jX0PiS+UN7J9w\\_\\_](http://www.infopedia.pt/$fp-25-%28forcas-populares-25-de-abril%29;jsessionid=VsO9NtzR0jX0PiS+UN7J9w__).

**Joint Improvised Explosive Device Defeat Organization. 2012-1026.** *Counter-Improvised Explosive Device Strategic Plan.* California : JIEDDO, 2012-1026.

**Jolkkonen, Mikael. 2012.** Update Computer Club. <http://www.update.uu.se>. [Online] Uppsala University, 2012. [http://www.update.uu.se/~jolkkonen/pdf/CRC\\_TD.pdf](http://www.update.uu.se/~jolkkonen/pdf/CRC_TD.pdf).

**Kirkpatrick, Allan T.** [www.engr.colostate.edu](http://www.engr.colostate.edu). *Colorado State University.* [Online] <http://www.engr.colostate.edu/~allan/thermo/page11/page11.html>.

**Koch, Ernst-Christian. 2002.** Metal-Fluorocarbon-Pyrolants IV: Thermochemical and Combustion Behaviour of Magnesium/Teflon/Viton (MTV). *Propellants, Explosives, Pyrotechnics*. 2002, Vol. 27, pp. 340-351.

**Kohno, Yuji, et al. 2003.** Theoretical Study of the Initial Decomposition Process of the Energetic Material Urea Nitrate. *J. Phys. Chem. A*. 2003, pp. 6444-6450.

**Kolaczkowski, A. 1980.** *Samorzutny Rozklad Saletry Amonowejv*. Wrocław. : Wydawnictwo Politechniki Wrocławskiej, 1980.

**Kubota, Naminosuke. 2002.** *Propellants and Explosives - Thermochemical Aspects of Combustion*. Weinheim : WILEY-VCH GmbH, 2002.

**Kuzik, L.A. and Yakovlev, V.A. 1999.** Effect of a noble metal coating o a natural aluminium oxide film. *Thin Solid Films*. 1999, Vol. 340, pp. 288 - 291.

**Lee, Chris. 2012.** The Bombing of Sterling Hall. *Leemark Communications*. [Online] Leemark Communications, September 2012. <http://www.leemark.com/sterlinghall/index.html>.

**Manual, Department of the Army Technical. 2007.** *Improvised Munitions Handbook (Improvised Explosive Devices or IEDs)*. United States of America : Headquarters, Department of the Army, 2007.

**McNesby, Kevin L. and Pesce-Rodriguez, Rose A. 2002.** *Applications of Vibrational Spectroscopy in the Study of Explosives*. USA : US Army Research Laboratory, 2002. pp. 1-17.

**Morgado, Joel, et al. 2003.** "Fast" thermite reaction of iron oxide/aluminium/nitrate mixtures. *34th International Annual Conference of ICT*. 24-27 June, 2003, pp. 1-14.

**Morgado, Joel, et al. 2002.** Iron oxide/aluminium fast thermite reaction using nitrate aditives. *New trends in research of energetic materials*. Proceedings of the V seminar, 2002, pp. 207-221.

**NASA. 2003.** NASA Thermobuild. *NASA Glenn Research Center*. [Online] 2003. <http://www.grc.nasa.gov/WWW/CEAWeb/ceaThermoBuild.htm>.

## BIBLIOGRAPHIC REFERENCES

**Neves, Andreia Catarina Cardoso das. 2010.** *Comportamento de espumas de poliuretano no processo de colagem à chama.* Department of Chemistry. Aveiro : Universidade de Aveiro, 2010.

**NICODOM. 2012.** NICODOM IR Explosives – FTIR Spectra Explosives. *IR-Spectra.* [Online] 2012. [http://www.ir-spectra.com/download/NICODOM\\_IR\\_Explosives.htm](http://www.ir-spectra.com/download/NICODOM_IR_Explosives.htm).

**NIST.** kinetics.nist.gov. *NIST Chemical Kinetics Database.* [Online] <http://kinetics.nist.gov/kinetics/ReactionSearch;jsessionid=4E3AD1CED8FC90EF56014F076BFF7205?r0=7782447&r1=0&r2=0&r3=0&r4=0&p0=17778802&p1=17778802&p2=0&p3=0&p4=0&expandResults=true&>.

**Oommen, C. and Jain, S.R. 1999.** Ammonium nitrate: a promising rocket propellant oxidizer. *Journal of Hazardous Materials A67.* 1999, pp. 253–281.

**Oommen, C. and S.r.Jain. 1999(2).** Phase Modifications of Ammonium Nitrate by Potassium Salts. *Hournal of Thermal Analysis and Calorimetry.* 1999(2), Vol. 55, pp. 903-918.

**Oosterhout, Marcel P.A. van, et al. 2007.** Visibility Platforms for Enhancing Supply Chain Security: a Case Study in the Port of Rotterdam. *International Symposium on Maritime Safety, Security and Environmental Protection.* 2007.

**Oxley, Jimmie C and al., . et. 2013.** Synthesis and Characterization of Urea Nitrate and Nitrourea. *Propellants, Explosives, Pyrotechnics.* 2013, pp. 1-10.

**Oxley, Jimmie C. and al., et. 2009.** Decompositions of Urea and Guanidine Nitrates. *Journal of Energetic Materials,*27. 2009, pp. 17–39.

**Oxley, Jimmie C., et al. 2002.** Ammonium nitrate: thermal stability and explosivity modifiers. *Thermochimica Acta* 384. 2002, pp. 23-45.

**Patil, Dilip G., Jain, Sampat R. and Brill, and Thomas S. 1992.** Thermal Decomposition of Energetic Materials 56. On the Fast Thermolysis Mechanism of Ammonium Nitrate and its Mixtures with Magnesium arnd Carbon. *Propellants, Explosives, Pyrotechnics.* 1992, Vol. 17, pp. 99-105.

**Pieterse, J.A.Z., et al. 2005.** Direct decomposition of N<sub>2</sub>O at low(er) temperature: the effect of NO, combining active metals and a synergistic effect. *Proceedings of the 4th International Conference on Environmental Catalysis*. 2005.

**Pires, A. and Campos, J. 1996.** Incineration of Explosives in a Fluidised Bed. *International Annual Conference of ICT*. 27th, 1996, pp. 80.1-80.14.

**Portugal, Paula, Campos, José and Portugal, António. 2000.** Combustion behaviour of pyrotechnic mixture based in ammonium and sodium nitrates with wood particles. *Proc. of the 31st International Annual Conference of ICT, Germany*. 2000.

**Quaresma, J., et al. 2013.** Flame velocity measurements of heterogeneous mixtures based in ammonium or urea nitrates. *44th International Conference of ICT*. 2013, pp. 1-17.

**Quaresma, Joana and Campos, José. 2013(2).** *Security level - selection and evaluation of open market reactants for homemade explosives*. LEDAP. Coimbra : CH-Secure, 2013(2). p. 34.

**Reichenbacher, Manfred and Popp, Jurgen. 2012.** *Challenges in Molecular Structure Determination*. Germany : Springer, 2012.

**Rheometric Scientific . 1995.** *Plus V - Software Manual*. Epsom : Rheometric Scientific Limited, 1995.

**Ryczkowski, Janusz. 2001.** IR spectroscopy in catalysis. *Catalysis Today*. 2001, Vol. 68, pp. 263 - 381.

*Science & Technology to Counter Improvised Explosive Devices*. **Doherty, Ruth M. 2010.** Florida : NDIA Conference on Combating Terrorist Use of Explosives, 2010.

**Silva, Marisa. 2013.** Ammonium Nitrate.  
<http://ammoniumnitrate.weebly.com/index.html>. [Online] 2013.  
<http://ammoniumnitrate.weebly.com/structure.html>.

## BIBLIOGRAPHIC REFERENCES

**Silverstein, Robert M. and Webster, Francis X. 1998.** *Identificação Espectrométrica de Compostos Orgânicos*. Rio de Janeiro : LTC - Livros Técnicos e Científicos Editora S.A., 1998.

**Simões, P.N., et al. 1998.** Study of the decomposition of phase stabilized ammonium nitrate (PSAN) by simultaneous thermal analysis: determination of kinetic parameters. *Thermochimica Acta*. 319, 1998, pp. 55-65.

**START. 2012.** National Consortium for the Study of Terrorism and Responses to Terrorism (START. *GTD Global Terrorism Database*. [Online] University of Maryland, 2012. <http://www.start.umd.edu/gtd/>.

**Stigset, Marianne, Kremer, Josiane and Treloar, Stephen. 2011.** Police in Norway Extend Terror Probe Across Europe After Breivik Attacks. *Bloomberg*. [Online] Bloomberg LP, 27 July 2011. <http://www.bloomberg.com/news/2011-07-27/norway-police-spreads-breivik-terror-probe-europe-wide-after-twin-attacks.html>.

**Tamiri, Tsippy. 2005.** Characterization of the improvised explosive urea nitrate using electrospray ionization and atmospheric pressure chemical ionization. *RAPID COMMUNICATIONS IN MASS SPECTROMETRY*. 2005, Vol. 19, pp. 2094–2098.

**Tamiri, Tsippy, et al. 2009.** Urea nitrate, an exceptionally easy-to-make improvised explosive: studies towards trace characterization. *Anal Bioanal Chem*. 2009, Vol. 395, pp. 421–428.

**Tang, Rose. 2001.** Bomber has confessed, China says. *CNN.com/WORLD*. [Online] CNN, 27 March 2001. <http://premium.europe.cnn.com/2001/WORLD/asiapcf/east/03/27/china.bomber.confess/index.html>.

**The White House. 2012.** *National Strategy for Global Supply Chain Security*. Washington : U.S. Department of Homeland Security, 2012.

**Théorêt, A. and Sandorfy, C. 1964.** Infrared spectra and crystalline phase transitions of ammonium nitrate. *Canadian Journal of Chemistry*. Volume 42. 1964, pp. 57-62.

**Tokmakov, Igor V., Alavi, Saman and Thompson, Donald L. 2006.** Urea and Urea Nitrate Decomposition Pathways: A Quantum Chemistry Study. *J. Phys. Chem. A*, 110, 2006, pp. 2759-2770.

**United Nations. 1994.** *49/60 Measures to eliminate international terrorism*. s.l. : General Assembly , 1994.

**US Code. 1992.** Legal Information Institute. *Cornell University Law School*. [Online] Cornell University Law School, 1992. <http://www.law.cornell.edu/uscode/text/18/2331>.

**Vyazovkin, Sergey, Clawson, Jacalyn S. and Wight, Charles A. 2001.** Thermal Dissociation Kinetics of Solid and Liquid Ammonium Nitrate. *Chem. Mater.* 13, 2001, pp. 960-966.

**Whitlock, Craig. 2007.** Homemade, Cheap and Dangerous: Terror Cells Favor Simple Ingredients In Building Bombs. *The Washington Post*. [Online] Washington Post Foreign Service, 5 July 2007. [http://www.washingtonpost.com/wp-dyn/content/article/2007/07/04/AR2007070401814\\_pf.html](http://www.washingtonpost.com/wp-dyn/content/article/2007/07/04/AR2007070401814_pf.html).

**Yinon, Jehuda and Zitrin, Shmuel. 1981.** *The Analysis of Explosives*. Israel : Pergamon Press, 1981. Vol. Analytical Chemistry Volume 3.